Investigation of superconductor tunnel junctions on YBCO high temperature superconductor

Chouial, Baghdadi

Award date:
1991

Awarding institution:
University of Bath

Investigation of superconductor tunnel junctions on YBCO high temperature superconductor

Submitted by Baghdadi Chouial
for the degree of PhD
of the University of Bath
1991

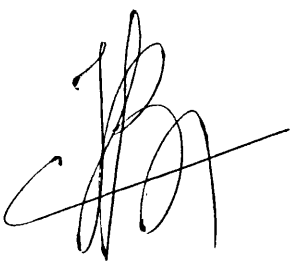

ProQuest LLC
789 East Eisenhower Parkway
P.O. Box 1346
Ann Arbor, MI 48106-1346

ABSTRACT

This thesis presents an investigation into superconducting tunnelling junctions based on high T_c superconducting materials. Seven YBCO samples were used to make superconductor tunnel junctions. IV curves of junctions were measured at different temperatures and voltage ranges using a computer controlled measurement system. The measurements gave well behaved nonlinear IV curves as well as IV curves with very strong non-linearities. Many properties such as the 0 volt anomaly and gap anisotropy were observed .

To my wife F. Zohra whose encouragement and support over the years have made the completion of this thesis possible .

To my children Besma and T.Yaakoub.

To my parents.

To the memory of my brother Tahar.

TABLE OF CONTENTS

CHAPTER 1: INTRODUCTION 1
1.1 Introduction 1
1.2 Superconductivity 1
1.3 The Meissner effect. 2
1.4 Penetration depth and coherence length 3
1.4.1 Penetration depth 3
1.4.2 Coherence length 5
1.5 Different types of superconductors 6
1.5.1 Type I superconductor 6
1.5.2 Type II superconductor 8
1.6 Heat capacity of superconductors 9
1.7 Low T_c superconductivity microscopic theory 9
1.7.1 The energy gap 10

CHAPTER 2: SUPERCONDUCTING TUNNELLING DEVICES 15
2.1 Introduction 15
2.2 Elements of tunnelling 15
2.3 Fabrication of MIM junctions and Superconductor tunnel junctions 19
2.4 Tunnelling process in Metal-Insulator-Metal junction 21
2.4.1 Normal metal electrons and superconductor quasiparticles 24
2.5 Energy level diagram of a superconductor 24
2.6 SIN junction tunnelling 28
2.7 SIS junction tunnelling 31
2.7.1 SIS junction with identical superconductors . 31
2.7.2 SIS tunnel junction with different superconductors 33
2.8 Super-Schottky diode tunnelling 35
2.9 Photon assisted tunnelling 37
2.10 Pairs tunnelling :the Josephson junction 39
2.10.1 Different type of Josephson junctions 41
2.10.2 IV curves of Josephson junction 42
2.10.3 IV curve of other weak links 44
2.11 Equivalent circuit and features of real junctions 45
2.12 The RSJ mode 52

CHAPTER 3: LOW T_c SUPERCONDUCTOR DEVICE APPLICATIONS .. 59
3.1 Introduction 59
3.2 Direct detection 59
3.2.1 Direct detector sensitivity 59
3.2.2 Quantum expressions of R_i and NEP 61
3.2.3 Direct detectors results 62

3.3 Mixer principles 63
3.3.1 Mixer properties 65
3.3.2 Conversion loss L_c 66
3.3.3 Noise temperature 66
3.3.4 Mixer receiver sensitivity 67
3.3.5 Superconductor mixer results 68
3.4 SQUIDS 70
3.4.1 Introduction 70
3.4.2 DC SQUIDS 71
3.4.3 Noise and sensitivity of DC SQUIDs 74
3.4.4 Results of practical DC SQUIDS 74
3.4.5 DC SQUID applications 75
3.4.6 RF SQUIDS 76
3.4.7 RF SQUID sensitivity 77
3.4.8 RF SQUID results 78
3.4.9 RF SQUID applications 78
3.4.10 Conclusions and remarks on DC and RF SQUIDs 79
3.5 Computer applications 79
3.5.1 Josephson junction as a switch 79
3.5.2 The superconducting computer: IBM contribution 82
3.5.3 Contribution of other labs and companies 82
3.5.4 Conclusion 86

CHAPTER 4: HIGH T_c SUPERCONDUCTING MATERIALS AND THEIR APPLICATIONS 94
4.1 Introduction 94
4.2 High T_c Superconductors 94
4.3 Other high T_c superconductors 96
4.4 Charge carriers 98
4.5 Superconductivity theories 99
4.5.1 Introduction 99
4.5.2 High T_c superconductivity theories 100
4.6 High Tc superconductors and the energy gap. 101
4.6.1 Introduction 101
4.6.2 Energy gap of high T_c superconductors. 101
4.6.3 Anisotropy of high T_c energy gap 102
4.7 High T_c Specific heat 103
4.8 High T_c parameters 104
4.9 Environmental and solvent effect on high T_c superconductors 105
4.9.1 Environmental effects 105
4.9.2 Reaction of YBCO with nonaqueous solutions 105
4.10 Dopant effect on high T_c superconductors 106
4.10.1 Effect of many dopants on $YBa_2Cu_3O_{(7-x)}$ 106
4.10.2 Effect of Zn and Ni on $YBa_2Cu_3O_{(7-x)}$ 107
4.10.3 Effect of Pr in $YBa_2Cu_3O_{(7-x)}$ 107
4.10.4 Effect of Titanate and Strontium Titanate on $YBa_2Cu_3O_{(7-x)}$ 107
4.10.5 Effect of fluoride on $YBa_2Cu_3O_{(7-x)}$ 108

4.10.6 Liquid nitrogen effect on YBCO 108
4.10.7 Effect of Beryllia (BeO) 109
4.10.8 Simulation of dopant effect on $YBa_2Cu_3O_{(7-x)}$ 109
4.10.9 Dopant effect on superconductor parameters . 109
4.10.10 Conclusion 110
4.11 High T_c applications 111
4.12 High T_c detectors 111
4.12.1 High T_c mm and microwave detectors 112
4.13 High T_c mixers 114
4.14 High T_c SQUIDs 116
4.15 High T_c computer applications 119
4.16 High T_c space applications 119
4.17 Other device applications 119

CHAPTER 5: SAMPLE PREPARATION, EXPERIMENTAL SET-UP, AND RESULTS 132
5.1 Introduction 132
5.2 Sample 1 referred to as S1P 132
5.2.1 Sample preparation 132
5.2.2 Experimental set up 132
5.2.3 Measurement Results 136
5.3 Sample 2 referred to as K1B 144
5.3.1 Sample preparation 144
5.3.2 Experimental set up 145
5.3.3 Results 145
5.4 Sample 3 :preparation and characterisation of YBCO pelletts 150
5.4.1 Sample S1B characterisation 151
5.4.2 R vs T anomaly of samples immersed in liquid N2 153
5.5 Sample 4 referred to as S1DE (S1D and S1E) 153
5.5.1 Experimental set-up 155
5.5.2 Results of the pellett S1D 156
5.5.3 Results of the Bar S1E 159
5.6 Samples 5 referred to as S2A 163
5.6.1 Sample preparation 163
5.6.2 Experimental set up 165
5.6.3 Measurement results 165
5.6.4 R vs T with increasing temperature 174
5.7 Sample 6 referred to as BD1 176
5.7.1 Sample preparation 176
5.7.2 Silicon oxide (SiO) deposition 176
5.7.3 Magnesium floride (MgF2) deposition 177
5.7.4 Silver deposition 177
5.7.5 Electrical contact layout 177
5.7.6 Experimental set up 178
5.7.7 Measurement results 179
5.8 Sample 7 referred to as SDO 183
5.8.1 Sample preparation 183
5.8.2 Experimental set up 187
5.8.3 Layout of run 1, 2, and 3 187

5.8.4 Measurement results of run 1 188
5.8.5 Measurement results of run 2 198
5.8.6 Measurement results of run 3 209
5.8.7 Layout of run 4 and 5 218
5.8.8 Measurement results of run 4 218
5.8.9 Measurement results of run 5 224
5.8.10 Layout of run 6 233
5.8.11 Experimental set-up 234
5.8.12 Measurement results of run 6 235
5.9 Thin film attempt 243
5.9.1 R vs T measurement of thin film on $SrTiO_3$ .. 245
5.9.2 R vs T measurement of thin film on allumina 246
5.9.3 Comparaison of the previous R vs T 246

CHAPTER 6: DISCUSSION OF RESULTS 249
6.1 Introduction 249
6.2 SAMPLE 1 S1P 250
6.3 SAMPLE 2 K1B 252
6.4 SAMPLE 4 S1DE (S1E and S1D) 253
6.5 SAMPLE 5 S2A 254
6.6 SAMPLE 6 BD1 255
6.7 SAMPLE 7 SDO 255
6.7.1 Run 1 255
6.7.2 Run 2 256
6.7.3 RUN 3 262
6.7.4 Run 4 263
6.7.5 Run 5 263
6.7.6 Run 6 265
6.8 Summary of gap parameters 268
6.9 General conclusion 270
6.10 Future work 271

CHAPTER 7: ACKNOULEGEMENTS 276

Appendix A1 277

Appendix A2 280

Computer program 291

CHAPTER 1: INTRODUCTION

1.1 Introduction

In this chapter the main fundamental aspects of superconductivity will be briefly reviewed using both macroscopic and microscopic approaches. In this discussion only those aspects which are related to this investigation will be emphasized .

1.2 Superconductivity

This term was first used by K.Onnes when he observed for the first time that the DC resistance of mercury (the only pure metal available at that time) vanished at Helium liquid temperature i.e 4.2 K [1] as shown in figure 1.1 .

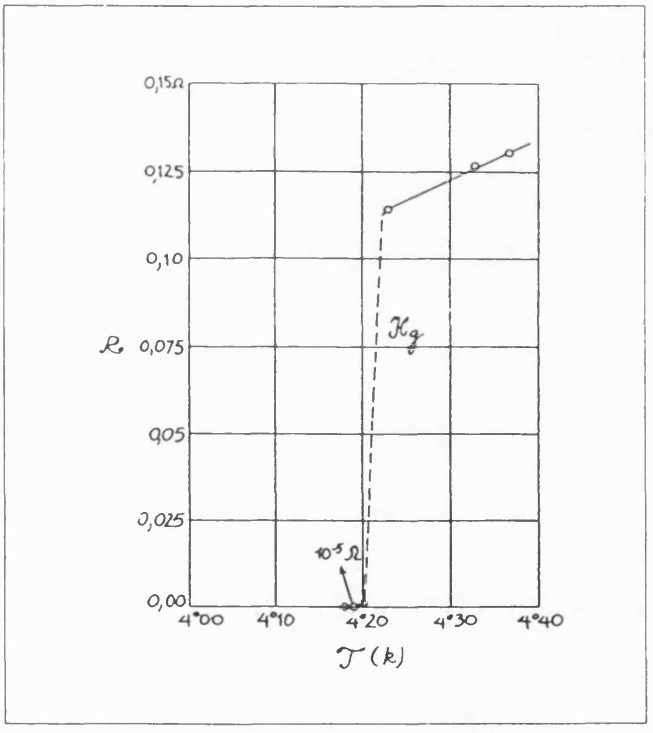

Fig.1.1 Resistance vs temperature measurement (after H. K. Onnes [1])

This discovery came three year later after the same man had succeeded in liquefying Helium , a major breakthrough in itself. At this time, a decade before the development of quantum theory , Onnes did not realise that the vanishing resistance

is in fact a striking manifestation on a macroscopic scale of quantum mechanical behaviour . The absence of resistance means that a supercurrent can be induced in a superconducting ring cooled below the transition temperature (critical temperature) T_C and may be expected to flow at uniform level for an indefinitly long time. Indeed supercurrents which persisted for extremely long period (years) have been observed .

1.3 The Meissner effect.

Three decades elapsed before the discovery of another effect related to the superconductive state of pure metals, the Meissner effect. This phenomenon was observed by Meissner and Ochsenfeld [2] who noticed that when a pure metal cooled through its transition temperature T_C in the presence of an applied magnetic field, all magnetic flux was expelled from within the bulk. This diamagnetic behaviour is created by persistent currents (screening current) that arise on the surface and circulate so as to cancel the flux density inside the superconductor as indicated in figure 1.2 .

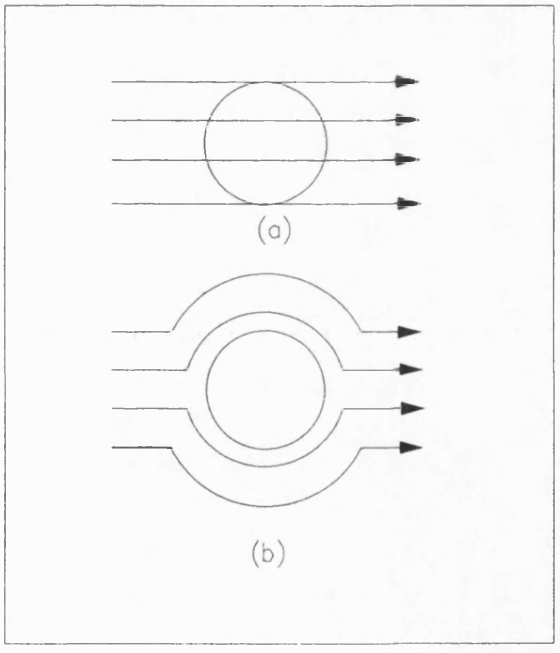

Fig.1.2 (a) Superconducting sample at $T>T_C$
(b) At $T<T_C$ the sample expels the magnetic flux

Two years later, the London brothers [3] [4] formulated the first phenomenolgical theory describing the properties of superfluid in the presence of electromagnetic fields and explained the Meissner effect. Subsequent major contribution in describing the phenomenology of the superconducting state were made by Ginzburg and Landau [5] and by Pippard [6].

1.4 Penetration depth and coherence length

1.4.1 Penetration depth

When a superconducting sample is in an applied magnetic field, the screening currents which circulate to cancel the flux inside the superconductor must flow within a very thin surface layer (current cannot be confined entirely to the surface otherwise the current density would be infinite, which is physically inconceivable). Consequently, the flux density does not fall abruptly to zero at the boundary of the superconductor but dies away within the region where the screening current are flowing. The thickness of the layer within which screening current can flow, and thus magnetic field can penetrate, is called the penetration depth λ . The variation of the magnetic field inside a thick superconductor is given by the following formula which is derived from the London equations .

$$B(x) = B_a \exp\left(-\frac{x}{\lambda}\right) \qquad (1.1)$$

B_a is the applied magnetic field, B(x) the magnetic field inside the superconductor and λ is the penetration depth . The curve B_a vs the distance x is shown in figure 1.3 . This figure was obtained using Nb penetration depth which is λ=90 nm .

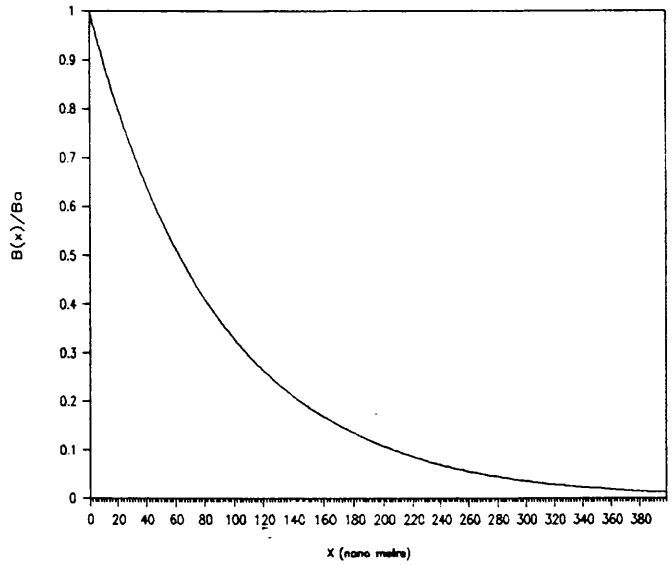

Fig. 1.3 Magnetic field attenuation as a function of the distance x inside the superconductor

The penetration depth is related to the superconducting electrons density n_s by the formula:

$$\lambda = \sqrt{\frac{m}{\mu n_s e^2}} \qquad (1.2)$$

where m is the mass of the electron, and e its electronic charge . The superconducting electron density varies with the temperature according to Gorter-Gasimir formula [7] :

$$n_s = n_0(1-t^4) \qquad (1.3)$$

where $t = T/T_C$ is the reduced temperature and n_0 is the maximum density at 0 K. Consequently the penetration depth varies with the temperature according to the equation:

$$\lambda(T) = \lambda(0)/\sqrt{(1-t^4)} \qquad (1.4)$$

where $\lambda(0)$ is the penetration depth at temperature T=0, as shown in figure 1.4.

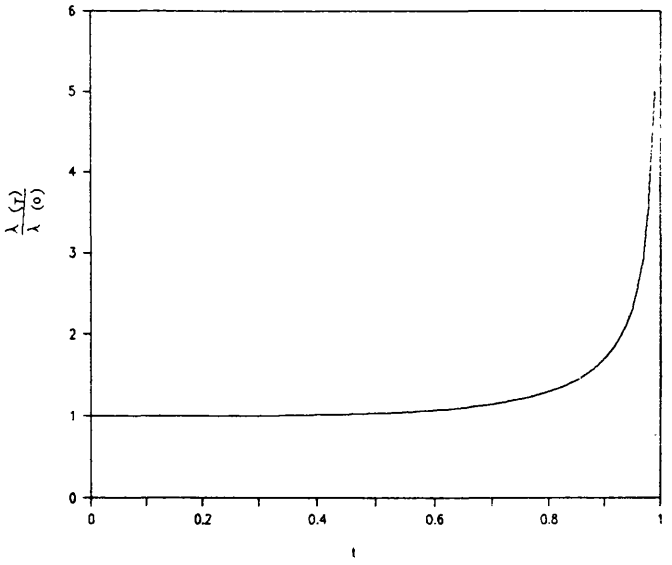

Fig.1.4 Penetration depth vs temperature.

For T just below T_C the above formula is replaced by:

$$\lambda(T) = \frac{1}{\sqrt{2}} \frac{\lambda(0)}{\sqrt{1-t}} \qquad (1.5)$$

1.4.2 Coherence length

The coherence length concept was first formulated by Pippard [8] who suggested that n_s cannot change rapidly with position, but can only change appreciably within a distance of the order of 10^{-6} m. It is this distance he called the coherence length ξ . From microwave surface impedance measurement he deduced that the coherence length of pure superconducting metals was reduced by the presence of impurities and suggested an empirical relation for it:

$$\frac{1}{\xi} = \frac{1}{\xi_0} + \frac{1}{\alpha l} \qquad (1.6)$$

where ξ_0 is the intrinsic coherence length, l is the electron mean free path, and α is a constant of the order of unity. The BCS theory gives the value :

$$\xi_0 = \frac{0.18 h v_F}{2\pi k_B T_c} \qquad (1.7)$$

where υ_F is the electron velocity at the Fermi surface. Like the penetration depth, the coherence length varies with the temperature as shown in figure 1.5 and this variation is given by the equation [5] :

$$\xi(T) = \frac{0.74}{\sqrt{1-t}}\xi_0 \qquad (1.8)$$

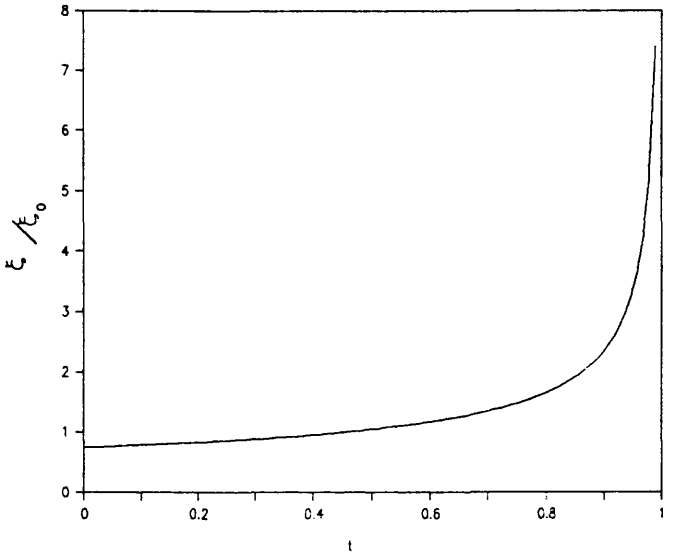

Fig.1.5 Coherence length vs temperature.

1.5 Different types of superconductors

According to their behaviour in a magnetic field, superconductors are divided in into two categories :type I and type II superconductors.

1.5.1 Type I superconductor

Type I superconductor is one that excludes magnetic field until superconductivity is destroyed completely. The value of magnetic field above which this transition occurs is called the critical field H_C for which the field enters completely the superconductor as shown in figure 1.6 .

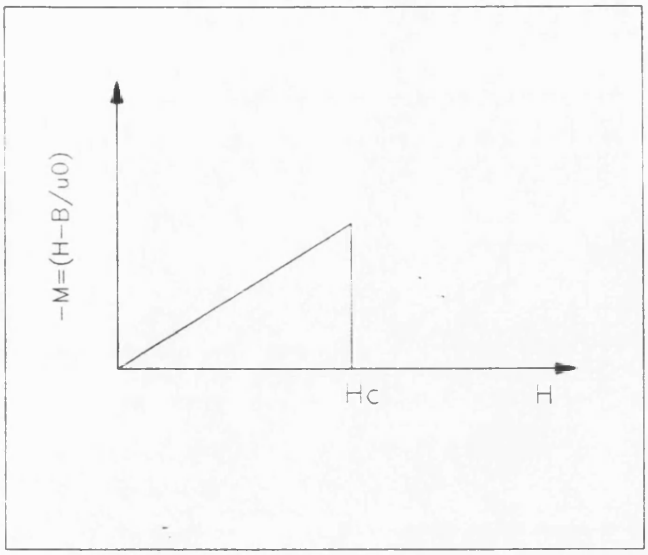

Fig.1.6 Magnetisation vs magnetic field of type I superconductor

H_C is temperature dependant and its relation with temperature is given by the formula :

$$H_c = H_0(1-t^2) \qquad (1.9)$$

where H_0 is the critical magnetic field at T=0 and t is the reduced temperature. The graph of $H_C(t)/H_0$ is shown in figure 1.7 .

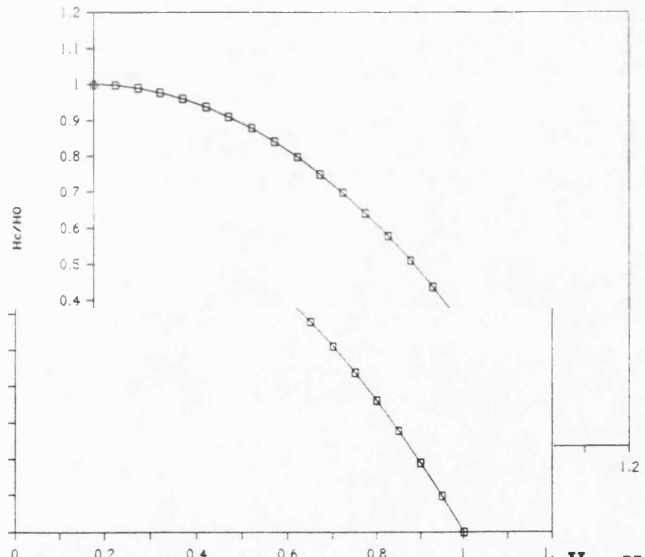

Fig.1.7 Critical magnetic field H_C vs the reduced temperature t

1.5.2 Type II superconductor

Type II superconductor excludes the field completely only for relatively weak field up to a value H_{c1}. Above H_{c1} the field is partially excluded but the specimen remains electrically superconducting. At higher field, the flux enters these superconductors completely and the superconductivity vanishes only after a second critical value H_{c2} is reached as indicated in the magnetisation M vs H curve which presented in figure 1.8 .

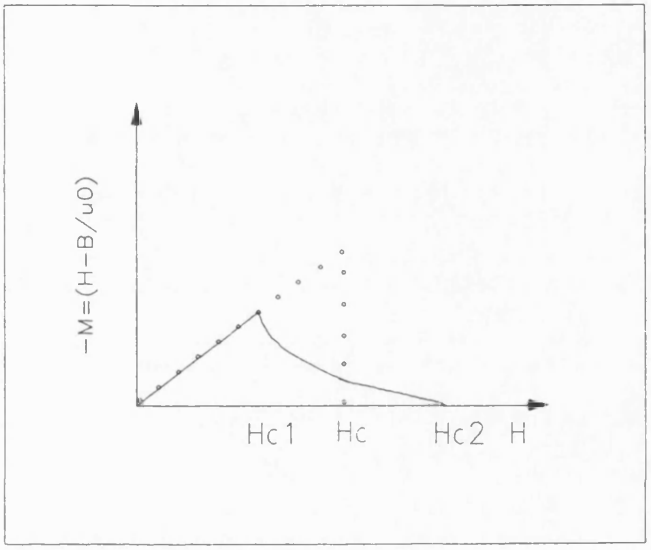

Fig.1.8 Magnetisation of type II supercondctors

Another way of differentiating between the two classes of supercondctors is the value of the Ginsburg-Landau constant K given by the equation :

$$K = \frac{\lambda}{\xi} \qquad (1.10)$$

For type I superconductor $K < \frac{1}{\sqrt{2}} = 0.71$

For type II superconductor $K > \frac{1}{\sqrt{2}} = 0.71$

1.6 Heat capacity of superconductors

The transition of a material from the normal state to a superconducting state causes a sharp and finite discontinuity in the specific heat as indicated in figure 1.9 where the specific heat of a typical superconductor, Nb, is presented .

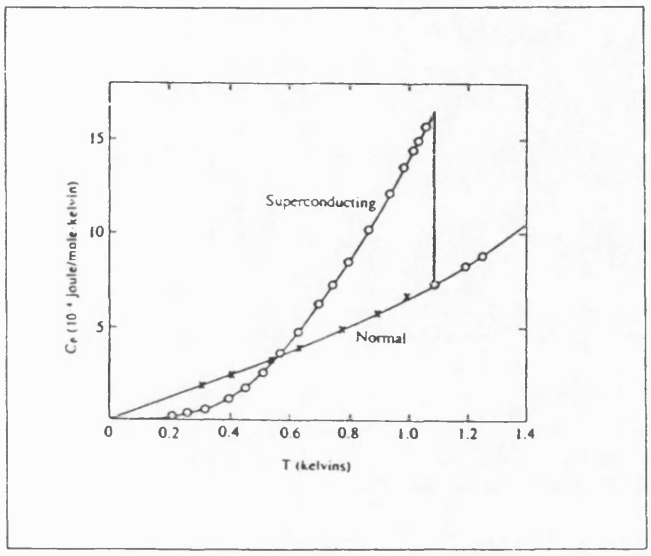

Fig.1.9 Specific heat of Nb vs temperature (ref [9])

At the time of the experiment there was no mathematical expression to fit the experimental curve.A few years later it was suggested that the electronic component of the specific heat varies exponentially with temperature [10] :

1.7 Low T_c superconductivity microscopic theory

The first successful microscopic theory of superconductivity was developed by Bardeen, Cooper and Schrieffer (BCS) [11]. This theory shows that unlike the normal conduction process involving single electrons whose repeated collision with the lattice are responsible for resistance of the metals the constituents of the supercurrent are pairs of weakly bound electrons, Cooper pairs, which do not collide with the atoms of the lattice. The absence of collision between the cooper pairs and the host lattice accounts for the zero resistance of the superconductor. The BCS theory involves a detailed

quantum mechanical analysis which is not required in this thesis. However the qualitative features of energy gap and pair conduction will be briefly discussed .

1.7.1 The energy gap

The bonding force between the electrons in a cooper pair is due to an interaction with the lattice. The negative charge on each of the electrons attracts the local positively charged metal ions and the lattice undergoes a slight distortion, thereby creating a region of enhanced positive charge which attracts the other electron. In terms of quantum mechanical language this attraction develops through the exchange of virtual phonon between electrons having opposite spin and opposily directed momentum . The formation of these pairs lowers the energy of the system below the Fermi level hence creating a gap Δ in the electronic excitation spectrum E of the superconductor as indicated in figure 1.10 (a) . The excitation energy of a normal metal does not possess a gap and is as indicated in figure 1.10 (b) .

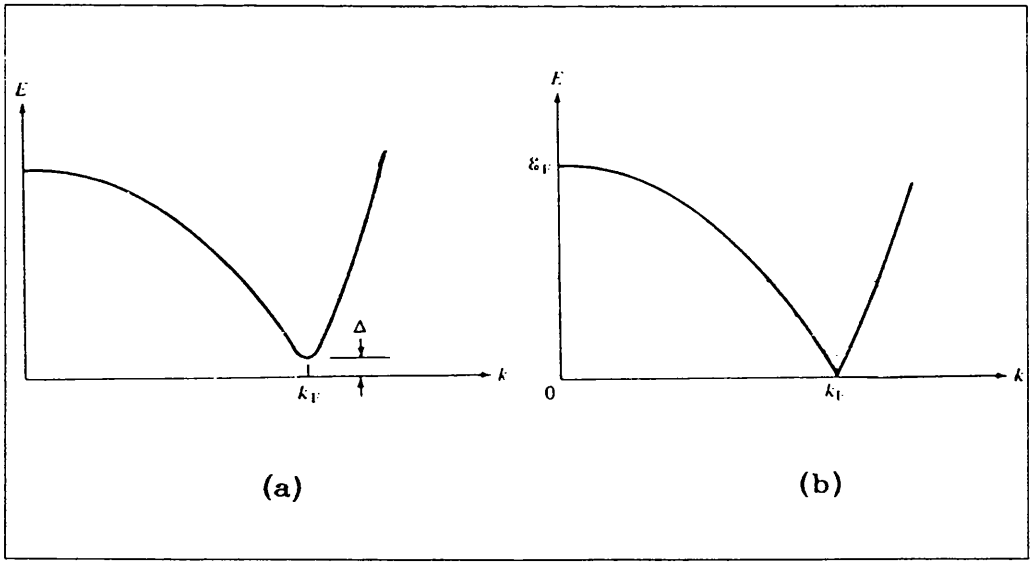

Fig.1.10 Excitation energy of a superconductor

The excitation energy E of a superconductor is related to the energy gap Δ and the free electron energy ϵ referred to the Fermi level, E_F , by the relation [11] :

$$E = \sqrt{\epsilon^2 + \Delta^2} \qquad (1.11)$$

and the density of excitation states of a superconductor is given by the approximate relation [11] :

$$N_s = \frac{N_N(0)E}{\sqrt{E^2 - \Delta^2}} \qquad (1.12)$$

where $N_N(0)$ is the normal-state density of states at the Fermi energy. This latter expression is usually plotted in a semiconductor-like representation which is indicated in figure 1.11.

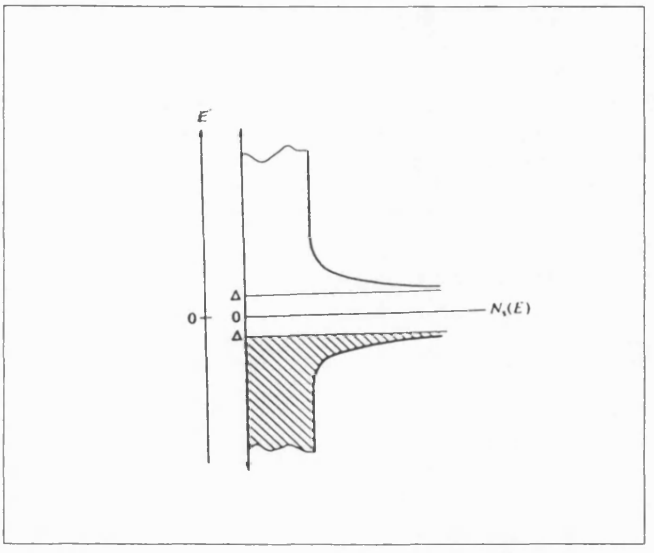

Fig.1.11 Density of state resulting from the BCS theory.

The energy gap varies with the temperature :

- at T= 0 the energy gap $\Delta(0)$ is related to T_C by [11] :

$$2\Delta(0) = 3.52 k_B T_c \qquad (1.13)$$

- For temperatures between 0 K and $T_C/2$, $\Delta(T) \sim \Delta(0)$

- For temperatures close to T_C, the dependance of $\Delta(T)$ on the temperature is approximated by [12]:

$$\frac{\Delta(T)}{\Delta(0)} = 1.74\sqrt{1 - \frac{T}{T_c}} \qquad (1.14)$$

This latter expression is plotted against the temperature and is shown in Fig.1.12 .

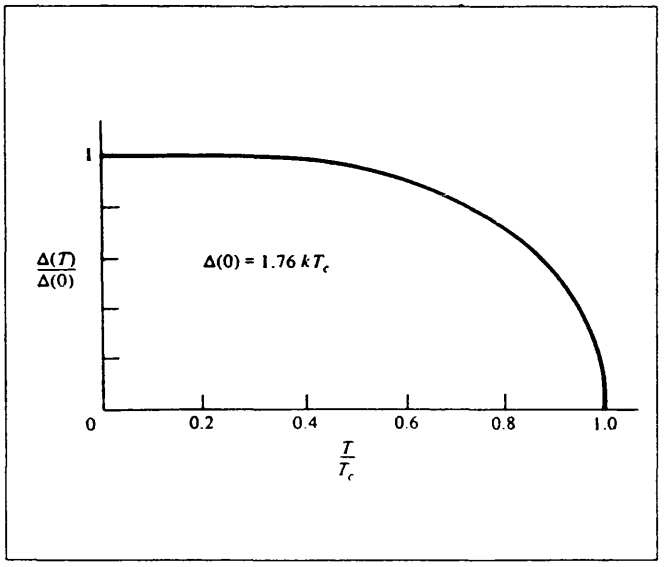

Fig.1.12 Energy gap vs normalized Temperature T/T_C

Numerically $2\Delta(0)$ is of the order of 10^{-4} eV. This gap (or binding energy as it is referred to sometimes) is so low that separation is easily caused by thermal fluctuation of electrons. That is why conventional superconductivity is usually only observed at cryogenic temperatures. For the same reasons it can be destroyed by an excessive magnetic field or by too large a current. In addition this weak attractive force by which the pairs are held together implies that pairs electrons are a large distance apart roughly 1 microns in typical low T_C superconductors . This size is large compared to the mean distance between two conduction electrons which of the order of 0.1 nm . Therefor Each cooper pair coexists in its own volume with a large number of electrons (10^6 to 10^7) which are themselves correlted into pairs [13] [14] . Thus there exist a large overlap in every pair volume in the superconductor. This then requires that the phase of the wave functions should be locked together over a microscopic length scale. This microscopic phase coherence which forces different points in a superconductor

to have a built-in phase relation is the fundamental feature of the superconducting state. It follows then that :

* Firstly a superconductor, which is in principle a many body system ,can be represented by the "single particle "wave function i.e:

$$\psi = |\psi| \exp(i\phi) \qquad (1.15)$$

Where the phase ϕ may be a function of position and $n_s = |\psi|^2$ is the density of pairs of effective charge 2e and masse 2m where e and m are respectively the charge and mass of the electron .

* Secondly it is extraordinarily difficult for such a macroscopic quantum state to be scattered by the microscopic impurities and defects which lead to resistance in normal metal.

Thus the BCS theory provides a mechanism which explains one important aspect of superconductivity namely the absence of resistance. In fact it accounts for all the parameters and properties of low T_C superconductors.

Chapter 1 references

1 H. K. Onnes, Akad Van, Wetenschapen (Amesterdam). Vol.14 pp 113,818,1911.
See also selected reprints of "Superconductivity".New York:American Institute of Physics 1964.

2 W.Meissner and R.Ochsenfeld "Ein Neuer effect bei eintritt der supraleitfatugkeit ",Nautrwissensschften vol.21,pp:787-788, 1933.

3 F.London and H.London, " Electromagnetic equations of the superconductor", Proc. Roy. Soc. A149, pp:71-88, 1935.

4 F.London and H.London, Physica 2, p.341, 1935.

5 V.L.Ginzburg and L.D.Landau, Zh. Eksp. Teor. Fiz.20, p.1064, 1950.

6 A.B. Pippard, " An experimental and theoritical study of the relation between magnetic field and current in a superconductor", Proc. Roy. Soc. A216, pp:547-568, 1953.

7 C. J. Gorter and H. B. G. Casmir 1934 according to:
A. B. Pippard "early supsuperconductivity Research ",IEEE Trans. Magn. Vol. MAG-23 ,pp: 371-375, 1987.

8 A.B. Pippard, Physica 19,765 (1953)

9 A. Brown, M.W. Zemansky, and H.A. Boorse, " The superconducting and normal heat capacities of Niobium", Phys. Rev. 92, p:52-58, 1953.

10 J. S. Blakemore "The superconducting state " in "solid state physics", 2nd edition , edited by W. B. Saunders Company 1974

11 J.Bardeen, L.N.Cooper and J.R Shrieffer ,Phys.Rev. 108, 1175 (1957).

12 M. Thinkham , " Intoduction to superconductivity ", Edited by McGraw-Hill , 1975 .

13 T. van Duzer, C. W. Turner ,"Principle of superconductive devices and circuits" , edited by Edward Arnold, London, 1881.

14 W. Buckel " Superconductivity, fundamental and applications", edited by VCH , FRG, 1991 .

CHAPTER 2: SUPERCONDUCTING TUNNELLING DEVICES

2.1 Introduction

Superconductivity and tunnelling became closely related topics when superconductor tunnel junctions appeared in the early sixties. Since then superconductive tunnelling has became a very useful tool for investigating certain fundamental properties such as the measurement of energy gaps. In addition the nonlinearity of the tunnelling characteristic of the superconductor tunnel junction found important applications in certain type of novel electronic devices. In this chapter general tunnelling concepts will be considered followed by a discussion on tunnelling in the most important superconducting tunnelling devices for microwave applications. In addition the electrical and physical properties of these junctions will be presented .

2.2 Elements of tunnelling

Consider two metallic plates separated by a thin vacuum gap of width w as shown in figure 2.1 .

When the distance $w \leq 100$ Å and a dc voltage is applied to them a current can flow between them which rises exponentially with decreasing w [1] . This current is due to a quantum mechanical phenomenon known as tunnelling . The origin of this can be understood by studying the one dimensional square barrier model indicated in figure 2.2

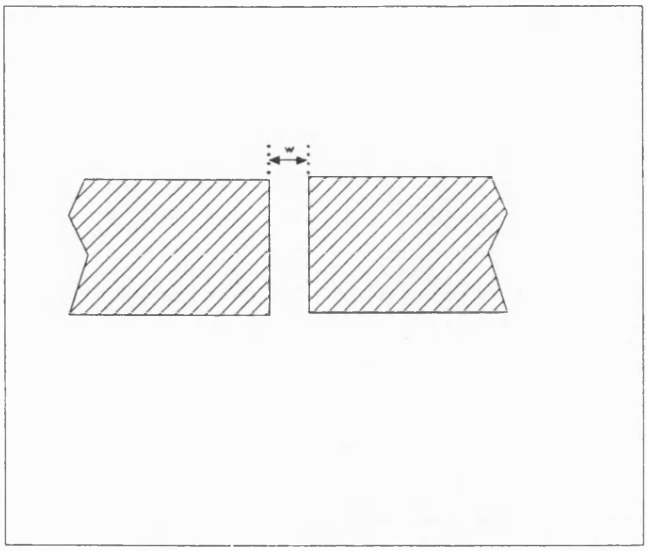

Fig.2.1 Schematic representation of two metal plates separated by a thin vacuum gap of width w

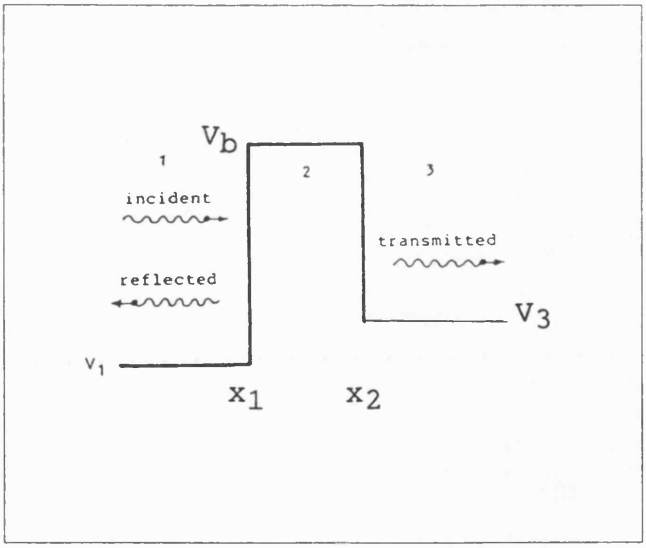

Fig.2.2 One dimensional abrupt potential barrier

The diagram is divided in three regions. The barrier has a potential height V_b and a width w. An electron having a kinetic energy E (in zero potential) is incident from the left onto the potential barrier. The probability of appearance of the electron at the right hand side of the barrier can be calculated using the time independent Schrodinger equation (2.1) and the boundary conditions on ψ at $x=x_1$ and $x=x_2$ as specified in figure 2.2 .

$$\left[-\frac{\hbar^2}{2m}\nabla^2+V\right]\psi=E\psi \qquad (2.1)$$

In region 1 the potential $V=V_1=0$ and $E-V>0$. Thus the solution of Schrodinger equation has the form :

$$\psi_1=A_1\exp(ik_1x)+B_2\exp(-ik_1x) \qquad (2.2)$$

with $\frac{\hbar^2k_1^2}{2m}=E$ and A_1 and B_1 constants.

In region 2 $V=V_b$ and $E-V<0$ then the solution becomes :

$$\psi_2=A_2\exp(\kappa_2x)+B_2\exp(-\kappa_2x) \qquad (2.3)$$

where $\kappa_2=\frac{2m}{\hbar}(V_b-E)$ and A_2 and B_2 are constants.

In region 3 $V=V_3$ and $E-V>0$ then the solution is

$$\psi_3=A_3\exp(ik_3x) \qquad (2.4)$$

with $\frac{\hbar^2k_3^2}{2m}=E-V_3$ and A_3 is a constant (in region 3 there is no reflected wave and hence $B_3=0$).

The constants A_i, B_i (with i=1, 2, 3) which appear in equations (2.2), (2.3), and (2.4) are determined using the continuity of both ψ and $\frac{d\psi}{dx}$ at $x=x_1$ and $x=x_2$. These matching conditions can be conveniently calculated using a 2x2 matrix and are carried out in Appendix A1 where the following results are obtained:

$$\left|\frac{A_3}{A_1}\right| = \frac{4k_1\kappa_2}{\sqrt{(k_1^2+\kappa_2^2)(k_3^2+\kappa_2^2)}}\exp(-\kappa_2 w) \qquad (2.5)$$

where w= x_2-x_1 . The ratio of current density is :

$$\frac{J_3}{J_1} = \frac{k_3}{k_1}\left|\frac{A_3}{A_1}\right| = \frac{16k_1k_3\kappa_2^2}{(k_1^2+\kappa_2^2)(k_3^2+\kappa_2^2)}\exp(-2\kappa_2 w) \qquad (2.6)$$

This equation is dominated by the exponential factor $\exp(-2\kappa_2 w)$ (the barrier penetration factor) and shows that if w increases the current decreases exponentially. This attenuation is as shown in figure 2.3

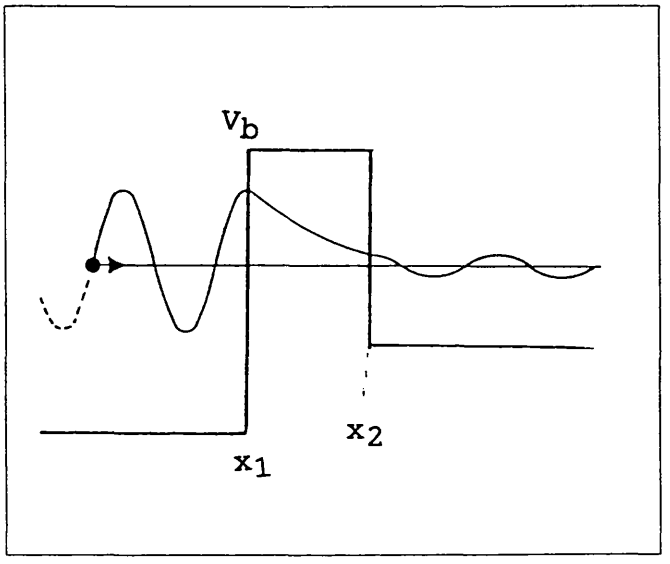

Fig.2.3 Quantum mechanical tunnelling process through an abrupt potential barrier.

The above calculation shows that the separation between conductors should be less than ~ 100 Å and ideally ~ 50 Å in order to observe a substantial tunnelling current. In practice this is very difficult to achieve because of the inherent roughness of material surfaces . A more convenient method for observing quantum mechanical tunnelling is the use of evaporated films whereby the metallic electrodes are separated by an insulating layer whose

thickness can be of the order of 20 Å . This insulating layer is usually an oxide resulting from exposure to air of the first metal surface prior to the evaporation of the second metal. Such a structure is called a metal-insulator-metal (MIM) junction and its fabrication procedure is discussed in the next section.

2.3 Fabrication of MIM junctions and Superconductor tunnel junctions

Both the MIM junction and the superconductor tunnel junction are fabricated using the procedure depicted in figure 2.4 [2] [3].

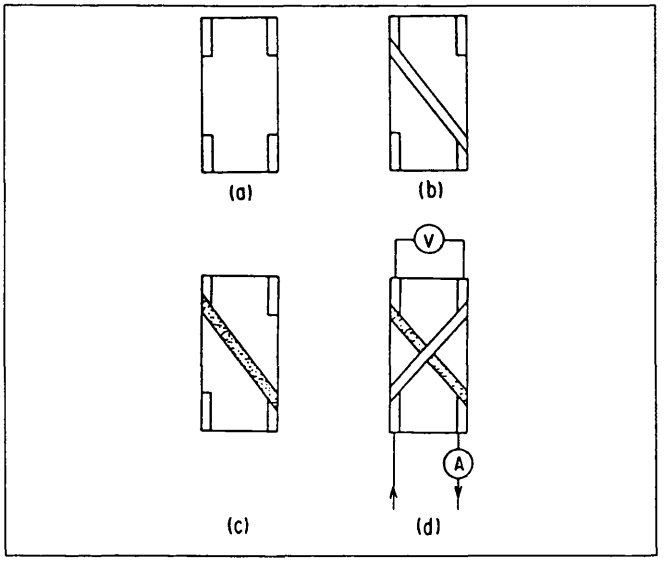

Fig.2.4 Fabrication procedure of a MIM junction

Firstly a glass slide or other suitable substrate is prepared by forming four Indium contacts one in each corner. An Aluminium strip is then evaporated as shown in figure 2.4(b). The strip is left to oxidize in air for the time required for the formation of the insulating layer (figure 2.4 (c)). Finally a second strip of Al or

a different metal like Pb is evaporated across the previous oxidised layer (figure 2.4 (d)). The result is a three layer device as shown in figure 2.5 .

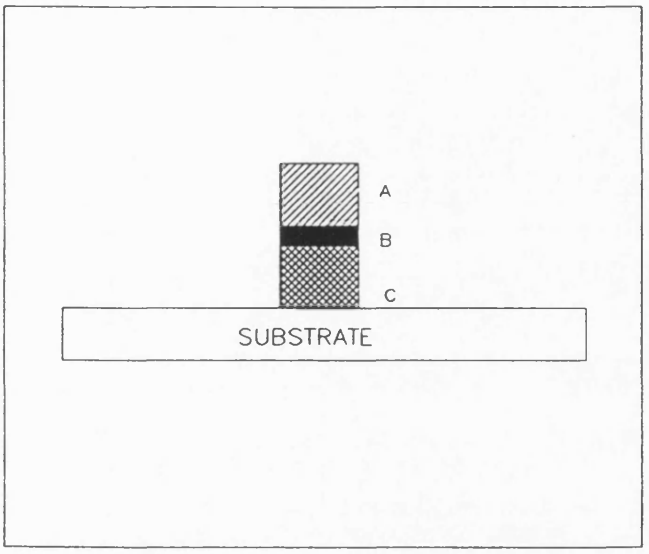

Fig.2.5 Schematic presentation of a three layer device

For temperatures above the critical temperature T_c of both layers A and C, the device is a MIM junction . In the case of a superconducting tunnel junction one of the outer layers, (A) for instance, is always a superconductor . The middle one (B) is an insulator whose thickness should be less than 40 Å (ideally 10 to 20 Å) if one is to observe a tunnelling current [3] [4] [5] . Depending on whether the third layer (C) is a normal metal (referred to by N) or a superconductor (referred to by S), the resulting devices are respectively called SIN or SIS junctions. The first superconductor tunnel junctions were fabricated using the process described above. There is another superconductor tunnel junction which is widely used in microwave applications that is the super Schottky diode. Although it is a two layer device, a superconductor and a semiconductor, its behaviour is very similar to that of the SIN junction.

2.4 Tunnelling process in Metal-Insulator-Metal junction

Tunnelling between normal metals is a good introduction to tunnelling in superconductors. Many aspects of tunnelling are best described using energy level diagrams . For The MIM junction the energy level diagram is shown in figure 2.6 [6] .

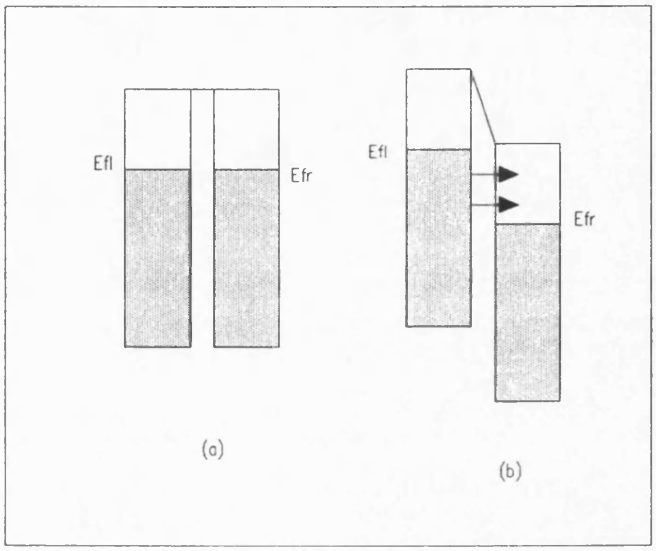

Fig.2.6 (a) energy band structure of a MIM junction
(b) A bias voltage is applied to the structure

There are two conditions which must be fulfilled for tunnelling to take place, apart from the obvious one that the separation w must not be too large as discussed previously. Firstly, energy must be conserved in the tunnelling process i.e: the total energy of the system including the two metals on both sides of the insulating film must be the same before and after tunnelling. Secondly, tunnelling can take place only if the states into which electrons are going to tunnel are empty, otherwise the process is forbidden by the Pauli principle. This is illustrated in figure 2.6(a) where the metals, separated by the insulators, are assumed to be at absolute zero. Here there could be no tunnelling

possible because the states which satisfy the first condition are occupied on both sides. However in figure 2.6 (b), the junction is biased by a voltage V_a positive on the right electrode. The biasing voltage causes the Fermi energy levels E_{FL} and E_{FR} to shift with respect to each other and thus creates empty states on the right opposite to occupied ones on the left. Both conditions are now satisfied and tunnelling can take place from left to right as indicated by the arrows. This discussion can be used to obtain a heuristic derivation of the IV curve of the MIM junction. This is achieved by making the assumption that the number of electrons which will tunnel from left to right in an interval of energy dE is proportional to the number of occupied states on the left and is given by:

$$N_L(E-eV)f(E-eV)dE \qquad (2.7)$$

where N_L is the density of states on the left side and f is the Fermi distribution . The energy E is measured from the Fermi level on the right. Because of the Pauli principle the electrons cannot move to the right unless there are unoccupied states and hence the current must be proportional to:

$$N_R(E)(1-f(E)) \qquad (2.8)$$

The flow of electrons from left to right is also proportional to the probability of transition across the barrier $P_{LR}(E)$. The proportionality of the current to these parameters can be used to write the expression of the current flowing from left to right I_{LR} as follow:

$$I_{LR} \propto P_{LR} N_L(E-eV)f(E-eV)N_R(E)(1-f(E))dE \qquad (2.9)$$

Following similar arguments, the current flowing from right to left can be written I_{RL}

$$I_{RL} \propto P_{RL} N_L(E-eV)(1-f(E-eV))N_R(E)f(E)dE \qquad (2.10)$$

By assuming that $P_{RL}=P_{LR}$ and integrating over the energy the net current can be written

$$I = I_{LR} - I_{RL} \propto \int_{-\infty}^{+\infty} P_{LR} N_L(E-eV) N_R(E)[f(E-eV)-f(E)]dE \quad (2.11)$$

A further assumption that is usually made is to consider $P_{LR}(E)$ as constant and take it out of the integral. For small voltages the density of states do not vary significantly and can be considered to be constant and equal to their values at Fermi level ie: $N_L(E-eV)=N_L(E)=N_L(0)$ and also $N_R(E)=N_R(0)$. After applying these approximations equation (2.11) becomes :

$$I = AN_L(0)N_R(0)\int_{-\infty}^{+\infty}[f(E-eV)-f(E)]dE \quad (2.12)$$

where A is constant of proportionality.

For small voltages f(E-eV)-f(E) can be replaced by the following equation

$$f(E-eV)-f(E) = -eV\frac{df}{dE} \quad (2.13)$$

At temperatures approaching zero -df/dE can be replaced by a delta function and thus the expression for the current I becomes:

$$I = G_{NN}V \quad (2.14)$$

where the conductivity is expressed by:

$$G_{NN} = AN_L(0)N_R(0)e \quad (2.15)$$

Equation (2.14) shows that at low voltages the current is linear with the voltage. However when the voltage is no longer small, the current is no longer proportional to the voltage and the tunnelling IV characteristic becomes non linear as illustrated in figure 2.7 [7].

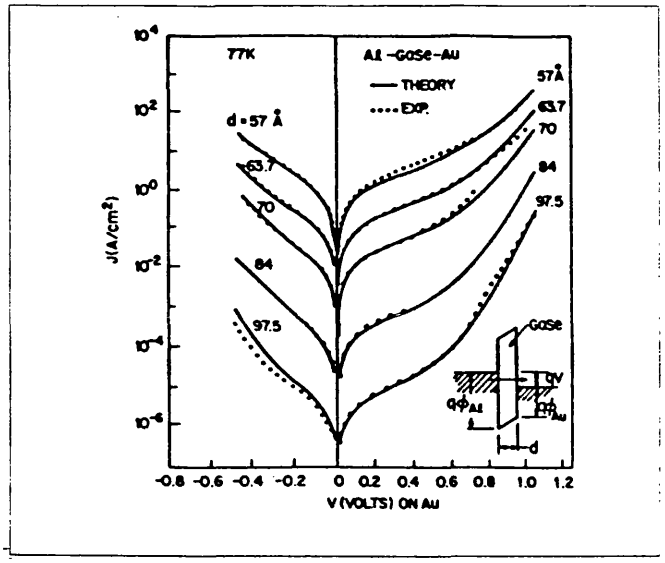

Fig. 2.7 I-V characteristic of a MIM (Al-GeSe-Au) junction at 77 K (from ref. [7])

A more detailed calculation of tunnelling current through a MIM junction has been carried out elsewhere [8] .

2.4.1 Normal metal electrons and superconductor quasiparticles

In a normal metal the electrons are independent of each other so that the energy of one electron is not affected by whether or not another level happens to be occupied . In a superconductor this is no longer true : the contribution of each electron to the total energy depends on whether it has a partner with equal and opposite momentum . This difference was expressed in models such as "the two fluids model "(one fluid electrons and the other electron pairs) [9] and the "holes and quasiparticles model" [10] .

2.5 Energy level diagram of a superconductor

In order to represent the energy level diagram of a superconductor three different diagrams have been suggested by different authors.

Firstly the representation which uses the excitation energy

or energy-momentum diagram [11] which was presented in chapter 1, figure 1.10 . Using this diagram an SIS junction formed by two different superconductors characterised by their different energy gaps Δ_1 and Δ_2 for instance is as shown in figure 2.8 .

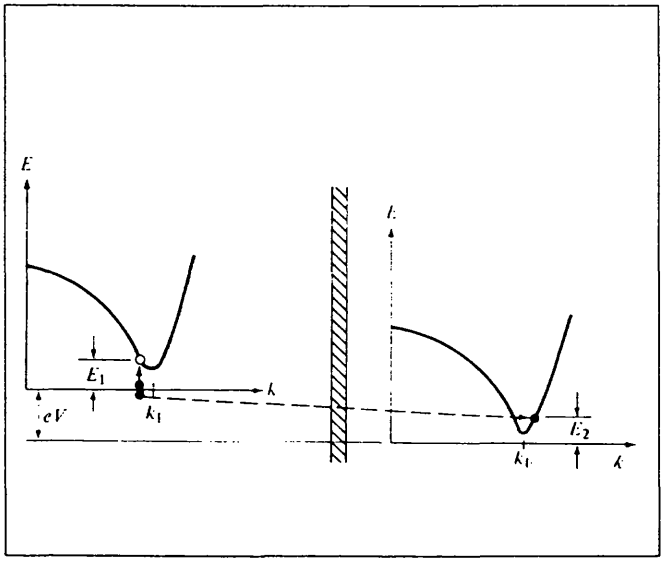

Fig.2.8 Energy momentum representation of SIS junction at a bias voltage eV=Δ_2+Δ_1

In this diagram (figure 2.8) the bias voltage causes a pair to split into two quasiparticles , one moves to the continuum on the left and the other tunnels to the continuum on the right . The use of this representation becomes complicated if the two branch of the excitation spectrum below and above K_F are considered as discussed elsewhere [12] .

A second presentation uses the analogy between super-conductors and semiconductors in that they both posses an energy gap. This has led to a semiconductor-like representation [2] [3] [4] . Using this representation the diagram of an SIS junction is as indicated in figure 2.9 .

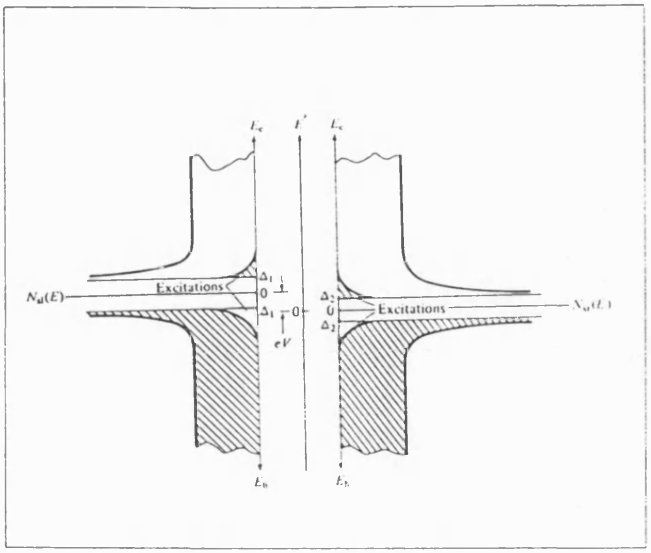

Fig.2.9 Semiconductor representation of SIS Junction

The weakness of this model is that the condensate level of pairs is not represented. In addition it has been found that it fails to account for the excess current due to pairs tunnelling [13] .

In view of the complexity of the first diagram (figure 2.8) and the shortcoming of the second (figure 2.9), a third idea has been suggested by Adkins [14] [15] . It can be thought of as a simplified version of the first diagram and is referred as the Adkins representation. In this representation the condensate energy level and the lower limit of the continuum of energies are depicted by two lines separated by Δ (the average energy per electron which is one half of the energy of a cooper pair) as shown in figure 2.10 .

The pairs are shown as two joint circles and electrons by single circles. This representation is to be compared to the case of a normal metal or a semiconductor where the energy band diagram represent the range of energies allowed to one single electron. At absolute zero temperature all

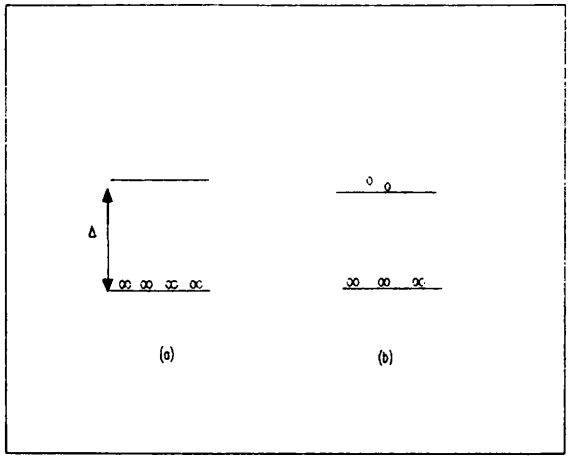

Fig.2.10 Energy level diagram of a superconductor using Adkins representation
(a) At T=0, (b) At 0< T <T_c

the continuum states are empty and all the Cooper are grouped in one single energy level as shown in figure 2.10 (a). At temperature between zero and T_c some pairs are split and the resulting quasiparticles promoted to the continuum states as indicated in figure 2.10 (b) .

Using this final representation the energy level diagram of SIS junction is as indicated in figure 2.11 . It is this represntation which will be adopted in the next sections for the discussion of tunnelling in superconducting tunnel junction.

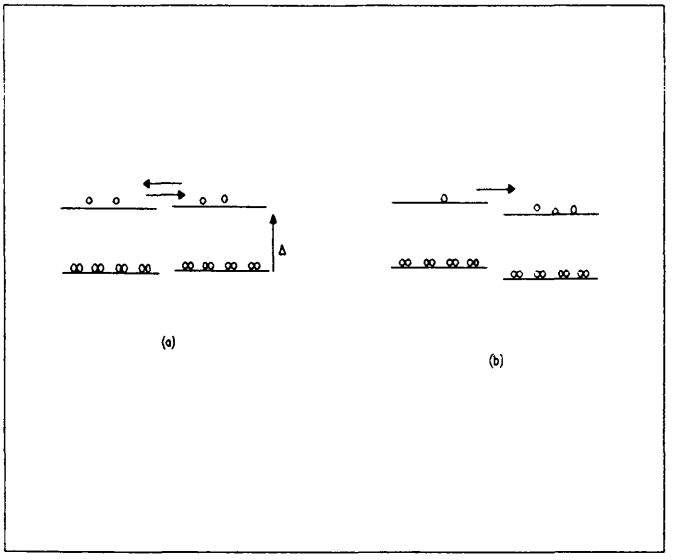

Fig.2.11 Adkins Representation of SIS junction at T≠ 0
(a) no biasing voltage applied
(b) a biasing voltage is applied

2.6 SIN junction tunnelling

The energy band diagram of an SIN junction is as indicated in figure 2.12 .

In the absence of any applied voltage the Fermi level E_F of the normal metal coincides with the level representing the condensed pairs in the superconductor and no tunnelling is possible as shown in figure 2.12 (a).
When a positive voltage V_a is applied to the superconductor side the condensed state and the Fermi level are shifted relatively to each other by an interval eV_a but no tunnelling is possible until V_a reaches the value $+\frac{\Delta}{e}$ where the bottom of the continuum of quasiparticles levels coincide with the Fermi levels of the normal metal as indicated in figure 2.12 (b). It now becomes possible for electrons in the normal metal to tunnel into empty quasiparticles states of the superconductor and the current flowing through the junction rises sharply. If the superconducting side is

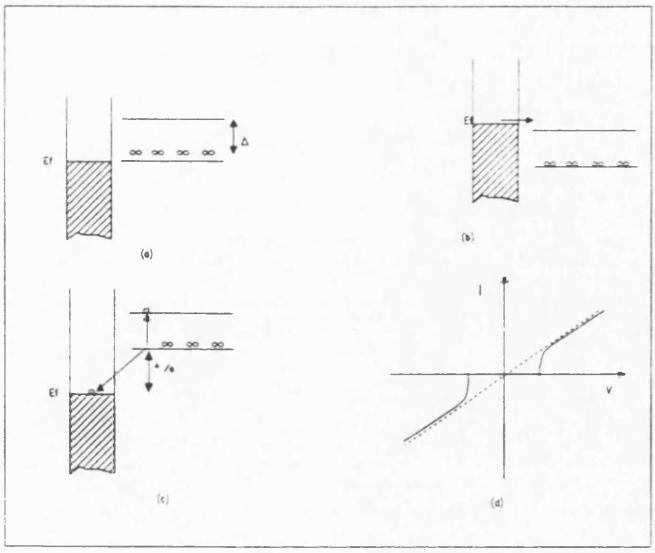

Fig.2.12 SIN junction at T=0 and different biasing voltages
(a) $V_a=0$, (b) $V_a=+\frac{\Delta}{e}$, (c) $V_a=-\frac{\Delta}{e}$,
(d) IV characteristic of SIN junction at T=0

negatively biased relatively to the normal metal, no tunnelling occurs until V_a reaches $-\frac{\Delta}{e}$ .In this position one of the single electrons resulting from a pair can tunnel to the states just above the Fermi level of the normal metal by loosing $-\frac{\Delta}{e}$ energy . The second electron can reach the continuum by gaining $+\frac{\Delta}{e}$ energy as indicated in figure 2.12(c) . It is by the means of this process which conserves the energy of the system that the tunnelling is allowed. If V_a increases or decreases beyond $+\frac{\Delta}{e}$ or $-\frac{\Delta}{e}$ respectively, the current becomes more and more linear while it approaches the dashed line of the normal conduction as indicated in figure 2.12(d). For the SIN junction the dependence of the current I on the voltage V ie the I(V) function is similar to that of MIM junction as expressed by equation (2.11) and is given by the formula [4] [13]:

$$I_{SN} = \frac{2\pi eA}{\hbar}\int_{-\infty}^{+\infty} |T|^2 N_N(E-eV)N_S(E)[f(E-eV)-f(E)]dE \quad (2.16)$$

where N_N is the density of state of the normal metal on the left, N_S is that of the superconductor as expressed in equation (1.12), and $|T|^2$ the tunnelling matrix element. By substituting N_S by its expression of equation (1.12), one obtains:

$$I_{SN} = \frac{2\pi eA}{\hbar}N_L(0)N_R(0)|T|^2\int_{-\infty}^{+\infty}\frac{E}{(E^2-\Delta^2)^{1/2}}[f(E-eV)-f(E)]dE \quad (2.17)$$

where $N_L(0)$ and $N_R(0)$ are as defined in equation (2.12).

At T=0 we have the following approximations :

(f(E-eV)-f(E)) =1 for 0<E<eV

(f(E-eV)-f(E)) =0 for E<0 and E>0

giving I_{SN}=0 for eV<Δ.

For Δ <E < eV I_{SN} is given by :

$$I_{SN} = \frac{2\pi eA}{\hbar}N_L(0)N_R(0)|T|^2\int_{\Delta}^{eV}\frac{E}{(E^2-\Delta^2)^{1/2}}dE \quad (2.18)$$

Using $G_{NN} = \frac{2\pi e^2 A}{\hbar}N_L(0)N_R(0)|T|^2$

and inergrating equation (2.18) one obtains :

$$I_{SN} = \frac{G_{NN}}{e}[(eV)^2-\Delta^2]^{1/2} \quad (2.19)$$

For $T \neq 0$ equation (2.17) becomes:

$$I_{NS} = 2G_{NN}\frac{\Delta}{e}\sum_{m=0}^{\infty}(-1)^{m+1}K_1\left(\frac{m\Delta}{K_BT}\right)\sinh\left(\frac{meV}{K_BT}\right) \quad (2.20)$$

and when $V \to 0$ this becomes

$$\lim_{V\to 0} I_{NS} = 2G_{NN}\frac{V\Delta}{K_BT}\sum_{m=0}^{\infty}(-1)^{m+1}mK_1\left(\frac{m\Delta}{K_BT}\right) \quad (2.21)$$

when $T \to 0$ this equation reduces to :

$$\lim_{\substack{V\to 0\\ T\to 0}} I_{NS} = I_{NN}\left(\frac{2\pi\Delta}{K_B T}\right)^{1/2} \exp(-\Delta/K_B T) \qquad (2.22)$$

2.7 SIS junction tunnelling

2.7.1 SIS junction with identical superconductors

The junction is considered to be at a temperature $0<T<T_c$ which is always the case in practice as absolute zero temperature is impossible to achieve. The energy level diagrams are as shown in figure 2.13 with various biasing voltages .

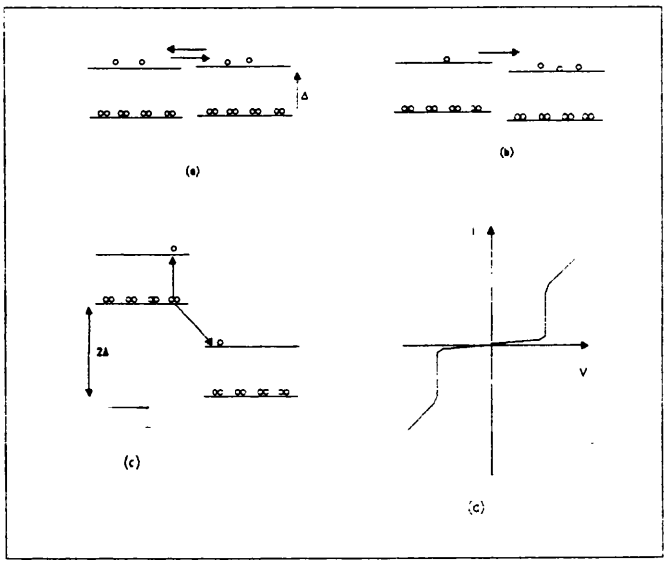

Fig.2.13 SIS junction at $0<T<T_c$ with different biasing voltages
(a) $V_a=0$, (b) $0<V_a<2\frac{\Delta}{e}$, (c) $V_a=2\frac{\Delta}{e}$,
(d) IV characteristic of SIS junction

The quasiparticle states are occupied on either side and thus it is possible for quasiparticles to tunnel in either direction as indicated by the arrows in figure 2.13 (a). At $V_a=0$ the numbers of quasiparticles tunnelling in opposite

direction are equal and no net current flows. When the right side is positively biased relatively to the left side, the energy levels are shifted allowing more quasiparticles to tunnel from left to right as shown in figure 2.13 (b) and hence a net small current flows through the junction and continues to increase proportionally to V_a until all the occupied states on the right face empty states under the bottom of the continuum on the left . This situation is reached when $Va = K_B T/e$. If V_a is increased further the current remains more or less constant because it is due to tunnelling of the left side quasiparticles alone whose number is constant. When V_a reaches the value of $\frac{2\Delta}{e}$ an additional process involving the splitting up of pairs is launched resulting in the tunnelling of one quasiparticle to the lowest quasiparticle state on the right and the transition of the other to the lowest quasiparticle state on the left. As the number of splitting pairs is large, the net tunnelling current rises sharply. Once again if the voltage V_a continues to increase, the current increases rapidly and soon reaches a critical value I_c beyond which the material looses its superconducting phase and regains its normal behaviour in which the current approaches the normal conduction curve whose slope is $\frac{1}{R_N}$ with R_N the normal state resistance of the junction. The corner occurring at $V_a = \frac{2\Delta}{e}$ is the strongest known nonlinearity in nature. The dc I-V curve is given by the formula:

$$I_{ss} = \frac{G_{NN}}{e} \int_{-\infty}^{+\infty} \frac{|E|}{(E^2-\Delta^2)^{1/2}} \frac{|E-eV|}{[(E-eV)^2-\Delta^2]^{1/2}} [f(E-eV)-f(E)]dE \quad (2.23)$$

When the temperature T=0 I_{SS} is given by :

$$I_{ss} = 0 \text{ if } V < 2\Delta/e \quad (2.24)$$

and when $V \geq 2\Delta/e$ I_{SS} is given by:

$$I_{SS} = \frac{G_{NN}}{e}\left[(2\Delta + eV)E(\alpha) - \frac{4\Delta(\Delta + eV)}{2\Delta + eV}K(\alpha)\right] \qquad (2.25)$$

where $\alpha = (eV - 2\Delta)/(eV + 2\Delta)$. Both $K(\alpha)$ and $E(\alpha)$ are complete elliptic integrals [16] .

2.7.2 SIS tunnel junction with different superconductors

The energy bands of an SIS junction made of two different superconductors are characterised by two energy gaps Δ_1 and Δ_2. Assume $\Delta_1 > \Delta_2$ as indicated in figure 2.14.

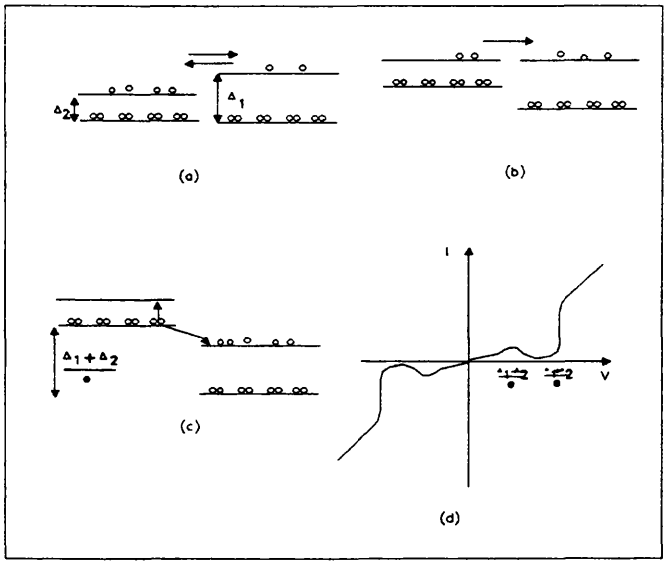

Fig.2.14 SIS junction made from different energy gap superconductors at $0<T<T_c$ and different biasing voltages
(a) $V_a=0$, (b) $0<V_a<\frac{\Delta_1-\Delta_2}{e}$; (c) $V_a=\frac{\Delta_1+\Delta_2}{e}$,
(d) IV characteristic of SIS junction $\Delta_1 \neq \Delta_2$

When $V_a=0$ thermal excited quasiparticles can tunnel to either side in equal number but opposite directions and thus no net current is observed as indicated in figure 2.14 (a). When V_a increases with the right side positively biased

relative to the left side, the number of quasiparticles tunnelling from left to right increases almost exponentially and reaches its maximum for $V_a = \frac{\Delta_1 - \Delta_2}{e}$ as shown in figure 2.14(b). In this position the gap edges are lined up with one another . Since the density of states at the gap edge is very large (infinite in BCS model as was shown in figure 1.11) in both sides , this causes the tunnelling current at the bias of figure 2.14(b) to be larger than for bias voltages less than or greater than $V_a = \frac{\Delta_1 - \Delta_2}{e}$. When V_a is increased further, the maximum of the density of states are no longer lined up, therefore the current decreases and reaches its minimum when V_a approaches $\frac{\Delta_1 + \Delta_2}{e}$. When $Va = \frac{\Delta_1 + \Delta_2}{e}$ the condition for the usual splitting up of pairs is satisfied as shown in figure 2.14(c). The tunnelling current is relaunched with a sharp increase and very quickly reaches the normal conduction process if V_a is increased further as indicated in figure 2.14(d).

For two different superconductors, the dc I-V curve is given by the formula :

$$I_{SS} = \frac{G_{NN}}{e} \int_{-\infty}^{\infty} \frac{|E|}{(E^2 - \Delta_R^2)^{1/2}} \frac{|E - eV|}{[(E - eV)^2 - \Delta_L^2]^{1/2}} [f(E - eV) - f(E)] dE \qquad (2.26)$$

When T=0 and $Va < \frac{\Delta_1 + \Delta_2}{e}$ $I_{SS} = 0$, but when $Va \geq (\Delta_1 + \Delta_2)/e$ the current is given by:

$$I_{SS} = \frac{G_{NN}}{e} \left[-2\Delta_1 \Delta_2 \beta K(\gamma) + \frac{1}{\beta} E(\gamma) \right] \qquad (2.27)$$

where $\beta = [(eVa)^2 - (\Delta_R - \Delta_L)^2]^{1/2}$ and $\gamma = \beta[(eVa)^2 - (\Delta_R + \Delta_L)^2]^{1/2}$

When $T \neq 0$ equation (2.26) can only be integrated numerically in order to obtain the I-V characteristic similar to that indicated in figure 2.14 (d) [3] .

2.8 Super-Schottky diode tunnelling

The Super-Schottky diode is a superconductor-semiconductor tunnelling junction. It consists of a Schottky barrier between a degenerate semiconductor and a superconducting metallic contact. The degenerate semiconductor is heavily doped to make the barrier sufficiently thin that the tunnelling of electrons near the Fermi surface becomes the dominant current carraying mechanism [17].

The energy band diagram of an n-type super-Schottky diode is as indicated in figure 2.15

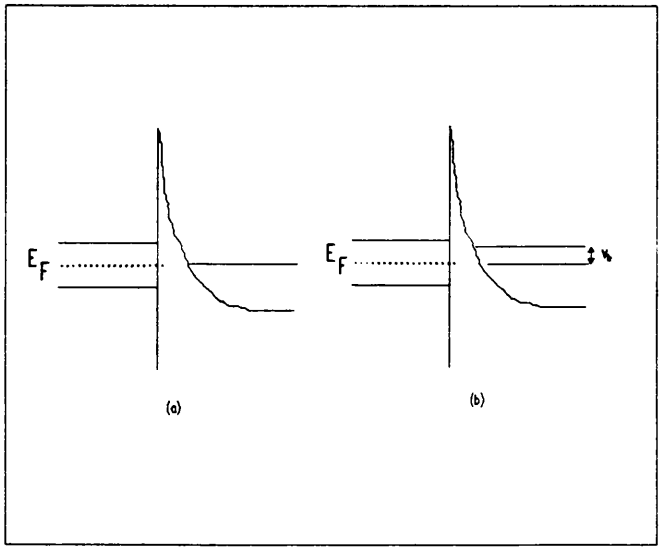

Fig.2.15 Band diagram of n-type super-schottky diode (a) without bias, (b) with a biasing voltage V_b

From this diagram (figure 2.15) it can be deduced that at temperature T=0 and for bias $V_b < \Delta/e$ electrons on the right of the barrier have no available states on the left to which they can tunnel and thus no current can flow. When $V_b=\Delta/e$ electrons start to tunnel to occupy the large number of free states which have become accessible.

Consequently a sharp rise in current occurs as indicated in figure 2.16(a). When V_b increases beyond Δ/e the IV curve approaches the normal state conductivity asymptote. When T $\neq$0 and $K_B T \ll \Delta$ a small proportion of electrons are thermally excited and start to tunnel even for $V_b << \Delta/e$ and give rise to a small current . When $K_B T/e < V_b < \Delta/e$ the current has been found to vary exponentially according to the formula $I = I_0 \exp(SVb)$ with $S = e/K_B T$ [18] [19] and T is the absolute temperature . When V_b increases beyond Δ/e the IV curves becomes linear as indicated in figure 2.16 (b) .

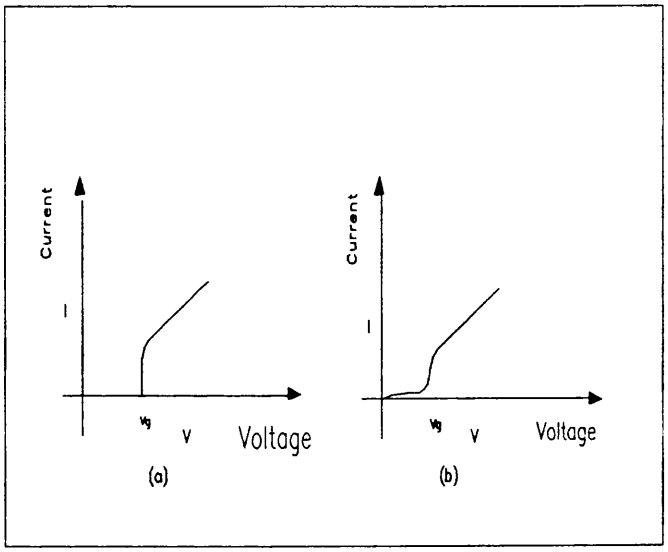

Fig.2.16 (a) IV curve of super-schottky diode at T=0 (b) IV curve of the same junction at T $\neq$0

The conventional Schottky diode has similar exponential relation $I = I_0 \exp(SVb)$ but with S determined empirically [20] by the relation $:S = \frac{e}{K_B(T+T_0)}$ where T_0 has a numerical value greater than 40 K for Shottky diode on n-type GaAs [21] . For the super-Schottky T_0 << 1 and hence can be neglected at operating temperature of few degrees [18]. At temperature T=1 K, the conventional diode has

S=11600/41 V^{-1} whereas the super-Schottky diode has S=11600 V^{-1}. This high parameter S of the super-Schottky diode leads to a stronger non-linear IV curve and hence makes this device attractive for microwave detection and mixing.

2.9 Photon assisted tunnelling

The IV curve of an SIS tunnel junction has been found to be affected by presence of a microwave field. When exposed to the electromagnetic radiation it acquires steps as shown in figure 2.17

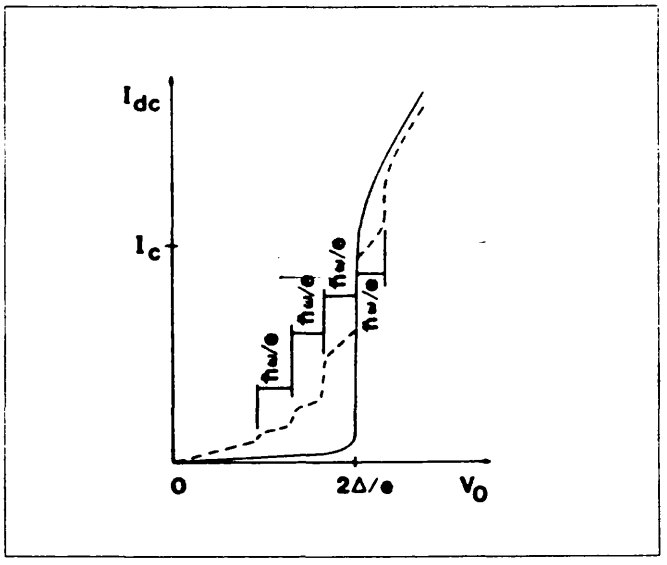

Fig.2.17 IV characteristic of SIS junction in the absence of microwave signal (solid line) , and in the presence of microwave signal (dotted lines).

This effect of the microwave field shown in figure 2.17, can be described by considering the energy level diagram shown in figure 2.18

From the discussion of the previous sections a single electron can tunnel only when the condition $eV\alpha = \Delta_1 + \Delta_2$ is fulfilled as indicated in figure 2.18 (a). When the junction

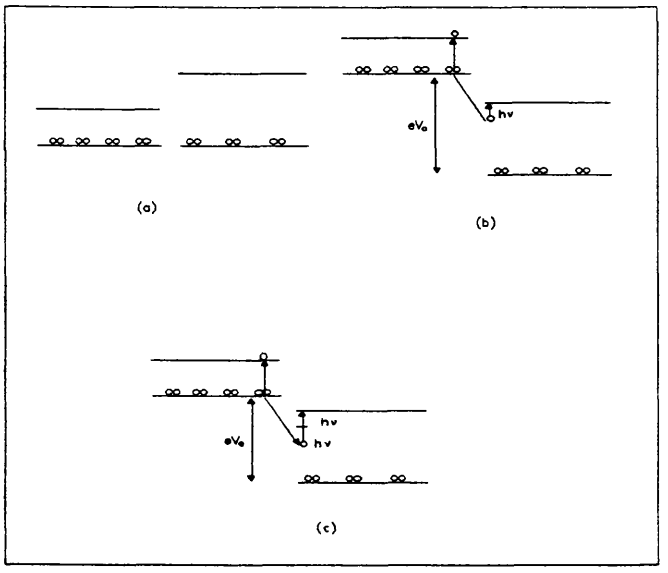

Fig.2.18 Photon assisted tunnelling process: (a) no photons present, (b) absorption of a one photon (c) absorption of two photons.

is illuminated with microwave signal photons at frequency ν, these latter provide an energy $h\nu$ that adds to that due to the biasing voltage V_a . Therefore the previous tunnelling condition becomes :

$$h\nu + eV_a = \Delta_1 + \Delta_2 \qquad (2.28)$$

This shows that even when the biasing voltage is less than the $(\Delta_1 + \Delta_2)/e$, an electron can absorb a photon and tunnel across the barrier as shown in figure 2.18 (b). This tunnelling process take place as a result of a joint action of the biasing voltage and the microwave field and hence it is referred to as photon assisted tunnelling. For lower biasing voltages electrons may absorb several photons so as to reach the bottom of the continuun as shown in figure 2.18 (c) where the absorption of two photons (n=2) is represented. Consequently equation (2.28) can be written under the general form :

$$nh\nu + eV\alpha = \Delta_1 + \Delta_2 \qquad (2.29)$$

It is this absorptions of different numbers of photons that causes sudden rises in current at the corresponding voltages between 0 and $(\Delta_1 + \Delta_2)/e$ and generates the step structure of figure 2.17.

The IV curve of tunnelling current in the presence of microwave signal which is represented by the dashed line in figure 2.17 has been formulated using detailed calculations [22] which led to the expression:

$$I = A \sum_{n=-\infty}^{\infty} J_n^2(\alpha) I_0(eV + nh\nu) \qquad (2.30)$$

where J_n is the n_{th} order Bessel function of the first kind, and $\alpha = (eV_s)/(h\nu)$, with Vs equal to the amplitude of the microwave signal.

2.10 Pairs tunnelling :the Josephson junction

A typical Josephson junction is an SIS junction where the insulator is an oxide of metals forming the junction and thin enough to allow pairs to tunnel through it. Pairs tunnelling was first predicted by Josephson [23] using quantum mechanical analysis similar to that used to describe quasiparticle tunnelling through the potential barrier of an SIS junction [24]. The results of his work are two equations known as the Josephson equations that describe the tunnelling of pairs. The first equation is given by:

$$I = I_c \sin(\delta\Phi) \qquad (2.31)$$

where I_c is the maximum dc current which can flow through the junction without developing any voltage across it. I_C depends on the physical structure of the junction. For an ideal SIS junction at absolute zero I_c is given by the relation [25] :

$$I_c = \frac{\pi \Delta(0)}{2eR_N} \qquad (2.32)$$

where R_N is the normal resistance of the junction and $\Delta(0)$ is half the energy gap at temperature T=0.

In equation (2.32) I_C is the height of the step in quasiparticle tunnelling at $V_g = 2\Delta/e$ [29]. The term $\delta\Phi = \Phi_1 - \Phi_2$ is the phase difference between the phases of the pairs wave function Ψ_1 and Ψ_2 on either side of the barrier a shown In figure 2.19.

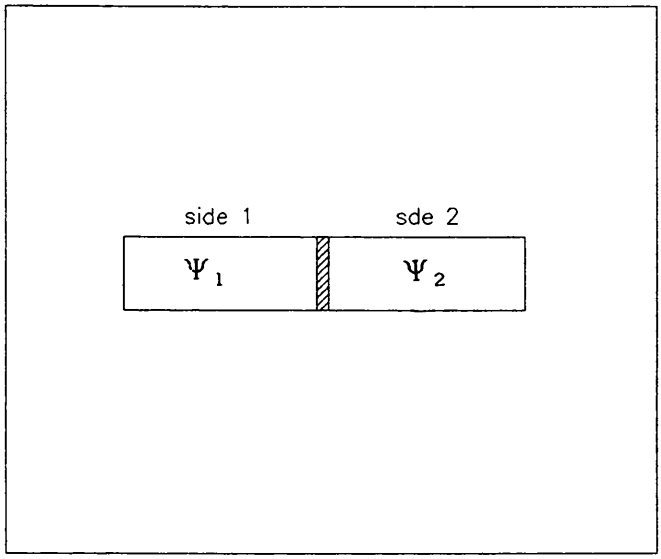

Fig.2.19 Schematic diagram of Josephson junction where two superconductors in side 1 and side 2 are separated by a barrier (shaded)

As discussed in chapter 1, The superconductor wave functions of pairs are given by the relations:
$\Psi_1 = \sqrt{n_{s1}}\exp(j\Phi_1)$ and $\Psi_2 = \sqrt{n_{s2}}\exp(j\Phi_2)$ where n_{s1} and n_{s2} are the densities of pairs on sides 1 and 2 respectively (figure 2.19).

The second Josephson equation relates the time derivative of $\delta\Phi$ to the voltage across the junction :

$$\frac{d\delta\Phi}{dt} = \frac{2eVa}{\hbar} \qquad (2.33)$$

If V_a is constant in time this equation can be integrated to give :

$$\delta\Phi = \frac{2eV_a t}{\hbar} + \delta\Phi_0 \qquad (2.34)$$

where $\delta\Phi_0$ is an integration constant . By substituting equation (2.34) into (2.31) one obtains :

$$I = I_c \sin(\omega_j t + \delta\Phi_0) \qquad (2.35)$$

with $\omega_j = 2eV_a/\hbar$. This equation shows that when a dc voltage V_a appears across the Josephson junction the pairs current becomes sinusoidal and oscillates at frequency:

$$\nu_j = \frac{2eV_a}{h} \qquad (2.36)$$

This is called the Josephson frequency and has the following numerical value: ν_j=484 GHz/mV .

2.10.1 Different type of Josephson junctions

In addition to the most common planar oxide Josephson junction (shown in figure 2.20 (a)) there exist several other types of junctions or weak links as they are referred to because critical supercurrent I_C in the active area of the device is lower than the current in the superconductor on either side of the junction. The most important types of weak link are shown diagrammatically in figure 2.20 . These and other types of weak links are discussed in more details elsewhere [26] .

Of these various types of J-J, the most widely used are the thin film bridge junction (also known as Dayem bridge) [27] and the point contact junction [28] [29] . The bridge junction consists of two bulk superconductors

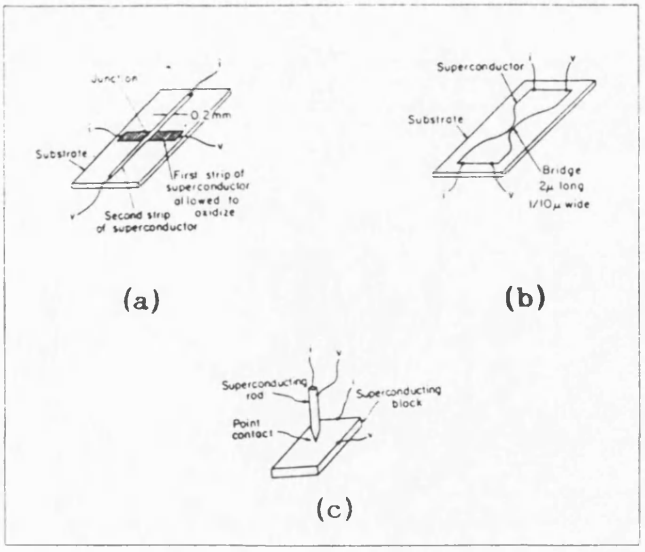

Fig.2.20 Different type of Josephson junctions:
(a) thin film tunnel junction
(b) Thin film bridge junction
(c) Point contact junction

connected by very small bridge with dimension of the order of the micron. The point contact is made by depressing a sharpened superconductor wire, Nb for instance onto a bloc of Nb or a different superconductor such as Indium .

2.10.2 IV curves of Josephson junction

The IV curve of an oxide Josephson junction is as shown in figure 2.21. It should be noted that the form of I-V curve obtained in a measurement depends on the apparatus used [30]. Here the junction is biased using a dc current supply whose internal impedance is greater than the junction impedance.

The IV curve consists of two branches :the supercurrent branch(or pairs branch) and the single electrons branch. The branch OA is the locus of dc supercurrent that flow through the junction without any voltage developed across

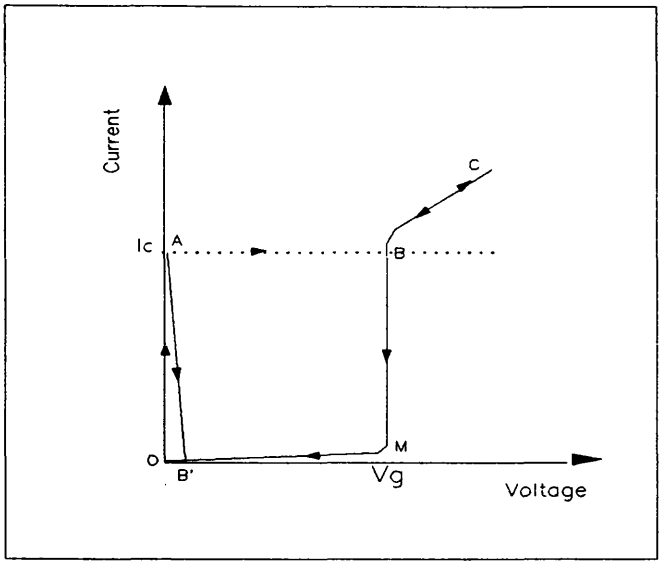

Fig.2.21 IV characteristic of an oxide Josephson junction

it. When the biasing current becomes greater than I_c, the junction is no longer able to withstand it and a jump to the single electrons branch occurs. This is indicated by the dashed line A-B . Single electrons start to tunnel and a voltage $V = 2\Delta/e$ appears across the junction. This voltage V causes the supercurrent to oscillate at very high frequency according to equation (2.35) which therefore has no significant further contribution on the I-V curve which is then mainly due to single electrons. If the dc biasing current is increased further the voltage increases and the IV curve moves from B towards c following the normal conduction curve which has a slope $1/R_N$. When the biasing current is decreased from the normal conduction value to zero, the voltage decreases correspondingly until B from where it either jumps back to A or continues to M and then to O.

However if now instead of using a dc current supply, a dc voltage supply whose internal impedance is less than that of the junction is used, a different result is obtained.

The current flowing through the junction is losseless as long as it is less than I_c. When the biasing voltage increases and causes the current to become greater than I_c a jump to the single electron branch occurs but from A to B' where $V < 2\Delta/e$. At B' a voltage $V_{B'}$ appears across the junction and causes the pairs current to oscillate and a limited tunnelling current due to single electrons starts to flow. When V reaches the value $V = 2\Delta/e$, a sharp rise of current is seen following the path from M to B . If V is increased further the current increases from B towards C. When V is decreased the current decreases following the path C B M B'. From there the current might jump back to A or continue to O.

2.10.3 IV curve of other weak links

The IV curve of the bridge junction has been found to be different from that of an oxide junction and is as indicated in figure 2 .22 .

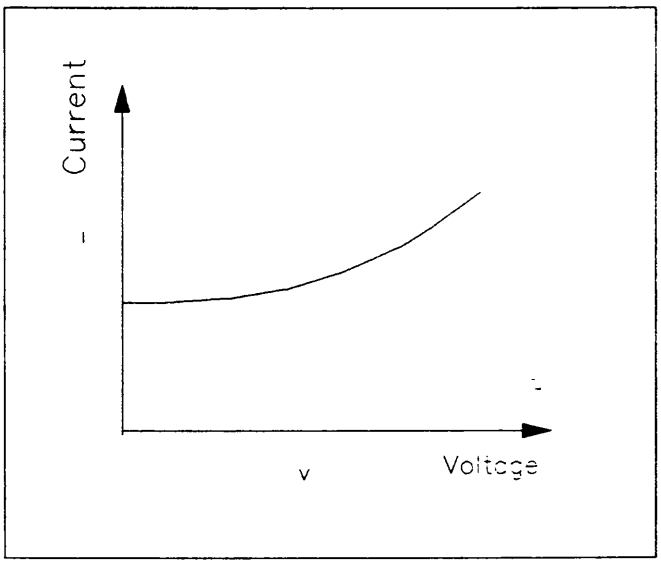

Fig.2.22 IV curve of bridge junction

This IV (figure 2.22) curve displays a zero-voltage current, and has no negative resistance region and no hysterisis. The IV curve of the point contact junction can be modified by varying the pressure on the contact point. Thus it can be made to give characteristics similar to thin film tunnel junctions or bridge junctions [30] .

2.11 Equivalent circuit and features of real junctions

It is often useful to represent the electrical characteristics of a device by an equivalent circuit. Such a representation provides means of analysing circuits into which the device is incorporated. Furthermore the equivalent circuit can serve to relate the electrical properties of the device to its physical parameters. Consequently the performance may be improved by modifying the physical parameters.

The equivalent circuits of an SIN junction, a super Schottky diode and an SIS junction are as shown in figure 2.23 [18] [31] [32] .

The quasiparticle tunnelling current is represented in the SIN diode, super-Schottky, and SIS junction by a nonlinear resistance R, which is shunted by the junction capacitance C. SIN junctions and super-Schottky diodes have series resistance R_S . For the SIN junction the capacitance C is due to the metallic electrodes of area A separated by an insulating layer of thickness d . R_S is due to the spreading resistance of the normal electrode. For the super-Schottky diode the capacitance is determined by the Schottky depletion width and the area of the junction A, and the series resistance is due to the spreading resistance of the semiconducting bar. The SIS junction has no series resistance for $T<T_C$ and possesses an additional parallel conduction path for the pairs tunnelling through the junction represented by the "opposite arrows" in figure 2.23 (C).

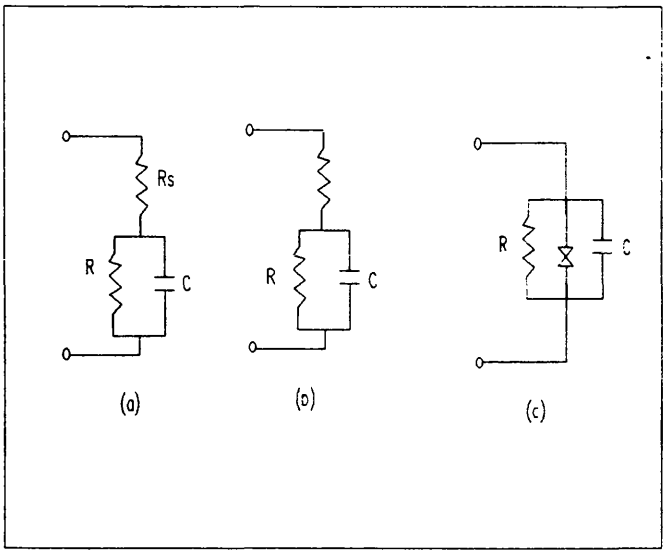

Fig.2.23 Equivalent circuits of: (a) SIN junction, (b) Super-Schottky junction , and (c) SIS junction

IF these devices are to be used at high frequencies their capacitance must be small enough so as to prevent shorting out the microwave signal. In addition their impedance level (which is set by their normal resistance R_N as will be discussed) has to be in the range of 50-400 Ω for matching to an input waveguide system [33].

The series resistance present in an SIN and super-Schottky diode produces parasitic losses as the junction capacitance charges and discharges through it . These losses have been determined from the junctions equivalent circuit [34] and are expressed by the equation:

$$L_p = 1 + \frac{R_S}{R_{RF}} + \omega^2 C R_{RF} R_S \qquad (2.37)$$

where ω is the signal angular frequency, R_{RF} is the RF impedance of the diode, and R_S and C are the parasitic resistance and capacitance. This equation shows that in order to reduce the parasitic loss it is necessary to reduce

R_S and C . For the super-Schottky diode the reduction of R_S has been attempted using different methods such as the use of a high mobility semiconductor like InSb [35], or the use of ultra-thin substrate [36] or the multiple contact geometries [37]. The parasitic capacitance can also be reduced substantially using the fact that the impedance level of the super-Schottky diode is set by the junction normal resistance R_N [38] which is given by the relation :

$$R_N \propto A^{-1} \exp(\gamma S V_B) \qquad (2.38)$$

in which A is the area of the contact, γ is a dimensionless parameter between 2/3 and 1 , V_B is the barrier height, and S is given by:

$$S = \frac{2}{e\hbar}\frac{\epsilon m^*}{N} \qquad (2.39)$$

where e is the electron charge, m^* the carrier effective mass, ϵ the permitivity of the semiconductor, and N the dopant concentration. Equation (2.38) can be transformed to give :

$$A \propto R_N^{-1} \exp(\gamma S V_B) \qquad (2.40)$$

For a chosen value of R_N, the area is exponentially dependant on V_B . The capacitance C of the diode is given by [39] :

$$C = A\left(\frac{eN}{2V_B}\right)^{1/2} \qquad (2.41)$$

where N is the concentration of the dopant . By substitution for A from equation (2.41) into equation (2.40) one obtains:

$$C \propto R_N^{-1}\left(\frac{eN}{2V_B}\right)^{1/2} \exp(\gamma S V_B) \qquad (2.42)$$

This equation shows that a decrease in V_B causes an exponential decrease in C. Conveniently the barrier height of GaAs super-Schottky diode was found to depend on the interaction between the chemical etchant used to prepare the surface before junction formation and the semiconductor [36] . However any reduction of the area A, causes the parasitic resistance R_S to increase because of the relation of this latter with the junction radius r [40] which is given by the formula:

$$R_s = \frac{\rho}{4r} \qquad (2.43)$$

where ρ is the resistivity of the semiconductor and r the radius of the contact. Inspite of this the reduction of C by lowering the barrier height has extended the use of the super-Schottky diode from 9 Ghz [18] at which it has performed nearly as an ideal low noise mixer to 30 GHz with similar sensitivity . Another team has successfully operated super-Schottky diode at 36 GHz and attempted to extend it to 90 GHz but the results were found to suffer from parasitic losses [41]. Consequently the use of super-Schottky diode seems to be limited to less than 40 GHz.

The absence of series resistance in SIS junction greatly reduces the parasitic losses and make this device attractive for operation at millimetre wavelengths [42].

For SIS junctions the cutoff frequency is found to be determined by the normal state resistance R_N and the capacitance C [33] according to the formula:

$$f_c = \frac{1}{2\pi R_N C} \qquad (2.44)$$

By introducing the junction area A and the junction conductance per unit area i.e $(R_N A)^{-1}$ which is equivalent to J_C, the previous expression of f_C was written [31, 33] as follows:

$$f_c = \gamma \frac{1}{2\pi \frac{2\pi}{\phi J_c} \frac{C}{A}} \tag{2.45}$$

where γ is a constant of order of one . This latter expression for f_C can be written in the form:

$$f_c = \gamma \frac{e}{4\pi^2} \frac{A}{C} J_c \tag{2.46}$$

A similar expression can be obtained using equations (2.32) and (2.44). The normal resistance R_N is calculated from (2.32) where I_C is replaced by it $J_C A$ to give the formula:

$$R_N = \frac{\pi \Delta(0)}{2eAJ_c} \tag{2.47}$$

The substitution of this expression for R_N into equation (2.44) gives :

$$f_c = \frac{e}{\pi^2 \Delta(0)} \frac{A}{C} J_c \tag{2.48}$$

Moreover J_C has been found to decay exponentially with the thickness d of the oxide barrier [43] according to the formula :

$$J_c = \frac{c_1}{d} \exp(-c_2 d) \tag{2.49}$$

where c_1 and c_2 are constant with $c_1=2.207\text{x}10^5$ and $c_2=1.5787$ when d is in nm and J_c in Acm^{-2} [44].

By substitution of J_c in the last expression of f_c (equation 2.48) into which C/A has been replaced by ϵ/d, one obtains:

$$f_c=\frac{1}{\pi^2\Delta(0)}\frac{c_1}{\epsilon}\exp(-c_2 d) \qquad (2.50)$$

This equation shows that the operating frequency is $\propto\exp(-c_2 d)$ and therefore for high frequency applications junctions with thin barriers are required .

From equation (2.47) and (2.49) one obtains :

$$R_N=\frac{\pi\Delta(0)}{2eAc_1}d\exp(c_2 d) \qquad (2.51)$$

From this equation it can be seen that the requirement of thin barrier is fulfilled by a junction having small R_NA product.

For SIS mixer application, the receiver performance has been found to be optimised for product $\omega CR_N\sim 4$ [45]. Thus most of the work in SIS mixers is being done using junctions with ωCR_N approaching this ideal limit of 4 . A 110 GHz SIS mixer made of eight Nb/AlOx/Nb junction was used for regular astronomical observations [46] . The junctions of this mixer were designed so that , the capacitance C and the normal state resistance R_N, of each junction satisfy the relation $\omega CR_N\sim 3$. For f=100 GHz , and $8R_N$ =100 Ω , and the specific capacitance of Nb/AlOx/Nb junction equals to 60 $fF/\mu m^2$, C should be 300 fF corresponding to a junction diameter of 2.5 μm . This order of junction dimension can be achieved by available processing [47] [48] .

In addition SIS mixers suffer from Josephson noise which increase with increasing frequency for a given voltage gap V_g. This leads to a limitation of the upper frequency limit at which an SIS mixer can be used without onset of Josephson noise .

Recently it has been found that using different material such as Nb/Nb-oxide/PbInAu junctions and sophisticated fabrication procedures [49], it was possible to operate SIS mixers at frequencies up to 345 GHz [50]. The junction used had the following characteristics: R_N = 100 Ω , C=35fF, A= 0.18 μm^2 and $\omega C R_N(345GHz)=3.8$.

In mixer applications the Josephson noise can be circumvented by either the use of magnetic field [51] (by reducing I_C), or the use of array of large SIS junctions. However if the magnetic field is not homogeneous this can smear the gap and result in a reduction of sensitivity [52]. An array of N SIS junctions has its normal resistance R_{Na} , its capacitance Ca, and its gap voltage V_{ga} given by the following equations respectively [53]:

$$R_{Na} = N R_N \qquad (2.52)$$

$$C_a = C/N \qquad (2.53)$$

$$V_{ga} = N\frac{2\Delta}{e} \qquad (2.54)$$

From equation (2.52) it can be seen that the use of an array can solve the matching problems caused by the small value of R_N for individual junctions. From the last 2 of these equations it can be seen that the capacitance Ca is smaller and the gap voltage V_{ga} is greater than the corresponding junction values . This means that the biasing

voltage, V_b, and the swing of the local oscillator V_{LO}, can occur without Josephson noise. However the use of an array introduces a series inductance which can alter the array impedance .

The SIN junction has no pairs tunnelling and thus does not exhibit any Josephson noise. Therefore SIN junction can present a solution extending mixing and detection by photon assisted tunnelling into the frequency domain above 200 GHz . In fact photon assisted tunnelling has been observed at 246 and 604 GHz [54] using small area SIN junctions which were made using the oblique evaporation method [55].

2.12 The RSJ mode

The hysterisis observed in the IV curves of thin film tunnel junction (figure 2.21) must be eliminated when these junctions are used in certain applications such as SQUIDs (SQUIDs will be discussed in chapter 3) [56] . These hysterisis are eliminated by adding an external shunt resistance R in parallel with the junction [56]. The resulting equivalent circuit of the Josephson junction with the shunting resistance is known as the "Resistively Shunted Junction " (RSJ) model and is shown in figure 2.24 .

This circuits have been analysed by writing the current i(t) as a function of v(t) and integrating numerically [32]. The effect of the shunting resistance is shown in figure 2.25 .

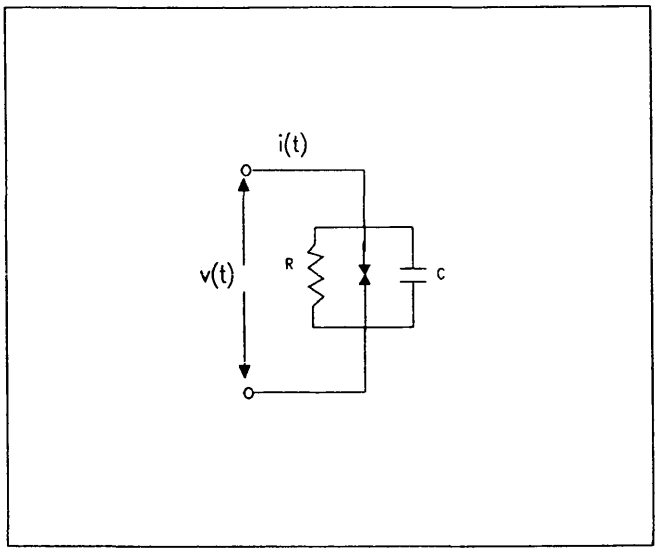

Fig.2.24 Equivalent circuit of a resistively shunted SIS tunnel junction

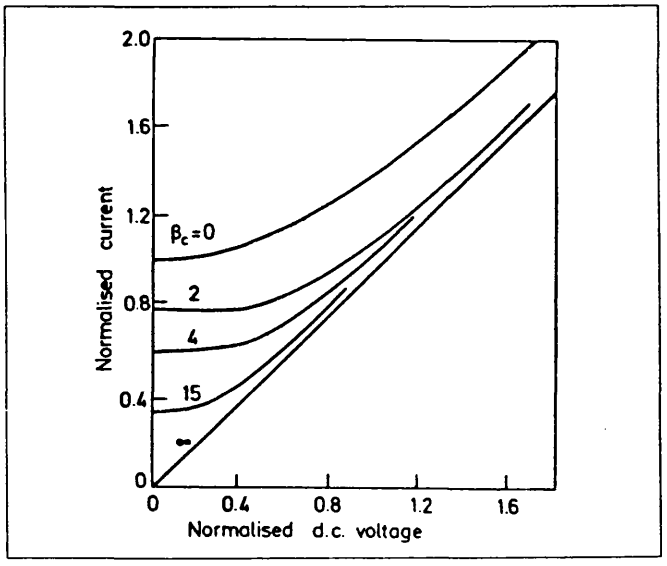

Fig.2.25 Normalised IV curves of (a) SIS tunnel junction for different β_c (from ref. [32])

The term β_c is given by the following equations [32].

$$\beta_c = \frac{2eI_cCR^2}{\hbar} \qquad (2.55)$$

From this figure it can be seen that:

- for $\beta_c >> 1$ there is a hysterisis effect
- for $\beta_c << 1$ there is no hysterisis effect

Most of the SQUIDs are operated in this second condition.

Chapter 2 references

1 M. D. Fiske and I. Giaver, "Superconductive tunnelling", Proceeding of the IEEE 52, pp:1155-1163, 1964.

2 I. Giaver, "Electron tunnelling between two superconductors ", Phys. Rev. Lett. 5, pp:464-466,1960 .

3 J. Nicol, S. Shapiro and P. H. Smith, "Direct measurement of the energy gap", Phys.Rev.Lett. 5, pp:461-463, 1961.

4 I. Giaver and K. Megerel, " Study of superconductors by electron tunnelling", Phys. Rev. 122 , pp:1101-1111, 1961.

5 I. Giaver, "Energy gap in superconductors measured by electron tunnelling", Phys. Rev. Lett. , 5, pp. 147-148, 1960 .

6 S. M. Sze ," Physics of semiconductor devices ", p.553, 2nd edition, John Wiley and sons, New York 1981.

7 S. Curtin, T. C. McGill, and C. A. Mead, "Direct interelectrode tunneling in GaSe", Phys. Rev. B3, p.3368, 1971.

8 C. B. Duke, "Theory of metal-Barrier-Metal tunnelling ", in " Tunnelling phenomenon in Solids" edited by E. Burstein and S. Lundqvist, Plenum Presse, New York, 1969.

9 C.J.Gorter and H.B.G Casimir ,Phys.Z 35, 787 (1933)

10 N.N.Bogoliubov, J.Exptl.Theoret.Phys.U.S.S.R. 34,58,73 (1958) .
[Translation :Soviet Phys.34,41,51 (1958)];Bogliubov,Tolmachev,and Shirkov, A New Method in the Theory of Superconductivity (Accademy of Sciences of U.S.S.R., Moscow, 1958).

11 J. R. Schrieffer and J. W. Wilkins, "Two-particles tunnelling process between superconductors", Phys. Rev. Letters 10, pp:17-20, 1963.

12 T. V. Duzer , C. W. Turner , "Principle of superconductive devices and circuit", p79-87, edited by Edward Arnold 1981.

13 B. N. Taylor and E. Burstein, " Excess Currents in electron tunnelling between superconductors ", Phys. Rev. Lett. 10, pp14-17, 1963 .

14 C. J. Adkins , " Multi-particle tunnelling between superconductors", Rev. Mod. Phys. 36 , pp:211-213, 1964 .

15 C. J. Adkins , " Two-particle tunnelling between superconductors", Phil. Mag. 8, pp:1051-1061 , 1963.

16 Jahnke-Emde-Losch, " Table of higher functions", McGraw Hill, New York, 1960.

17 M. F. Mellea, M. McColl, and C. A. Mead, "Schottky barrier on GaAs", Phys. Rev. 177, pp:1164-1172, 1969.

18 F.L. Vernon,Jr., M.F. Bottjer, A.H. Silver, R. J. Pedersen and M. McColl, "The super-Schottky diode ", IEEE Trans. Microwave Theory Tech. MTT-25, pp:286-294, 1977.

19 M. McColl, M. F. Millea, A. H. Silver, M. F. Bottjer, R. J. Pedersen, and F. L. Vernon, " The super-Schottky microwave mixer ", IEEE Trans. Magn. MAG-13,pp:221-227, 1977.

20 F.A. Padovani and G.G. Samner, "Experimental studies of Gold-Galium Arsenide Schottky barriers", J.Appl. Phys. 36, pp.3744-3747, 1965 .

21 F.A. Padovani , "Graphical determination of the barrier height and excess temperature of a Shottky barrier", J.Appl. Phys. 37, pp.921-922, 1966.

22 P. K. Tien and J.P. Gordon " Multiphoton process observed in the ineraction of microwave fields with the tunneling between superconductor films ", Phys. Rev. 129, pp:647-651, 1963.

23 B.D. Josephson, " Possible new effects in superconductive tunnelling ", Phys. Lett. 1, p:251-253, 1962 .

24 M.H. Cohen , L.M. Falicov and J.C. Phillips, " Superconductive tunnelling " , Phys. Rev. Lett. 8, 316, 1962 .

25 V. Ambegoaker and A.Baratoff,"Tunneling between superconductors", Phys. Rev. Lett. 10, pp:486-489, 1963 . Erratum Phys. Rev. Lett. 11, p. 104, 1963.

26 J. Clarke "The Josephson effect and e/h", Am. J. Phys. 38, pp:1071-1095, 1970.

27 P. W . Anderson, and A. H. Dayem, Phys. Rev. Letters, 13, p.195, 1964.

28 H. J. Levinstein and J. E. Kunzler, "Observation of energy gap in beta-tungsten and other superconductors using a simplified tunnelling technique", Physic lett. 20, pp:581-583, 1966 .

29 J. E. Zemerman and A. H. Silver, " Macroscopic quantum effect through superconducting point contacts", Phys. Rev. 141, pp:367-371, 1966.

30 D. N. Langenberg, "AC Josephson tunnelling-experiment", p:519-539, in "Tunnelling phenomenon in solids", edited by Ellias Burstein and Stig Lindqvist, Plenum Press, New York 1969.

31 P.L. Richards and T. M. Shen, "Superconducting devices for millimetre waves detection, mixing, and amplification", IEEE Trans. Electron Device ED-27, pp:1909-1920, 1980.

32 D.E. McCumber, "Effect of ac Impedance on dc Voltage-current characteristics of superconductor weak link junctions", J. Appl. Phys. 39, pp: 3113-3118, 1968.

33 G. J. Dolan , T. G. Phillps, and D. P. Woody,"Low noise 115 Ghz mixing in superconducting oxide barrier tunnel junctions, " Appl. Phys. Lett., 34, pp. 347-349 , 1979 .

34 G. C. Messenger and C. T. McCoy, "theory and operation of crystal diodes as mixers", Proc. IRE 45, pp:1269-1283, 1957.

35 M. McColl and M. F. Millea, " Schottky barrier on InSb", J. Electronic Mat. 5, pp:191-207, 1976.

36 C. L. Hung and T. Van Duzer," Schottky diodes and other devices on thin silicon membranes", IEEE Trans. Electron. Devices ED-23, pp:579-583, 1976.

37 M. McColl, D. T. Hodges, and W. A. Garber, " Submillimeter-wave detection with submicron-size Schottky barrier diode ", IEEE Trans. Microwave Theory Tech. MTT-25, pp:463-467, 1977.

38 M. McColl, M. F. Bottjer, A. B. Chase, R. J. Pedersen, A. H. Silver, and J. R. Tucker, "The super-Schottky diode at 30 GHz", IEEE Trans. Magn. MAG-15, 1979.

39 S. M. Sze, "Physics of semiconductor devices ", p. 248, 2nd edition John Wiley and sons, New York 1981 .

40 H. K. Henish, " Rectifying Semiconductor contacts", p. 219, Oxford University press, London, 1957.

41 A.H. Silver, R. J. Pederson, M. McColl, R. L. Dickman, and W. J. Wilson, "The millimetre wave super-Schottky diode detector", IEEE Trans. Magn. MAG-17, pp:698-701,1981.

42 Y. Taurr and A. R. Kerr, " Low noise Josephson mixer at 115 GHz, using recyclable point contacts ", Appl. Phys. Lett. 32, pp:775-777, 1978.

43 S. Basavaiah, J. M. Eldridge, and J. Matisoo, "Tunnelling in lead-lead oxide-lead junctions", J. Appl. Phys. 45, pp:457-464, 1974.

44 G.G. McDonald, R. L. Pederson, C.A.Hamilton, R. E. Harris, and R. L. Kautz, "Picosecond applications of Josephson junctions", IEEE trans. Electron devices ED-27, pp:1945-1965, 1980.

45 J. R. Tucker and M. J. Fledman, " Quantum detection at millimeter wavelengths", Rev. of modern physics 57, pp:1055-1113, 1985.

46 H. Ogawa, A. Mizuno, H. Hoko, H. Ishikawa, and Y. Fukui, "A 110 GHz, SIS Receiver for radio astromy ", Int. J. of Infrared and Millimeter wasves 11, pp:717-726, 1990 .

47 M.Gurvich, M. A. Washington, and H. A. Huggens, "High quality refractory tunnel junctions utilasing thin alluminium layers ", Appl. Phys. Lett. 42, p472-474, 1983 .

48 M. Yuda, K. Kuroda, and J. Nakamo, Jap. Jour. Of Appl. Phys. 26, march 1987.

49 W. C. Danchi, E. C. Sutton, P. A. Jaminet, and R. H. Ono, "Nb edge junction process for submillimeter waves SIS mixers", IEEE Trans. Magn. MAG-25, pp:1064-1067, 1989.

50 E. C. Sutton, W. C. Danchi, P. A. Jaminet, and R. H. Ono, "A superconducting tunnel junction receiver for 345 GHz ", Int. J. Infrared millimetre waves 11, pp:133-151, 1990.

51 S. Runder, M. J. Fledman, E. Collberg, and T. Cleasson, J. Appl. Phys. 52, pp.6366,1981

52 T. G. Phillips, D. P. Woody, G. J. Dolan , R. E. Miller, and R. A. Linke, "Dayem-Martin (SIS tunnel junction) mixers for low noise heterodyne receivers", IEEE Trans. Magn. MAG-17, pp:684-689, 1981.

53 M. J. Fledman, and S. Runder, Review of Infrared and millimetre waves 1, p.47, Edited by K. J. Button (Plenum, New York), 1983.

54 F. Habbal, W. C. Danchi, and M. Thinkham, " Photon-assisted tunnelling at 246and 604 GHz in small-area superconducting tunnel junctions", Appl. Phys. Lett. 42, pp:296-298, 1983.

55 W. C. Danchi, F. Habbal, and M. Thinkham, "Ac Josephson effect in small-area superconducting tunnel junctions at 604 GHz", Appl. Phys. Lett. 41, pp:883-885, 1982.

56 J. Clarke, "SQUIDs : principles, Noise, and applications", in "superconducting devices", p. 51, edited by S. T. Ruggiero, and D. A. Rudman , Academic press, London 1990.

CHAPTER 3: LOW T_c SUPERCONDUCTOR DEVICE APPLICATIONS

3.1 Introduction

As discussed in chapter 2 the quasiparticle tunnelling currents of the super-Schottky diode, SIN and SIS junction are characterised by an abrupt rise when the voltage is increased above the voltage corresponding to the gap. As a result a strong nonlinearity in the IV curve is obtained which makes it possible for the device to be used as a direct detector or as a mixer in the millimetre and submillimetre regions.

3.2 Direct detection

When an RF signal is applied to a superconductor tunnel junction (SIS for example) its dc IV characteristic (solid line) acquires steps as shown by the dashed line of figure 2.17 [1] . From the figure one can see that the sudden rise of current is displaced to lower voltage by multiples of $h\nu/e$. These current steps are due to single electron tunnelling resulting from pairs which were broken by the energy $h\nu$ of the RF field. This quantum effect is called photon assisted tunnelling. Following the discovery of this phenomenon, in the early sixties [2], device interest started in the seventies when the first super-Schottky diode was invented [3]. This interest was further stimulated when a quantum mixer theory was developed [4] and made the extraordinary prediction that a quasiparticle detector could approach unity quantum efficiency, ie one tunnelling electron for each incident microwave photon.

3.2.1 Direct detector sensitivity

The performance of a direct detector is characterised by its current responsivity and its noise equivalent power NEP.

These two parameters will be defined for a microwave diode (super-Schottky diode or normal Schottky diode). Such diodes have similar IV curves to the SIN and SIS junctions and their sensitivity is related to the degree of nonlinearity of the IV Characteristics. The IV characteristic of these devices is given by the formula [5]:

$$I = I_0(\exp(SV) - 1) \tag{3.1}$$

where I is the current, V the voltage and I_0 a constant related to the material parameters of the diode. The responsivity R_i is expressed by the relation [5] :

$$R_i = \frac{1}{2}\frac{d^2I/dV^2}{dI/dV} = \frac{S}{2} \tag{3.2}$$

and the sensitivity of the detector is expressed by its noise equivalent power NEP which is given by [3]:

$$NEP = \frac{<i_n^2>^{1/2}}{R_i} \tag{3.3}$$

where $<i_n^2>^{1/2}$ is the rms current generated by the detector. If the diode is shot noise limited then [6] .

$$<i_n^2> = 2q(I_{DC} + 2I_0)B = \frac{2qB}{R_d S} \tag{3.4}$$

where I_{DC} is the DC diode current, R_d the dynamic resistance of the diode and B the bandwidth. Using equations (3.2, 3.3, and 3.4) leads to the relation :

$$NEP = \left(\frac{2qB}{R_d}\right)^{1/2}\frac{2}{S^{3/2}} \tag{3.5}$$

This equation shows that a sensitive detector (low NEP) requires a large S.

3.2.2 Quantum expressions of R_i and NEP

The previous expressions are derived from the classical approach as opposed to the quantum one [4] . This latter analysis shows that when $S/2 > e/\hbar\omega$ the derivative of the classical relation of R_i should be replaced by an equivalent finite difference expression to give the quantum responsivity R_{iQM} :

$$R_{iQM} = \frac{e}{\hbar\omega} \frac{I(V+\hbar\omega/e) - 2I(V) + I(V-\hbar\omega/e)}{I(V+\hbar\omega/e) - I(V-\hbar\omega/e)} \qquad (3.6)$$

where all the terms are as defined in figure 3.1 caption .

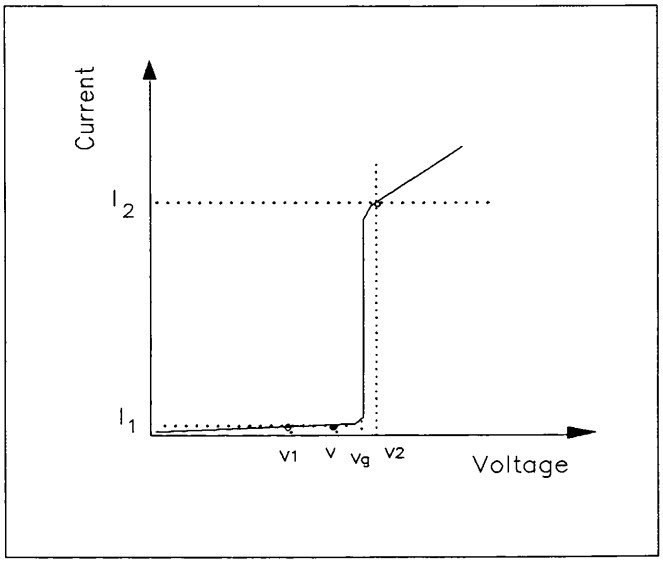

Fig.3.1 DC IV characteristic of an SIS tunnel junction:
V: bias voltage ; V_g: gap voltage ;
$V_1 = V - \hbar\omega/e$; $V_2 = V + \hbar\omega/e$
$I_1 = I(V - \hbar\omega/e)$; $I_2 = I(V + \hbar\omega/e)$

This equation shows that if the non linearity of the IV curve is strong enough so that $I(V-\hbar\omega/e) = I(V) \ll I(V+\hbar\omega/e)$, then R_{iQM} approaches the quantum limited value :

$$R_{iQM} = \frac{e}{\hbar\omega} \qquad (3.7)$$

The implication of this result is that in the quantum limit one electron crosses the junction for each photon absorbed . Thus the junction is considered to be a microwave photon detector with unit responsive quantum efficiency.

The NEP has the same expression as before but with R_i replaced by R_{iQM} to give

$$NEP_{QM} = \frac{< i_n^2 >^{1/2}}{R_{iQM}} = \frac{(2eIB)^{1/2}}{R_{iQM}} \tag{3.8}$$

Using equation (3.7) this then becomes:

$$NEP_{QM} = \hbar\omega\left(\frac{2IB}{e}\right)^{1/2} \tag{3.9}$$

It is worth noting that these superconductor based devices can have classical or quantum mechanical behaviour according to the strength of the RF field voltage $h\nu/e$ in comparison with the nonlinearity scale of the IV characteristic. When $h\nu/e$ is smaller than the nonlinearity scale the device behaves classically. When $h\nu/e$ is greater than the nonlinearity scale, the response is quantum mechanical [7].

3.2.3 Direct detectors results

Some of the main results achieved using superconductor based devices as direct detector are listed in table 3.1 .

Table 3. 1. Direct detectors performance

Frequency (GHz)	R_i (A/W)	NEP ($W/H^{1/2}$)	References
9	2200	5.410^{-16}	[8]
36	3500	2.610^{-16}	[9]
70	0.46 $e/\hbar\omega$	1.710^{-15}	[10]
604	0.4 $e/\hbar\omega$		[11]

3.3 Mixer principles

A mixer can be thought of as a device that reduces the frequency of an incoming signal to a lower frequency which can more easily be processed by conventional electronics. This frequency reduction is achieved by beating the signal (ω_s) with a second locally generated signal (ω_{LO}) in a non-linear device . The beat is generated at the difference frequency (ω_s- ω_{LO}) . Any non-linear current-voltage relation will achieve this, for example a square law i.e:

$$I = \alpha V^2 \tag{3.10}$$

This process is schematically shown in figure 3.2 .

The two signals are simultaneously applied to the diode so that the net resultant voltage e is given by the sum:

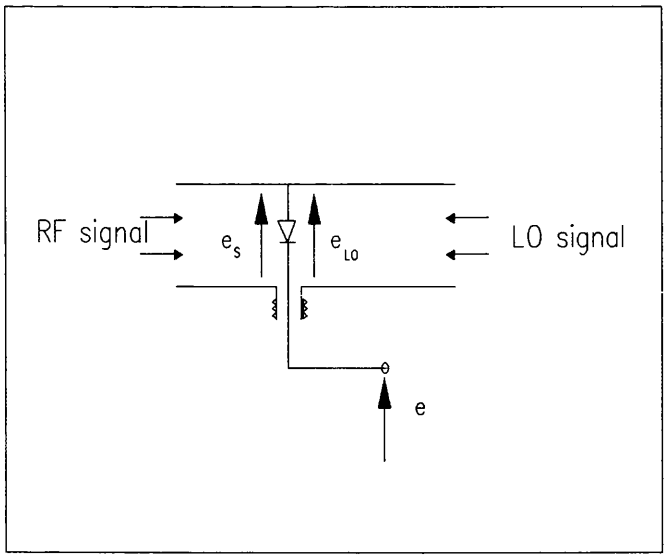

Fig.3.2 Schematic representation of mixing process

$$e = e_s + e_{LO} \tag{3.11}$$

Suppose e_s and e_{LO} are of the form :

$$e_s = E_s \cos(\omega_s t) \tag{3.12}$$

and

$$e_{LO} = E_{LO} \cos(\omega_{LO} t) \tag{3.13}$$

For the square law device the current is given by :

$$i = \alpha\{E_s \cos(\omega_s t) + E_{LO} \cos(\omega_{LO} t)\}^2 \tag{3.14}$$

this leads to :

$$i = \frac{\alpha}{2}\{E_s^2 + E_{LO}^2 + E_s \cos(2\omega_s t) + E_{LO} \cos(2\omega_{LO} t) \tag{3.15}$$

$$+ 2E_s E_{LO} \cos((\omega_s + \omega_{LO})t) + 2E_s E_{LO} \cos((\omega_s - \omega_{LO})t)\}$$

The nonlinearity of the device has produced terms at frequencies different from ω_s and ω_{LO} as indicated in figure 3.3 .

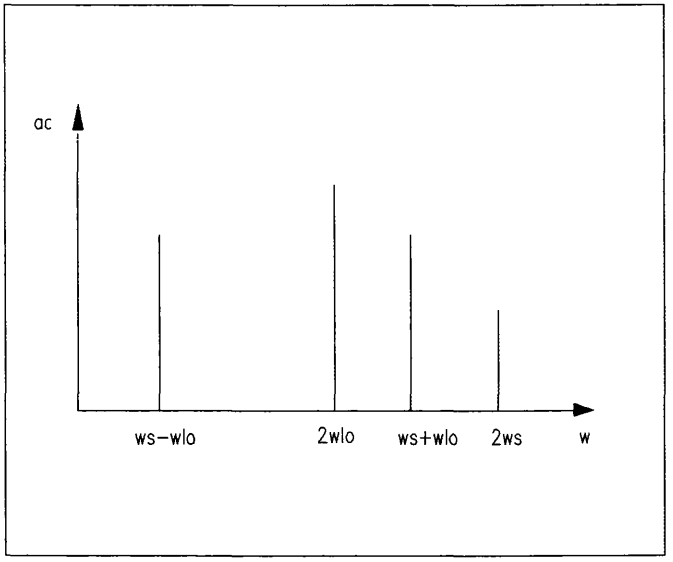

Fig.3.3 Harmonics obtained from mixing process

It is the component whose frequency is $\omega_s - \omega_{LO} = \omega_{IF}$ which is of interest. The DC and higher frequencies components are shunted and filtered by appropriate circuits.

A more elaborate quantum mechanical theory of the superconducting mixer was developed in the late seventies [4] . Recently a theory that is considered to be a complement of the previous one has been developed and has made the striking predictions that SIS mixers will be usable at frequency up to 3000 GHz [12] .

3.3.1 Mixer properties

The main characteristic of a mixer are its conversion loss L_C and its equivalent input noise temperature T_M. These two parameters will be briefly discussed in the next section. More details of these and other related factors can be found in the literature [13] .

3.3.2 Conversion loss L_C

The conversion loss of a mixer is defined as the ratio of the available power, P_{av}, from the RF signal to the absorbed power, P_{ab}, in the IF load.

$$L_c = \frac{P_{av}}{P_{ab}} \tag{3.16}$$

The inverse L_c^{-1} is called conversion gain. L_C is expressed in dB . For the case where $P_{av} = P_{ab}$, $L_C = 1$ thus $L_C(dB) = 0$.

3.3.3 Noise temperature

The noise temperature of a device is defined by considering the increase in noise at the output compared to an equivalent, noise free device. If we imagine both devices to be connected at the input to a matched thermal noise source at temperature Tin, then to make the output noise power of both system equal we must increase Tin in the case of the noise free device. The noise temperature T_N of the noisy device is just equal to this required temperature increase. From the mixer quantum theory, T_N is noted T_M and has been found to have a lower bound $\frac{\hbar\omega}{K_B}$. The mixer is used as a part of a receiver as indicated in figure 3.4 .

The total receiver noise temperature T_R [14] is given by the relation :

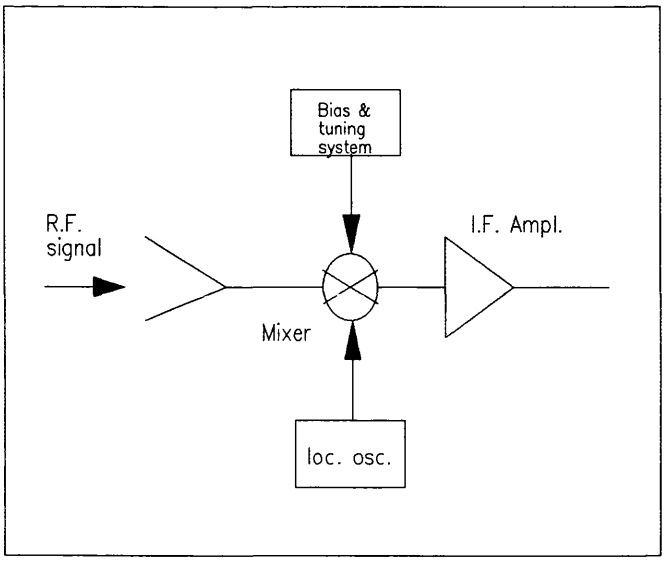

Fig.3.4 Heterodyne receiver block diagram

$$T_R = T_M + L_c T_{IF} \tag{3.17}$$

where T_M is the mixer temperature, L_C is the conversion loss and T_{IF} noise temperature of IF amplifiers.

3.3.4 Mixer receiver sensitivity

The minimum power of a signal that a receiver can detect is given by the relation [13]

$$P_{smin} = K_B T_R B_{IF} \tag{3.18}$$

By substitution for T_R from the preceding equation this becomes :

$$P_{smin} = K_B (T_M + L_c T_{IF}) B_{IF} \tag{3.19}$$

In order to obtain the best possible sensitivity, T_M , T_{IF} , and particularly L_C should be minimised. This latter can be expressed as the product of two terms :

$$L_c = L_0 L_1 \tag{3.20}$$

with L_0 the loss associated with the conversion process and L_1 is related to the loss due to parasitic elements R_S and C which were discussed in section 2.11 (chapter 2). For a super-Schottky diode it has been shown that L_0 is a decreasing function with $e\Delta/K_BT$ as indicated in figure 3.5.

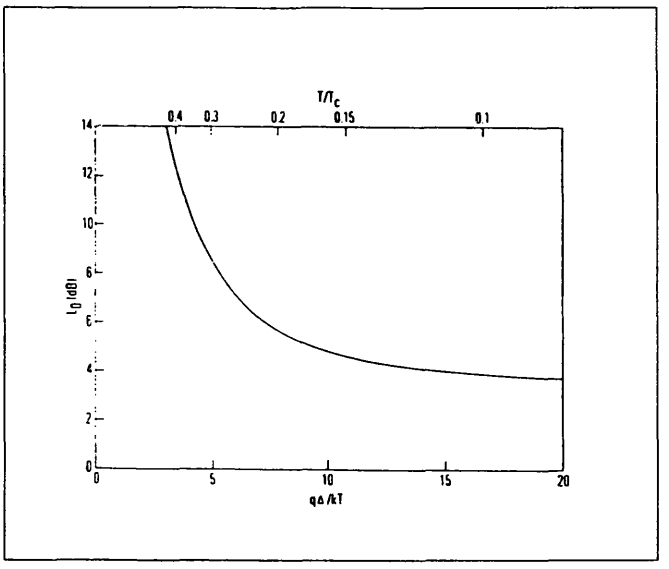

Fig.3.5 Conversion losse vs $e\Delta/K_BT$ (from ref. 13)

From this plot one can obtain an estimate of L_0 knowing Δ and T. It also shows that in order to obtain a lower L_0 one has to reduce the temperature and increase Δ by using a higher T_C material for which the following relation holds [13] .

$$2e\Delta = 3.5K_BT_c(1-T/T_c)^{\frac{1}{2}} \qquad (3.21)$$

3.3.5 Superconductor mixer results

In this section results obtained by different researchers using various types of mixers are cited in table 3.2 . Some of them have been treated in more details in an earlier review [15].

Table 3. 2 Mixer results.

Frequency (GHz)	Conversion gain (dB)	Mixer Temperature (K)	References
36	-8	14	[16]
115	-10	99	[17]
36	-2	3	[18]
36	+ 4.3	9.6	[19]
115	-7.6	62	[20]
55	-7.4	27	[21]
46		55	[22]
241	-10.5	305	[23]
90-120	-3	40	[24]
30-40	6.2	9.2	[25]
85-115		150 to 250	[26]
100 800	+2.6 +0.35	21 48	[27]
115 345 525 761		33 215 470 1100	[28]
90 180	-4.8 -4.4	150 200	[29]
114	-0.1	5.6	[30]

3.4 SQUIDS

3.4.1 Introduction

The term SQUID is an acronym of Superconducting QUantum Interference Device. A SQUID is a flux to voltage transducer which provides an output voltage that is periodic in the applied flux with a period of one flux quantum or fluxion $\Phi_0 = h/\ 2e\ = 2.07 \cdot 10^{-15}\ Wb = 2.07 \cdot 10^{-7}\ g-cm^2$ [31]. It consists of a superconducting ring containing one or two Josephson junctions (or weak links). A double junction ring is biased by a dc current and thus called a DC SQUID whereas a single junction ring is coupled to an ac current circuit and hence called AC SQUID or RF SQUID. Both kind of SQUIDs are shown in figure 3.6

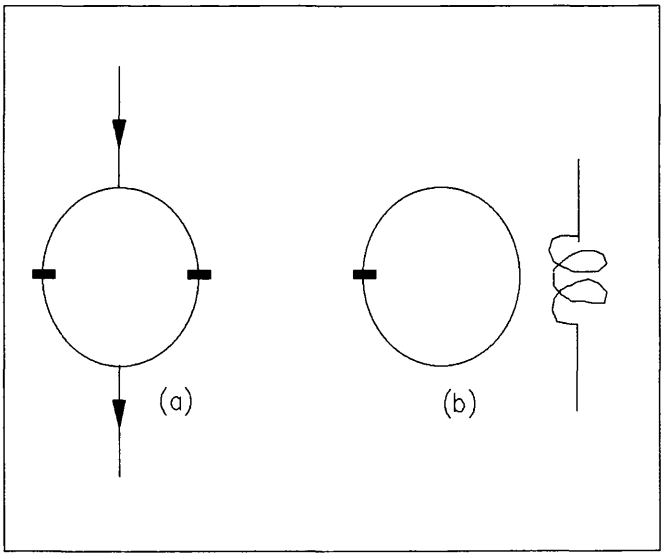

Fig.3.6 (a) DC SQUID , (b) AC SQUID

The minimum flux variation that can be measured by SQUIDs is of the order of $10^{-5}\Phi_0$ [32]. It is this sensitivity that made the SQUIDs the best magnetic flux detector ever known.

Excellent reviews on SQUIDS can be found in the literature [32] , [33], [34] . In the next sections the basic principles of operation of both DC and RF SQUID will be discussed. This will be followed by a selection of some practical results of both kind of SQUIDs and some of their applications.

3.4.2 DC SQUIDS

Figure 3.7 Shows the DC SQUID with the junction represented by their equivalent circuit .

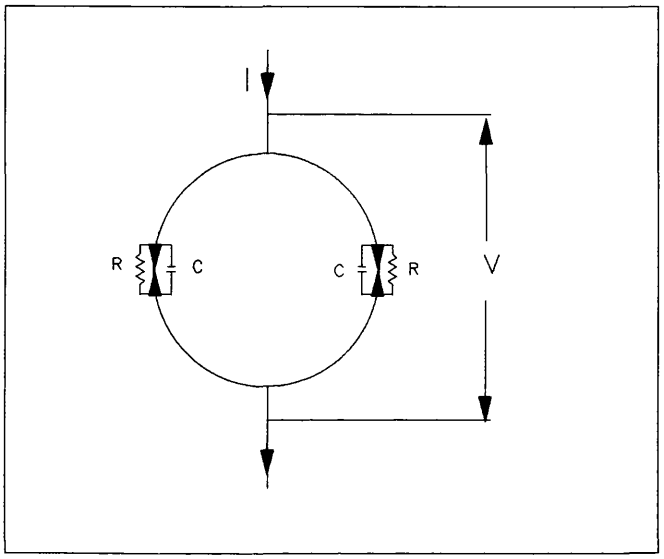

Fig.3.7 Equivalent circuit of DC SQUID

The junctions are assumed to have the same critical current I_C and the same capacitance C. R is the shunt resistance added externally so as to eliminate the hysteresis effect, ie the junction are in the RSJ mode. When magnetic flux is applied to the loop (and gradually increasing), the maximum zero voltage current (critical current) that can be passed through the ring oscillates as a function of the flux Φ of the magnetic field with a period of one fluxion [31].

Accordingly the I-V curve swings with same period between two extremum positions (C1) and (C2) which are reached consecutively for $\Phi = n\Phi_0$ and $\Phi = (n + 1/2)\Phi_0$ as indicated in figure 3.8.

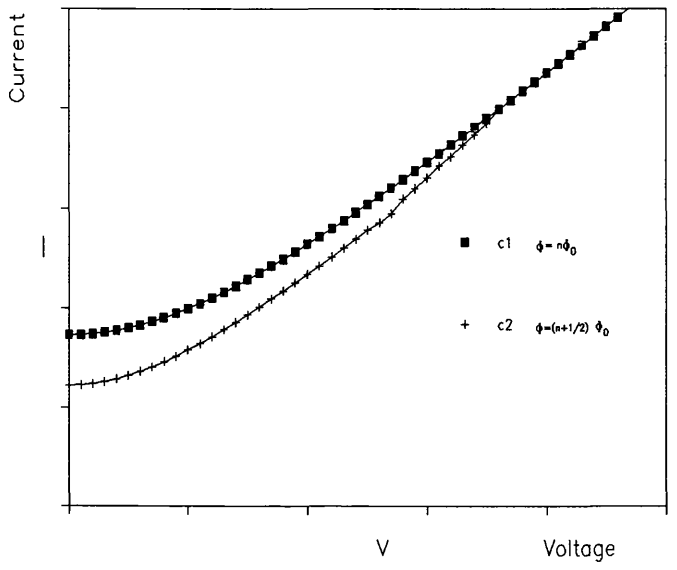

Fig.3.8 Effect of applied magnetic flux on IV curve of DC SQUID

The SQUID is biased by a dc current I_B greater than the junction critical current I_C as indicated in figure 3.9 . I_B causes a voltage V to be created across the loop . When the IV curve is in position C_1 the voltage across the junction is V_1 and when the IV curve is in C_2, the voltage is V_2 as indicated in figure 3.9 .

Hence when the flux varies and the IV curve is displaced between (C_1) and (C_2) with the period Φ_0 the voltage V varies between V_1 and V_2 with the same period as indicated in figure 3.10 .

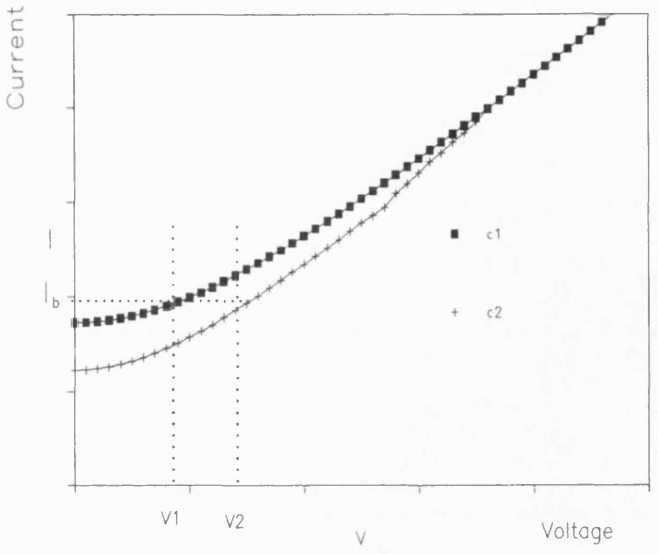

Fig.3.9 Effect of applied magnetic flux on IV curve of a DC SQUID biased by a dc current I_b

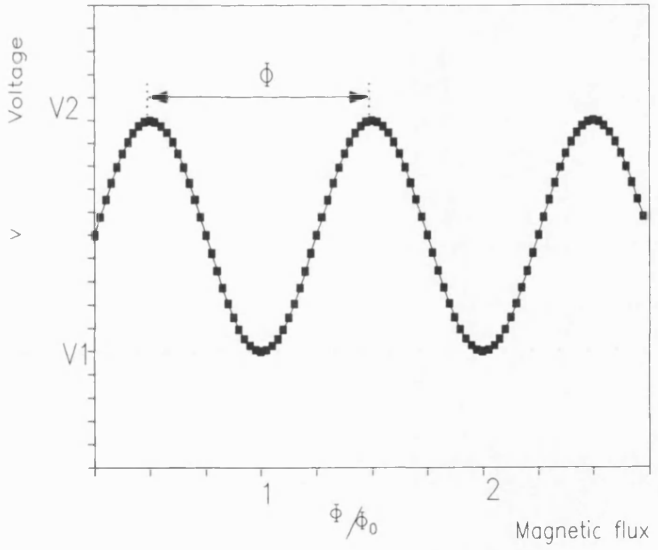

Fig.3.10 Voltage V vs Φ/Φ_0 at a biasing current Ib

The DC SQUID is operated on the steep part of the curve of V against flux Φ where $V_\Phi = \frac{dV}{d\Phi}|_{I_B}$ is maximum ie when the flux in the SQUID is near $(2n+1)\frac{\Phi}{4}$ [32].

3.4.3 Noise and sensitivity of DC SQUIDs

The shunt resistor of the DC SQUID (figure 3.7) creates a Johnson noise that results in a current flowing through the loop and a noise voltage across the SQUID . The noise current creates a noise flux through the loop . The equivalence between energy and the magnetic flux makes it possible to express the noise flux in the SQUID in terms of Joules per unit bandwidth $\epsilon/1Hz$ which is given by [34].

$$\epsilon/1Hz = 8K_B T\sqrt{(\pi LC)} \qquad (3.22)$$

In order to obtain the best sensitivity one has to have the lowest $\epsilon/1Hz$. To achieve this the previous equation predicts that T, L, and C have to be reduced to their minimum values possible while bearing in mind that if L is too small the coupling of the SQUID to the input coil becomes difficult. In another investigation it has been found that $\epsilon/1Hz$ has a minimum value given by [35] :

$$\epsilon/1Hz = \hbar \qquad (3.23)$$

3.4.4 Results of practical DC SQUIDS

Enormous progress has been made towards reaching the quantum limit. Table 3.3 summarises the results achieved with some practical DC SQUIDs

Table 3.3. Performance of some practical DC SQUIDs

R (Ohms)	L (pH)	Sensitivity	References
		$1.2\ 10^{-33}$ J/Hz	[36]
		$5 fT/Hz^{1/2}$	[37]
2.7	51	34 h	[38]
		$710^{-6}\ \Phi_0$ $/Hz^{1/2}$	[39]
0.58	6	$2.310^{-6}\ \Phi_0$ $/Hz^{1/2}$	[40]
	28	1400 h	[41]
	200	$0.22\ 10^{-30}$ J/Hz	[42]
3	110 to 240	$10^{-6}\ \Phi_0$ $/Hz^{1/2}$	[43]
7.5	500	4.5 $fT/Hz^{1/2}$	[44]

3.4.5 DC SQUID applications

DC SQUIDs have been used in a great range of applications not only in the laboratory but also in many other important areas such as :

* Biomedical applications or more specifically bio-magnetism: the SQUID are used to measure the tiny magnetic fields generated by the heart that are of the order of 100 pT [45], and those of the brain which are of the order of 100 fT [46]. The effort of research in this field led to

important progress [47] [37] [48] .

* Gravity wave detection [49] .
* Superconducting Computer applications [50] .

3.4.6 RF SQUIDS

An RF SQUID is a superconducting loop interrupted by a single Josephson junction usually in the hysteretic mode. The loop has an inductance L and is inductively coupled to an LC circuit as shown in figure 3.11.

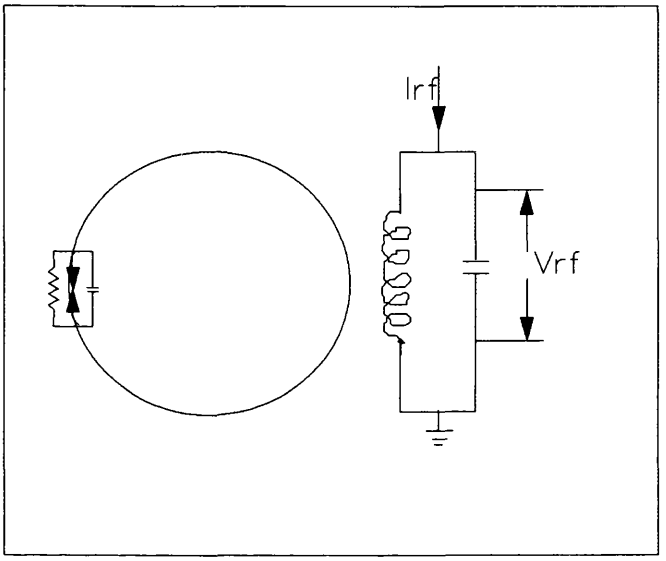

Fig.3.11 RF SQUID basic circuit

The resonant frequency of the tank circuit lies in the range between 10 MHz to 10 GHz as is shown in table 3.4. An RF current I_{RF} at the resonant frequency of the LC circuit drives this latter at a level that causes the peak current induced in the RF SQUID to be just above the critical current I_C of the junction. When a magnetic flux is applied to the loop the output voltage V_{rf} oscillates with a period Φ_0 with a waveform that has the shape of a triangular pattern as shown in figure 3.12 [33] .

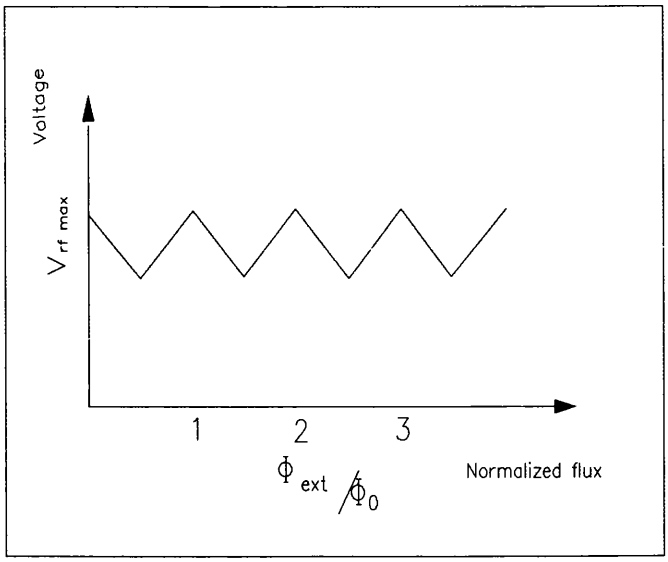

Fig.3.12 Output voltage V_{rfmax} of an RF SQUID vs applied magnetic field

3.4.7 RF SQUID sensitivity

For the RF SQUID the noise is again expressed in term of the noise energy per unit bandwidth $\epsilon/1Hz$. This is given by the relation [34] :

$$\epsilon/1Hz = \frac{1}{\omega_{RF}}\left(\frac{\pi\alpha^2\Phi_0^2}{2L} + 2\pi\alpha K_B T_a^{eff}\right) \tag{3.24}$$

Where L is the SQUID inductance , T_a^{eff} is the effective temperature of the amplifier , $\omega_{RF}/2\pi$ is the pump frequency, and α is given by :

$$\alpha = \frac{1.3(LI_0)^2}{\pi\Phi_0}\left(\frac{2\pi K_B T}{I_0\Phi_0}\right)^{4/3} \tag{3.25}$$

where I_0 is the junction critical current and T is the temperature.

From the expression for $\epsilon/1Hz$ it is apparent that the best sensitivity can be obtained by cooling the amplifier and using a high pump frequency

3.4.8 RF SQUID results

The results of some work on Rf SQUID are indicated in table Table 3.4

Table 3.4 RF SQUID performance

F(MHz)	L (pH)	$\epsilon/1Hz \times 10^{-30}$ (J/Hz)	References
20	800	21	[51]
430	500	1.3	[52]
		0.7	[53]
430	500	1.3	[54]
		$0.03(pT/m)^2/Hz$	[55]

3.4.9 RF SQUID applications

RF SQUID have been used in many applications such as :

* Magnetoseismometry:The measure the magnetic fluctuation caused by the seismic wave stress on earth crust [55].

* A component in gravitational wave detectors [53]

* Superconducting computer applications [56] .

3.4.10 Conclusions and remarks on DC and RF SQUIDs

The very high sensitivities achieved in both RF and DC SQUID have been made possible by the combination of better understanding of noise factors, the use of refractory materials (Nb, NbN etc), and the more and more sophisticated fabrication techniques . All these factors will help widen the range of application of SQUIDs particularly commercial level applications .

3.5 Computer applications

3.5.1 Josephson junction as a switch

The I-V curve of a Josephson junction tunnelling junction consists of two branches :the supercurrent branch due to the tunnelling pairs at zero voltage and quasiparticle branch which is due to the tunnelling of single electrons, this is resistive and has a sharp knee at $V_g = 2\Delta/e$ as indicated in figure 3.13.

The maximum supercurrent that a Josephson junction can withstand in the absence of a magnetic field is the critical current I_c. In the presence of a magnetic field I_c is depressed to a lower value . Whenever the current flowing through the junction is greater than the critical current, the junction switches to the non zero voltage branch. In computer application the junction switches between the zero voltage state and a finite voltage state, $2\Delta/e$ usually . In order to accomplish this operation the junction has to be biased by a current I_b just below I_c and shunted by a resistor R_L to give two working points P1 and P2 as indicated in figure 3.14.

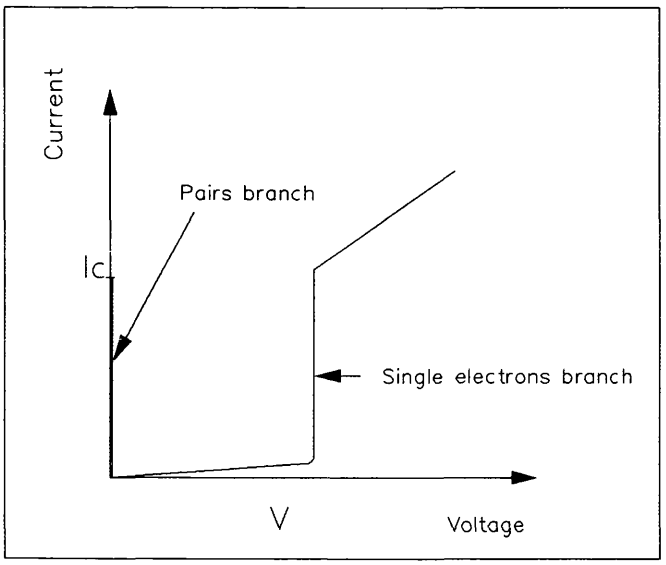

Fig.3.13 IV characteristic of Josephson junction

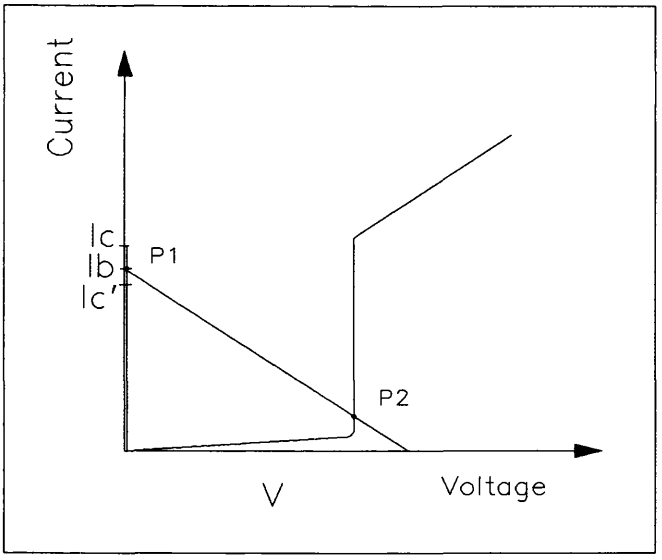

Fig.3.14 IV characteristic with a load

For $I_b < I_c$ the operating point is at the point P1(0,Ib). There is no voltage drop and the junction is in the "0" state. If an extra current I_a is applied to the junction

so as the condition $I_a + I_b > I_c$ is fulfilled, the operating points jumps to point P2($2\Delta/e$, $2\Delta/eR_L$) and the junction is in the "1" state .

If instead of additional current , a magnetic field is applied to the junction and results in decreasing the critical current from I_c to $I_c' < I_b$ the same result is obtained : the operating point moves to P2($2\Delta/e$, $2\Delta/eR_L$).

When I_a or the magnetic field is removed the operating point stays at P2. This is called a latching mode. For the operating point to return to P1, the biasing current has to be reduced to a very low value and then raised to I_b again . This causes the operating point to move to O(0, 0) and then P1. Hence unlike semiconductors that need a DC supply, the Josephson junction requires an alternating or pulsed supply as shown in figure 3.15.

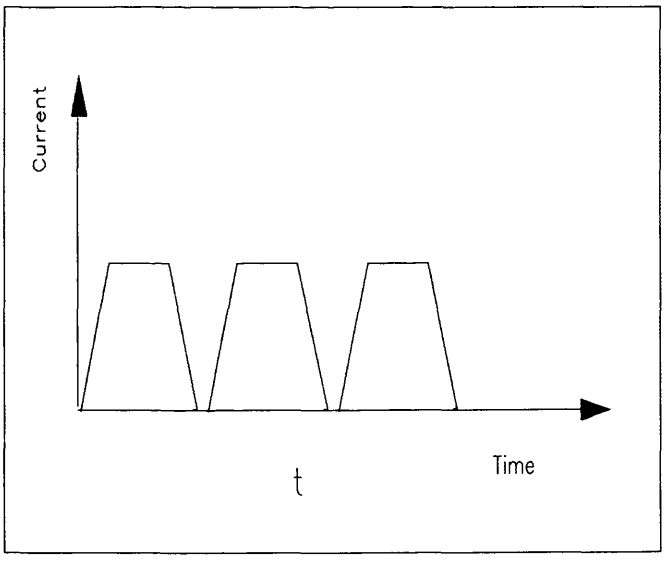

Fig.3.15 Supply of Josephson logic circuit

Depending on the method used to switch the Josephson junction , two kind of circuits can result:logic circuits that are magnetically coupled and circuits using direct injection of current.

3.5.2 The superconducting computer: IBM contribution

These switching properties of Josephson junctions combined with their inherent low power consumption attracted IBM's attention in the mid 1960's. This led the company to start investigating the feasibility of a superconducting computer using Josephson junctions for its logic circuits and memories. Just one year after the launch, they succeeded in producing the first logic circuit with subnanosecond operation [57]. Since then IBM have taken the lead in developing many logic circuits and gates needed for the superconducting computer. They also developed two major techniques . One for the fabrication of large scale integration of lead alloy chips [58], and the other for the all refractory Nb based chips which has been given the acronym SNAP for Selective Niobium Anodisation Process [59]. They also developed a technique for packaging all the chips (10,000) into a box of 10 cmx10 cm which not only ensured the dissipation of the heat generated by the 100 million switching junctions but also made sure that the signal travels without distortion in one cycle time which was measured to be 3.7 nanoseconds [60] .

However and despite all the progress achieved, IBM decided to end the Josephson supercomputer project. This decision was caused by a combination of the delay caused by problems encountered in realising a fast memory chip and the nearing of the availability of a semiconductor computer whose performance is not far from that of the supercomputer [61].

3.5.3 Contribution of other labs and companies

The progress achieved by IBM caught the attention of many other institutions such as Bell Labs, and many Japanese companies such as ETL, NTT, and NEC. Unlike IBM these institutions continued their efforts towards developing a superconducting computer. Following the finding of IBM, most

groups shifted to producing Josephson junction entirely made from refractory materials such as $Nb/NbO_x/Nb$,Nb/Si:H/Nb, and $Nb/Al\text{-}Alo_x/Nb$ [62]. These junction have more stable and reproducible switching properties than those made of lead alloy which were particularly sensitive to thermal cycling between room temperature and liquid Helium . New fabrication processes were developed and improved allowing large scale integration of logic circuits based on NbN [63] [64] . During the decade many circuits have been developed . However the major obstacle has been the realisation of Josephson junctions memories that are essential for the superconducting computer. Recently a Japanese group at ETL has successfully developed and operated a 1 K-bit random access memory RAM [50] . It was fabricated using $Nb/Alo_x/Nb$ and consists of 1024 memory cells known as MVTL (Modified Voltage Threshold Logic) cell and 1028 logic gates making a total of 8512 Josephson junctions integrated an chip of 3.7 mm^2 . The access time (time to read out information stored in the RAM) of this RAM is 500 ps and the total power dissipation is 1.9 mW. Another Japanese team has developed a 4K RAM [56] using new gates and a capacitively coupled single flux quantum (SFQ) memory cell [65]. A comparison of these latest RAMs with previously developed ones is as indicated in table 3.5.

From this table it can be seen that even the best reported RAM still has a 2% bit failure. However these were explained by the authors to be due to deviation from the design for some cells and the presence of microscopic dust for other cells . In other words these difficulties can be easily circumvented and 100% operational bit RAM should be obtained. It is also worth noting that this same RAM is the most successful non destructive readout (NDRO) RAM developed so far.

Table 3.5. Josephson RAM performance

RAM Size & institution	Technology	Memory cell	Access time(ps)	Power (mW)	Operational bits
IBM [66]	Lead-alloy /Nb edge	Henkels	700		
1 K-Bit NTT [67]	Lead-alloy	Henkels	3500	2.0	
1K-Bit NEC [68]	Nb	Henkels	570	6.0	40%
1K-Bit NEC [69]	Nb		570	13	40%
1 K-Bit [50] ETL	Nb	Variable threshold	500	1.9	98%
4 K-Bit FUJITSU [56]		SFQ	590	19	

Another essential element for the superconducting computer is a superconducting microprocessor. A breakthrough has been achieved at Fujitsu (Japan) where the first microprocessor was developed [70]. More recently the same team improved the design of the previous microprocessor and integrated with it on the same chip an instruction ROM, a multiplier, and an accumulator . The result is a processor operating at 1.1 GHz [71] . The materials involved in the fabrication of this processor are summarised in table 3.5 and a cross-section of the Josephson circuit is given in figure 3.16.

Table 3. 5. Process summary (from [71])

Materials				Minimum sizes	
Josephson junction	Insulator	Resistor	Wiring	Junction diameter	Line width
$Nb/AlO_x/Nb$	SiO_2	Mo	Nb	1.5 μm	2.0 μm

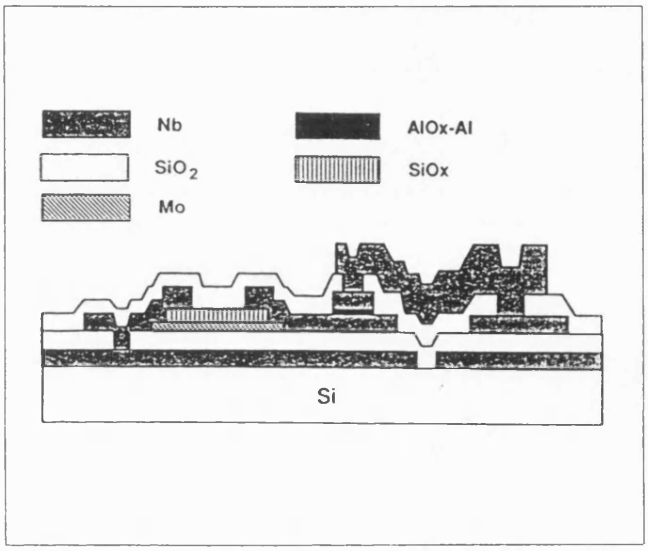

Fig.3. 16. Cross section of integrated circuit with Nb/AlOx/Nb Josephson junction (from ref [71])

A comparison between the performance of the new processor and the previous microprocessor followed by that of semi-conductor based micro-processor is given in Table 3.6.

Table 3.6 Microprocessor performance from (ref [71])

Item	Present	Previous
Minimum size	1.5 μm	2.5 μm
Number of gates	3,056	1,841
Instruction ROM	100 ps	-
Bit-slice microprocessor	1.1 Ghz	770 Mhz
Multiplier-accumulator	200 ps	
Power dissipation	6.1 mW	5.1 mW
Cf. Bit slice microprocessor	Si:30 Mhz/1.4 W [72] GaAs :72 Mhz/2.2 W [73]	

3.5.4 Conclusion

Eight years have elapsed since IBM terminated its project and the superconducting computer is yet to be built. More over their prediction of the entry into service of fast semiconductor computers has proven to be correct . There exist now a generation of fast semiconductor computers that are also called supercomputers whose microprocessor clock time is around 1.5 nanoseconds for the fastest, made by NEC [74] . This performance is not far from that predicted for the superconducting computer.

Nevertheless it is interesting to note that companies like Fujitsu and NEC which are on the forefront in realising a semiconductor supercomputer are not far from developing a

superconductor supercomputer . This is a clear indication that the superconducting computer is holding a firm position in the race for developing the fastest computer.

Chapter 3 references

1 P. K. Tien and J. P. Gordon "Multiphoton process observed in the interaction of microwave fields with the tunnelling between superconductor films ", Physical Rev. 129, pp:647-651 1963.

2 A. H. Dayem , and R. J. Martin, "Quantum interaction of microwave radiation with tunnelling between superconductors", Phys. Rev. Lett. 8, pp:246-248, 1962.

3 M. McColl, M. F. Millea, and A. H. Silver, "The superconductor-semiconductor Schottky barrier diode detector ", Appl. Phys. Lett. 23, pp:263-264, 1973.

4 J. R. Tucker," Quantum limited detection in tunnel junction mixers", IEEE J. Quantum electron., QE-15,pp:1234-1258,1979.

5 H. C. Torrey, and C. A. Whitmer, " Crystal rectifiers ", p. 337, (MTT Radiation Labs Series, Vol. 15), McGraw-Hill, New York, 1948.

6 A. Van Der Ziel, "Fluctuation phenomena in semiconductors", p:88, New York, Academic press, 1959,

7 J. R. Tucker and M. F. Millea , Appl. Phys. Lett. 33, 611, 1978.
See also ref. [4] in this chapter .

8 F. L. Vernon, M. F. Millea, M. F. Bottjer, A. H. Silver, R. J. Pederson, and M. McColl," The super-Schottky diode", IEEE Trans. Microwave theory Tech. MIT-25, pp:286-294, 1977.

9 P. L. Richards, and T. M. Shen, "Superconductive devices for millimetre wave detection, mixing, and amplification ", IEEE Trans. Electron. Devices ED-27, pp:1909-1920, 1980.
P. L. Richards, and T. M. Shen, R. E. Harris , and F. L. Lloyd, "Superconductor -insulator -superconductor quasiparticle junctions as microwave photon detector ", Appl. Phys. Lett. 36, pp:480-482, 1980.

10 H. J. Hartfuss and K. H. Gundlach , Int . J. Infrared millimetre Waves 4, p. 993, 1981

11 F. Habbal , W. C. Danchi, and M. Thinkham ,"Photon-assisted tunnelling at 246 and 604 in small area superconducting tunnel junction", Appl. Phys. Lett. 42, pp:296-298, 1983.

12 M. J. Wengler and D. P. Woody, "Quantum noise in heterodyne detection ", IEEE J. Quantum Electron QE-23, p:613-622, 1987.

13 M. McColl, M. F. Millea, A. H. Silver, M. F. Bottjer, R. J. Pedersen, and F. L Vernon , "The super-Schottky microwave mixer ", IEEE Trans. Magn. MAG-13, pp:221-227, 1977.

14 T. G. Philips, D. P. Woody, G. J. Dolan, and R. E. Miller, " Dayem-Martin (SIS tunnel junction) mixers for low noise heterodyne receivers", IEEE Trans. Magn. MAG-17, pp:684-689, 1981.

15 J. R. Tucker and M. J. Fledman "Quantum detection at mm wave lengths", pp:1055-1113 , 1985.

16 P. L. Richard, T. M. Shen, R. E. Harris, and F. L. Lloyd, "Quasiparticle heterodyne mixing in SIS tunnel junctions", Appl. Phys. Lett. 34, pp:345-347, 1979.

17 G. J. Dolan, T. G. Phillips, and D. P. Woody "Low noise 115 GHz mixing in superconducting oxide barrier tunnel junctions ", Appl. Phys. Lett. 34,pp:347-349, 1979.

18 T. M. Shen, P. L. Richards, R. E. Harris, and F. L. Lloyd, "Conversion gain in mm-wave quasiparticle heterodyne mixers ", Appl. Phys. Lett. 36, pp:777-779, 1980.

19 W. R. McGrath, P. L. Richards, A. D. Smith, H. Van Kempen, R.A. Bachelor, D.E. Prober, and P. Santhanam, "Large gain, negative resistance, and oscillations in superconducting quasiparticle heterodyne mixers ", Appl. Phys. Lett. 39, pp:655-658, 1981.

20 G. J. Dolan, R. A. Linke, T. C. L. G. Sollner, D. P. Woody, And T. G. Phillips, "Superconducting tunnel junctions as mixers at 115 GHz", IEEE Trans. Microwave Theory Tech. MTT-29, pp:87-91, 1981.

21 A. C. Callegari, and R. A. Buhrman, "Millimetre wave mixing with submicron area Nb tunnel junctions", J. Appl. Phys. 53, pp:823-827, 1982.

22 S. K. Pan, M. J. Feldman , A. R. Kerr , and P. Timbie, "Low noise 115 Ghz receiver using superconducting tunnel junctions", Appl. Phys. lett. 43, pp:786-788, 1883

23 E. C. Sutton "A superconducting tunnel junction receiver at 230 GHz", IEEE Trans. Microwave Theory Tech. MTT-31, pp:589-592, 1983

24 L. R. D'Addario "An SIS mixer for 90-120 GHz with gain and wide bandwidth ", Int. J. Infrared Millimetre waves 5,pp: 1419-1442, 1984.

25 W. R. McGrath, A. V. Raisanen, P. L. Richards , R. E. Harris , and F. L. Lloyd, "Accurate noise measurements of superconducting quasiparticle array mixer", IEEE Trans. Magn. MAG-21, pp:212-215, 1985.

26 D. P. Woody, R. E. Miller, and M. J. Wengler, "85-115 GHz Receiver for radio astronomy ", IEEE Trans. Microwave Theory Tech. MTT-33,pp: 90-95, 1985.

27 W. C. Danchi and E. C. Sutton " frequency dependence of quasiparticle mixers", J. Appl. Phys. 60, pp:3967-3977, 1986.

28 T. H. Buttgenbach, R. E. Miller, M. J. Wengler, D. M. Watson, and T. G. Phillips, "A broad -band low noise SIS receiver for submillimetre astronomy", IEEE Trans. Microwave Theory Tech. MTT-36, pp:1720-1725,1988.

29 Qing Hu, C. A. Mears, P. L. Richards, and F. L. Lloyd, "Mm wave quasioptical SIS mixers", IEEE Trans. Magn. MAG-25, pp:1380-1383, 1989.

30 S. K. Pan, A. R. Kerr, M. J. Fledman, A. W. Kliensasser, J. W. Stasiak, R. L. Sandstorm, and W. J. Gallagher, "An 85-116 SIS receiver using inductively shunted edge junction", IEEE Trans. Microwave Theory Tech MTT-37, pp:580-592, 1989.

31 R. C. Jakvelic, J. Lambe, A. H. Silver, and J. E. Mercereau, "Quantum interference effect in Josephson tunnelling", Phys. Rev. Lett. 12, pp:159-160, 1964.

32 C. Tesch and J. Clarke " DC SQUID: noise and optimization", J. Low temperature physics 29, pp:301-331, 1977.

33 J. C. Gallop and B. W. Petley " SQUIDS and their applications", J. Phys. E9, pp:417-429, 1976.

34 J. Clarke "Advance in SQUID magnetometers", IEEE Trans. Elect. Devices ED-27, pp:1996-1908, 1980.

35 R. H. Koch, D. J. Van Harlingen, and J. Clarke, " Quantum noise theory for the DC SQUID", Appl. Phys. Lett. 38, pp: 380-382, 1981.

36 R. R. Voss, R. B. Laibwitz, S. I. Raider, and J. Clarke, "All-Nb low noise DC SQUID with 1 μm tunnel junction", J. Appl. Phys. 51, pp:2306-2309, 1980.

37 J. Knuutilla, S. Ahlfors A. Ahonen J. Halstrom, M. Kajola O. V. Lounsasmaa, V. Vilkman, and C. Tesche, "Large-area low-noise seven- channel DC SQUID magnetometer for brain research", Rev. Sci. Instrumemt. 58, pp:2145-2156, 1987.

38 T.Takami, T. Nogushi, and K. Hamanaka, "A DC circuit amplifier with a novel tuning circuit", IEEE Trans. Magn. MAG-25, pp:1030-1033, 1989.

39 F. C. Welstood, C. Urbina, and J. Clarke, " Low-frequency noise temperature in dc superconducting quantum interference devices below 1 K", Appl. Phys. Lett. 50, pp:772-774, 1987.

40 M. W. Cromar, J. E. Bell, D. Go, K. A. Massarie, R. H. Ono, and R.W. Simon, "Noise in DC SQUID with Nb/Al-Oxide/Nb Josephson Junctions", IEEE Trans. MAG-25, p:1005-1007, 1989.

41 P. Carelli, V. Foglietti, R. Leoni, and M. Pullano," Reliable DC SQUID", IEEE Trans. MAG-25, p.1026, 1989.

42 P. Yang et al "A planar all Nb edge junction DC SQUID ", cryogenics 30, pp:556-560, 1990

43 H. J. M. Ter Brake, J. Flokstra, E. P. Howman, D. Veldhuis, W. Jaszczuk, A. Martinez, and H. Rogala et Al, "Design and construction of 19 channels DC SQUID neuro-magnetometer", Physica B 165-166, pp:95-96, 1990.

44 D.Drung, R. Cantor, M. Peters, H. J. Scheer, and H. Koch, " Low noise high-speed dc superconducting quantum interference device magnetometer with simplified feedback electronics ", Appl. Phys. Lett. 57, pp:406-408, 1990.

45 D. Cohen, "Magnetic fields around the Torso:Production by electrical activity of the human heart", Science 156, pp:652-654, 1967.

46 D. Cohen, "Magnetoencephalography: Evidence of magnetic fields produced by Alpha-Rhythm currents.", Science 161, pp:784-786, 1968.

47 G. L. Romani, "Biomagnetism : an application of SQUID sensors to medicine and physiology ", Physica B-126, pp:70-81, 1984.

48 R. Hari and O. V. Lounasmaa, "Recording and interpretation of cerebral magnetic fields", Science 224, pp:432-436, 1989.

49 C. Cosmelli, P. Carelli, M. G. Castelano, and V. Foglietti,"Long term operation of low noise DC-SQUID coupled to a very high Q gravitational radiation detector", IEEE Trans. Magn. MAG-23, pp:454-457, 1987.

50 I. Kurosawa, H. Nakagawa, S. Kosaka, M. Aoyagi, and S. Takada "A 1 K-bit Josephson random access memory using variable threshold cells", IEEE J. Solid-State Circuit 24, pp:1034-1039, 1988.

51 R. A. Kamper and J. E. Zemmerman, "Noise thermometry with the Josephson effect", J. Appl. Phys. 42, 132-136, 1971.

52 A. Long, T. D. Clark, R. J. Prance, and M. G. Richards , "High performance UHF SQUID magnetometer", Rev. Sci. Instrum. 50, pp:1376-1381, 1979.

53 J. N. Hollenhorst and R. P. Giffard, "High sensitivity microwave SQUID", IEEE Trans. Magn. MAG-15, pp:474-477, 1979.

54 A. P. Long, T. D. Clark,and R. J. Prance, " Varacator tuned ultra-high frequency SQUID magnetometer", Rev. Sci. Instrum. 51, pp: 8-13, 1980.

55 P. V. Czipott, and W. N. Podney, "Measuring magnetic fluctuation from seismic waves using a superconductive gradiometer ", IEEE Trans. Magn. MAG-23, pp:465-468, 1987.

56 H. Suzuki, N. Fujimaki, H. Tamura, T. Imamura, and S. Hasua, "A 4 K Josephson memory", IEEE Trans. Magn. MAG-25, pp:783-788, 1989.

57 J. Matisoo , " Subnanosecond pair tunnelling to single-particle tunnelling transition in Josephson junctions ", Appl. Phys. Lett. 9, pp:167-168, 1966.

58 J. H. Greiner , C. J. Kircher, S. P. Klepner, S. K. Lahiri, A. J. Warneck, S. Basavaiah, E. T. Yen, J. M. Baker, P. R. Brosious, H. C. W. Huang, M. Murakami, I. Ames, "Fabrication process for Josephson integrated circuits", IBM J. Res. Develop. 24, pp:195-205, 1980.

59 H. Kroger, L. N. Smith, and D. W. Jillie, "Selective Niobium anodisation process for fabricating Josephson tunnel junction ", Appl. Phys. Lett. 39, pp:280-282, 1981.

60 A. L. Robinson, " A computer is not just chips", Science 215, pp:42-43, 1982.

61 R. Lewin, "IBM drops superconducting computer project", Science 222, pp:492-494, 1983.

62 M. Gurvich, M. A. Washington, and H. A. Huggens, "High quality refractor Josephson tunnel junction utilising thin aluminium layers", Appl. Phys. Lett. 42 , pp:472-474, 1983.

63 A. Shoji, F. Shinoki, S. Kosaka, M. Aoyagi, H. Hayakawa, Appl. Phys. Lett. 41, p.1097, 1982.

64 A. Shoji, S. Kosaka, F. Shinoki, M. Aoyagi, H. Hayakawa, "All refractor Josephson tunnel junctions fabricated by reactive ion etching ", IEEE Trans. Magn. MAG-19, pp:827-830, 1983.

65 H. Suzuki and S. Hasao, " A capacitively coupled SFQ Josephson memory cell", IEEE Trans. Electron Device ED-35, pp:1137-1143, 1988.

66 Henkel et Al , "Experiment on cross-section of a Josephson RAM chip", Proc. 1983 IEEE Int. Conf. Computer des. pp:570-573, 1983.

67 M. Yamamoto, Y. Yamauchi, K. Miyahara, k. Kuroda, F. Yanagawa, and A. Ishada, " An experimental nanosecond Josephson 1 K RAM using 5-μm Pb-Alloy technology ",IEEE Electron. Devices Lett. EDL-4, pp:150-152, 1983.

68 Y.Wada, S. Nagasawa, and I. Ishida , " AC- and DC-powred subnanoseconds 1 K-bit Josephson cache memory design ", IEEE J. Solide State circuits 23, pp:923-932, 1988.

69 S. Nagasawa, Y. Wada, H. Tsuge, M. Hidaka, I. Ishida, and S. Tahara, "Nb multilayer planirazation technology for a subnanosecond Josephson 1 K-bite RAM ", IEEE Trans. Magn. MAG-25, pp:777-781, 1989.

70 S. Kotani, N. Fujimaki, T. Imamura, and S. Hasuo, " A Josephson 4b microprocessor", in IEEE ISSC Dig. Tech. Papers, pp: 150-151, Feb. 1988.

71 S. Kotani, T. Imamura, and S. Hasuo, " A subnanosecond clock Josephson 4-bit processor", IEEE J. Solid-State Circuits 25, pp: 117-124, 1990.

72 J. Mick, " Am 2900 bipolar processor family ", in IEEE Proc. 8th Annu. Workshop microprogramming, pp:56-63, 1975.

73 N. Hendrickson, B. Larkins, R. Bartolotti, R. Deming, and I. Deyhimy, " A GaAs I_C bit-slice microprocessor chip set", IEEE Proc. GaAs IC Symp. pp:197-200, Oct. 1987.

74 E. Corcoran, "Calculating reality ", Scientific American 264, pp:74-83, 1991

CHAPTER 4: HIGH T_C SUPERCONDUCTING MATERIALS AND THEIR APPLICATIONS

4.1 Introduction

The superconducting materials can be divided in two main groups. The first one consists of superconductors that were discovered before September 1986 having the highest critical temperature T_C =23.2 K achieved with Nb_3Ge [1]. They are referred to as conventional superconductors or low T_C superconductors (LTS). The second and more exotic group first became known in September 1986 when Bednorz and Muller published their discovery of the first of a completely new class of superconductors [2]. This event triggered world-wide intense research among the scientific community and led to the attainment of T_C as high as 125 K because of which these materials have been called high T_C superconductors (HTS). In this chapter, progress within the second group, will be discussed .

4.2 High T_C Superconductors

The compound discovered by Bednorz and Muller consisted of mixture of Barium, Lanthanum, copper and oxygen ($La_{(2-x)}Ba_xCuO_4$) and remained superconducting up to a temperature of 36 K which is far higher than the critical temperature of Nb_3Ge . A few months later the transition temperature rose sharply to 90 K [3] [4] [5]. This is well above the boiling point of liquid Nitrogen and will have considerable consequences on both scientific and commercial instrumentation using devices based on superconducting materials. This T_C of 90 K was achieved with the discovery of a ceramic material that belong to the "Oxygen defect perovskite ". It consists of Yttrium, Barium, Copper and Oxygen . The first three are in the proportion 1 2 3

respectively leading to the chemical formula of the compound $YBa_2Cu_3O_{(7-x)}$ (0< x <0.5) or YBCO in short and whose structure is orthorhombic as shown in figure 4.1 (a) [6] and (b) [7] .

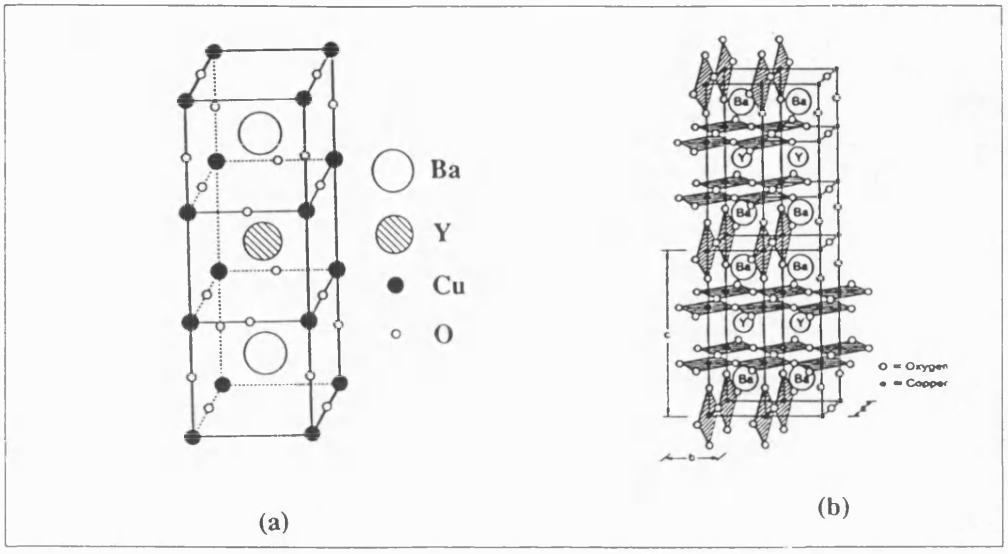

Fig.4.1 Structure of YBCO (from ref. [6],[7])

The crystalographic structure of YBCO shows two main features: Firstly the structure of planes parallel to (a,b) which are referred to as planes layers, and those parallel to c and referred to as chains. These planes and chains have different properties as indicated by measurement of the resistivity for instance where different behaviour is observed as shown in figure 4.2

Secondly the structure of YBCO has oxygen missing from different location within the crystal (oxygen deficient perovskite). The oxygen content is critical as it has direct implications on the properties of YBCO: the quality of the superconductivity of this material increases with the quantity of oxygen within the lattice . Inversely if the oxygen is decreased, ie x increased from 0.5 to 1,

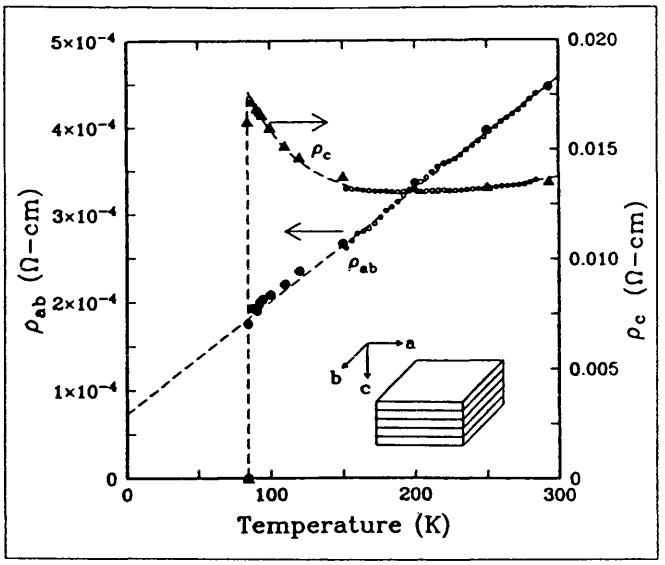

Fig.4.2 Resistivity component of YBCO single crystal (from [8])

a transition to a tetragonal structure occurs. For x approaching 1 the ceramic becomes a semiconductor [9] [10] [11] . Thus oxygen is a key element.

4.3 Other high T_C superconductors

Since YBCO's T_C breakthrough, the list of high T_C superconducting materials has been increasing and table 4.2 summarises the important ones .

From this table (4.2) one can notice that unlike all other compounds BaKBiO3 is a copper free compound and has a cubic structure . The compounds containing Lead belong to the Lead cuprate familly which is expected to have promising potential among high T_C materials which have T_C higher than 100 K [32] [33]. Superconducting features at very high temperatures T_C= 210 [34], 230 [35] , 240 [36], and even 260 K [37] have been observed with YBCO, and the question of room temperature superconductors has rejuvenated research with intense and spirited rivalry.

Table 4.2 High temperature superconductors and their T_c

Compound or system	T_c (K)	References
$La_{(2-x)}Ba_xCuO_4$	36	[2]
$YBa_2Cu_3O_{(7-x)}$ $0<x<1$	90	[4] [12]
$La_{(2-x)})Sr_xCuO_4$ $x=0.2$	36	[13]
$Bi_2Sr_2CaCu_{(8+x)}$ (2212 phase)	85	[14]
$Bi_{(2-x)}Pb_xSr_{(2-y)}Ca_{(2+y)}Cu_3O_{10}$	108	[15] [16]
$Bi_2Sr_2Ca_2Cu_3O_{(10+x)}$ (2223 phase)	110	[17]
Bi-Al-Ca-Sr-Cu-O	114	[18]
Tl-Ba-Cu-O	90	[19]
Tl-Ca/Ba-Cu-O	120	[20]
$Tl_2Ca_2Ba_2Cu_3O_{(10+x)}$	125	[21] [22]
$BakBiO_3$	30	[23]
$YBa_2Cu_xNiO_{(7-x)}$ $0 \leq x < 0.5$	$Tc \leq 90$, $Tc=f(x)$	[24]
$Ln_{(2-x)}Ce_xCuO_{(4-y)}$ Ln=Nd, Pr, or Sm	24 for Ln=Nd	[25]
$Pb_2Sr_2A_{(1-x)}Ca_xCu_3O_{(8+\delta)}$ A:rare earth	70	[26]
Tl-based 2223	127	[27]
$DyBa_2Cu_4O_8$	77	[28]

Sb-Pb-Bi-Sr-Ca-Cu-O	132 112 111	[29] [30] [31]

4.4 Charge carriers

Prior to the discovery of $Ln_{(2-x)})Ce_xCuO_{(4-y)}$ the charges carriers of all high Tc superconductors were holes (electrons vacancies) [38] [39] . However in the $Ln_{(2-x)}Ce_xCuO_{(4-y)}$ family where Ln stands for the lanthanide Nd, Sm, or Pr, the charge carriers are electrons [26]. These compound have the $Nd_2CuO_{(4-y)}$ or $La_2CuO_{(4-y)}$ structure which are shown in figure 4.3 .

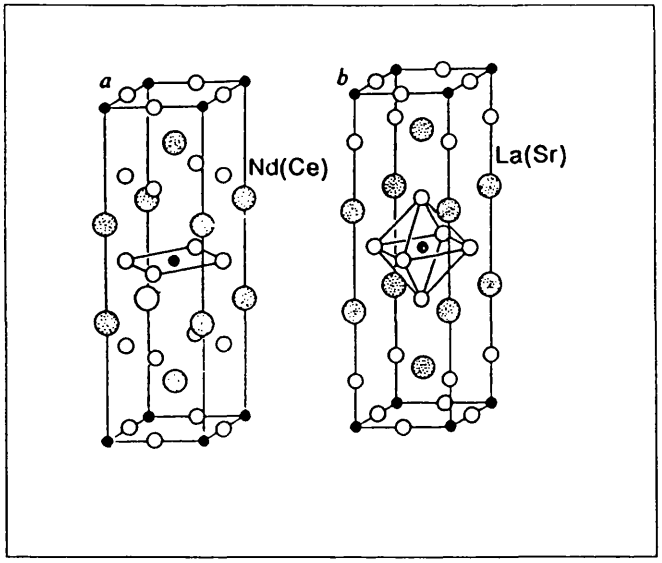

Fig.4.3 Crystal structure of Nd_2CuO_4 (a) and La_2CuO_4 (b) (from ref. [25])

This new family of copper oxide superconductors are believed to have significant implication in the understanding of high temperature superconductivity [40] .

4.5 Superconductivity theories

4.5.1 Introduction

Prior to the discovery of high T_C superconductors , the superconductivity in most materials was described by the BCS theory as briefly discussed in Chapter one. However this theory has been of limited value in predicting properties of materials from consideration such as band structure, electrons-electrons interaction, electrons-phonons interaction. This is particularly true for superconductors with high T_C and Hc values which happened to be the most complicated structurally . This is why all major advances in discovering new superconducting materials have been made experimentally. In an attempt to provide a prediction tool Mathias [41] [42] proposed his semi-empirical rule which states that the T_C of superconductor is determined by the ratio of its valence electron Ne to atom concentration Na i.e. Ne/Na. For the occurrence of superconductivity it is necessary that this ratio should be between 2 and 8 . This rule led to the discovery of the most useful superconductors, particularly the very important class of superconductors known as A15 compounds . This class of superconductors is well documented and many reviews have been carried out [43] [44].

The absence of predictive theory caused many authors to announce contradictory declarations. Some authors [45] [46] suggested that high T_C superconductivity is impossible, whereas others predicted the possibility of the sudden appearance of high T_C superconductors ($T_C \geq$ 100 K) [47]. This latter guess was proved correct by the major discovery of high T_C superconductors. Nevertheless a great deal of effort is required in order to unravel the secrets of these materials particularly the mechanism responsible for their superconductivity at such high temperature . In fact one theorist has shown that 40 K is the upper boundary for phonon mediated superconductivity [48]. Following this line

of thinking there is an almost general consensus that high temperature superconductivity cannot be explained by the BCS theory. This idea seems to be backed by the findings of experimentalists who have reported that high T_C superconductors do not possess the isotopic effect [49], [50]. Others workers found that the specific heat has linear features that cannot be described by the phonon-mediated electron-electron interaction [51] [52] [53] . However this linearity does not appear in recent specific heat measurement [54] . All these anomalies and controversies show the complexity of the phenomenon producing high T_C superconductivity and stress the need for a more adequate theory based on appropriate mechanism which enable it to describe all aspect of these new materials. This has not been developed so far and many theories instead of one are suggested .

4.5.2 High T_C superconductivity theories

The new high T_C superconductivity has spurred a remarkable surge of interest and research activity among theorists attempting to give the appropriate explanation of electron attractive interactions. This has resulted in a rapidly escalating number of theories and models based on different concepts such as phonon mediated pairing [48] , magnetic excitations [55], excitons [56] [57] , bipolarons [58] [59] [60], plasmons [61], solitons [62] [63] , and the resonating valence bond (RVB) [64] [65] . The issue of high T_C superconductivity theories is addressed in a single book [66] in which the author divided these theories in three categories :

- BCS like theories .
- Resonating valence band models .
- Hubbard-like models explicitly including oxygen .

These are just few of the numerous reports that were published on the topic which indicate the intense interest in these intriguing materials .

4.6 High Tc superconductors and the energy gap.

4.6.1 Introduction

For microwave applications, the most important parameter of a superconducting material is the energy gap . Since the discovery of high T_C materials, one of the main preoccupation for the researchers was to prove whether high T_C superconductors, like the conventional superconductors, have an energy gap and if so what can be its value ? Presently the question of the existence is settled positively but many different gap values have been suggested by different authors as will be discussed in the next section.

4.6.2 Energy gap of high T_C superconductors.

There have been many estimate of the values of the gap parameter for YBCO and other HTS superconductors. For YBCO the value of $2\Delta/K_BTc$ was found to vary between 1.6 [67] [68] and 16.7 [69] . Large number of reports have been published describing the different techniques that have been used to measure the gap and the results obtained. In this section the results of only few selected reports will be discussed . One group of researchers [70] was among the first to use both native and artificial barrier YBCO/Nb SIS junctions. Their measurements gave $\Delta_{YBCO}+\Delta_{Nb}=36mV$ which leads to $2\Delta_{YBCO}/K_BTc=8.3$ for T_C(YBCO)= 90 K . However the authors suggested that this value of $2\Delta_{YBCO}/K_BT_c$ was too large and assumed the existence of an YBCO/YBCO junction in series with YBCO/Nb. This correction gives $2\Delta_{YBCO}/K_BTc=2.9$. Another group [69] combined both point contact tunnelling and infrared techniques to measure the gap in YBCO and found $3.7\leq 2\Delta/K_BT_c\leq 5.6$ when using the first method , and $1.6\leq 2\Delta/K_BT_c\leq 3.4$ with the second.

These few examples show the lack of uniformity in the

determination of $2\Delta/K_BT_c$. This turns out to be true of all published reports. A good way to summarise the large variety of gap values is a statistical sketch as shown in figure 4.4 [71] .

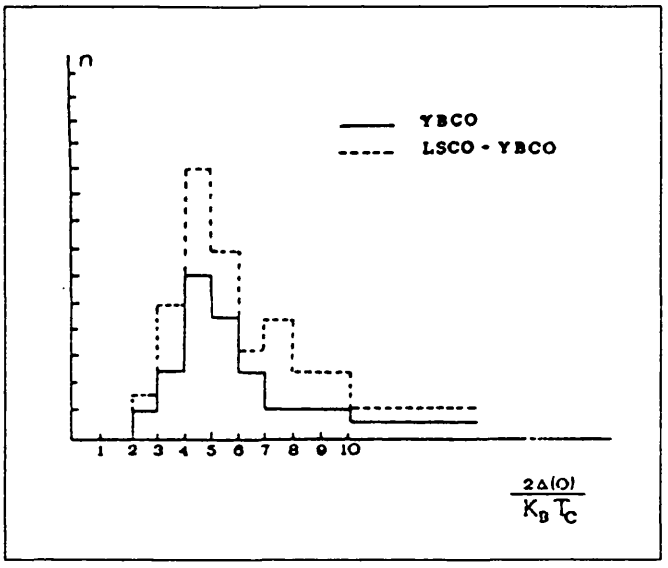

Fig.4.4 Reported values of $2\Delta/K_BT_c$ (from ref [71])

From this graph it can be seen that the most largely reported value tend to collect around $2\Delta/K_BT_c = 4-5$.

4.6.3 Anisotropy of high T_C energy gap

Energy gap anisotropy has been reported by many authors . One team used a broken film edge junction [72]. This consists of breaking a film of the high T_C material along the desired orientation and bringing a Pb electrode in contact with the exposed film edge to form tunnel junctions . The breaking of the film and the contact with Pb is carried out under liquid He in order to obtain a clean surface for tunnelling. The normalised energy gap $2\Delta/K_BT_c$ was measured in the CuO plane ie (a, b) plane and perpendicularly to the

CuO plane ie in the C direction . The results obtained are $2\Delta/K_BT_c = 5.9$ and $2\Delta/K_BT_c = 3.6$ in the direction parallel and perpendicular to the CuO plane respectively.

Another team [73] suggested the existence of two gaps $2\Delta_1/e = 4mV$ and $2\Delta_2/e = 29mV$. In addition this same group observed double peaks features with the higher peak at 400 mV.

Another measurement obtained from a YBCO (thin film)/AlOx/Pt SIN junction gave a gap parameter $\Delta = 11.5meV$ in the direction perpendicular to CuO plane [74] . This YBCO single crystal thin film was epitaxially grown on $SrTiO_3$ and had T_C=85 K which gave $2\Delta/K_BT_c = 3.2$. In the direction parallel to CuO plane two features were obtained at 5 and 17 mV .

A recent investigation on YBCO/I/Pb has led to the identification of anisotropic gap values Δ_{ab} in the plane (a,b) and Δ_c along the c axis having the following values respectively [75] :

$$\Delta_{ab} = 16 - 20meV$$

$$\Delta_c = 5meV$$

4.7 High T_C Specific heat

The specific Heat of HTS is one of the physical properties which is of paramount importance and which can help in the understanding of the nature of superconductivity in these HTS materials. However many unusual features in behaviour have been found in comparison with conventional superconductors. In an early report an anomaly at 220 K was reported [51]. Another specific heat measurement on YBCO has shown a jump at T_C which is sample dependant , a linear term at

$T < T_c$, a large upturn of Cp/T at very low temperatures, and a double peak near T_c showing a double transition from one of the samples [76] as shown in figure 4.5 .

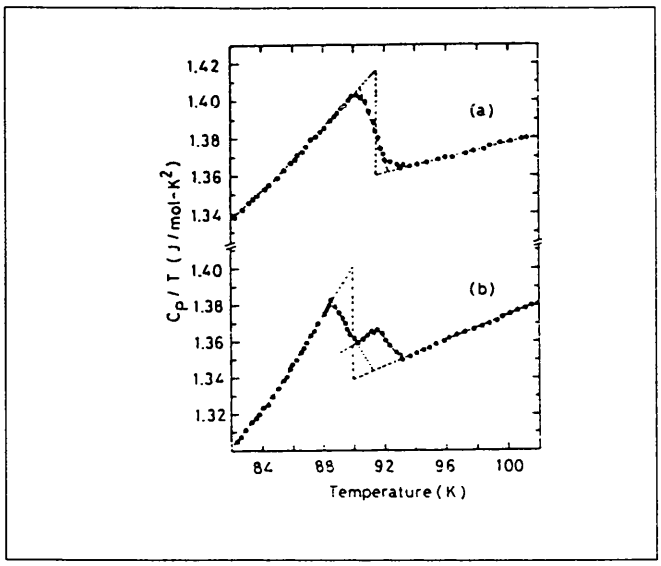

Fig.4.5 Specific heat curves Cp/T vs T from two different samples (From ref [76])

4.8 High T_c parameters

The parameters of HTS have been evaluated by different authors and the following values are mainly extracted from one of the reports [77] and are as indicated in table 4.3 .

In this table λ is the penetration depth, ξ_0 the coherence length and H_{c2} the second critical magnetic field .

Table 4.3 Parameters of high T_c superconductors

Parameter	LTS	HTS YBCO	HTS LaSrCuO
T_c (K)	23<	95	40
λ(Å)	60 (for Nb)	270, 1800 [78]	80, 430
ξ_0(Å)	10^3 -10^4	15, 7	20
H_{c2} (Tesla)	< 60 T	140 T, 280 T	< 90 T

4.9 Environmental and solvent effect on high T_c superconductors

4.9.1 Environmental effects

The high Tc superconductor YBCO is affected by the environment by reacting with water vapour and carbon dioxide . The reaction results in the formation of non superconducting species such as $BaCO_3$ and $Ba(OH)_2$ on the exposed surface of the superconductor [79] [80] [81] [82] [83] . In order to prevent this corrosion effect different researchers used different methods to protect their samples. Some researchers sealed their sample in quartz tubes [84] and reported satisfactory results.

4.9.2 Reaction of YBCO with nonaqueous solutions

The sensitivity of YBCO to moisture must be considered when seeking an etchant, which should be non-aqueous at least. Although other techniques can be used to eliminate surface layers, nonaqueous etching is necessary for depth profiling. Various nonaqueous chemicals have been investigated and a successful etchant, Br in absolute ethanol for YBCO thin film, has been reported [85]. This etchant is said to be effective at removing non-superconducting

sepices while leaving the surface close to the ideal stoichiometry . Moreover its use has been found to be suitable for depth profiling with YBCO films [86] .

4.10 Dopant effect on high T_c superconductors

There are three main reasons for the study of dopants on high T_c superconductors :

First the effect of substituants on properties such as T_c can provide a way of probing high T_c superconductivity.

Second it is desirable to obtain a dense ceramic body approaching the theoretical density and the microstructure having the optimal grain size for high mechanical strength, high critical current density and high critical temperature.

Third interfacial reaction between thin films and substrates or between thin films, single crystals and YBCO pellets and deposited metals or dielectrics can have important effects on high T_c materials. The dopant investigations lead to the determination of the materials that have detrimental effects on HTS and hence their use can avoided.

4.10.1 Effect of many dopants on $YBa_2Cu_3O_{(7-x)}$

Many workers have addressed this issue in numerous investigations [87] [88] . The authors of [87] investigated the effect of seventeen different dopants on YBCO and ended up dividing them into four (4) categories according to their solubility in the lattice of the material :

1) Zn, Mg and Li at 2 mole% dopant level dissolve and substitute in the copper sublatice producing a reduction of T_c to 66, 65, and 82 K respectively.

2) Sr, substitutes in Ba and Y sites and have no significant effect on T_c.

3) Al_2O_3, SiO_2 have limited solubility but have a strong tendency to decompose the superconducting phase by leaching out some component of YBCO.

4) Other anions such as Fe, Co, Ga and Al have been found to substitute for copper in the chain sites [89] .

4.10.2 Effect of Zn and Ni on $YBa_2Cu_3O_{(7-x)}$

The drastic effect of Zn on T_c has been confirmed and Zn anions have been found to substitute for copper in Cu(2) plane [90] [91] . Ni also is found to substitute for copper in Cu(2) plane [90] [91] . In one of the previous investigations [89], Zn and Ni substitution in YBCO was found to give the formula $Ba_2Y(Cu_{1-x}M_x)_3O_y$ (M=Zn or Ni). The authors found that for both M=Zn and Ni with $x=<0.02$, T_c vs y remains flat for $6.8 \leq y \leq 7$ and decreases for $y<6.8$. But for $x = 0.05$ T_c decreases rapidly with decreasing y . For both M=Zn and Ni the variation of T_c against doping level shows that for $y \geq 6.9$ T_c vs x curves are almost identical. However for lower content of oxygen $y<6.90$, T_c vs x curve decreases more quickly. At equal oxygen content the substitution by Zn causes a lower T_c than substitution by Ni which indicates that Zn has a more poisonous effect than Ni.

4.10.3 Effect of Pr in $YBa_2Cu_3O_{(7-x)}$

Incorporated Pr in $YBa_2Cu_3O_{(7-x)}$ was found to substitute for Y and the resulting compound has the formula $Y_{(1-x)}Pr_xBaCu_3O_{(7-x)}$ [92]. When x varies from 0 to 1, T_c decreases monotonically to reach a non superconducting state for $x=0.6$.

4.10.4 Effect of Titanate and Strontium Titanate on $YBa_2Cu_3O_{(7-x)}$

Titanium substitutes for copper according to the formula $YBa_2(Cu_{1-x}Ti_x)_3O_{7-\delta}$ and its effect on T_c seems

to be promising [93]. For $0.02 =< x =< 0.25$ T_c shifted upward to reach the interval between 100 K and 102 K with $T_c(\rho=0)=100$ K for most of the x values .

4.10.5 Effect of fluoride on $YBa_2Cu_3O_{(7-x)}$

The effect of Fluorid doping of YBCO caused excitement among physicist after reports claiming a T_c =155 K [94] . However when this experiment was repeated by other workers in the field [95] higher T_c did not materialise and the highest T_c achieved was 93 K which decreases if fluoride concentration was varied from its optimum value x=0.2 that gave T_c = 93 K as shown in figure 4. 6

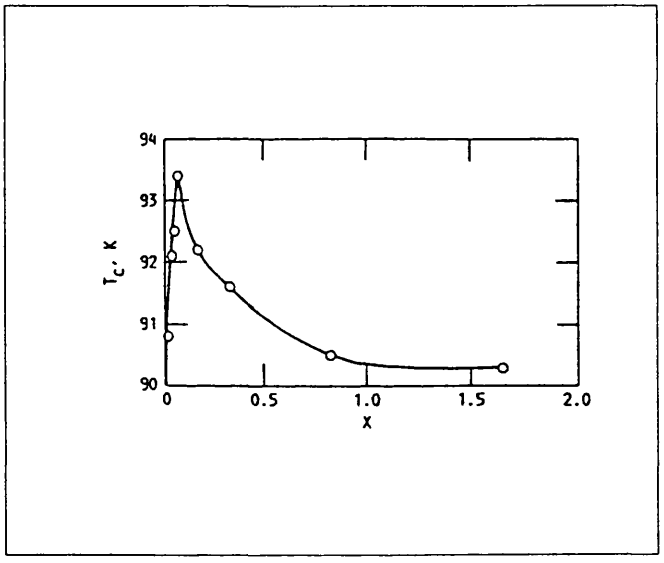

Fig.4.6 Effect of Fluoride on T_c of YBCO (From ref. [95])

4.10.6 Liquid nitrogen effect on YBCO

Many workers have studied the effect of liquid nitrogen on the transition temperature of YBCO and contradictory views have been expressed . Some groups found that exposure of YBCO to cold gas or liquid nitrogen can increase T_c [96] [97] [98] . An increase of T_c by nearly 40 K was observed

by a second group who suggested that this increase could be explained by condensation of nitrogen gas in porous ceramic [99]. Another group investigated the same effect and observed no increase in T_c [100].

4.10.7 Effect of Beryllia (BeO)

The effect of beryllia (BeO) on YBCO has been investigated and was found to have non detrimental effect on the superconducting properties of YBCO [101] and thus its potential as a nonpoisonous substrate is promising . In addition its lower dielectric constant and higher thermal conductivity relatively to $SrTiO_3$ and $LaAlO_3$ make of BeO a better substrate material for device applications based on YBCO .

4.10.8 Simulation of dopant effect on $YBa_2Cu_3O_{(7-x)}$

Simulation of the effect of dopant substitution in YBCO using computers has been carried out striking similarities with the previous dopant experiments were obtained [102].

4.10.9 Dopant effect on superconductor parameters

As an example of doping that can occur between a film and its substrate and which usually result in a depression of T_c, it may be useful to show the effect of different substrates on the T_c of YBCO thin film [103] . This is indicated in figure 4.7 .

The doping of high T_c superconductors affects not only T_c but also the energy gap parameter Δ which was found to be depressed when the superconductor is in direct contact with metal such as Pb, Nb, Au, and Pr [104] [105] .

Other parameters which characterise the superconductors such, the coherence length ξ, the penetration depth λ, the critical current Jc, and the critical magnetic Field Hc are

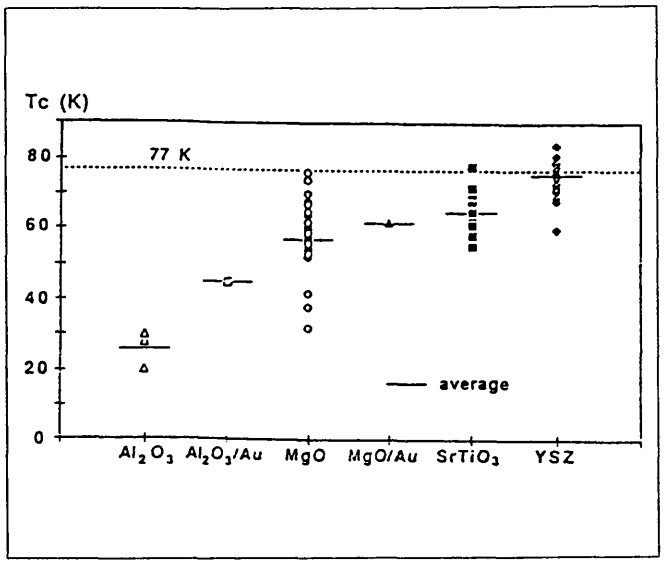

Fig.4.7 Substrate effect on T_C of YBCO thin film (from ref. [103])

related to T_C and Δ . Each of these parameters can prove to be crucial for different applications. Therefore particular attention must be given to the doping levels during sample preparation.

4.10.10 Conclusion

From the results of YBCO doping discussed above, one can divide the dopants into three main classes. First the elements with drastic poisonous effects which should be avoided: Zn, Ni, Al, Pr. Second the elements with intriguing effects on T_C such as N_2, and F_2 for which more thorough investigations is needed before drawing final conclusions . Third elements which have neutral or slightly positive effect on YBCO such as Ti, $SrTiO_3$, YSZ, BeO, and even MgO. These can be used as substrate materials in the manufacturing of HTS electronic devices.

So far the effect of doping has mainly been considered in YBCO as this is the material used for sample making in

this thesis. Nevertheless a great deal of doping work is being carried out with all HTS and the number of reports published is increasing rapidly and doping investigations are almost becoming a subject on their own.

4.11 High T_c applications

The unprecedented enthusiasm that has accompanied the discovery of HTS was due partly to the breakthrough in achieving such a high T_c, and partly to the wider application horizons opened up the possible use of liquid nitrogen instead of cumbersome liquid Helium cryogenic systems. Liquid nitrogen is not only about 12 times cheaper than liquid helium, but it is also a more effective cooler because of its larger heat of vaporisation . This will help bring certain large scale applications (e.g levitated trains) closer. In addition to a high T_c these materials must also possess a critical current Jc of the order of $10^4 A/cm^2$ if they are to replace conventional superconductors. Although current density of that order have been achieved in single crystals and thin films, they are still lower by one to two orders of magnitude in sintered pellets because of their granular structure . Small coherence length and anisotropy characterise these materials. Further more standard methods for fabricating electronic devices are not effective for these materials. These characteristic make it difficult to produce and operate electronic devices made from high T_c superconductors. Nevertheless a wide range of applications using HTS have been reported and the most important will be briefly reviewed in the next sections.

4.12 High T_c detectors

The device at the heart of many superconductor device application is the superconductor tunnel junction . Unfortunately it was found very difficult to extend the

existing technologies to SIS junction made from high T_c superconductors such as YBCO. The basic reason for this is that HTS are processed at a temperature of about 600 C . At such high temperature it is impossible to maintain the integrity of an insulating layer. As a consequence and until recently other types of weak link such as the microbridge and point contacts or even weak links formed in granular films have been used as will be discussed in the next sections. In addition these devices are operated at liquid nitrogen temperature and hence they will inevitably exhibit higher noise than their conventional counterparts.

4.12.1 High T_c mm and microwave detectors

Most of the high T_c microwave detectors rely on the so called "native junction" or weak link which is due to the granular nature of these materials. The use of granular superconducting films as detectors was investigated and demonstrated in the seventies using granular thin films of conventional superconductors [106] [107]. The observation of ac Josephson effect in YBCO can be explained by considering it to be a network of Josephson junctions [108]. The evidence for the existence has been reenforced by the detection of microwave signals emitted by granular thin films [109] . Direct detection of microwave power by an YBCO film deposited on MgO has been investigated and a responsivity of 1 KV/W at a temperature of 50 K with a biasing current of 1 mA [110] . This was achieved using a square film . When a strip structure was used, a responsivity of 10 KV/W was obtained at a biasing current of 100 μA . Another team of researchers [111] have used granular thin film of YBCO and BCSCO (Bi-Ca-Sr-Cu-O) deposited on MgO or ZrO_2 to observe detection mixing and emission of microwave radiation. The samples used were strips 80-300 μm wide and 2-3 mm long . The measurement were carried out at frequencies

between 25 to 110 GHz. The sensitivity was found to increase with decreasing temperature for YBCO-on-ZrO_2 and BCsCO-on-MgO as shown in figure 4.8 (a) and (b) .

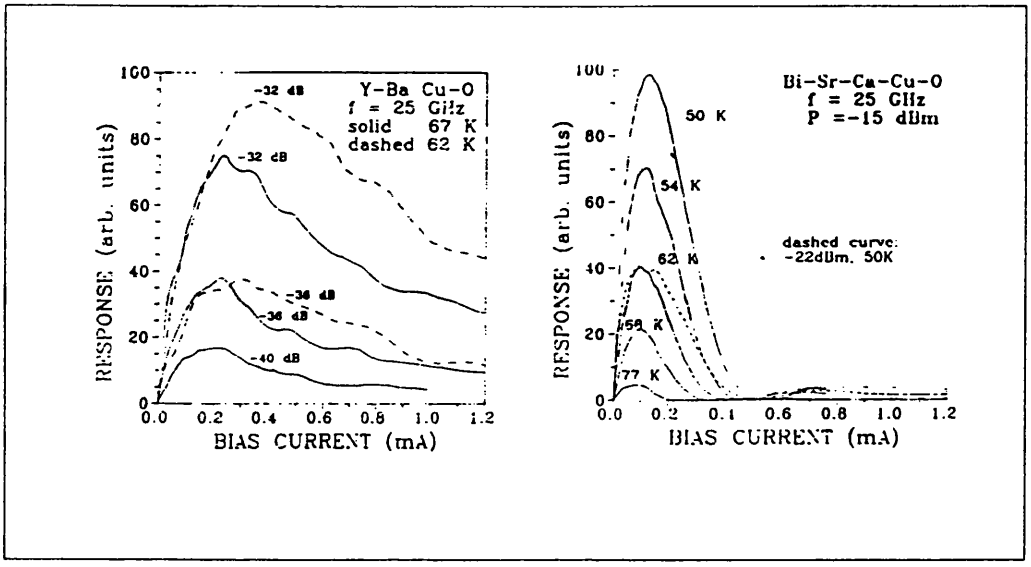

Fig.4.8 (a) Video response of YBCO-on-MgO Vs Bias current at two Different temperatures (b) Video response of BCSCO-on-MgO Vs Bias current at different temperatures (From ref. [111])

However In the case of the YBCO-on-MgO detector, the reduction of operating temperature under 65 K, rendered the properties of the detector sensitive to bias current in a complicated manner. This is also true for YBCO-on-ZrO_2 for a temperature below 50 K the response of the detector is shown in figure 4.9 .

The performance of this detector at 110 GHz was found to be only 6 dB worse than a 1N53 commercial crystal detector. Despite these encouraging results the authors admitted that the lack of a complete understanding of the relevant physical mechanisms makes these devices difficult to optimize and a challenging research problem . In addition the high frequency limit which is determined by the energy gap falls

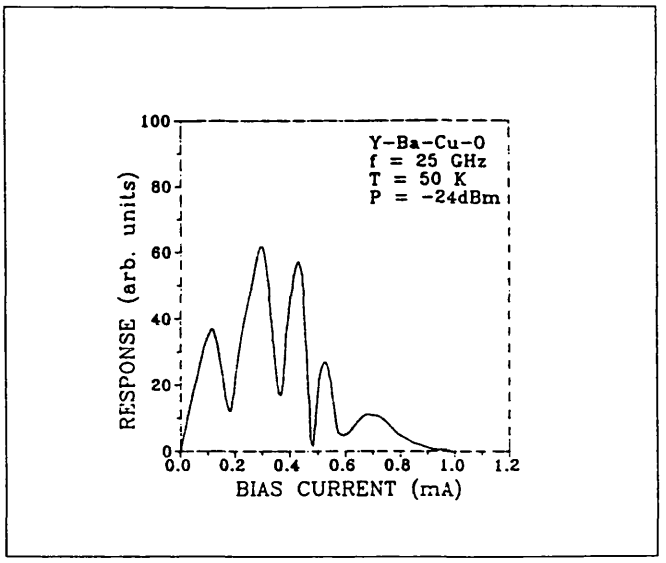

Fig.4.9 Video response of YBCO-on-ZrO_2 detectors at 50 K (From ref. [111])

in the terahertz range. Preliminary experiment made by the team, show that the video response decreases by one order of magnitude as the carrier frequency increases from 100 and 300 GHz [112].

4.13 High T_c mixers

From the experience of SIS conventional mixers it is known that one requirement is a sharp current onset at the gap voltage. Mixing has been found to occur up to the energy gap V_g [113] . If an average value of V_g= 14 meV is assumed this leads to a potential mixing up to 10 THz.

Mixing experiments at 25 GHz have been carried out using the granular thin film strip described in the previous section [117]. The mixing action is also thought to be due to the presence in the granular film of a network of Josephson-type weak-links . The YBCO mixer IF output is indicated in figure 4.10

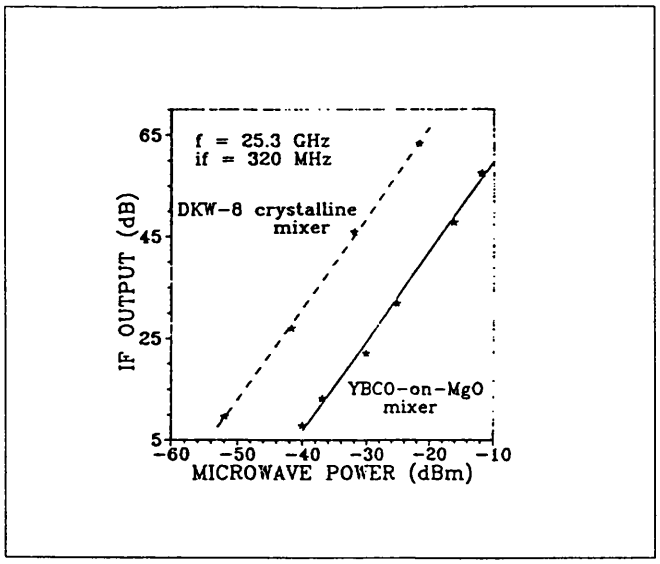

Fig.4.10 IF output vs microwave signal for YBCO-on-MgO (From ref. [111])

In this figure, the output of DKW-8 mixer is also shown for comparison purpose. Heterodyne mixing using YBCO microbridge has been carried at a 20 GHz [114] . The mixer was found to operate stably at temperature below 60 K and has potential for high sensitivity and good impedance matching because of its large dynamic resistance and high R_N (Normal state resistance) .

Mixing experiment at 61 GHz using weak link grain boundary in a $Tl_2CaBa_2Cu_2O_8$ thin film has been reported [115]. A narrow band IF output was obtained at 1 GHz as indicated in figure 4. 11. The signal to noise ratio was about 10^4

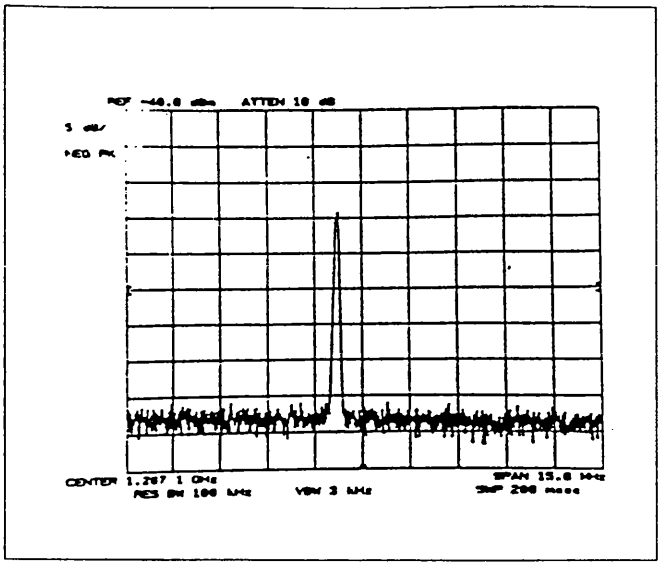

Fig.4.11 Output IF signal centred at 1 GHz (From ref. [115])

4.14 High T_c SQUIDs

High T_c SQUIDs constitute one of the potentially most important area of high T_c superconductor device application if one considers the number of reports presented on both RF and DC SQUIDs . This is due to the structure of these devices which allow the use of the technique known as the "break junction" [116], thin film microbridge [117] [103], and also the point contact [118] [119]. The results of some published work is summarised in the following tables.

Table 4. 10 High T_C DC SQUID performance

Performance	Operating temperature.	Type of DC SQUID	References
$4.10^{-4}\Phi_0/\sqrt{Hz}$	77	Bridge on YBCO	[120]
5.10^{-28} JHz^{-1}	78	Two holes on YBCO	[121]
$0.2\ 10^{-7}$ Φ_0^2/Hz (at 100 Hz)	77	Single grain boundary	[122]
$0.8\ 10^{-7}\Phi_0^2/Hz$ at 1000 Hz	77		

Although HTS SQUID operation is similar to the LTS counterpart , there are differences such as non-uniform quantum magnetic field periods in the triangular pattern, hysterisis effects, a reduction of the flux noise at 4.2 K which does not follow the thermal noise temperature dependence [125].

Table 4. 11 High T_C RF SQUID performance

Performance	Operating temperature	Type of Rf SQUID	References
4.510^{-4} $\Phi_0/\sqrt{Hz}$	77	Break junctions	[116]
$10^{-3}\Phi_0/\sqrt{Hz}$	77	Two holes made of YBCO	[123]
5 10-4$\Phi_0/\sqrt{Hz}$	77	Double hole made of YBCO	[124]
$6.010^{-4}\Phi_0/\sqrt{Hz}$	77	Single and double hole made of YBCO pellet	[125]
$1.510^{-4}\Phi_0/\sqrt{Hz}$	82	YBCO step edge	[126]
2 $10^{-4}\Phi_0/\sqrt{Hz}$	42	Ion implanted microbridge	[127]
8 $10^{-4}\Phi_0/\sqrt{Hz}$	38		
5 $10^{-4}\Phi_0/\sqrt{Hz}$	74	Step edge microbridge	

4.15 High T_c computer applications

Like low temperature superconductors high T_c superconductors have good potential for computer applications . In this respect a family of logic gates (AND, EXOR, EXNOR) based on the YBCO SQUID have recently been reported [128]. The best inverter operated at 36 μV with 2 nW of gate dissipation. These logic circuits are key components of digital system and hence of the future HTS computer.

4.16 High T_c space applications

The weight and volume of cryogenic systems needed by conventional superconductor have prevented the use of these latter in space except in special cases . With the discovery of HTS the refrigeration burden has been greatly reduced and made the use of superconductor in space more acceptable. In order to demonstrate the possibility of the practical use of HTS superconductor devices in space, the US Naval Research Laboratory launched a program in 1988 known as the High Temperature Superconductivity Space Experiment (HTSSE) [129]. This program aims to produce devices which are essentially passive microwave and millimetre wave components. After space qualification these will be incorporated into a specially designed cryogenic measurement system which will constitute the space package to be launched in 1992.

4.17 Other device applications

In addition of the major applications discussed in the previous sections, HTS applications extend to many other equally important such as optical and infrared detectors [130] [131] [132] [133], and superconducting base transistors SBT [134] [135] [136] which are expected to be used as microwave amplifiers operating at several hundred GHz [137].

HTS microwave filter have also been fabricated using YBCO thin film [138] [139] . One of the YBCO pass-band filter was found to be found to have a pass-band insertion loss of 0.3 dB compared to that of gold (2.8 dB) in the

same measurement conditions ie T= 77 K and centre frequency f=4 GHz . A microwave cavity made of bulk YBCO has been fabricated and was found to be resonant at 7 GHz with a quality factor of 10^5 at 25 K [140] . Finally it has been found that high T_c granular film can generate radiations which were found to be in the X band for the particular film strip reported [141].

This wide range of HTS device applications alone show that these materials will play a major role in microwave technology in the future .

Chapter 4 references

1 L. R. Tesdari Physics Today 26 , p.17, 1973.

2 J.G.Bednorz and K.A.Muller, "Possible High T_C superconductivity in the Ba-La-Cu-O system", Z.Phys.B 64, pp:189-193, 1986 .

3 C. W. Chu, P. Hore , R. L. Meng, L. gao, Z. J. Huang , and Y. Q. wang, " Evidence for superconductivity above 40 K in la-Ba-Cu-O compund system ", Phys. Rev. Lett. 55, pp.405, 1987.

4 M. K. Wu, J. R. Ashburn, C. J. Torng, P. H. Hore, R. L. Meng, L. Gao, Z. J. Huang, Q. Wang, C. W. Chu, "Superconductivity at 93 K on new mixed phase Y-Ba-Cu-O compound system at ambiant presuure ", Phys. Rev. Lett. 58, p.908, 1987.

5 P. K. Callghar , H. M. O'brayan , S. A. Sunshine , and D. W. Murphy, Mat. Res. bull., 22, pp:995-1006, 1987.

6 S. I. Koriyama, K. Sakuyama, T. Meada, H. Yamauchi, and S. Tanaka "Superconductivity in Pb-based layered copper oxides $(Pb_{0.5}Cu_{0.5})(Sr, Ba)_2(Y,Ca)Cu_2O_7$", Physica C 166, pp:413-416, 1990.

7 J. B. Torrence , Y. tokura, and Nazzai, Chemtronix 2, p.120, 1987.

8 S. W. Tozer, A. W. Kleinsasser, T. Penney, D. Keiser, and F. Holtzberg, " Measurement of anisotropic resistivity and hall effect constant for single crystal $YBa_2Cu_3O_{7-x}$", Phys. Rev. Lett. 59, p.1768, 1987.

9 E. T. Muromashi, Y. Uchida, M. Isii, T. tanaka, and K. Katao, "High Tc Superconductor $YBa_2Cu_3O_{7-y}$ ", Jap. J. Appl. Phys. 26,pp:1156-1158, 1987.

10 Z. Z. Wang, J. Clayhold, N. P. Ong, J. M. Tarascon, L. H. Green, W. R. Muckinnon, and G. W. Hull, " Variation of superconductivity with carrier concentration in oxygen doped $YBa_2Cu_3O_{7-y}$ ", Phys. Rev. B36, pp:7222-7225, 1987.

11 R.J. Cava, A. H. Hewat, E. A. Hewat B. battlogg, M. marezio, K. M. Rabes, J. J. Krajewski, W. F. Peck, and L. W. Rupp, " Structural anomalies, oxygen ordering, and superconductivity in deficiant $YBa_2Cu_3O_{7-x}$ ", Physica C 165, pp.419, 1990.

12 R. J. Cava, B. Battlog ,C. H. Chen, E. A. Rietman, S. M. Zahurak, and D. Werder, "Oxygen stoichiometry, Superconductivity and normal states properties of YB2C3O(7-x) ", Nature 329, pp.423, 1987.

13 R.J. Cava, R. B. Van Dover, B. Batlogg, and E. A. Rietman " Bulk superconductivity at 36 K in $La_{1.8}Sr_{0.2}CuO_4$", Phys. Rev. Lett. 58, pp:408-410, 1987.

14 H. Meada, Y. Tanaka, M. Fukutumi, and Asano, Japn. J. Appl. Phys. 27, L209, 1988.

15 N. Kitima, H. Endo, J. Tsuchiya, A. Sumyama, M. Mizuno, Y. Oguri, Jpn . J. Appl. Phys. 27, p.1852, 1988.

16 T. Brousse, R. Retoux, G. Poulain, J. Provst, H. Murray, D. Bloyet, B. Raveau, Appl. Phys. A 49, p.217, 1989.

17 J. M. Tarascon, W. R. McKinnon, P. Barboux, D. M. Hwang, B. G. Bagley, L.H. Green, G. W. Hull, and Y. Lepage, Phys. Rev. B 38, p.8885, 1988.

18 C. W. Chu, J. Bechtold, L. Gao, P. H. Hor, Z. J. Huang, R. L. Neng, Y. Y. Sun, Y. Q. Wang, and Y. Y. Xue, "Superconductivity up to 114 in the Bi-Al-Ca-Sr-Cu-O compound system without rare earth element", Phys. Rev. Lett. 60, pp:941-943, 1988.

19 Z. Z. Sheng, A. M. Herman, and A. El Ali, C. Almasan, J. Esterda, and T. Datta, "Superconductivity in the Tl-Ba-Cu-O system", Phys. Rev. Lett. 60, pp:937-940, 1988.

20 Z. Z. Sheng, and A. M. Hermann, "Bulk superconductivity at 120 K in the Tl-Ca-/Ba-Cu-O system", Nature 332, pp:138-139, 1988.

21 R. M. Hazen, L.W. Finger, R. J. Angel, C. T. Prewit, N. L. Ross, C. G. Hidiacos, P. J. Heaney, D. R. Veblem, Z.Z. Sheng, A. El Ali, and A. M. Hermann, Phys. Rev. Lett. 60, pp. 1657, 1988.

22 D. S. Ginley, E. L Venturini, J. F. Kwak, R. J. Baughman, M. J. Carr, P. F. Hlava, J. E. Schirber , and B. Morosin, Physica C 152, p.217, 1988.

23 R. J. cava, B. Batlog, J. J. Krajewski, R. Farrow, L. W. Rupp Jr., A. E. White, K. Short, W. F. Peck, and T. Kometani, "Superconductivity near 30 K without copper: The $Ba_{0.6}K_{0.4}BiO_3$ perovskite", Nature 332, pp:814-816, 1988.

24 Z. Yong, S. Shifang, S. Zhenpeng, C. Zuyao, and Z. Quirui, "Localisation of electrons and superconductivity in $YBa_2Cu_{(3-x)}Ni_x$", Sol. State Communications 67, pp:31-33, 1988.

25 Y. Tokura, H. Takagi, and S. Uchida, " A superconducting copper oxide compound with electrons as the charge carriers", Nature 337, p.245, 1989.

26 R. J. Cava, B. Battlog, J. J. Krajewski, L. W. Rupp, L. F. Schneemeyer, T. Siegrist, R. B. Van Dover, P. Marsh, W. F. Peck, P. K. GallAgher, J. H. Marshall, R. C. Farrow, J. V. Waszczack, R. Hull and P. Trevor, Nature 336, p.211 , 1988.

27 T . Kaneko, H. Yamouchi, and S. Tanaka, " Zero-resistance of Tl-based 2223 superconductor increased to 127 K ", Physica C 178, p:377-382, 1991.

28 R. M. Hazen, L. W. Finger D. E. Morris, "Crystal structure of a new 77 K bulk superconductor ", Appl. Phys. Lett. 54, pp:1057-1059, 1989.

29 L. Hongabo, C. Liezhao, Z. Ling, M. Zhgiang, L. Xiaoxian, Y. Zhidong, X. Bai, M. Zianglei, Z. Guien, R. Yaozhong, C. Zhaojia, and Z. Yuheng, Solid State comm. 69, p.867, 1989.

30 M. R. Chandrachood, I. S. Mulla, and A. P. B. Sinha, Appl. Phys. Lett. 55, p. 1472, 1989.

31 N. Kijima, R. Gronsky, H. Endo, Y. Ogari, S.K. McK ernan, and A. Zettl, Jpn. J. Appl. Phys. (To be published) . See also , Appl. Phys. Lett. 58, p.188, 1991.

32 B. Raveau, C. Michel, M. Hervieu, D. Groult, and J. Provost, " Layered Lead cuprates : promising high Tc superconductors", Adv. Mater. 2, p.299, 1990.

33 S. Koriama, K. Skuyama, T. Meada, H. Yamauchi, and S. Tanaka, "Superconductivity in Pb-based layered copper oxides, $Pb_{0.5}Cu_{0.5}(Sr, Ba)_2Cu_2O_7$", Physica C 166, pp:413-416, 1990.

34 D. Djurek, M. Prester, S. Knezovic, Dj. Drobac, O. Milat, E. Babic, N. Brincevic, K, Furik, Z. Medunic, and T. Vukelja, "Low Resistance state up to 210 K in mixed compound Y-Ba-Cu-O", Physics Letters A 123, pp:481-484, 1987.

35 C. X. Huang, L. J. Dries, P. H. Hor, R. L. Meng, C. W. Chu, and R. B. Frankel, " Observation of possible superconductivity at 230 K ", Nature, 328,pp:403-404, 1987.

36 J. T. Chen, L. E. Wenger, C. J. McEwan, and E. M. Logothetis, Phys. Rev. Lett. 58, pp:1972-1975, 1987.

37 P. Ayyub, P. Guptasamara, A. K. Rajarajan, L. C. Gupta, R. Vijayarghavan, and M. S. Multani, " Evidence for transient superconductivity near 260 K", J. Phys. C: Solid State Phys. 20, L673-L676, 1987.

38 J.T. Chen, C. J. McEwan, L.E. Wenger, E. M. Logothetis, "Determination of charges carriers in superconducting La-Ba-Cu-O by thermoelectric measurements", Phys. Rev. B 35, pp:7124-7125, 1987.

39 M. Galffy and E. Zirngiebl, "Hall-effect of bulk $YCa_2Cu_3O_{(7-x)}$", Solid State Commun. 68, pp. 929-933, 1988.

40 V. J. Emery , "Electron doping tests theories", Nature 337, p.306, 1989.

41 B.T Matthias, "superconductivity in the periodic system", Progress in low- Temperature physics 2, p.138, 1957.

42 B.T. Matthias, Phys. Rev. 97, p. 74,1955

43 B. T. Mathias, T. H. Gebbal, S. Geller, and E. Corenzwit, Phys.Rev. 95, p. 1435, 1954

44 J. Muller, " A15-type superconductors", Rep. Prog. Phys. 43, pp:641-687, 1980.

45 J. C. Phillips, "Superconductivity mechanism and covalent stabilities", Phys. Rev. Lett. 29, pp:1551-1154 , 1972.

46 M. L. Cohen and P. W. Anderson,"Sperconductivity of d and f band metals ", A. I. P. Conference (Rochester ,New York), 1971.

47 V. L. Ginzburg and D. A. Kirzhintz, "High temperature superconductivity", New York :Plenum , 1982 .

48 W. Weber, Phys. Rev. Lett. 58, p.1371, 1987.

49 L. C. Bourne, M. F. Crommie, A. Zettle, Hans-Conrad Zur Loye, S. W. Keller, K. L. Leary Angelia M. Stag, K. J. chang, Marvin L. Cohen, and Donald e. Morris, "search for isotopic effect in superconducting material", Phys. Rev. Lett. 58, pp:2337-2339, 1987.

50 B. Battlog, R. J. Cava ,A. Jayrama, R. B. Van Dover,G. A. Kourouki, S. Sunshine, D. W. Murphy L. W. Rupp, H. S. Shen, A. White, K. T. Short, A. M. Mujsce, and E. A. Rietman, "Isotopic effect in high T_c superconductors $YBa_2Cu_3O_7$ and $Ba_2EuCu_3O_7$", Pys. Rev Lett. 58, pp:2333-2336, 1987.

51 T. Lagreid, K. Fossheim, E. Sanvold, and S. Julsrud, " Specific heat anomaly at 220 K connected with superconductivity at 90 K in ceramic YBa2Cu3O(7-δ)", Nature 330, pp:637-638,1987.

52 R. A. Fisher, J. E. Gordon and N. E. Phillips, "Specific heat, clues for theory", Nature 330, pp:601-602, 1987.

53 P. W. Andrson and E. abrahams, "Superconductivity theories narrow down", Nature 327, pp:363-363, 1987.

54 M. Sera, S. Kondoh, K. Fukuda and M. Sato, "Absence of the T linear term in low Temperature specific heat of high T_c oxides Bi-Sr-Ca-Cu-O system", Sol.State .Comm. 66, pp:1101- 1103, 1988.

55 V. J. Emery "does magnetism hold the key ", Nature 328 pp:756-757,1987
V. J. Emery " Theory of high T_c superconductivity in oxide ", Phys. Rev. Lett. 58, pp:2794-2797, 1987.

56 B. halperin and R. Englman, "Excitons-mediated electron-pairing and high T_c Superconductivity ", Sol. St. Com. 66, pp:711-714, 1987.

57 D. Allender, J. Bray, and J. Bardeen , "Model for an exciton mechanism of superconductivity ", Phys. Rev. B 7, pp:1020-1028, 1973.

58 N. F. Mott, "Is there any explanation ?", Nature 327, pp:185-186,1987 .

59 A. S. Alexandrove, J. Ranninger, S. Robaszkiewicz, "Biplaronic superconductivity : Thermodynamics , magnetic properties, and possibility of existence in real space ", Phys. Rev. B 33, pp:4526-4546, 1986.

60 L.J. De Jongh "An exchange bipolaronic model for high T_c superconductivity", Sol. St. Com. 65, pp:963-972, 1988.

61 J. Rujvalds "Plasmons and high T_c superconductivity in alloy copper oxides", Phys. Rev. B 35, pp:8869-8872, 1987.

62 A. Bishop "Solitons and superconductivity ", Nature 330, p.418, 1987.

63 T. D. Lee "Possible relevance of solitons solution to superconductivity", Nature 330, pp:460-461, 1987.

64 P. W. Anderson, Science 235, pp:1196-1198, 1987.

65 P. W. Anderson et al., Phys. Rev. Lett. 58,p. 2790, 1987.

66 J. Woods Hally "Theories of high temperature superconductivity ", Addison-Wesley Publishing company, 1988.

67 J. R. Kirtley, R. T. Collins, Z. Schlesinger, W. J. Gallagher, R. L. Sandstorm, T. R. Dinger, and D. A. Chance, " Tunnelling and infrared measurement of the energy gap in the high critical temperature superconductor Y-Ba-Cu-O", Phys. Rev. B 35, pp:8846-8849, 1987.

68 P. E. Slewski, A. J. Silver, S. E. russek, H. D. Hallen, D. K. Lathrope, and R. A. Buhrman, Phys. Rev. B 35, p.5330, 1987.

69 J. C. Wan, A. M. Goldman, and J. Maps, " Electron tunnelling in single crystal of $YBa_2Cu_3O_{7-x}$ ", Physica C 153-155 , pp:1377-1378, 1988.

70 M. G. Balmir, G. W. Morris, R. E. Somekh and J. E. Evette, " Fabrication and properties of superconducting devices structures in YBa2Cu0(7-x) thin films", J. Phys. D 20, pp:1330-1335, 1987.

71 A. Barone , " Tunnelling spectroscopy on high Tc superconductors : certainties clues and ambiguities", Physica C 155-155, pp:1712-1717, 1988.

72 J. S. Tsai, I. Takeuchi, J. Fujita, T. Yoshitake, S. Miura, S. Tanaka, T. Terashima, Y. Bando, K. Iijima, and K. Yamamoto, " Observation of gap anisotropy in $YBa_2Cu_3O_{7-\delta}$, Physica C 153-155, pp:1385-1386,1988.

73 M. Reiffers et Al ,"Point contact properties of YBaCuO", Physica C153-155, pp:1387-1388, 1988.

74 J. Takad, T. Terashima, Y. Bando, H. Mazaki, K. Lijima, K. Yamamoto, and K. Hirata, " Tunnel junctions using oxide superconducting thin films epitaxially grown on $SrTiO_3$ ", Appl. Phys. Lett. 53, pp:2689-2691, 1988.

75 I. Igushi and Z. Wen, "Tunnel gap structure and tunnelling model of the anisotropic YBaCuO/I/Pb junctions", Physica C 178, pp:1-10, 1991.

76 M. Ishikawa, Y. Nakazawa, T. Takabatake, A. Kishi, R. Kato, and A. Measono, " Specific heat study on samples of Ba2YCu3O7 with a double superconducting transition ", Solid State Communications 66, pp:201-204, 1988.

77 S. A. Wolf, V. S. Kreisin, "Major parameters of high T_c oxides", IEEE Trans. Magnet. MAG- 27, pp:852-853, 1991.

78 W. J. Callagher, " Studies at IBM on anisotropy in single crystals of high temperature oxide superconductors YB2Cu3O(7-x)", J. Appl. Phys. 63, p.4126, 1987.

79 N.P. Bansal and A. L. Sandkuhl, "chemical durability of high-temperature superconductor in aqueous environments", Appl. Phys. Lett. 52, pp:323-325,1988.

80 M. F. Yan, R. L. Barnes, H. M. O'Brian, P. K. Gallagher, R. C. Sherwood, and S. Jin, "Water interaction with the superconducting YBa2Cu3O7 phase", Appl. Phys. Letters 51, pp:532-534, 1987.

81 R. L. Barns and R. A. Laudise, " Stability of superconducting YBa2Cu3O7 in the presence of water", Appl. Phys. Lett. 51, pp: 1373-1375, 1987

82 G. N. A. Van Veen, T. S. Baller, J. W. C. De Vries and G. M. Stollman, " Degradation of oriented superconducting thin films", Physica C 152, pp:267-271, 1988.

83 I. Kershner, T. Trager, J. Matrai, T. Porjes and J. Gyorgy,"Corrosin effects in Y-Ba- Cu-O ceramic superconductors", Physica C 153-155, pp:1419-1420, 1988.

84 G. E. Peterson, R. P. Stawicki and U. C. Peak," Radio frequency properties of ceramic high-T_c superconductors", IEE Pinceton Section, Sarnoff symposium, pp:159-167, 1988.

85 R. P. Vasques,B. D. Hunt, and M. C. Foot, " Nonaqueous chemical etch for YBa2Cu3O(7-x), Appl. Phys. Lett. 53, pp:2692-2694, 1988.

86 R. P. Vasques, M. C. Foot, and B. D. Hunt, " Nonacqueous chemical depth profiling of $YBa_2Cu_3O_{(7-x)}$, Appl. Phys. Lett. 54, pp:1060-1062, 1989.

87 M. F. Yan, W. W. Rhodes, and P. K. Gallagher, " Dopant effects on the superconductivity of $YBa_2Cu_3O_7$ ceramics", J. Appl. Phys. 63, pp:821-827, 1988 .

88 T. Siegrist, L. F. Schneemeyer, J. V. Waszczak, N. P. Singh, R. L. Opila, B. Batlogg, L. W. Rupp, and D. W. Murphy, "Aluminium substitution in $Ba_2YCu_3O_7$", Phys. Rev. B 36, pp:8365-8368, 1987.

89 R. Liang, T. Nakamura, H. Kawaji, M. Itoh, and T. Nakamura, "Superconductivity, magnetism and oxygen non-stoichiomery of $Ba_2Y(Cu_{1-x}M_x)_3O_y$ (M=Zn and Ni)", Phisica C 170, pp: 307-314, 1990.

90 G. Xiao, M. Z. Cieplak, D. Musser, A. Gavrin, F. H. Streitz, C. L. Chien, J. J. Rhyne, and J. A. Gotaas, Nature 332, p.238, 1988.

91 H. Meada, A. Koizumi, N. Bamba, E. M. Muromachi, F. Izumi, H. Asano, K. Shimzu, H. Moriwaki, H. Maryuma, Y. Kuroda, and H. Yamazaki, Physicac 157, p.483, 1989.

92 L. Soderholm, K. Zhang, D. G. Hinks, M. A. Beno, J. D. Jorgensen , C. U. Segre, and Ivan K. Shuller, " Incorporaion of Pr in YBa2Cu3O(7-δ):electronic effects on superconductivity ", Nature 328, pp:604-605, 1987.

93 E. Talik, J. Szad and J. Heimann, "T_c enhancement in Y-Ba-Cu-O by Titanium addition ", Physica C 165 , pp:434-436, 1990.

94 S. R. Ovshinsky ,R. T. Young , D. D. Allerd, G. DeMaggio, and G. A. Vander Leeden , Phys. Rev. Lett. 58, p.2579, 1987.

95 N. P. Bansal and A. L. Sandkuhl," Effect of fluoride doping on transition temperature of YBa2Cu3O(6.5+δ)", Appl. Phys. Lett. 52, pp: 838-840, 1988.

96 D.N Matthews , A. Baily, R. A. Vaile, G. J. Russell, and K. N. R. Taylor, Nature 328, pp:786-787, 1987.

97 K. N. R. Taylor, G. J. Russell, D.N Matthews , and A. Baily, Nature 328, p.214, 1987.

98 K. N. R. Taylor, A. Baily, D.N Matthews ,R. A. Vaile, and G. J. Russell, Physica C 153-155, pp.349, 1988.

99 D. D. Sarma, C. T. Simmons, and G. Kindl, Nature 330, p.213, 1987.

100 N. D. Collis , A. C. Rose-Innes, "Effect of N_2 on superconductors ", Nature 338, pp:383-384, 1988.

101 K. V. Paulose, J. Koshy, K. R. Rain, and A.D. Damordaran, " Effect of beryllia substitution and addition in YBa2Cu3O(7-x) compound ", Apll. Phys. Lett. 58, pp:176-178, 1991.

102 M. S. Islam and R. C. Beatzold ," Atomistic simulation of dopant substitution in YBa2C3O7", Phys. Rev. B 40, pp:10926-10953, 1989.

103 K. Betts, M. B. Burbank, A. Cragg, A. A. Fife, P. R. Kubik, S. Lee, J. McCubbin, D. McKenzie, M. Tillotson, B. Taylor, H. Tran, J. Vrba, A. C. D. Chaklader, g. Roemor, B. Heinrich, J. chrzanowski, J. C. Irwin," High T_c Thin film and device development", IEEE Trans. Mag. MAG-25, pp:965-969, 1989.

104 A. Plecenik, S. Benacka, M. Darula, S. Chromic, P. Mikusik, M. Grajcar, " The energy gap depression in YBa2Cu3O(7-x)/metal contacts", Solid State Communications, 78, pp:809-813,1991.

105 C. Thomsen, B. Friedl , M. Cieplak, and M. Cardona, "Effect of substitutional impurities on the superconducting gap of YBa2Cu3O(7-δ) ", Solid State Communications 78, pp:727-733, 1991.

106 K. Rose, C. L. Bertin, and R. Katz, "Radiation detectors", in Applied superconductivity, V. L. New House Ed. New York: academic, 1975, pp:268-208, 1975.

107 C. L. Bertin and K. Rose " Enhanced-mode radiation detection by superconducting films ", J. Appl. Phys. 42, pp:631-642, 1971.

108 S. Z. Cai, Y. S. Hou, E. X. Yu, J. W. Qiu, and W. A. Luo, " An experimental study of Josephson effect in bulk YBaCuO", Int. J. Inf. Millimetre waves 10, pp:231-236, 1989.

109 J. Knopka and G. Jung, " Emission of microwave from dc biased Y-Ba-Cu-O thin films", Europhysics lett. 8, pp:549-553, 1989.

110 J. Y. Jeong and K. Rose "Mm wave detection by superconducting thin films: application of high temperature superconducting films ", Int. J. Of Infrared and Millimeter Waves 10, pp:1441-1449, 1989 .

111 J. Kanopka, R. Sobolewski , G. Jung, W. Kula, P. Gierlowski, A. Kanopka, and S. J. Lewandowski, "Microwave detectors based on granular high-T_c thin films", IEEE Trans. Microwave Theory and techniques MTT-38, pp:160-165, 1990.

112 V. B. Anzin et Al "Submillimeter conductivity of Y-BaCu-O films and prospects of their applications", in Proc. European Conf. High T_c Superconductivity, 1990.

113 D. Winkler and T. Cleason, J. Appl. Phys. 62, p.4482, 1987.

114 Y. Yoshisa, M. Takai, K. Niki, S. Yoshkawa, T. Hirano, and S. Nakano, "Mixing characteristics of a microwave detector using a granular YBCO superconductor", IEEE Trans. Magnet. MAG-27, pp:3073, 1991.

115 S. T. Ruggiero, A. Cardona, and H. R. Fetterman, " Mixing in TlCaBaCuO superconducting films at 61 GHz", IEEE Trans. Magnet. MAG-27,pp:3070-3072, 1991.

116 J. E. Zemerman, J. A. Beall, M. W. Cromar, and R. H. Ono "Operation of Ya-Ba-Cu-O rf SQUID at 81 K ", Appl. Phys. Lett. 51, pp:617-618, 1987.

117 R. H. Koch , C. P. Umbach, G. J. Clarke, P. Chaudari, and R. B. Laibowitz, "Quantum interference devices made from superconducting oxide thin films", Appl. Phys. Lett. 51, pp:200-202, 1987.

118 U. Kawabe, "Application of high temperature superconductors to SQUID and other devices", Physica C 153-155, pp:1586-1591, 19988.

119 A. T. A. M. de Weal, W. A. Draisma, V. A. M. Brabers, W. J. M. de Jonge, and R. W. Van der Heijden, "SQUID operation of point contacts from YBACuO", Physica C 153-155, pp:1415-1416, 1988.

120 C. X. Fan, Y. J. Qian, L. S. Dai, and Z. Y. Hua, " A DC SQUID magnetometer operated at 77 K", Physica C 153-155, pp:1413-1414, 1988.

121 V. N. Polushkin, S. P. Shtanko, S. V. Uchaikin, and B. V. Vasilev, "An investigation of $YBa_2Cu_3O_{(7-x)}$ Josephson contacts", Supercond. Sci. Technol. 3, pp:404-408, 1990.

122 R. Crosse, P. Chaudari, M. Kawasaki, M. Ketchen, and A. Gupta, "Noise Characteristics of single grain boundary junction DC SQUID s in $YBa_2Cu_3O_{(3-7)}$", Physica C 135-155, pp:315-318,1990.

123 S. Harrop, C. M. Murhead, M. S. Coloclough, and C. E. Gough, " Two holes SQUID behaviour in a bulk YBCO SAMPLE AT 77 K", Physica C 153-155, pp:1411-1412, 1988.

124 L. Zhou, J. Qiu, X. Zhang, Z. Tang, Y. Cai, Y. Qian, "High Temperature SQUID suceptometer and its applications", Physica B 165 & 166, pp:85-86, 1990.

125 Z. Xiafung, Q. Jinwu, T. Zhiming, and Q. Yongjia, "Physical structure effects on the response characteristics of an RF-SQUID at 77", Sol. State com. 74, pp:479-481, 1990.

126 K. P. Daly, J. Burch, S. Coons, R. Hu, " YBa2Cu7 Step edge RF SQUID biased at 10 GHz", IEEe Trans. Magn. MAG-27, pp:3066-3069, 1991.

127 G. Cui, Y. Zhang, K. Herrmann, Ch. Buchal, J. Schubert, W. Zander, A. T. Braginski, and C. Heiden, " Properties of rf-SQUIDs fabricated from epithaxial YBa2Cu3O7 films", Supercond. Sci. Technol. 4, S130-132, 1991.

128 S. M. schwarzbek, R. A. Davidheuser, G. R. Fisher, J. A. Luine, and N. J. Scheier, "Digital logic with $YBa_2Cu_3O_{(7-x)}$ DC SQUIDs ", Appl. Phys. Lett. 59, pp:866-868, 1991.

129 J. C. Ritter, M. Nisenoff, G. Price and S. A. Wolf,"High temperature superconductivity space experiment (HTSSE)", IEEE Trans. Magnetic MAG-27, pp2534-2536, 1991.

130 M. Leung & al, "Optical detection in thin granular films of Y-Ba-Cu-O at temperature between 4.2 and 100°K", Appl. Phys. Let. 51, pp:2046-2048, 1987.

131 M. G. Forrester et al, "Optical response of epithaxial films of $YBa_2Cu_{3-\delta}$, Appl. Phys. lett. 53, pp:1332, 1988.

132 U. Storm et al, "Photoconductive response of granular superconducting thin films", IEEE Trans. Mag. 25 , pp:1315-1318, 1989.

133 Y. Enomoto, T. Murakami, and M. Suzuki, " Infrared optical detector using superconducting oxide film", Physica C 153-155, pp:1592-1597, 1988.

134 H. Tamura, S. Hasao , and T. Yamaoka, Jap. J. Appl. Phys. 24, L709, 1985.

135 D. J. Frank, M. J. Brandy, and A. Davidson, IEEE Trans. Magnet. MAG-21, p.721, 1985.

136 H. Tamura, A. Yoshida, K. Gotoh, and S. Hasuo, T. Van Duzer, "A superconducting resonant tunneling transistor with insulating layer ", IEEE Trans. Magnet. MAG-27, pp:2594-2597,1991.

137 K. Hashimoto, R. Kawasaki, and H. Abe, " Analysis of the high frequency performance of high T_c superconducting-base hot electron transistors", Solid-State Electronics 34, pp:629-633, 1991.

138 W. G. Lyons, R. R. Bonetti, A. E. Williams, P. M. Mankiewich, M. L. O'Malley, J. M. Hamm, A. C. Anderson, R. S. Wither, A. Meulenberg, R. E. Howard, " High-T_c Superconductive microwave filters", IEEE Trans. Magnet. MAG-27, pp:2537-2539,1991.

139 S. H. Talisa, M. A. Janoko, C. K. Jones, B. R. McAvoy, J. Talavacchio, and G. R. Wagner, " Microwave superconducting filters", IEEE Trans. Magnet. MAG-27, pp:2544-2547, 1991.

140 E. Minehara, R. Nagai, and M. Takeuchi, "The TM010 microwave cavity made of $YBa_2Cu_3O_{(7-d)}$", Jap. J. Appl. Phys. 28, pp:L100-L101, 1989.

141 G. Jung, J. Konopka, and S. Vitale, " Synchronization of radiating intrinsic high T_c Josephson junctions", Physica B 165 & 166, pp:105-106, 1990.

CHAPTER 5: SAMPLE PREPARATION, EXPERIMENTAL SET-UP, AND RESULTS

5.1 Introduction

This chapter is devoted to a description of the different samples and experimental set ups used with the results obtained. Early samples were processed using photolithographic techniques in which the sample was exposed to wetting solutions. However it was subsequently found that these materials are sensitive to wet solutions as discussed in section 4.8. Consequently, results obtained using these samples are not considered. In the next eight sections, eight different samples will be described. Each section will be divided into three parts: firstly the sample description, secondly the experimental set up used, and thirdly the measurement results.

5.2 Sample 1 referred to as S1P

5. 2. 1 Sample preparation.

The sample was cut from material supplied by B.Ae. On a part of it aluminium was deposited and heated for 10 minutes in an oven at 100 C to yield Al_2O_3. Silver dots were then evaporated to form the normal metal electrodes of the junctions on one side and the back contact on the other side. The fabricated sample was as shown in figure 5.1

5.2.2. Experimental set up .

The sample was mounted onto the sample holder of a large cryostat as shown in figure 5.2.

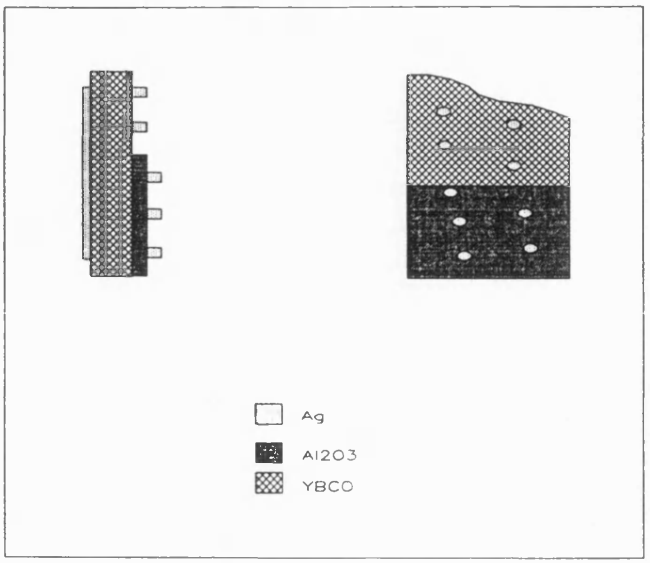

Fig.5.1 Sample S1P

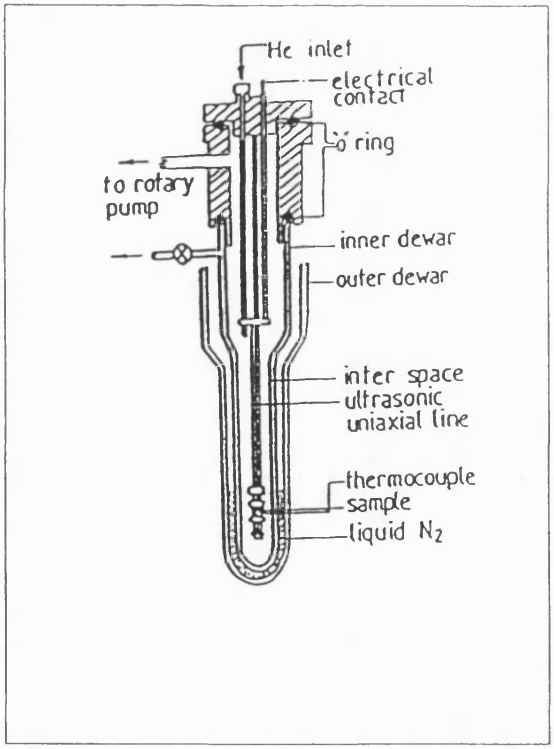

Fig.5.2 Low temperature cryostat

Several different ranges of temperature can be reached with this cryostat :

The 80 K range is obtained by keeping the sample under vacuum and filling the outer jacket with liquid N_2. The system allows the temperature to be lowered to 54 K by introducing Liquid N_2 into the sample compartment and pumping it out gradually . Lower temperatures down to 4.2 K can be reached by filling the sample compartment with liquid Helium. The sample dots were connected to the four electrical contacts available according to the layout shown in figure 5.3 .

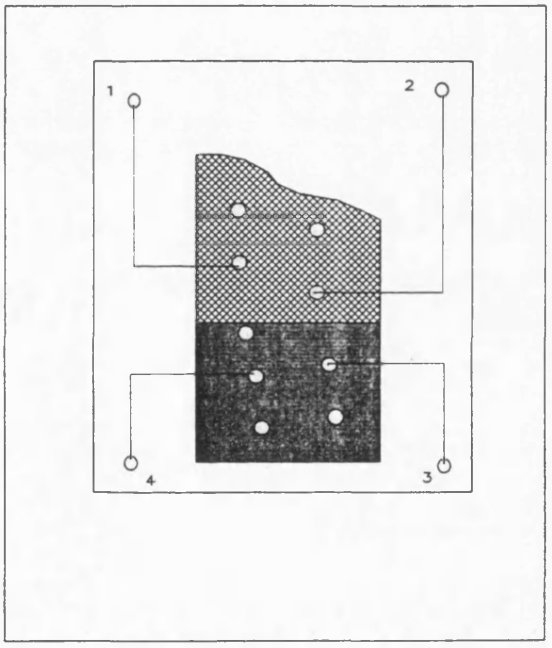

Fig.5.3 Electrical contacts layout of S1P

The dots or junction will be numbered according to the electrical contact to which they were connected . Thus the junctions connected to the electrical contacts 1, 2, 3, and 4, will be called J1, J2, J3, and J4 respectively . This method of numbering the junction is used for almost all of the samples.The sample temperature was reduced to 56 K using

the procedure described above and IV curve measurements were carried out using a computer controlled experimental set-up which is represented in figure 5.4 .

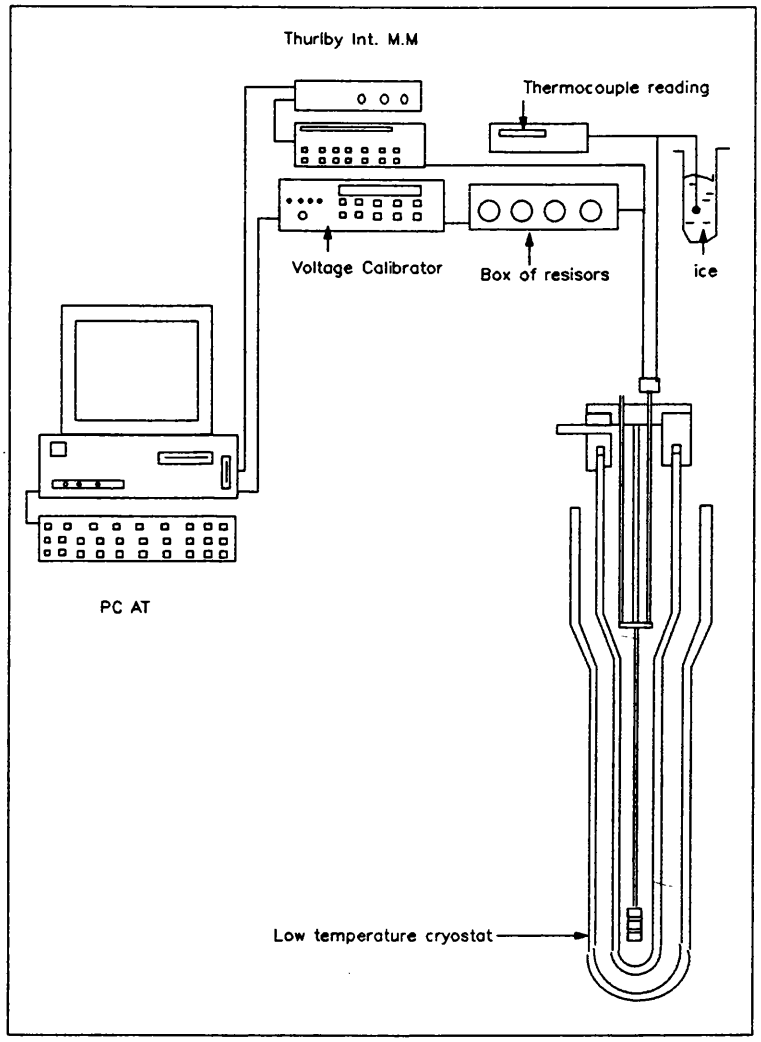

Fig.5.4 Experimental set up used with sample S1P

This experimental set up consists of a programmable dc voltage source which generates the required voltage, V_g, into a circuit containing a box of resistances in series with the junction . In parallel with sample is a Thurlby intelligent multimeter which is used to measure the voltage

V_j across the connected junction . The measurement system can be represented by a simplified circuit as shown in figure 5.5 .

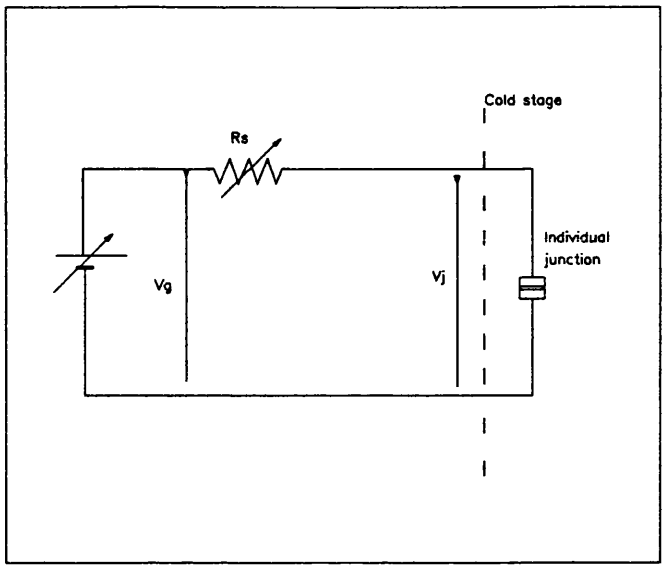

Fig.5.5 Equivalent circuit of the experimental set up

The computer varied V_g over a certain voltage range (the range can be chosen taken between +/- 10 mV to +/-300 mV). For each voltage the current flowing through the junction I_j is calculated by the same program using the formula :

$$I_j = \frac{V_g - V_j}{R_s} \qquad (5.1)$$

The corresponding values of V_j and I_j obtained constitute the data which were stored in the computer and can be processed to yield the I-V and dI/dV-V characteristics.

5.2.3. Measurement results

Two of the four junctions gave non-linear IV curves which will be presented in the following sections .

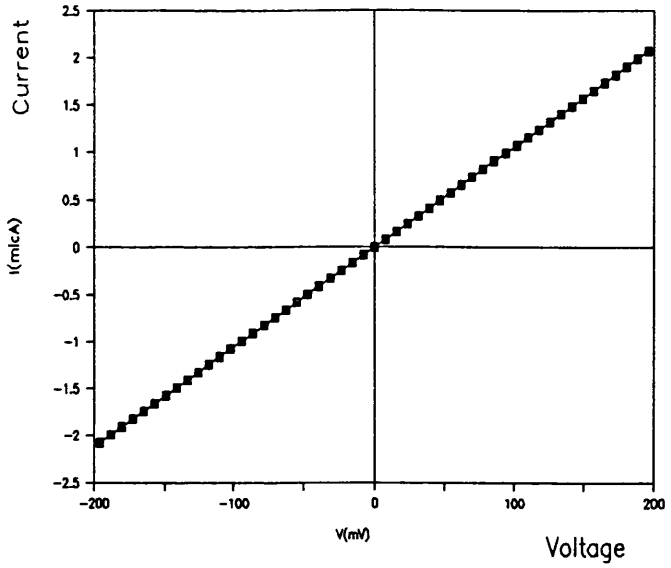

Fig.5.6 IV curve of J3 ,T= 81 K, Rs=500 Ω

Figure 5.6 shows that at T=81 K, the I-V curve of J3 is a straight line . Its slope gives a resistance of 100 Ω .

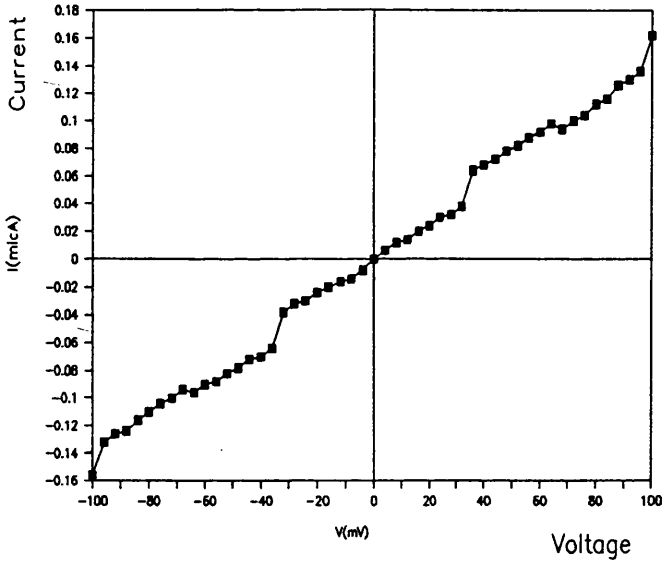

Fig.5.7 IV curve of J3, T= 66 K, Rs=500 Ω

Figure 5.7 shows that when the temperature decreased to 66 K a dramatic change of the I-V curve occurred. This change is characterised by the appearance of a slight increase in current around 0 V, two strong non-linearities at +/- 35 mV , and two small NDR-like features at +/- 65 mV .

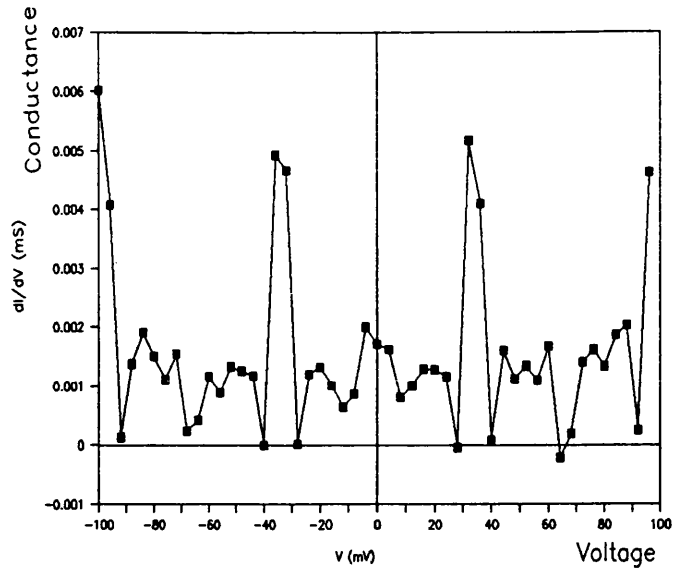

Fig.5.8 Conductance vs voltage of J3 , T=66 K

The conductance plot shown in figure 5.8 highlights the feature of figure 5.6 . The major features are two symmetrical peaks +/- 33 mV and a smaller peak at 0 V which is 22 mV wide. Two other peaks can be seen at -100 mV and +97 mV .

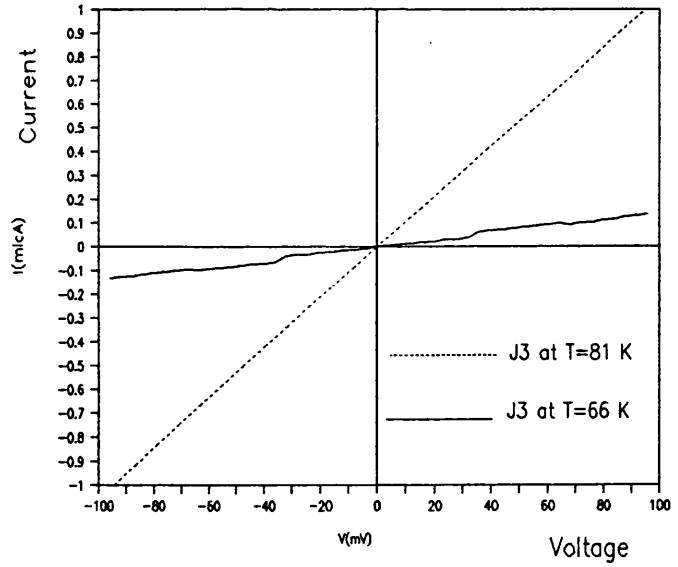

Fig.5.9 IV curve of J3 at T=81 K, and T=66 K

The I-V curves of figures 5.6 and 5.7 are presented together in figure 5.9. This shows more clearly the difference between the two curves when the temperature decreased from 81 K to 66 K.

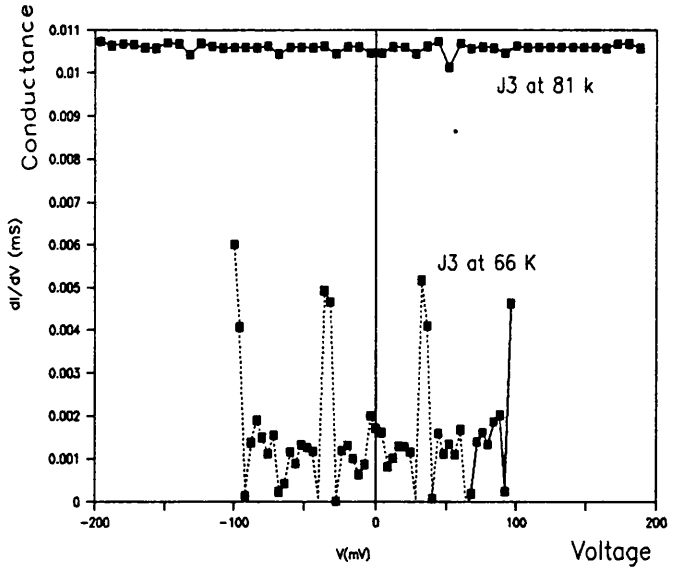

Fig.5.10 Conductance of J3 at T=81 K, and T=66 K

The difference between the two curves (5.6 and 5.7) is also shown in figure 5.10 where a simultaneous presentation of the conductances vs voltage is given.

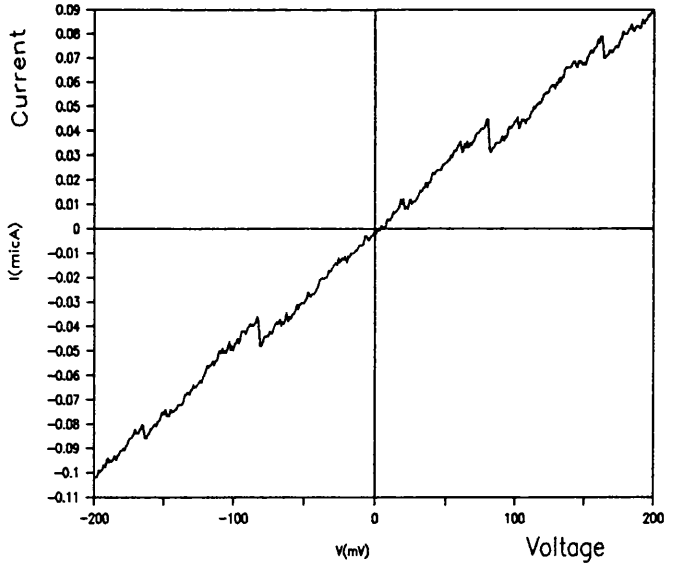

Fig.5.11 IV of J2 T=54 K, Rs= 1000 Ω

Figure 5. 11 shows the IV curve of J2 which exhibits a very pronounced NDR-like features at +/- 83 mV. Additional but less pronounced features can also be seen at V=+/- 19 mV and +/- 162 mV.

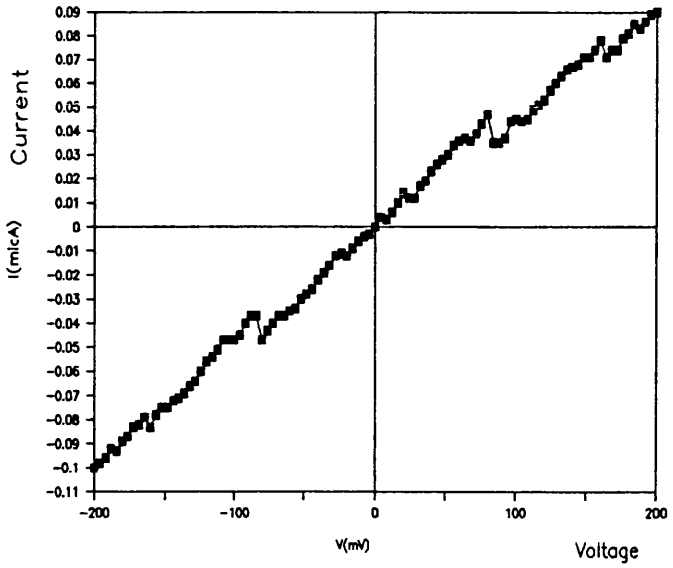

Fig.5.12 IV of J2 T=240 K, Rs= 1000 Ω

One of the five I-V curves was measured at T=240 K and is shown in figure 5.12. All the feature found in figure 5.11 are also found at this higher temperature measurement.

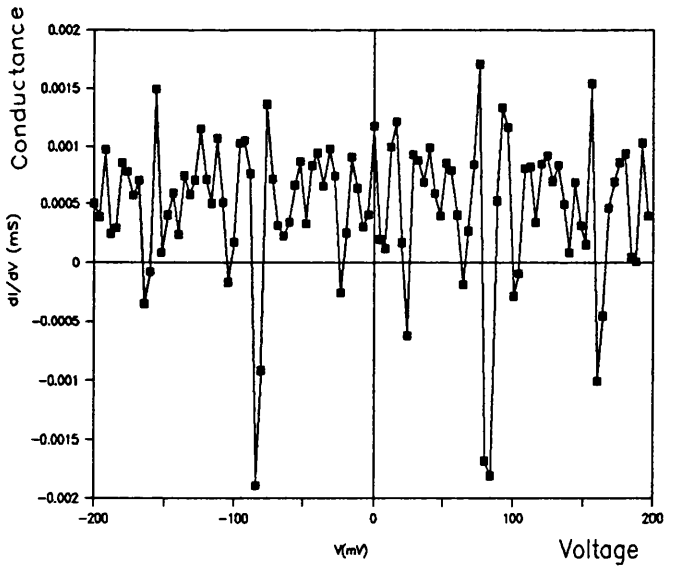

Fig.5.13 Conductance vs voltage of J2 at T=240 K

Figure 5.13 shows the conductance vs voltage obtained from the data of figure 5.12 . This conductance curve has striking symmetrical features such as peaks at 0 V, +/-41.5 mV, and +/-127.7 mV . The peaks at +/- 41.5 mV are enfolded by negative conductances resulting from very pronounced valleys at +- 83 mV . These valleys possess some shoulder-like features .

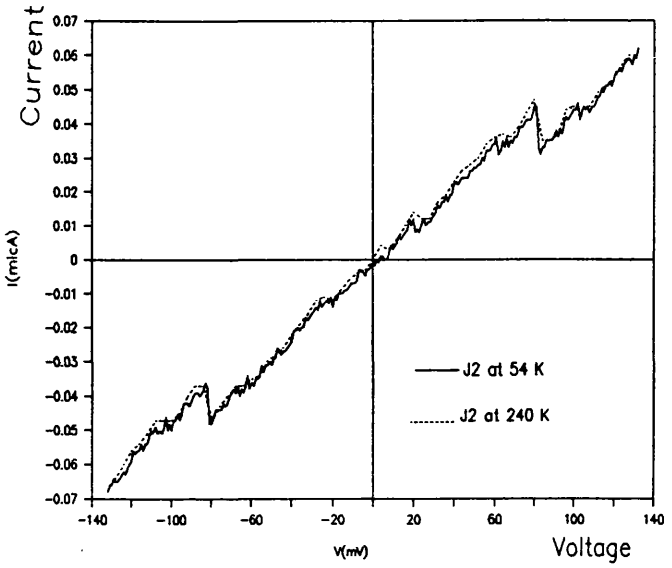

Fig.5.14 I-V curve of J2 at the two indicated temperatures

A simultaneous presentation of figure 5.11 and 5.12 is shown Figure 5.14. From this latter it can be seen that temperatures up to 240 K have only a minor effect on the IV curve of J2 .

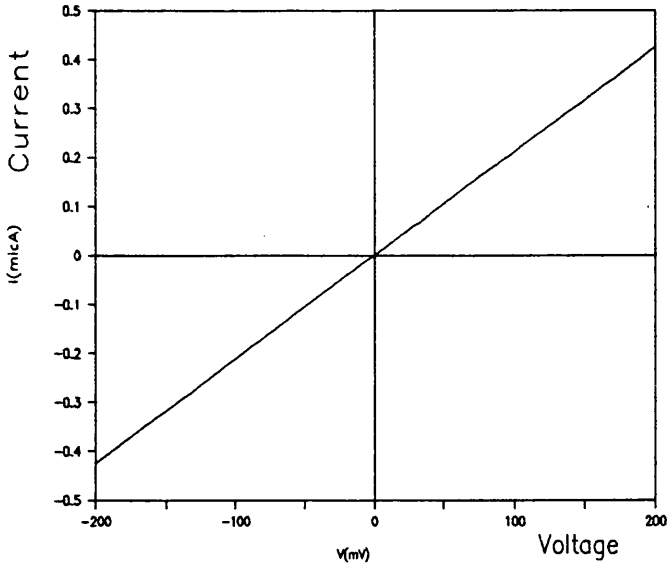

Fig.5.15 IV of J2 T=296 K, Rs= 1000 Ω

Figure 5.15 shows that at room temperature, all the low temperature features of junction J2 including the NDR have vanished leaving a straight line whose slope gives a resistance of 483 KΩ .

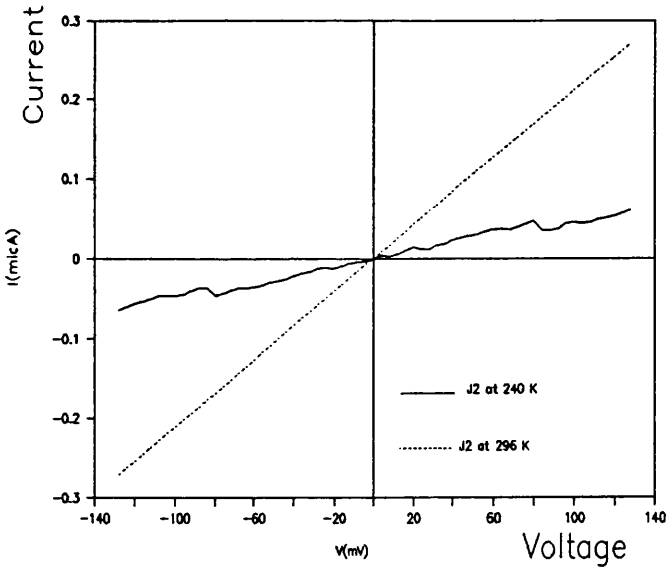

Fig.5.16 IV of J2 at the two indicated temperatures

The I-V curves of J2 at 240 K and 296 K are simultaneously presented in figure 5.16. This shows that the I-V curve of J2 changes dramatically from a non-linear curve to a straight line .

5. 3. Sample 2 referred to as K1B

5. 3 . 1. Sample preparation.

Sample K1B was an 8 mm diameter pellet cut from the 25 mm pellet provided by BAE . Its original thickness of 2mm was reduced to 0.8 mm by lapping on emery paper first and then polishing using Al_2O_3 powder. The pellet was annealed in air at 500 C for 72 hours, sputter cleaned using an ion beam facility and annealed at 500 C in flowing oxygen for 36 hours. Silver dots were evaporated directly onto the polished sides of the pellet whereas the back surface was fully coated with Ag to allow for the back contact. In the measurement the back contact was soldered to the sample holder of the continuous flow cryostat. The layout of Ag dots of the sample fixed to the sample holder is as shown in figure 5.17 .

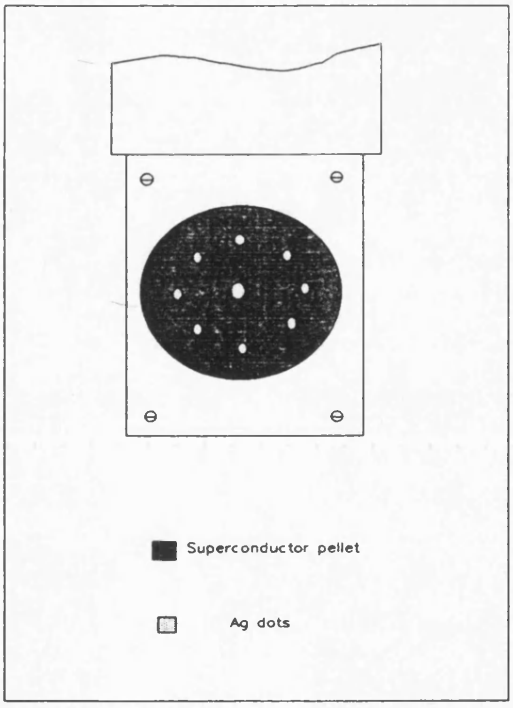

Fig.5.17 Layout of Ag dots on superconductor surface.

5. 3. 2. Experimental set up .

These measurements were carried out using a continuous flow cryostat that uses liquid Helium allowing it to reach temperatures as low as 7 K . Figure 5.18 shows the experimental set-up used in these measurements. The I-V measurement rig was basically the same as used in the previous arrangement except that the Thurlby multimeter was replaced with a Keithley 617 electrometer . This resulted in improved accuracy since the electometer is capable of measuring currents as small as 1 pA.

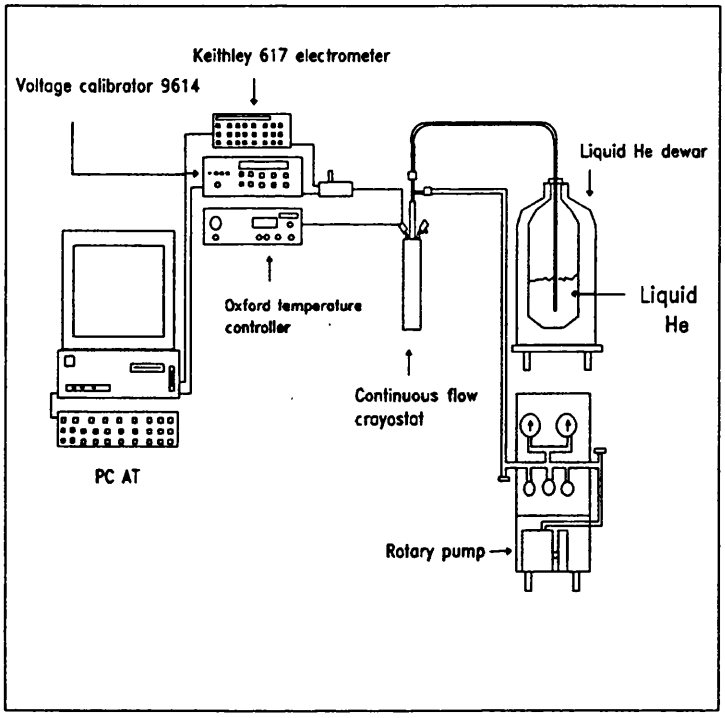

Fig.5.18 Experimental set up used with K1B

5.3.3 Results.

Measurements were carried out on only one dot, J1, since the other dots were damaged during the contacting process. The measurement on J1 gave five non-linear IV curves which were taken at temperatures between 13 and 17 K using different voltage ranges on the voltage calibrator as indicated in the following figures . Only three out of the five are presented because of the similarity of the curves.

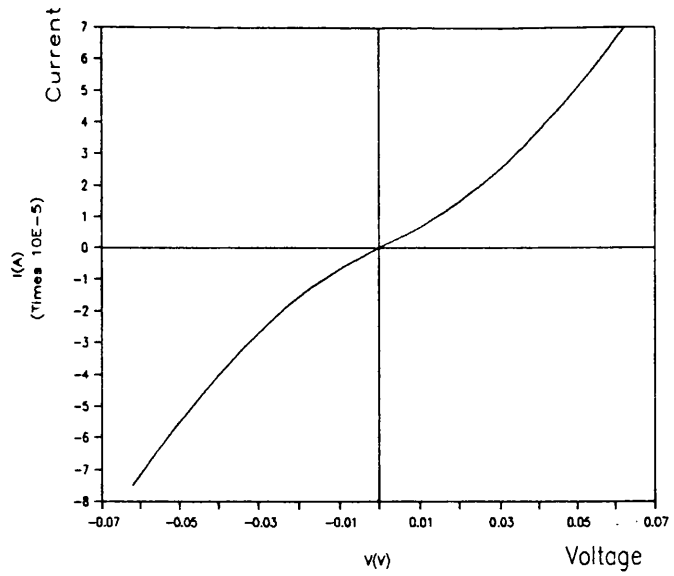

Fig.5.19 IV curve of J1 T=13.5 K

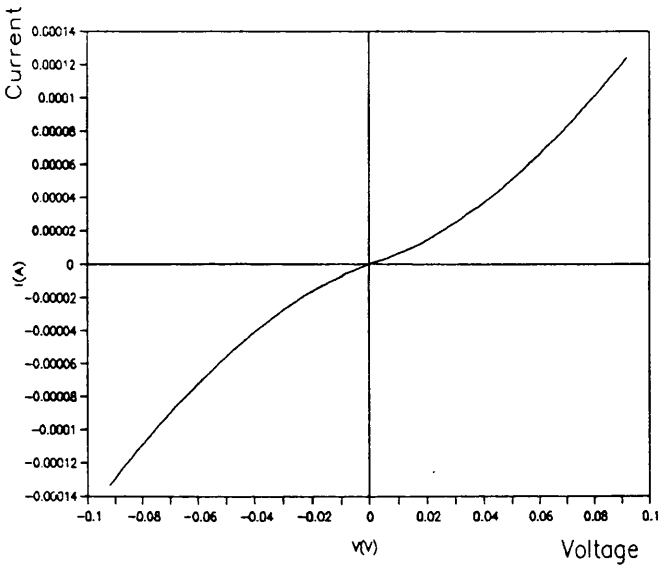

Fig.5.20 IV curve of J1, T= 16 K

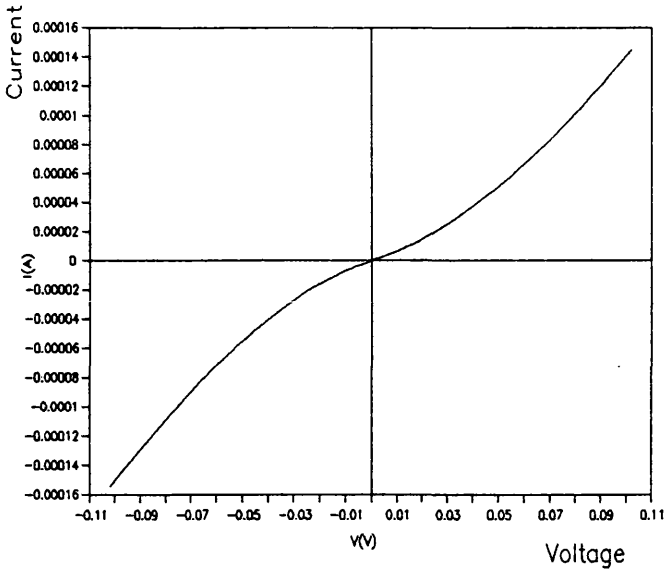

Fig.5.21 IV curve of J1, T=17 K

The I-V curves shown in figures 5.19, 5.20, 5.21 all exhibit non-linear behaviour. This non-linearity of the I-V curves may be due to the formation of an insulting layer resulting from the reaction of the compound with the environment (water vapor present in air) with the surface of the sample as discussed in chapter four.

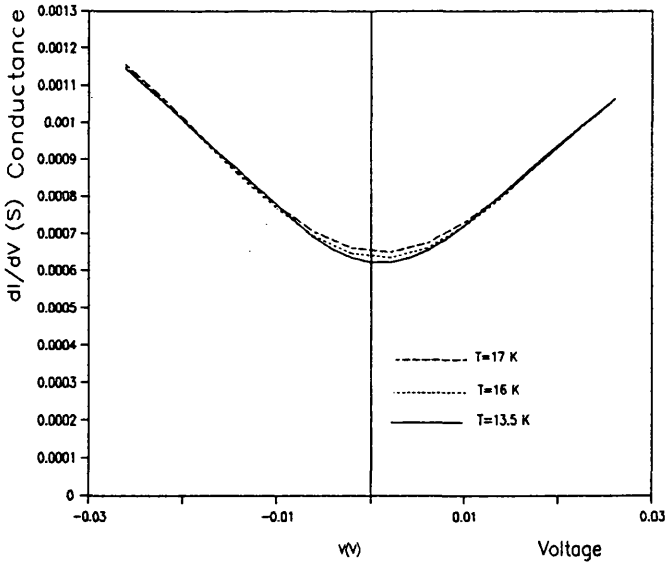

Fig.5.22 Conductance vs voltage of J1 at the indicated temperatures

Figure 5.22 shows the conductances vs voltage obtained from the data of figure 5.19, 5.20, and 5.21. A slight effect of the temperature can be seen on these curves consisting of an increase of conductivity with temperature for voltages between -10 mV and +10 mV. Beyond this interval the three curves almost coincide and increase monotonously with increasing voltage.

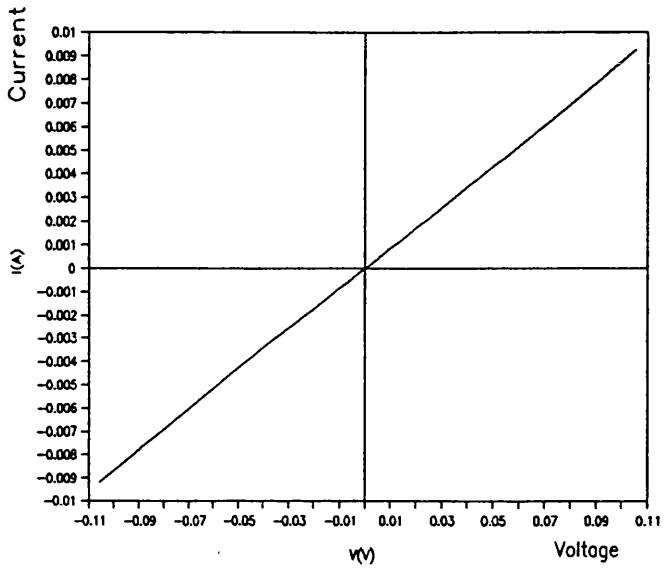

Fig.5.23 IV curve of J1 at room temperature

At room temperature, junction J1 gave four identical IV curves from which one curve only is presented in figure 5.23 .

Figure 5.24 shows the conductance vs voltage of one of four of the IV curve of J1 at room temperature which is identical to that of 5.23 . This is almost two order of magnitude higher than the conductance vs voltage curve of J1 at low temperature shown in figure 5.22.

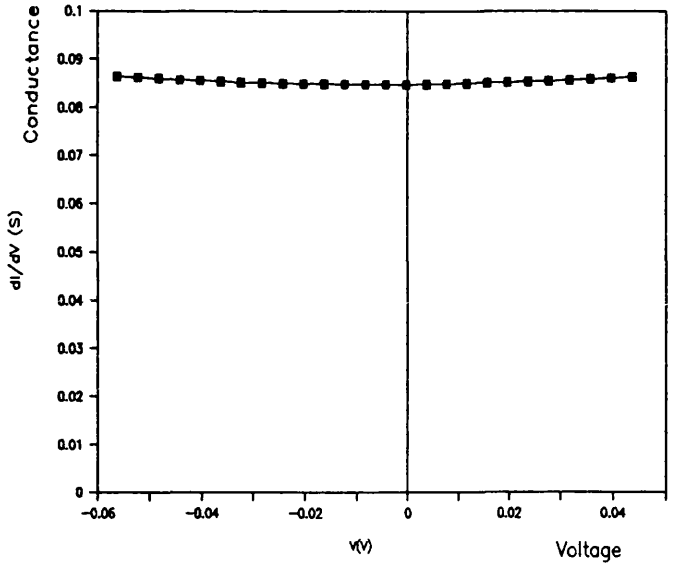

Fig.5.24 Conductance of J1 at room temperature

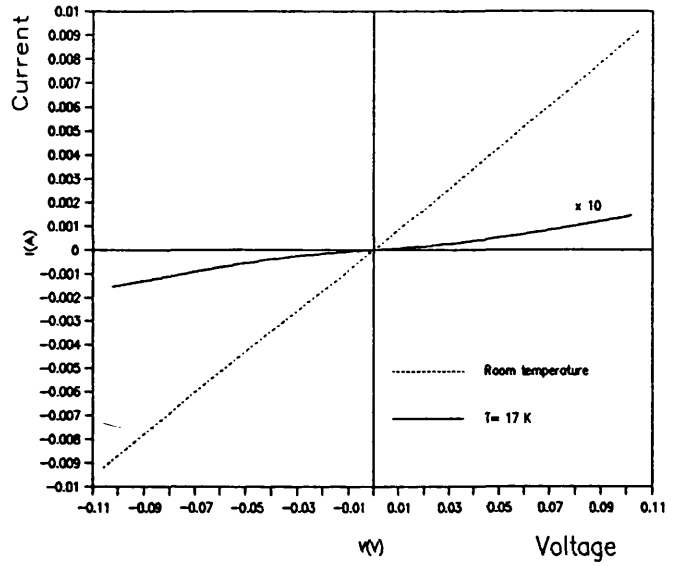

Fig.5.25 IV curve of J1 at the indicated temperatures

In figure 5.25, two curves from previous figures (5.21 and 5.23) are presented together. The I-V curve of J1 at T=17 K has been multiplied by ten (x 10) so that it can be presented in this way . Again this shows the dramatic change of the junction resistance between these two temperatures.

5.4 Sample 3 :preparation and characterisation of YBCO pellets

At this stage of the project , it became difficult if not impossible to find an HTS pellets supplier, let alone single crystals or thin films. The only way out of this situation was to start preparing my own samples . The material of choice was YBCO. A large quantity of YBCO powder (20 g) was synthesized from Y_2O_3, $BaCO_3$ and CuO with the atomic ratio of (Y:Ba:Cu)=(1:2:3). The three kinds of powders were thoroughly mixed and heated to 925 C for 36 hours in air and cooled in place in the oven. The result was a cylinder of black material with green spots on the side upon which it was lying in the oven . The cylinder was ground using mortar and pestle and sieved through a 125 μ mesh sieve. A set of six pellets weighing from 1.5 to 2 g were pressed at 700 MPa . These were fired to 925 C for 24 hours in flowing oxygen and cooled to ambient at a rate of 60 C/hour. These six pellets were referred to as batch S1A . Four pellet of this batch were reground with mortar and pestle again giving a shiny black powder that characterises YBCO. The powder was fired at 925 C for 36 hours in flowing oxygen and cooled at a rate of 50 C/hour . After this treatment the powder was reground, sieved through a 125 μ sieve, pelletized, and sintered in flowing oxygen following the diagram shown in figure 5.26. The pellets resulting from this treatment are referred to as batch S1B. Pellets from both batches, S1A and S1B, were used in the following experiments.

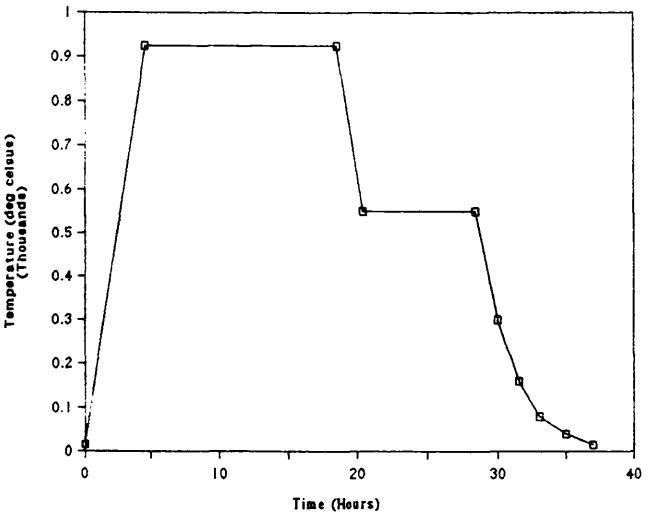

Fig.5.26 Sintering diagram of S1B

5.4.1 Sample S1B characterisation

A) Meissner effect

A small piece YBCO was cut from one of the pellet of S1B and fixed to a very thin wire and suspended to from a pin. After immersing the YBCO in liquid nitrogen a magnet was quickly brought up to it . When the magnet approached, the cold YBCO was observed to move away. Once the sample warmed up it was observed to move back into the magnetic field. In behaving in this way, the sample exhibits Meissner effect, thereby demonstrating that it was superconducting.

B) X Ray diffraction

Another piece from the same pellet was finely ground and analyzed by X-ray diffraction (XRD). The XRD pattern resulting from the sample analysis is shown in figure 5.27. Most of the features coincide with a reported XRD of an YBCO single phase powder as shown in figure 5.28 .

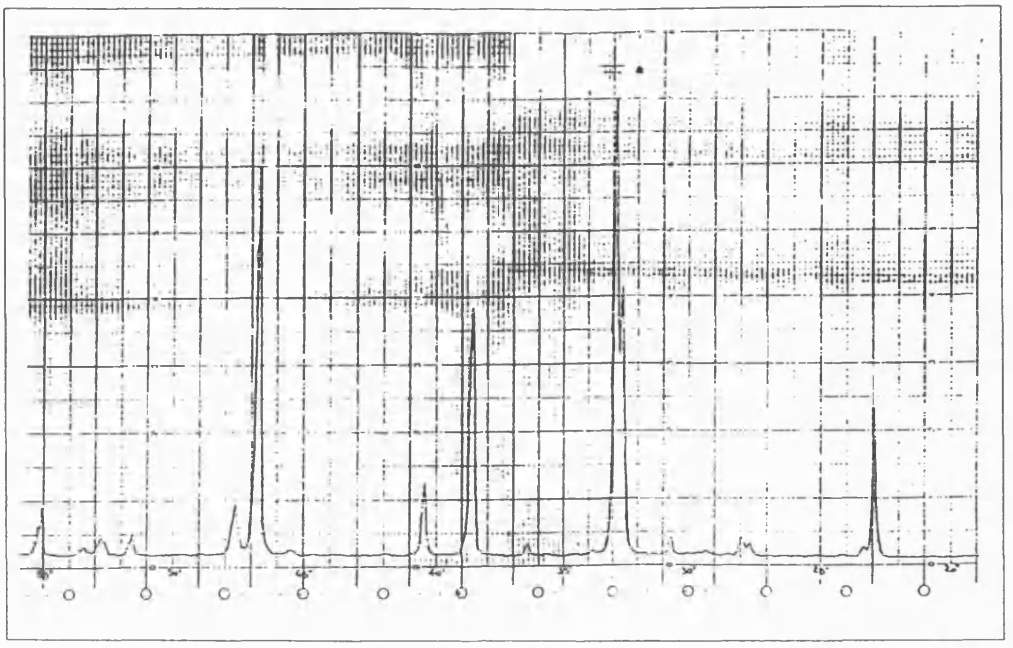

Fig.5.27 XRD pattern of sample S1B

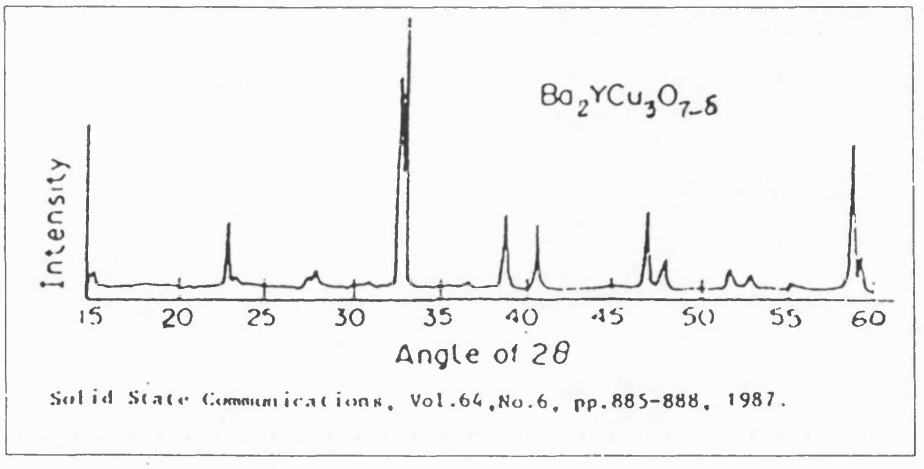

Fig.5.28 XRD pattern of YBCO single phase sample

5.4.2 R vs T anomaly of samples immersed in liquid N_2

A first bar, referred to SHS1B, of dimension 1x1.5x11 mm^3 was cut from one of the pellets of S1B , fixed to a sample holder and immersed directly in liquid N2 container . The result of R vs T measurement gave an anomalous low temperature minimum at T= 198 K followed by higher resistance at T=77 K . This behaviour was observed twice one during the cooling down of the sample and the second during the warming up.

A second bar of dimension 1x1x5 mm^3, and referred to as S1C, was cut from a pellet of batch S1B after sintering it following a diagram similar to that of figure 5.29 . Its R vs T measurement gave similar anomalous behaviour as the first bar. In addition IV curves were measured at temperature where R shown a minimum and intriguing results were obtained .

As these samples did not show a total superconducting transition, their anomalous results are described in appendix A2.

5.5 Sample 4 referred to as S1DE (S1D AND S1E)

Two pellets one from batch S1A, and the other from batch S1B sample were annealed in flowing oxygen according to the diagram shown in figure 5.29

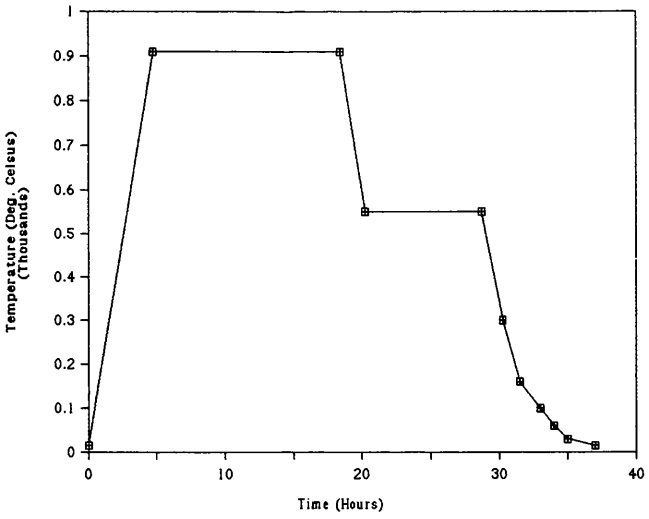

Fig.5. 29 Sintering diagram of SAMPLE S1DE

After this treatment, the pellets were separately exposed to DC glow discharge in an atmosphere of Ar under high tension so as to eliminate the upper layer which was exposed to the environment . For each pellet, the exposure to the glow discharge lasted three hours. This operation was carried out in a 12" chamber where Argon gas pressure was maintained at 0.08 mbar resulting in current of 200 mA.

A bar of dimension 1x1.5x6 mm^3 and referred to as S1E was cut from pellet of batch S1A . The second pellet of batch S1B was used as it is and referred to as S1D. Both the pellet S1D and the bar S1E had Ag dots evaporated onto them . Both were fixed to the sample holder of the continuous flow cryostat as shown in figure 5.30 .

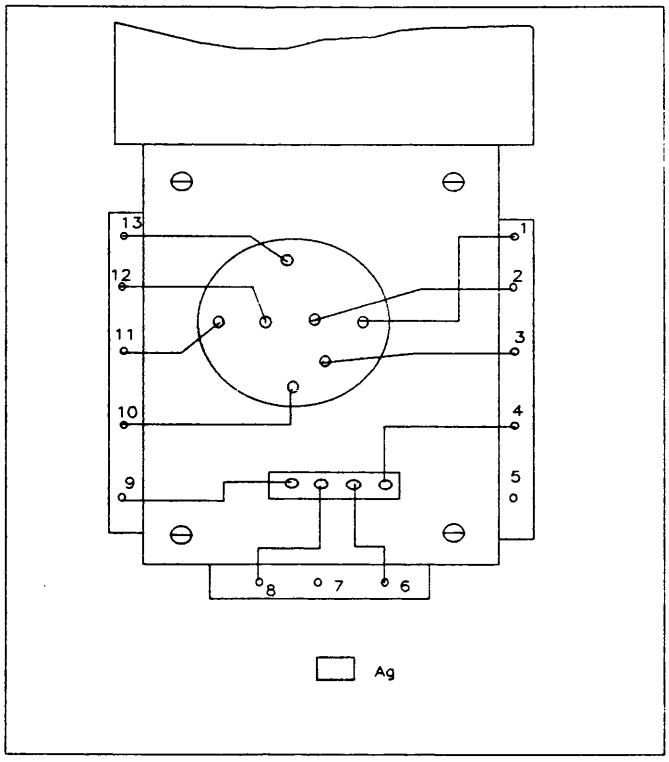

Fig.5.30 Layout of S1DE: PELLET S1D, AND BAR S1E

This layout was used for measuring R vs T of both the bar S1E, and the pellet S1D . In addition I-V curves were measured between near dots, referred to as NJ, and the far dots referred FJ, on both the pellet and the bar . For the pellet, the near dots NJ are connected to pins 2 and 12 whereas the far dots are connected to pins 1 and 11 shown in figure 5.30 . For the bar the near dots, NJ, are connected to pins 6 and 8 and the far dots FJ to pins 4 and 9. The results from both the pellet and the bar will be presented separately in the following section .

5.5.1 Experimental set-up

The experimental set up used in this experiment was similar to that described previously and shown in Fig.5.18 .

5.5.2. Results of the pellet S1D

Before cooling down the sample a series of measurement of the resistance R of the sample were carried out at room temperature . This was done using the four point probe method. Following this, I-V curves were taken at room temperature. During the cooling down of the sample measurement of R vs T were taken. More IV curves were taken at low temperature between the near dots NJ, and the far dots FJ. The measurement of the resistance R of the sample at room temperature was made using a constant current of 10 mA. The measurement of R was repeated 10 times and is and the following values of the mean and the standard deviation of the mean were obtained:

$$R=(1.585 +/- 0.007) \text{ milli } \Omega .$$

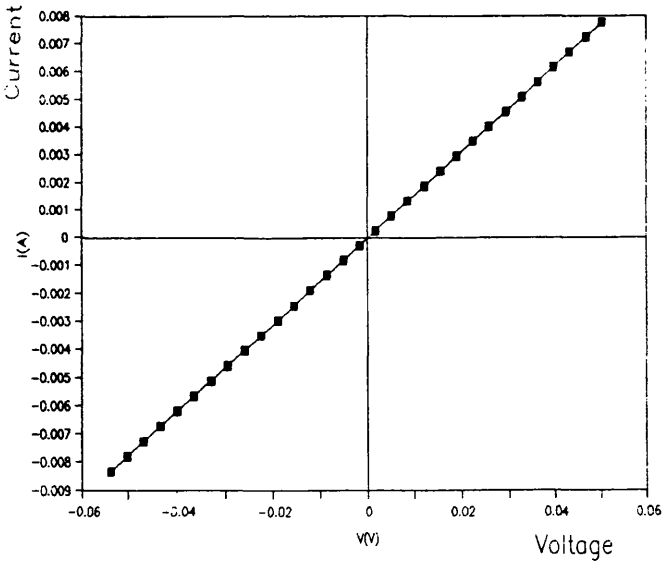

Fig.5.31 IV curves of NJ at room temperature

The I-V curve of NJ at room temperature is shown in figure 5.31 to be a straight line. Its slope yields a resistance of 6 Ω .

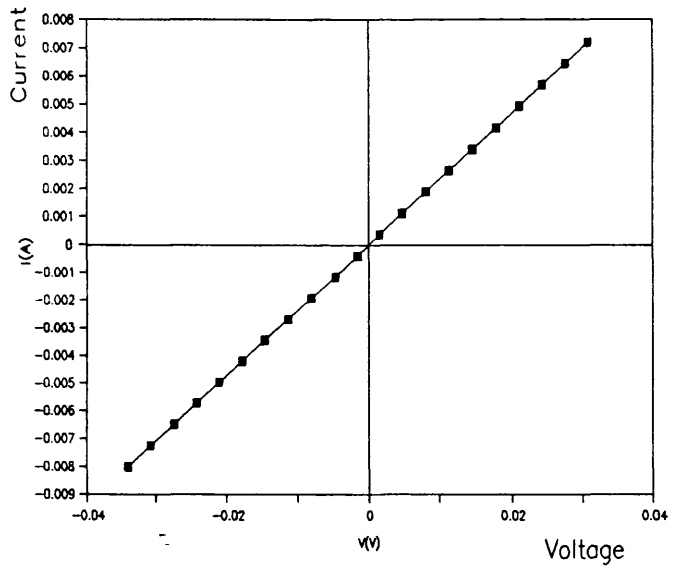

Fig.5.32 IV curves of FJ at room temperature

For the far dots FJ, the slope of the I-V curve shown in figure 5.32, gives a resistance of 4.7 Ω .

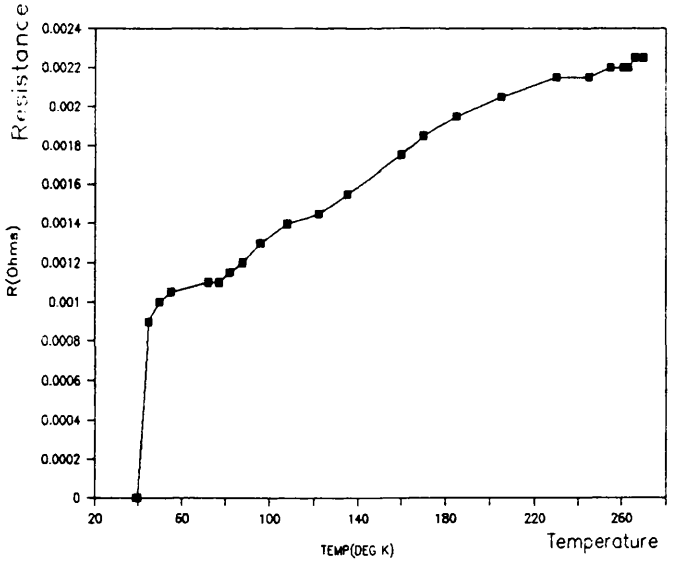

Fig.5.33 R vs T during the cooling down with I=20 mA

In figure 5.33 the R vs T curve of the pellet, (measured using the four point probe method) is shown to be steadily decreasing with decreasing temperature until the transition to the superconducting state occurs around 45 K.

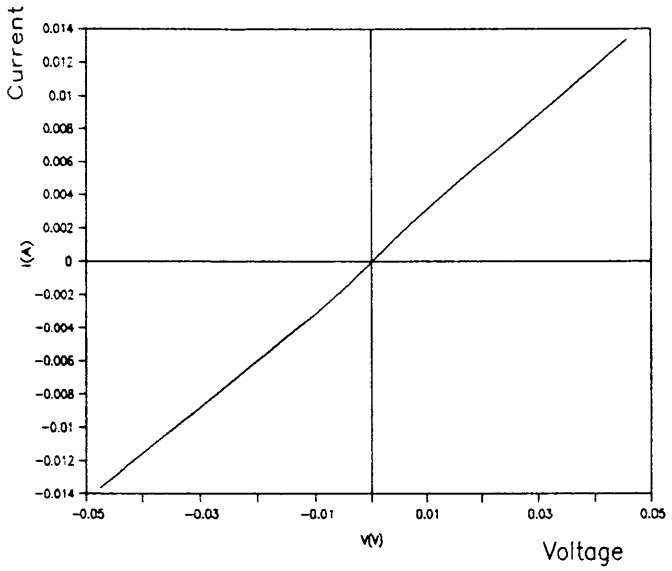

Fig.5.34 IV curve of NJ at T=18 K

Figure 5.34 shows that the I-V curve measured between the near dots at a temperature of 18 K which is well below the superconducting transition temperature. Aclose look at the figure shows that the right side of the curve is displaced upward relatively to the left. In other words there is an increase of current at 0 V.

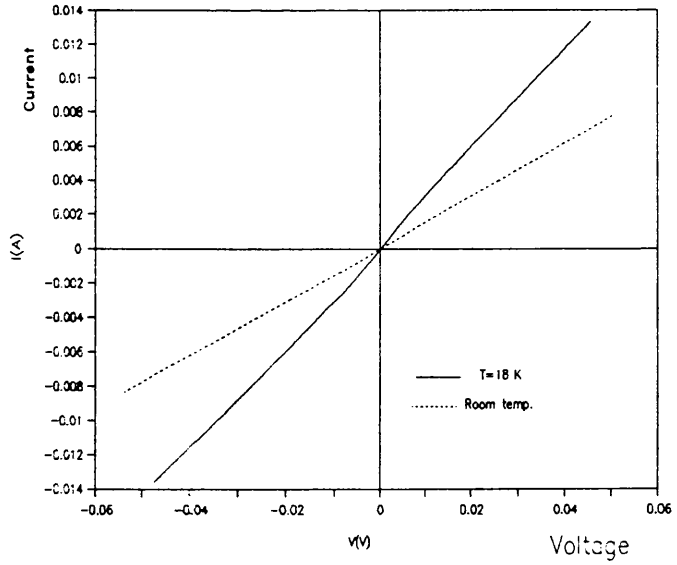

Fig.5.35 IV curves of NJ at the indicated temperatures

The IV curves of figures 5.31 and 5.34, are simultaneously shown in figure 5.35 where it can be seen that the conductivity of the curve at low temperature is higher than that at room temperature .

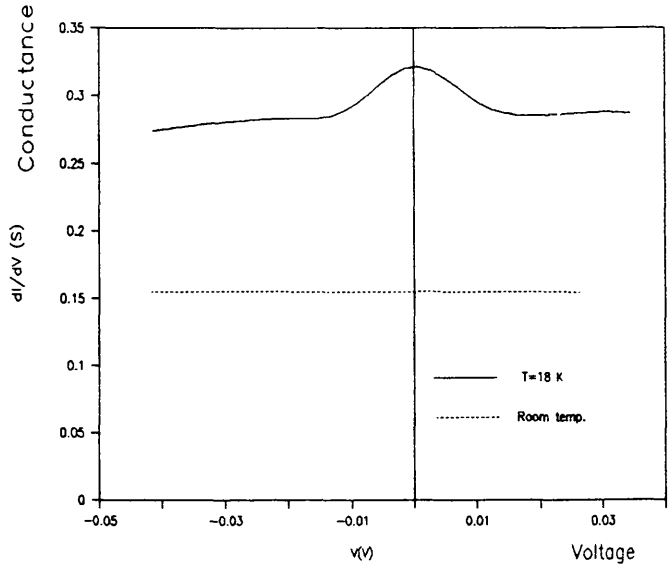

Fig.5.36 Conductance of NJ at the indicated temperatures

Figure 5.36 shows the conductances vs voltage obtained from the data of the IV curves of figures 5.31 and 5.34 . The conductance vs voltage graph (solid line) corresponding the IV curve at low temperature (figure 5.34) shows that the increase in current starts at -10 mV and continues to do so until it reaches its maximum at V=0 and then decreases until V=+10 mV where it becomes constant . The conductance vs voltage curve (dashed line) corresponding to the IV curve at room temperature (figure 5.31) is a straight line . The conductance at low temperature is higher than the conductance at room temperature .

5.5.3 Results of the Bar S1E

Similar measurement to those made on the pellet were carried out on bar. The resistance R of the sample was measured at room temperature 10 times and the following value of the mean and the standard deviation of the mean were found: R=(18.69 +/- 0.07) milli Ω . IV curves were measured at

room temperature and low temperature for both NJ and FJ . R vs T of the bar was measured during the warming up of the sample.

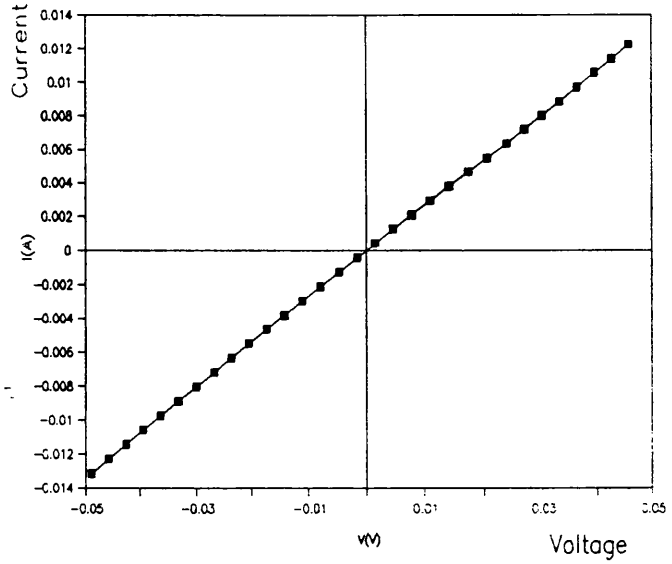

Fig.5.37 IV curve of NJ of the bar at room temperature

The IV curve of near dots of the bar shown in figure 5.37, at room temperature, is a straight line whose slope yields a resistance of 3.8 Ω .

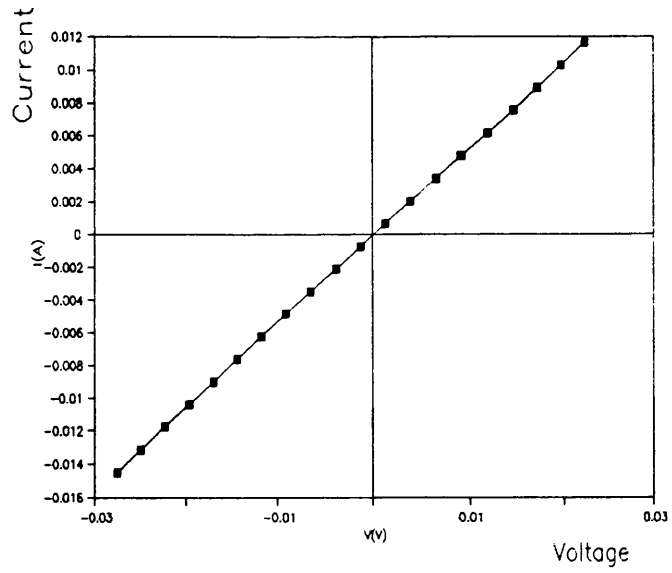

Fig.5.38 IV curve of FJ of the bar at room temperature

The IV curve of far dots of the bar shown in figure 5.38, is also a straight line at room temperature with a slope yielding a resistance of 2Ω . This is a very low resistance.

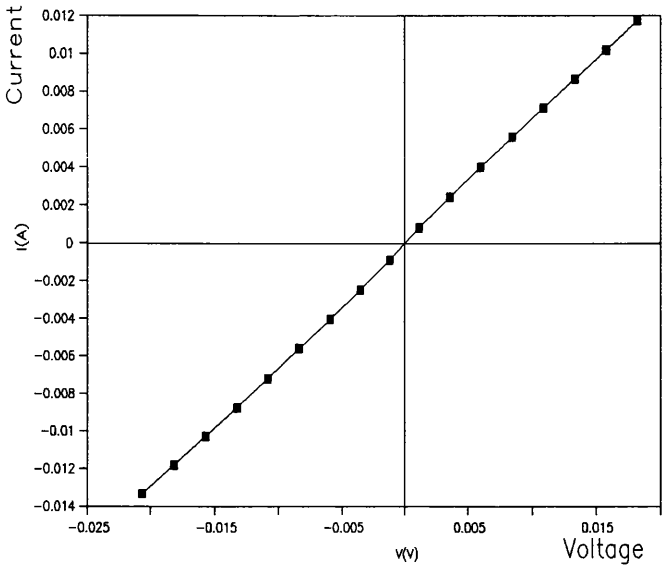

Fig.5.39 IV curve of NJ of the bar, T=30 K

Figure 5.39 shows the IV curve of near dots (NJ) . This IV curve also exhibit a slight increase of the current around 0 V.

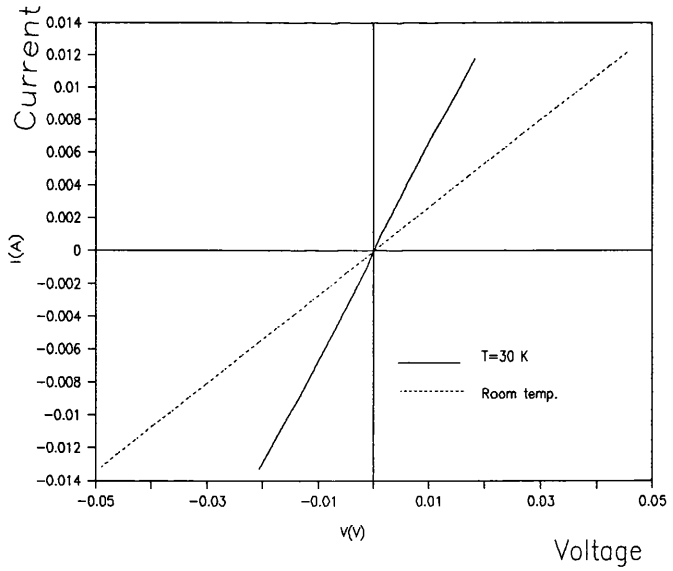

Fig.5.40 IV curves of NJ of the bar at the indicated temperature

Figure 5.40 shows that the conductance of NJ increase with decreasing temperature .

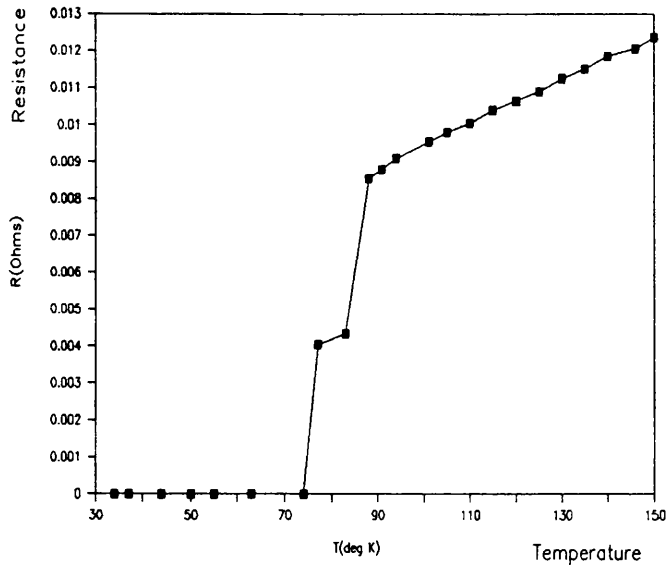

Fig.5.41 R vs T of the bar during warming up

Figure 5.41 shows the resistence R vs T of the bar measured during the warming up of the sample . The superconducting transition is seen to be at 74 K with knee between 77 and 83 K. This is known as double transition and is usually due to the presence of two different phases with different critical temperatures.

5.6 Sample 5 referred to as S2A

5. 6. 1 Sample preparation.

Fresh powder of YBCO was prepared from a stoicheometric mixture of Y_2O_3, CuO, and $BaCO_3$. This mixture was thoroughly homogenised and fired according to the diagram shown in figure 5.42.

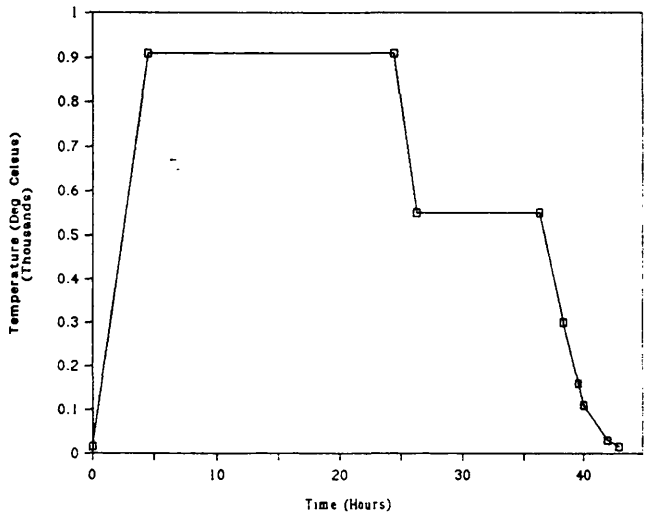

Fig.5.42 Firing of S2A YBCO sample

This resulted in a black powder mixed with few green particles which was then mixed, ground, sieved through 125 μm mesh, and sintered in air according to the previous diagram. The resulting product was completely black indicating the reaction had been complete and YBCO powder had resulted. This was finely reground and sieved again through the 125 μ mesh. This powder was then used to make pellets of 13 mm in diameter. Their weight was approximately 1 g and they were pressed at a pressure of 7 tons. These pellets were sintered in flowing oxygen according to the diagram indicated in figure 5.43. A thickness of about 250 Å of Al was evaporated as a stripe on the pellet. This was

left to oxidize in air for 2 hours. Ag dots were then evaporated and the pellet was fixed onto the sample holder of the continuous flow cryostat as shown in figure 5.44.

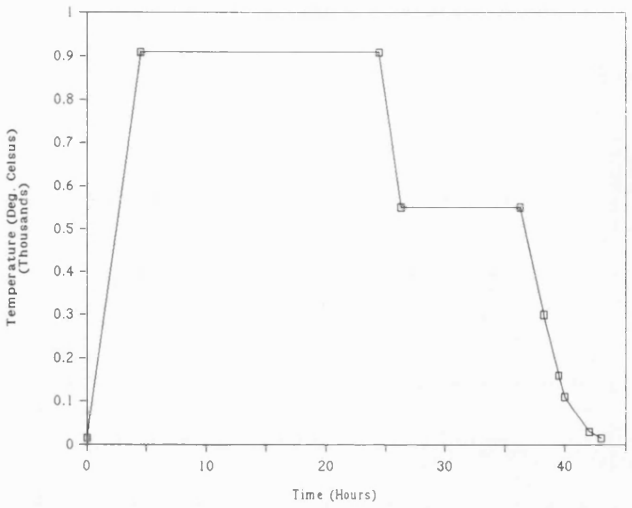

Fig.5.43 Sintering of S2A pellets

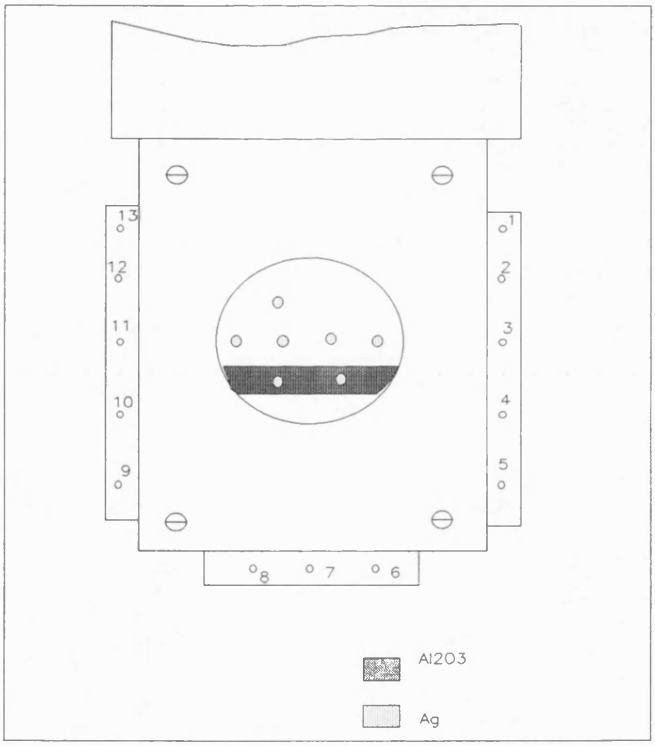

Fig.5.44 Layout of the AlOx and Ag dots on S2A pellet

5.6.2. Experimental set up .

Electrical contacts were soldered to the cryostat connectors and the pellet dots as shown in figure 5. 45 and the measurement were carried out using the same experimental rig shown in figure 5.18 .

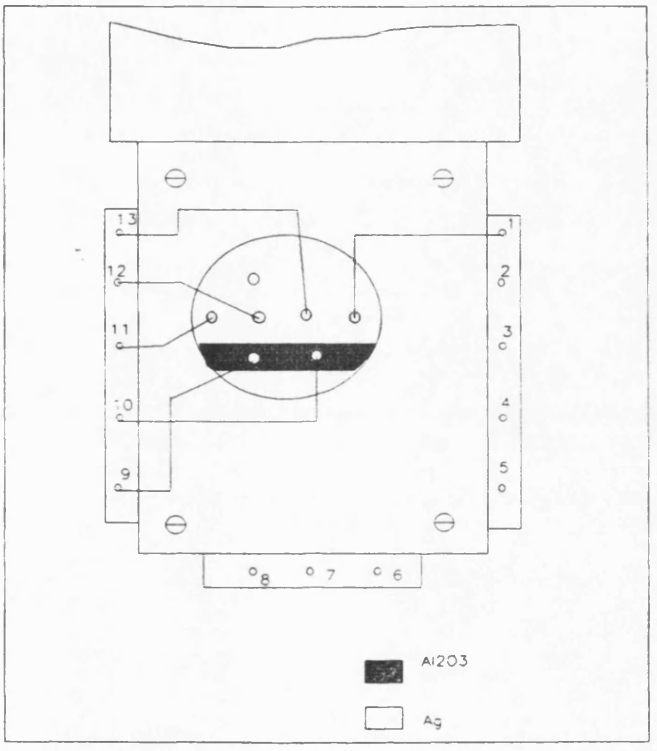

Fig.5.45 Contact Layout of S2A pellet

5.6.3. Measurement results.

The junctions used in this experiment will be referred to by alphabetical letters . A schematic representation of the pellet indicating the different junctions positions, is shown in the following figure.

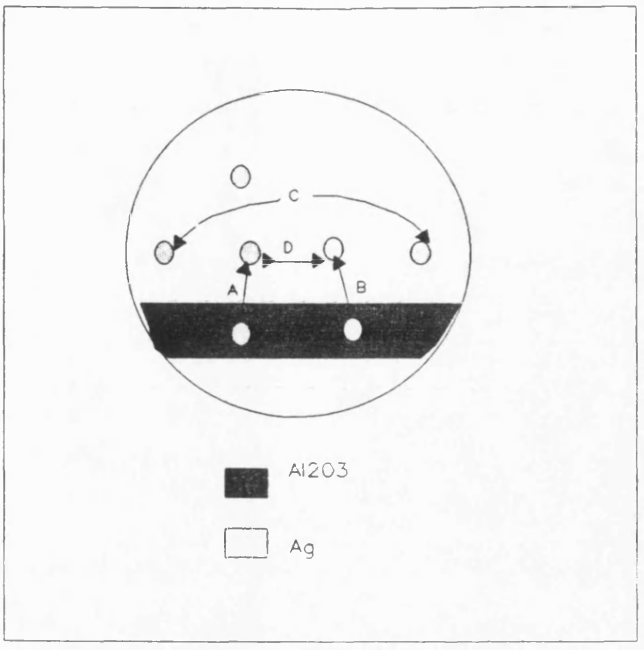

Fig.5.46 Junctions layout of sample S2A

The different junctions shown in the layout of figure 5.46 were connected to the following sample holder pins:

Junction A between pin 12 and 9

Junction B between pin 13 and 10

Junction C between pin 1 and 11

The resistance R of the sample was measured at room temperature using the four point method and the value obtained was 7 mΩ . The IV curves of junctions A and B which have an artificially deposited dielectric layer were also measured at room temperature and the results are presented in the following figures

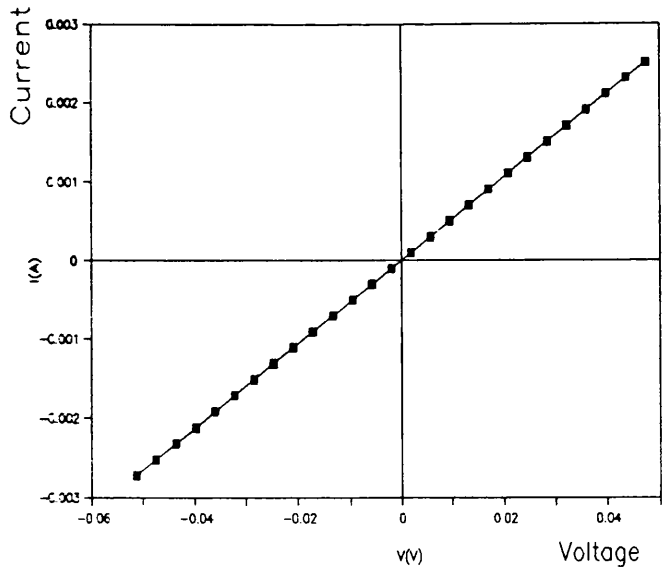

Fig.5.47 IV curve of junction A at room temperature

Figure 5.47 shows the IV curve of junction A at room temperature. The slope of this IV curve yields a junction resistance of 19 Ω

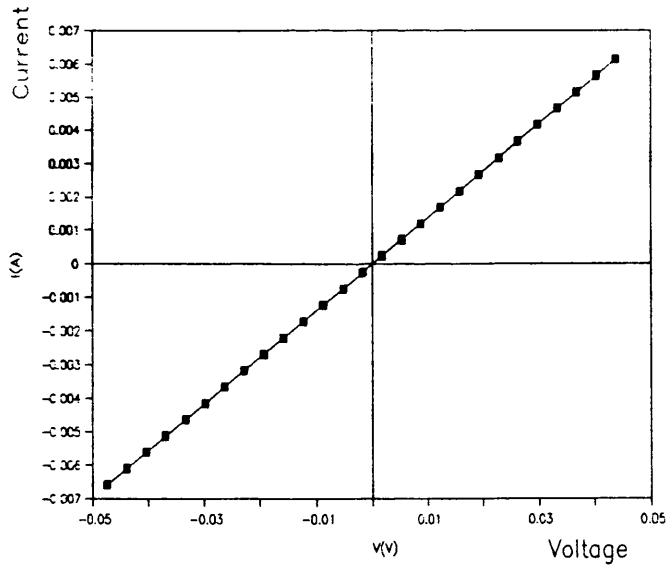

Fig.5.48 IV curve of junction B at room temperature

Figure 5.48 shows the IV curve of junction B at room temperature . The slope of the curve yields a junction resistance of 7 Ω . Although junction B is on the same insulating layer as junction A, its resistance is lower than that of B.

After these room temperature measurements the continuous flow cryostat was connected to helium dewar and the and the sample temperature decreased rapidly to 10 K . At this temperature the resistance of the sample was checked using the four point method and found to be zero indicating that the sample is fully superconducting . Subsequently IV curves of different junctions were measured at low temperatures using different voltage ranges. The results are presented in the following sections .

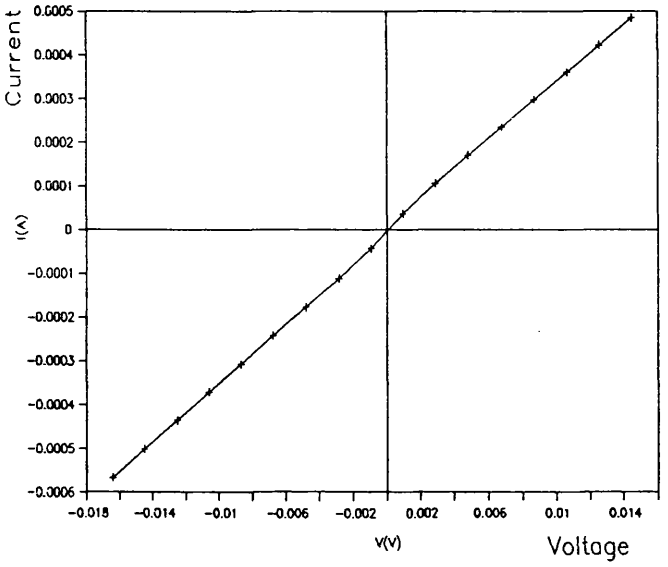

Fig.5.49 IV curves of junction A, T=10 K

Figure 5.49 shows the IV curve of junction A at 10 K. On this range of voltages (-18 mV< V < 14 mV), a slight increase of current around the origin can be seen . This behaviour has been observed in previous measurements .

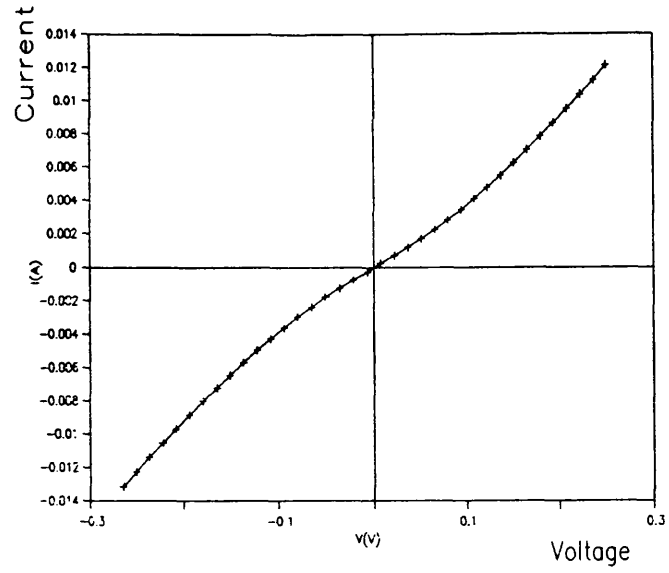

Fig.5.50 IV curves of junction A, T=10 K

Figure 5.50 shows one of three identical IV curve of junction A taken at T=10 K using a higher voltage range ie -280 mV <V < +280 mV in the case of this one. For this higher voltage ranges the IV curves of junction A slightly non-linear . The small current increase observed in figure 5.49 is indistinguishable in this high voltage range scan, however this feature is reflected in the conductance vs voltage as can be clearly seen in the following figure

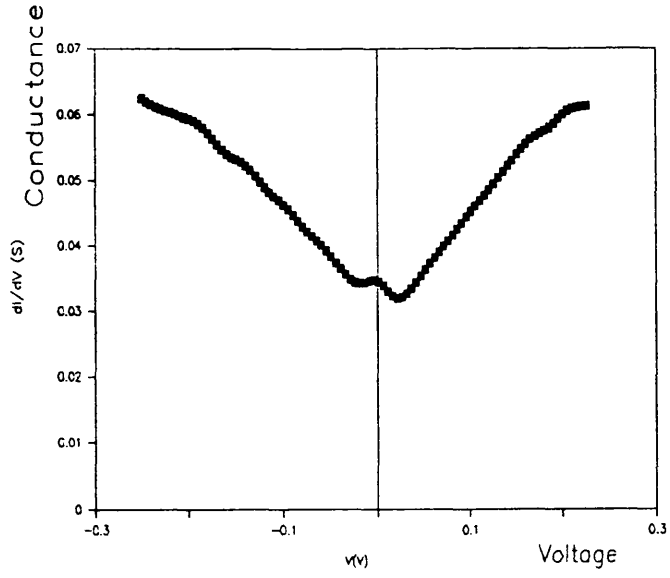

Fig.5.51 Conductance vs voltage of junction A

Figure 5.51 is the conductance vs voltage derived from the data of figure 5.50 . This graph shows that the increase of current around V=0 is asymmetrical. Beyond about +/- 15 mV the conductivity increases with increasing voltages and starts to flatten about +/-180 mV.

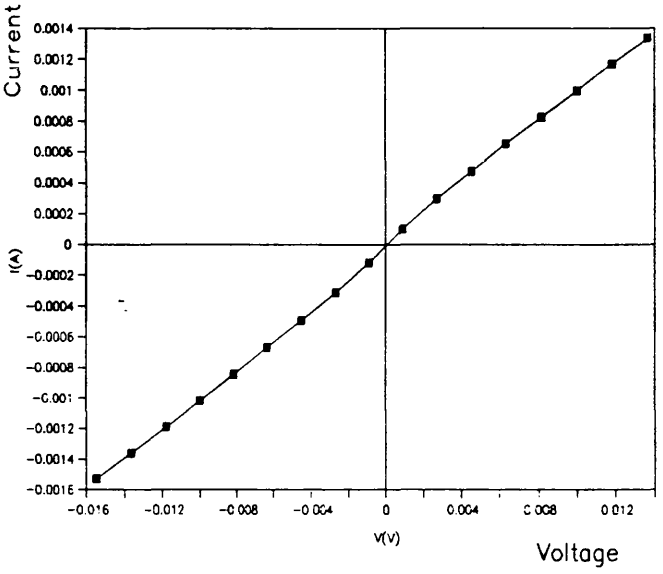

Fig.5.52 IV curve of junction B, T=10 K.

Figure 5.52 shows the IV curve of junction B at T=10 K using voltages between -18 mV and +18 mV. The upward displacement of the right side of the IV relative to the left side can be clearly seen .

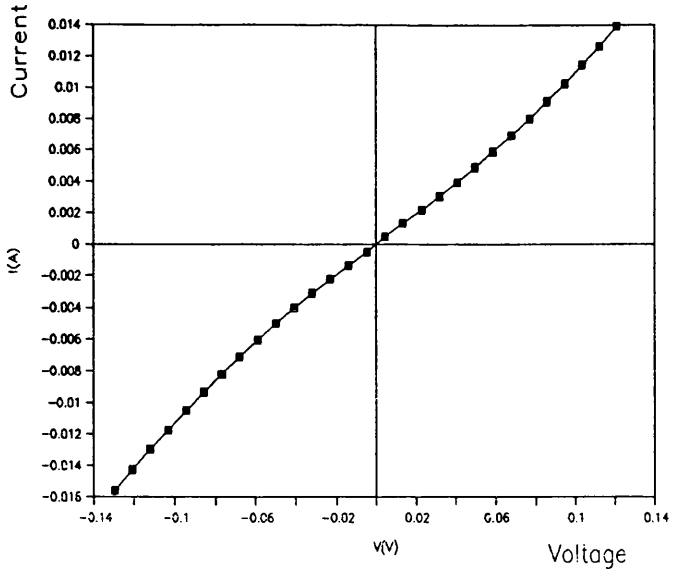

Fig.5.53 IV curve of junction B, T=10 K

Figure 5.53 shows the IV curve of junction B at T=10 K using voltages from -140 mV to +140 mV.

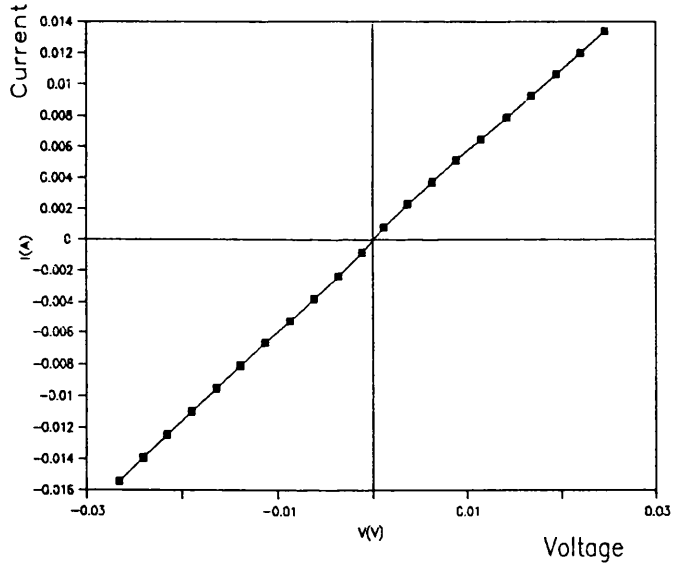

Fig.5.54 IV curve of junction C, T=9.5 K

Figure 5.54 shows the IV curve of junction C which has no insulating layer at T=9.5 K using voltages between -30 mV to +30 mV. A slight increase of current around V=0 can be seen. The slope of the linear part of the IV curve is 1.9Ω .

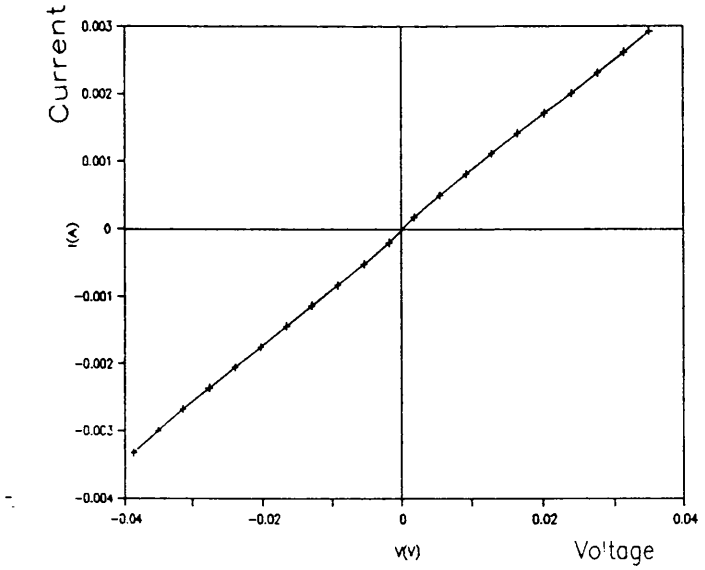

Fig.5.55 IV curve of junction D, T=9.5 K

Figure 5.55 shows the IV curve of junction D which has no insulating layer at T=9.5 K . A slight increase of current around 0 V can be seen. The slope of its linear part is 12.5 Ω . This is almost 7 times higher than that of C.

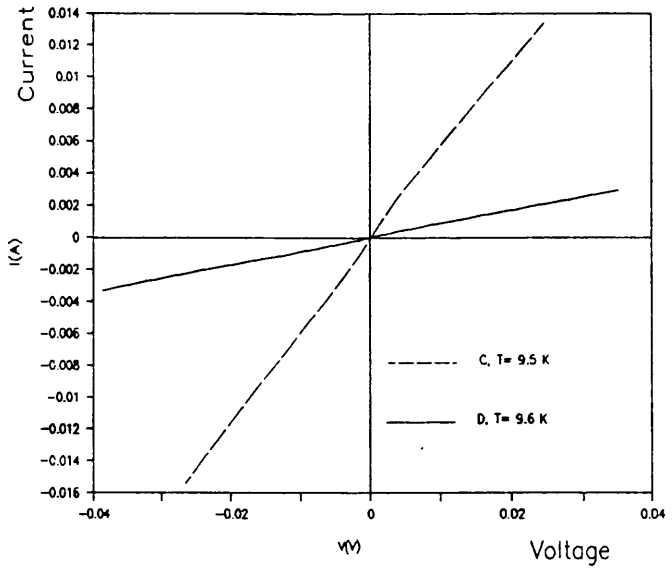

Fig.5.56 IV curves of junctions C and D (direct contacts)

Figure 5.56 is simultaneous presentation of the IV curves of figures 5.54 and 5.55 . This figure (5.56) brings out more clearly the difference between contact C and D which was expressed in term of the resistance obtained from the slope of the linear part of the IV curves. These values indicates that C approached the short circuit behaviour (resistance =1.6 Ω) whereas that of junction D was 12.5 Ω ie 7 times higher . Thus one can conclude that the surface layer of the sample is not homogeneous. This has been observed in many reports as will be discussed in chapter 6.

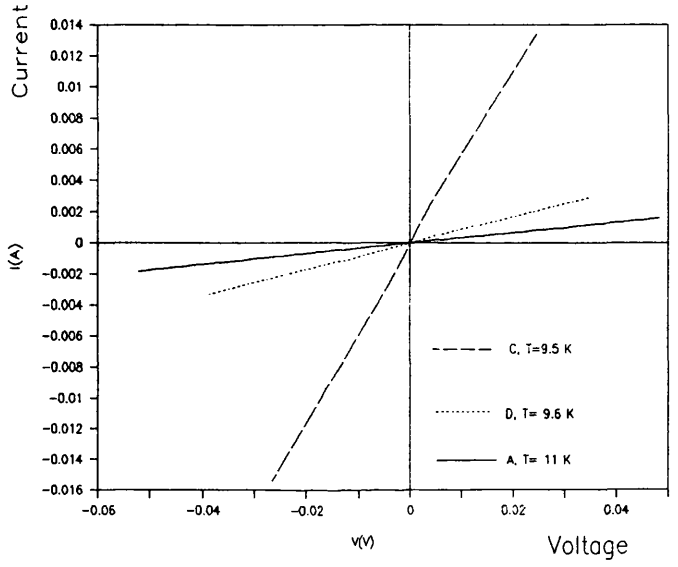

Fig.5.57 IV curves of dot C, D, and A

Figure 5.57 shows that the behaviour of junction D is nearer to that of A rather than C despite the fact that junctions C and D have no artificial dielectric deposited whereas junction A has such a layer .

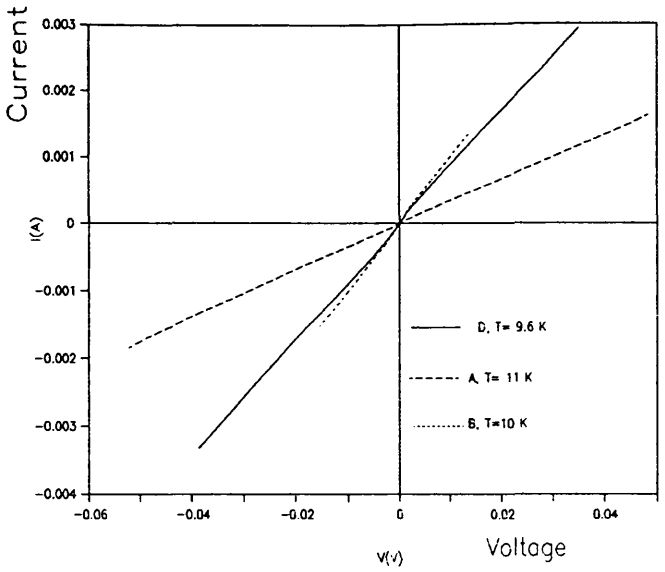

Fig.5.58 IV curves of D, A, and B.

Figure 5.58 shows that although junction B has the same artificial barrier as junction A their behaviour is different. Note that the IV curve of junction B which has an insulating barrier on one of the contacts (dot 10 in figure 5.45) is very similar to that of junction D which has no such a layer . This suggests that the insulating layer under dot 10 is shorted out .

5.6.4 R vs T with increasing temperature

When the above measurements were finished and the temperature started to rise, R vs T data was taken and the results are presented in the following graph.

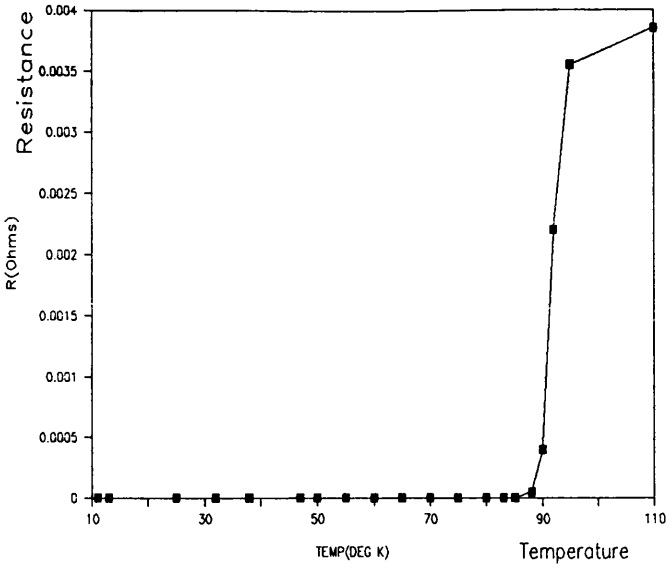

Fig.5.59 R vs T during warming up

Figure 5.59 shows that the sample kept its superconducting state up to 85 K. For this experimental set up (liquid helium cooled continuous flow cryostat) , the cooling down is very fast and hence does not allow precise measurement of R against T. On the contrary the warming up is very slow and results in a more precise determination of the measurement of R vs T and hence the critical temperature Tc .

5.7 Sample 6 referred to as BD1

5.7.1 Sample preparation.

The sample used for this experiment is a pellet which was prepared from a stoichiometric powder of YBCO acquired from BDH . A mass of 2 grammes was pelletized at 10 tons and subsquentely sintered in flowing oxygen according to the diagram shown in figure 5.60 .

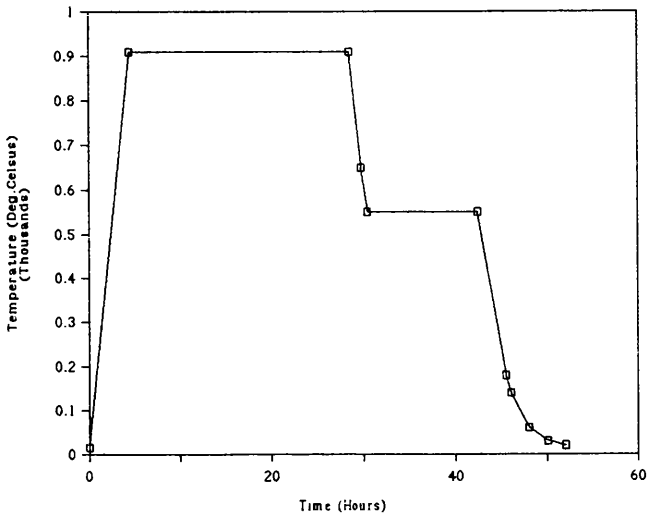

Fig.5.60 Sintering diagram of BD1

Prior to dielectric deposition the pellet was sputter cleaned for 20 minutes .

5.7.2 Silicon oxide deposition

A pressure of (7+/-2)10^{-6} mbar was maintained and a thickness of 220 Å of SiO was evaporated at an average rate of 0.5 Å/s onto a slice of the pellet as shown in figure 5.61 (a).

A second pellet that had been used previously and shown a Tc of 88 K was inserted into the jar and 520 Å of SiO was evaporated onto it the same conditions as above . These pellets with SiO were then heated for 5 min in an oven at 80 C to allow the formation of SiO_2 .

5.7.3 Magnesium fluoride (MgF_2) deposition

The pellet onto whith 220 Å of SiO_2 was inserted again into the evporator and a layer of MgF2 of 600 Å thickness was deposited as indicated in figure 5.61 (b) .

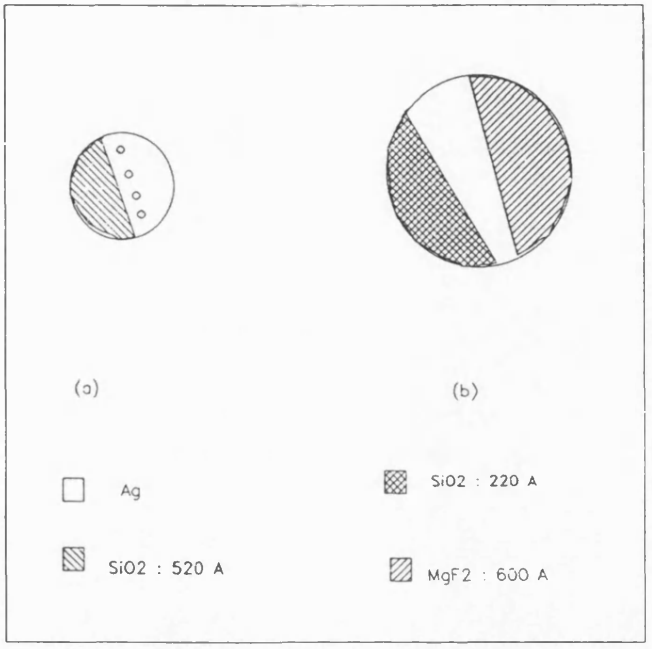

Fig.5.61 Layout of BD1 dielectric thicknesses

5.7.4 silver deposition

Although the pellet was accidentally broken into smaller pieces, three of these were of reasonable size silver dots were evaporated onto them so as to allow for R vs T and IV curve measurement from junctions having different dielectric layer thicknesses. Ag dots were also evaporated on the sample which had 520 Å a of SiO_2 .

5.7.5 Electrical contacts layout

The above selected pieces were fixed to a sample holder and electrically connected to the cryostat sample holder pins as shown in figure 5.62 .

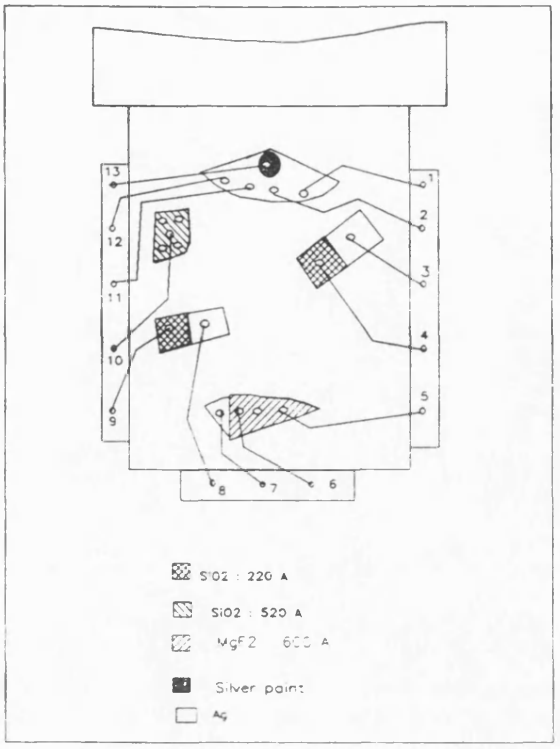

Fig.5.62 Layout of BD1 samples

In this experiment the different junction will be named after the two pins between which they are connected. For instance the junction between pins 3 and 4 will be referred to as J3-4 . The junction which is connected to pin 10, has the base electrode connected to the cryostat and thus it is referred to as Jc-10. The pin 13 is connected a junction that has been made of silver paint directly painted on the pellet surface.

5.7.6 Experimental set up .

The sample was mounted in the continuous flow cryostat and the measurement were carried out using the computer controlled set up which was described previously and represented in figure 5.18 .

5.7.7 Measurement results.

Prior to the cooling down of the sample its resistance was measured at room temperature using the four point method. The measurement was repeated 10 times and the gave the following mean and the standard deviation of the mean: R = (12.11 +/- 0.01) milli Ω .

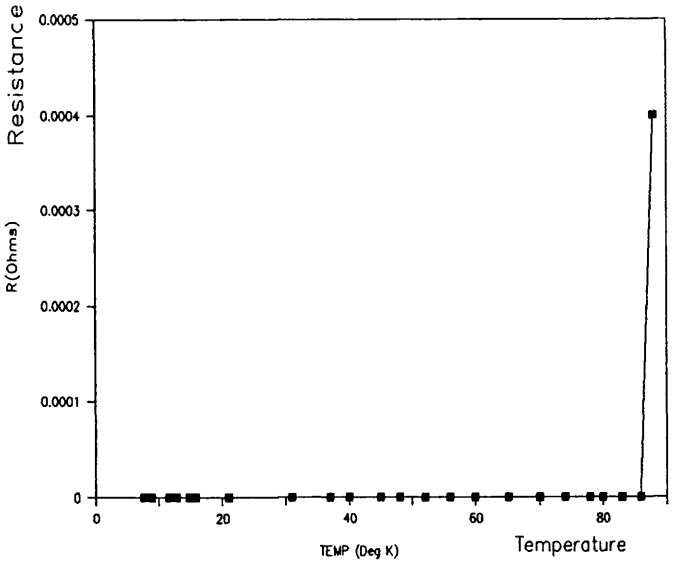

Fig.5.63 R vs T measurement of BD1.

Figure 5.63 shows that the transition temperature of this sample is Tc=86 K.

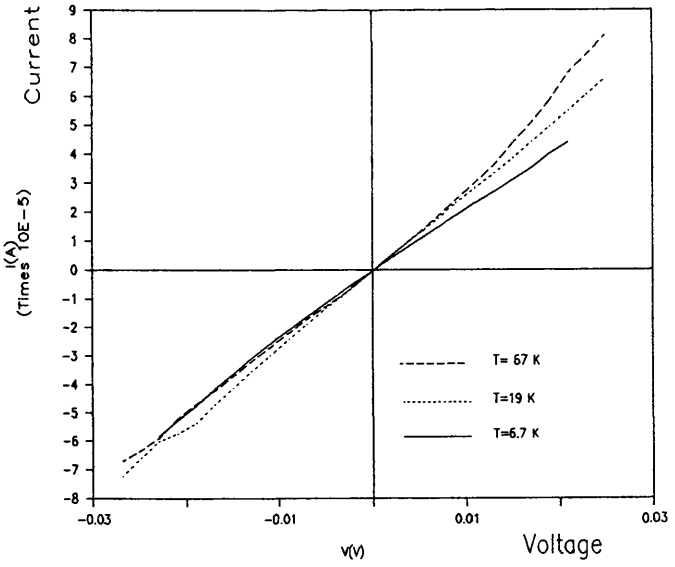

Fig.5.64 IV curves of J7-6 at different temperatures

In figure 5.64 the IV characteristics using a low voltage range of the same junction, J7-6, at different temperatures, are presented. Some features can be seen on some of the curves at -20 mV and +18 mV for the curve at T=19 K and T=67 K respectively. This graph shows also that these curves are asymmetric .

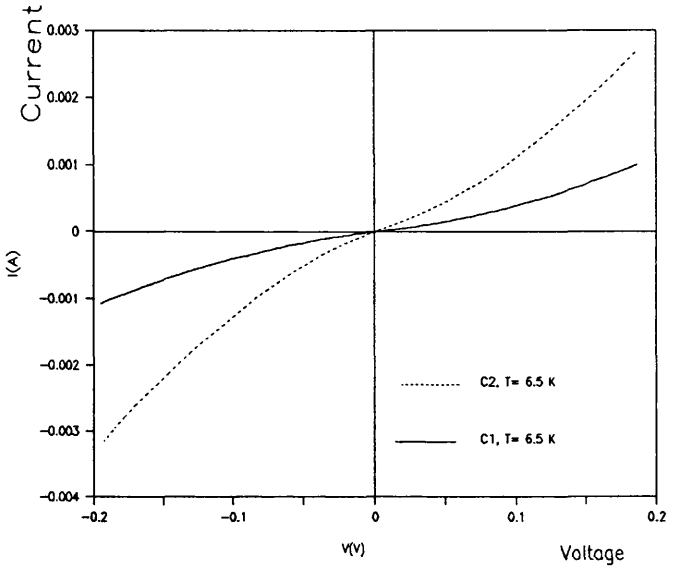

Fig.5.65 IV curve of J7-6 and J7-5, T= 6.5 K

Figure 5.65 shows a simultaneous presentation of the IV curves of junctions J7-6 (curve C1 in the graph) and J7-5 (curve C2) which have MgF_2 as dielectric and were measured at the same temperature T= 6.5 K . Despite the fact that the two junctions are onto the same sample and prepared under the same conditions, their IV characteristics are different .

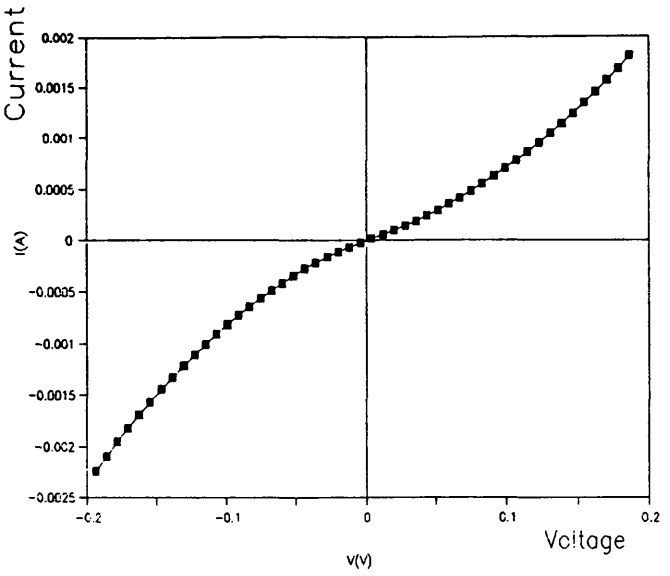

Fig.5.66 IV curve of junction JC-10 at T= 6 K

Figure 5.66 shows the IV curve of junction JC-10 whose artificial barrier is SiO_2 which is 520 Å thick .

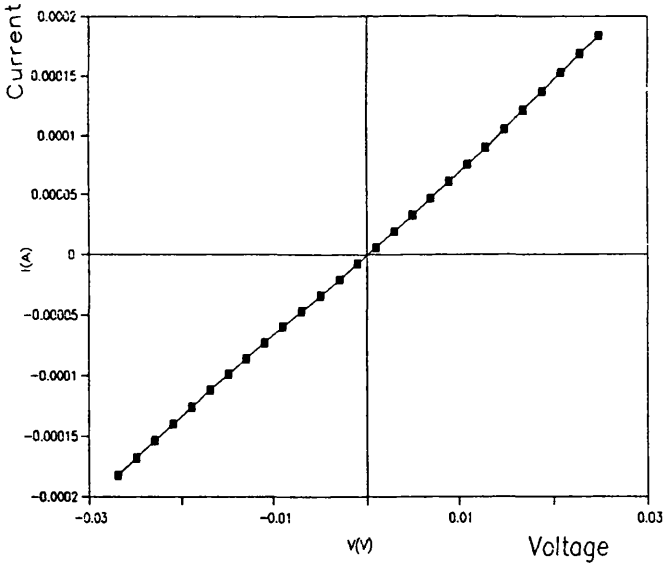

Fig.5.67 IV curve of J11-1 without artificially deposited dielectric T= 24 K (Small voltage range)

Figure 5.67 shows the IV curve measured between dots 11 and 1 (J11-1). This is junction without an artificial

barrier. From the slope of this curve one can deduce a resistance of around 160 Ω . This implies the existence of non-superconducting layer between the two contacts.

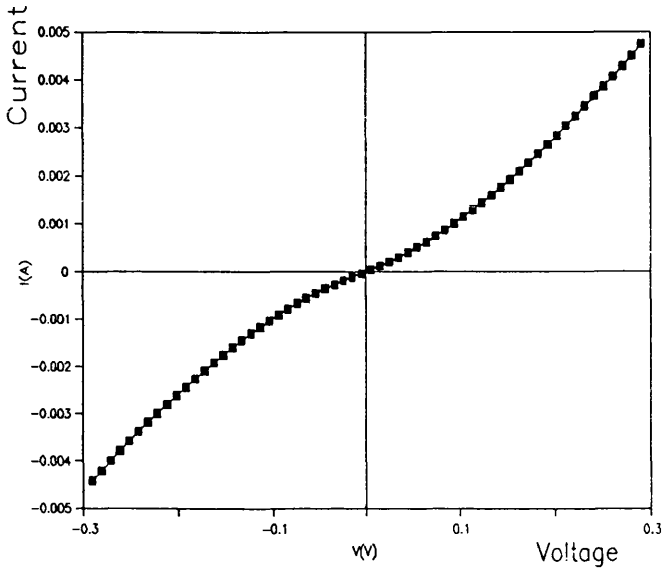

Fig.5.68 IV curve of J11-1 without artificially deposited dielectric, T= 26 K (Wide voltage range).

Figure 5.68 shows the IV of J11-1 (junction betwen dots 11 and 1 obtained by directly depositing Ag on the superconductor surface) measured using a wide voltage range. The IV curve exhibits a non-linear behaviour. This phenomenon is usually due to the formation of non superconducting layer (dead layer as it is often called) on the surface.

5.8 Sample 7 referred to as SDO

5.8.1 Sample preparation

The sample is a 19 mm diameter pellet prepared from Y_2O_3, $BaCO_3$ and CuO powders stoichiometrically mixed according to the formula $YBa_2Cu_3O_7$ and fired at 915 C for 48 hours in air . The mixture was pulverised and fired again at 915 C for 24 hours in air . The resulting black material was then finely ground , pressed at 8 tonnes into pellets and sintered into flowing oxygen according to the diagram in figure 5.69.

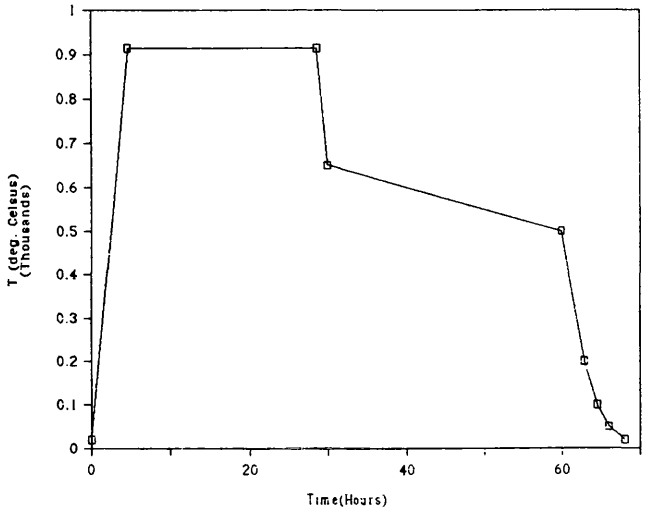

Fig.5.69 Sintering diagram of SDO

One face of the pellet was sputter cleaned using an ion beam facility . Then different thicknesses of SiO_2 were deposited using the same facility. The dielectric thickness patterns is shown in the following figure .

In figure 5.70 the areas having different dielectric thicknesses are specified . The area where no dielectric was deposited is indicated by the letter "A" . Normal metal (Ag) was evaporated through a suitable mask allowing the deposition of silver dots onto the different dielectric thicknesses, and also on the area without dielectric . The position of the dots on the different areas is indicated in figure 5.71

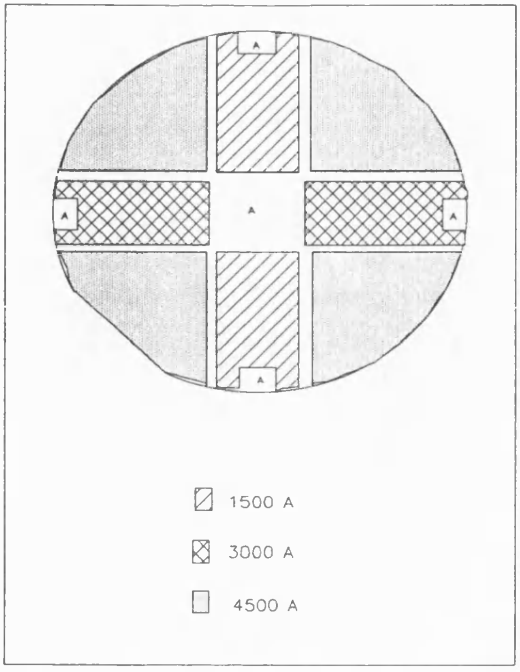

Fig.5.70 Layout of different thicknesses of SiO_2

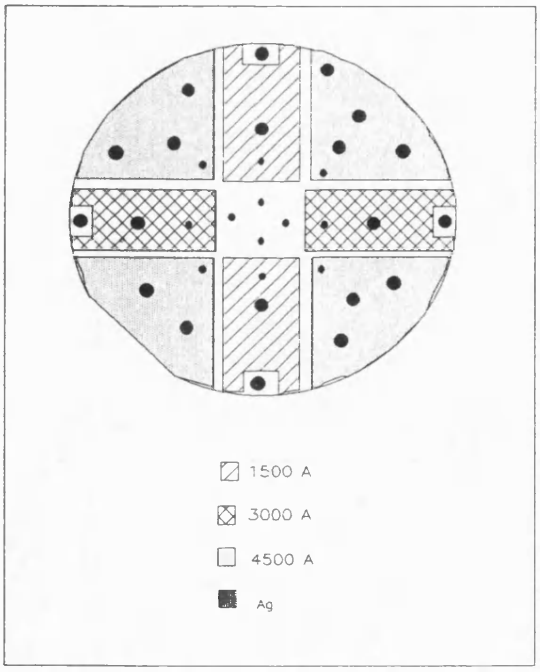

Fig.5.71 Layout of Ag dots on SDO sample

The dots on the dielectric constitute the normal electrode of the junction whereas those on area "A" (figure 5.70) are

direct contacts to the superconductor surface. Four of the direct contacts which are situated on the periphery of the pellet were used for the four points method which served to investigate the transition to the superconducting state of the pellet. Inside the cryostat, the sample was positioned on a sample holder fixed to the cold body of the cryostat between two sets of pin-strip headers allowing for fourteen dots to be used. The pins are numbered clockwise as shown in figure 5.72. During the measurement the junctions used were given the same number as the pins to which they were connected. The capital letters inside the circles designate the corresponding pins of the connectors outside the cryostat. The letters Tc designates a thermocouple which was added to allow temperatures readings.

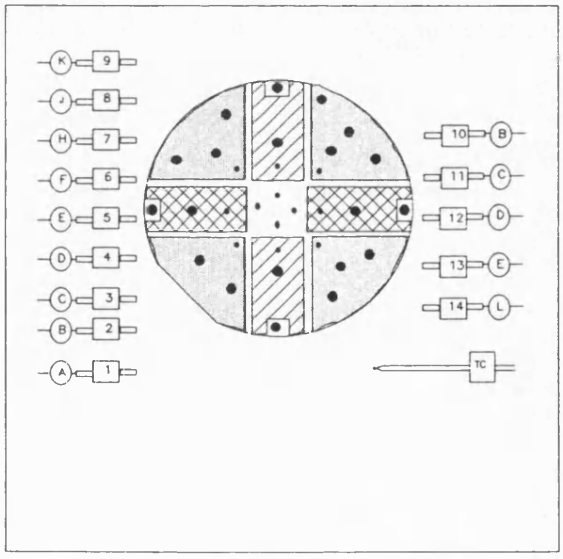

Fig.5.72 Layout of different contacts inside the cryostat

The cryostat used is versatile and can be used at both liquid nitrogen or liquid helium temperatures. The details of the cryostat are as shown in figure 5.73 .

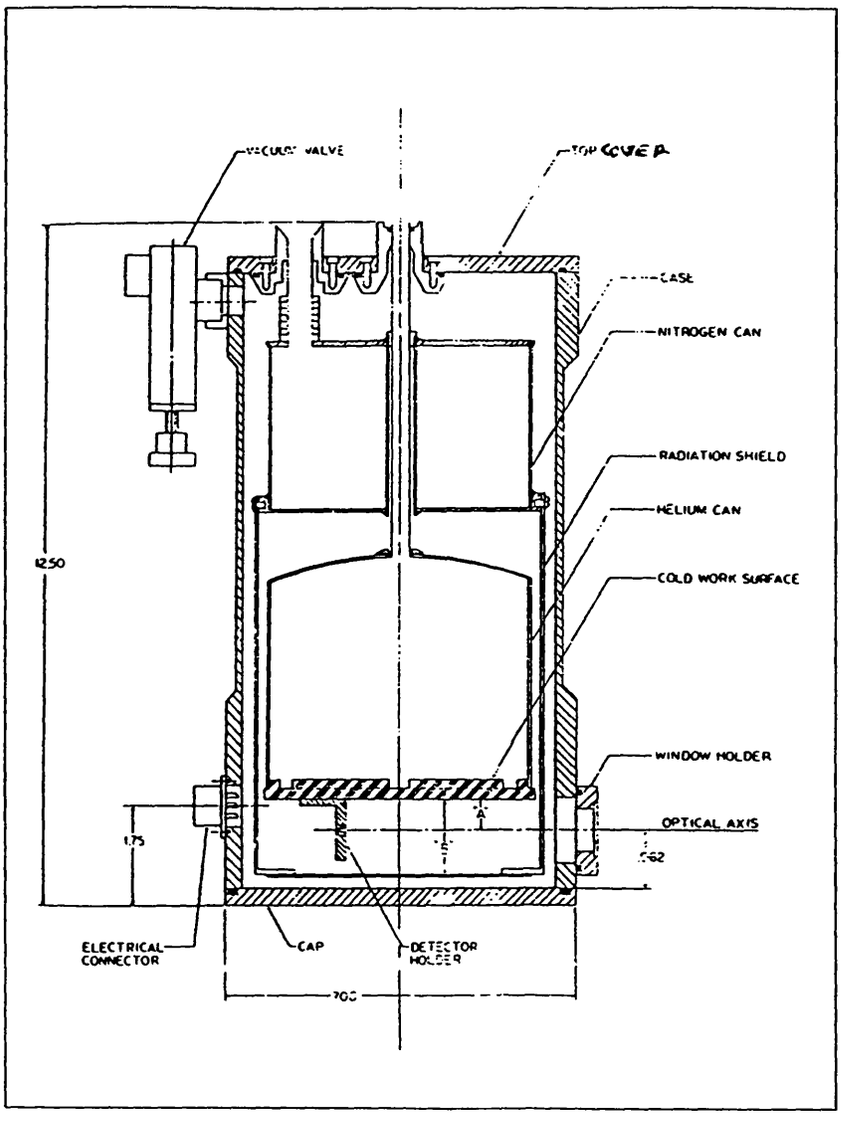

Fig.5.73 Helium cooled cryostat

5.8.2 Experimental set up .

The experimental set up used for measuring the IV characteristics of different junctions of this sample is shown in figure 5.74 .

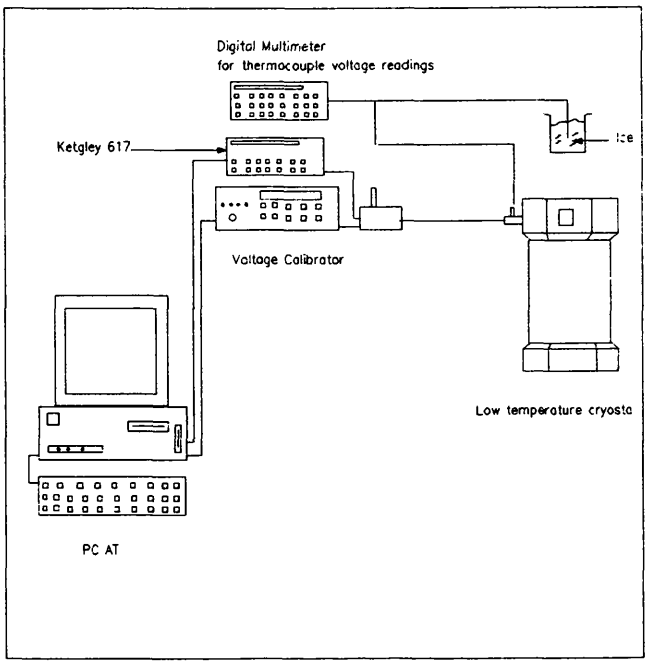

Fig.5.74 Experimental set up used with SDO

5.8.3 Layout of run 1, 2, and 3

During the first three runs, the sample dots were connected to the two sets of pin-strip headers using very thin gold wires (35 microns in diameter) as shown in figure 5.75 .

The different junctions will be referred to according to the two pins between which they are connected. In this measurement pin 9, which is connected to one of the dots in the centre of the pellet, was chosen to be the common electrode . Therefore a junction between pin number (N) and the common pin (C) will be referred to as JN&C . For N=7, 11, and 14 for instance, the junctions will be called J7&C, J11&C, and J14&C respectively.

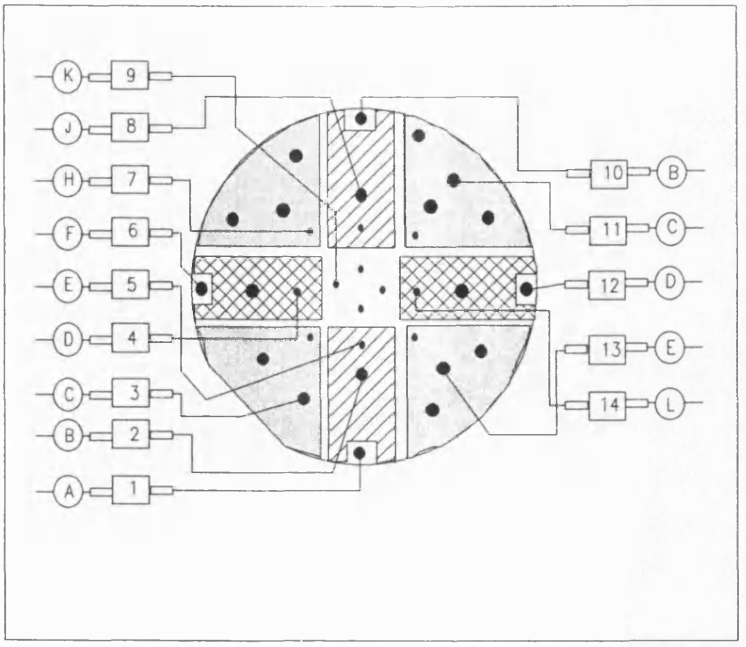

Fig.5.75 Contact layout used for run 1, 2, and 3

5.8.4 Measurement results of run 1

Measurement of IV characteristics were carried out on most of the dots on the different dielectric layer thicknesses. The measurement at low temperature were carried out at 77 K . Prior to the IV curve measurements at 77 K , the sample resistance was determined by the the four probes method using pins 1, 6, 10 and 12, and found to be zero . During the first run, the measurement was concentrated on one particular junction J7&C which gave striking non-linear behaviour. The measurement on J7&C was made over different voltage ranges and resulted in 17 reproducible non-linear IV curves . Because of the similarities of these IV curves, only six of them are presented in the following figures .

Figure 5.76 shows the first of these 17 IV curves which was measured for voltages between -153 mV and +153 mV. This curve is asymmetric and exhibits non-linear features. Over the voltage range from 25 mV to 150 , the current was zero.

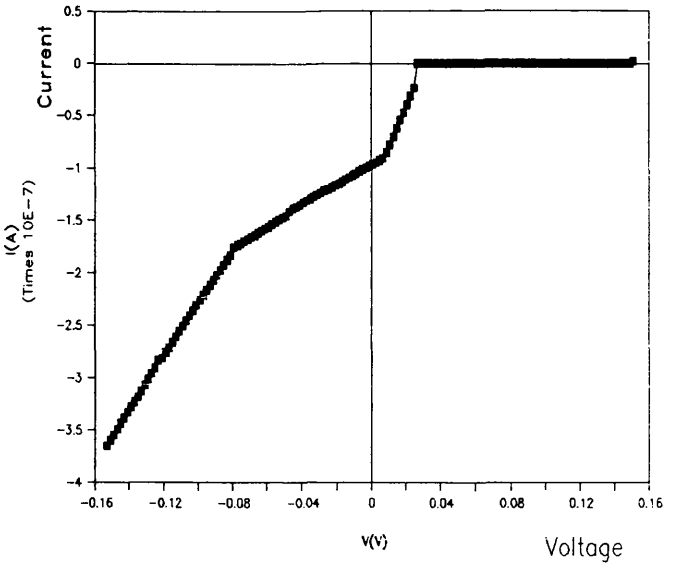

Fig. 5.76 IV curve of J7&C, T=77, V=+/- 153 mV

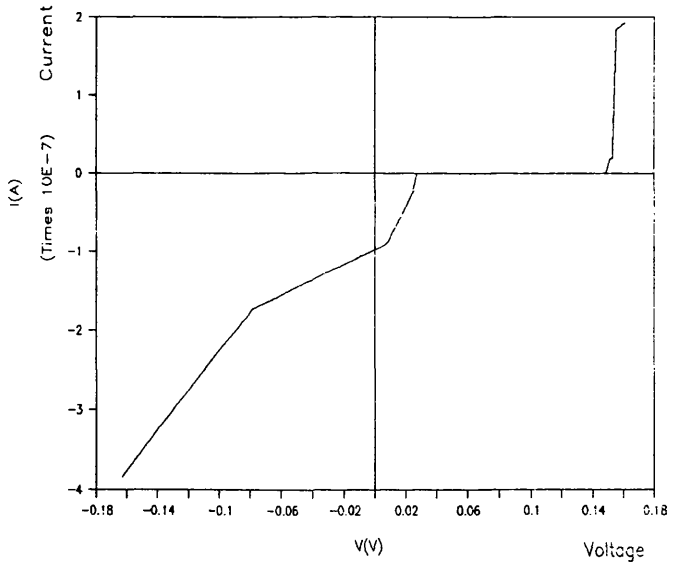

Fig. 5. 77 IV curve of J7&C, T=77, V=+/- 163 mV

Figure 5.77 shows the IV curve of J7&C for voltages between -163 mV and 163 mV. The current which was zero between 25 mV and 150 mV starts to rise above 150 mV. At about 151 mV the current shows a small but sharp increase followed by a small knee. At V=155 mV, a higher and sharper increase can be seen followed by linear features.

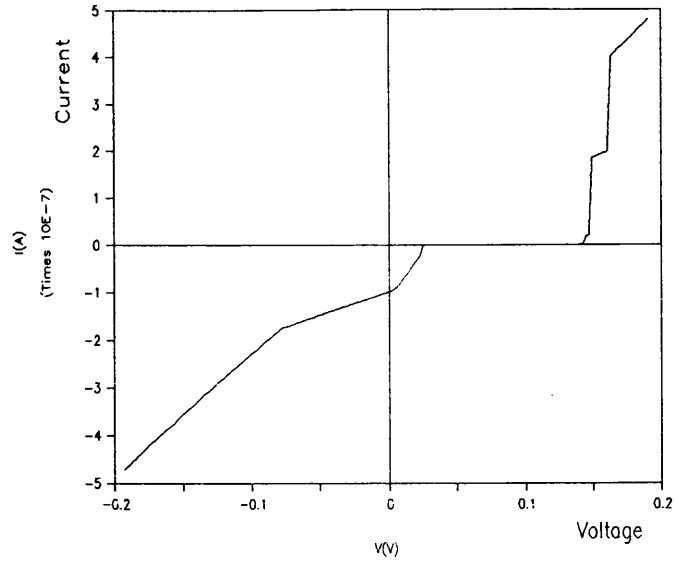

Fig. 5.78 IV curve of J7&C, T=77, V=+/- 193 mV

Figure 5.78 shows that the linear region observed starts at 155 mV , extends only to about 166 mV where the current rises very sharply again. For voltage greater than 166 mV, the curve is once again linear .

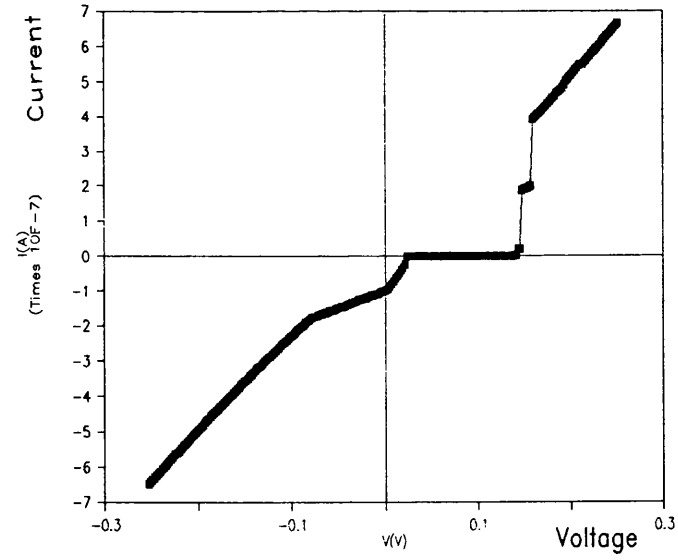

Fig. 5.79 IV curve of J7&C, T=77, V=+/- 253 mV

Figure 5.79 shows the IV curve of J7&C for V between -253 mV and 253 mV. All the features observed in the previous curves are also seen here .

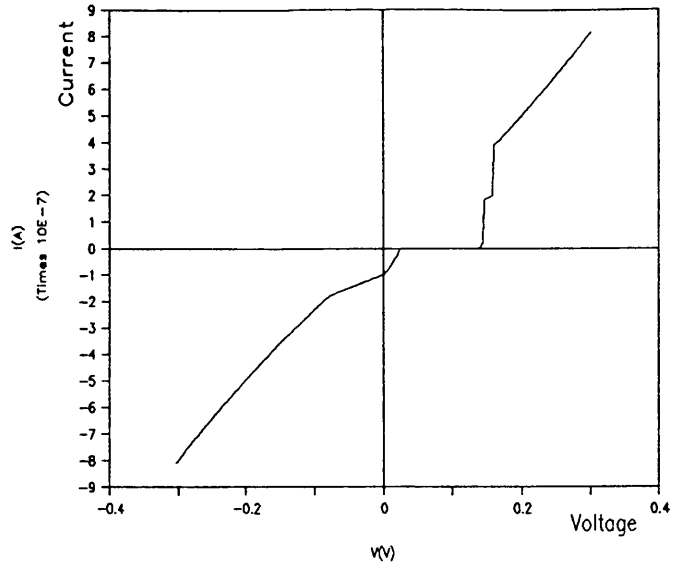

Fig. 5.80 IV curve of J7&C, T=77, V=+/- 303 mV

Figure 5.80 shows the IV curve of J7&C for V between -303 mV and 303 mV. This is the last of the 17 curves obtained. These curves are asymmetric and characterised by a strong non-linearity. In addition, a knee is present in the middle of the region of sharply increasing current.

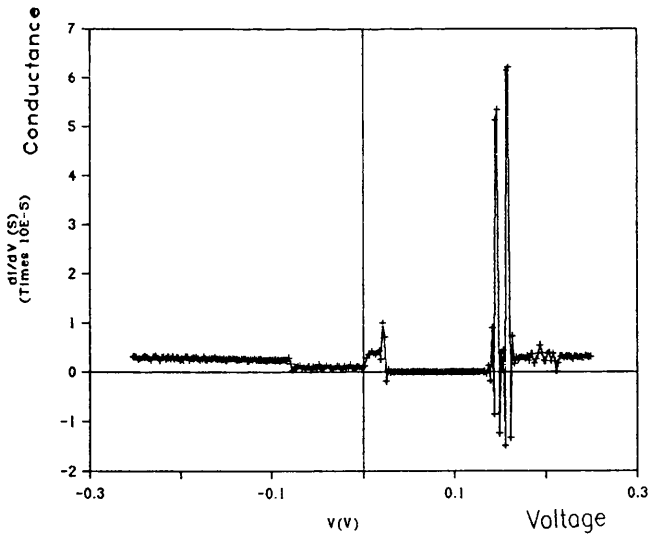

Fig. 5.81 Conductance vs voltage of J7&C, T=77, V=+/-253 mV

Figure 5.81 Shows conductance against voltage of J7&C obtained from the data of the IV curve of figure 5.79 . This figure shows that there is no current flow for voltages between 37 mV and 125 mV . This zero current region is enclosed by two small negative conductance valleys followed by two peaks with the right hand peak having an amplitude almost three times that of the left peak. The first peak on the right is followed by a slight decrease of conductance and then a second peak which is higher than the first one. Beyond the second peak on the right the conductance decreases rapidly and exhibits some oscillation-like features around 0.3 S. For voltages less than zero, the conductance has two levels : 0.5 S down to -90 mV and almost 0.3 S for voltages less than -90 mV .

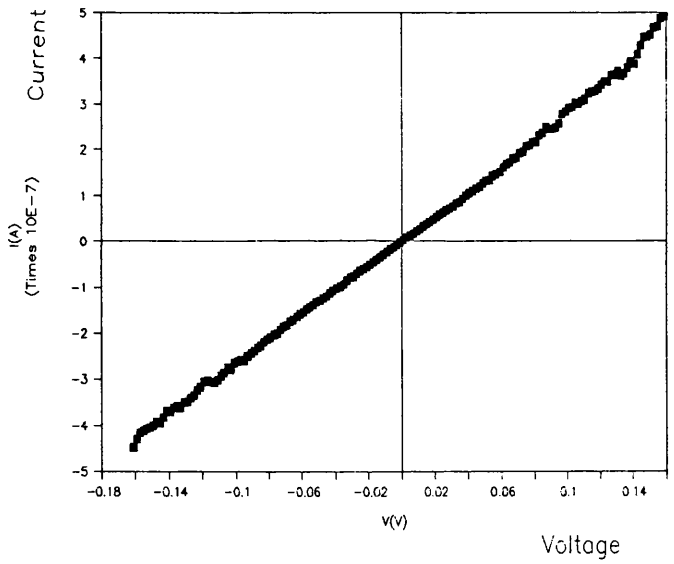

Fig. 5.82 IV of J7&C at room temperature, V=+/-161 mV

Figure 5.82 shows the IV curve of J7&C measured at room temperature. The slope of this curves yields a junction resistance of 356 MΩ .

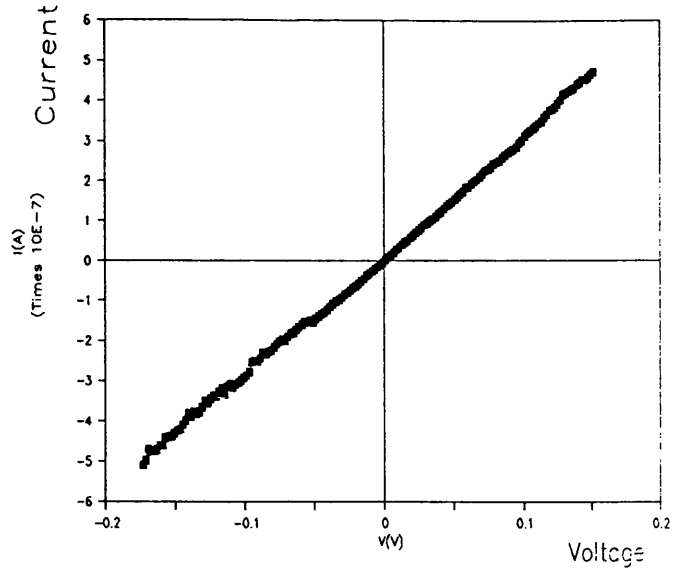

Fig. 5.83 IV of J7&C at room temperature, V= +/- 173 mV

Figure 5.83 shows a second IV curve of J7&C taken at room temperature and is also linear . However, both room temperature IV curves of J7&C exhibit some small features which occur for voltages beyond |100| mV .

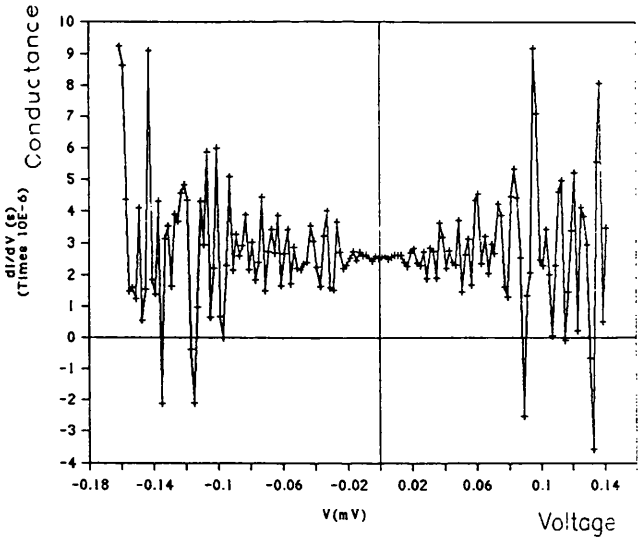

Fig. 5.84 Conductance vs voltage of J7&C at room temperature

The conductance vs voltage shown in figure 5.84 has symmetrical oscillations whose amplitudes become more damped as the voltage approaches zero. This damping is very strong for the voltages between +/- 40 .

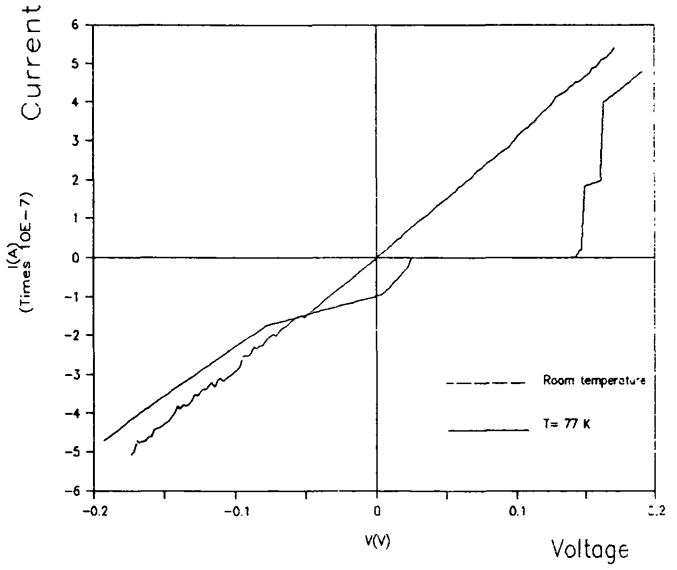

Fig. 5.85 IV curves of J7&C at T= 77 K and room temperatures

Figure 5.85 shows a simultaneous presentation of the IV curves of figure 5.78 and 5.83 . The asymmetry of the non-linear curve relative to the linear one can be clearly seen.

Figure 5.86 shows the same data as figure 5.85 but with the non-linear curve translated along the voltage axis to make it symmetrical (V=0 in the middle of the zero current region) . In this modified position, the room temperature curve is shown to have almost the same slope as the low temperarure curve outside of the non-linear region .

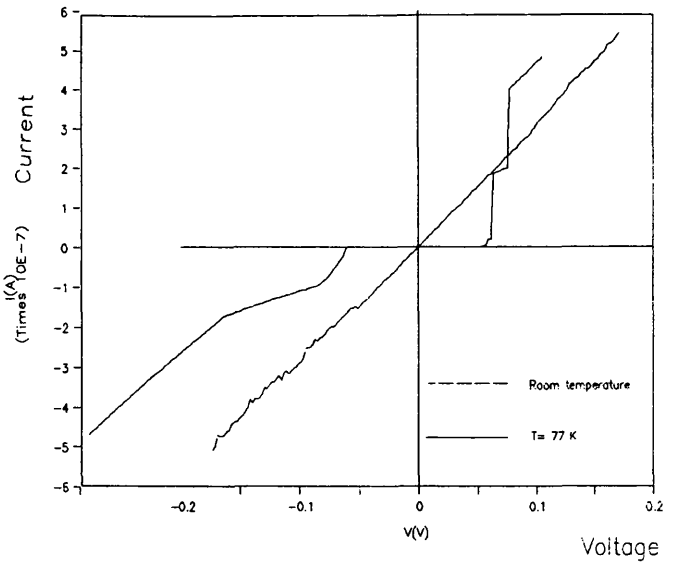

Fig. 5.86 IV curves of J7&C at T= 77 K and room temperatures

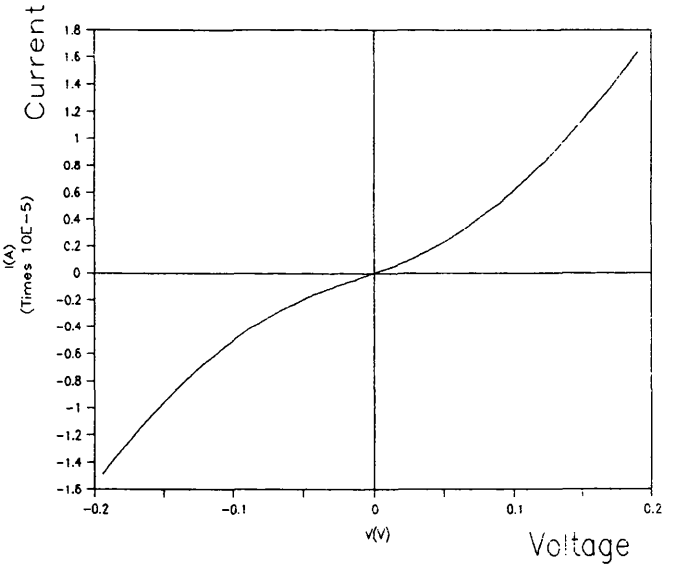

Fig. 5.87 IV curve of J3&C, T=77 K

Figure 5.87 shows the IV curve of J3&C . This is characterised by a smooth non-linear behaviour.

Figure 5.88 shows the conductance variation of J3&C corresponding to the IV curve of figure 5.87.

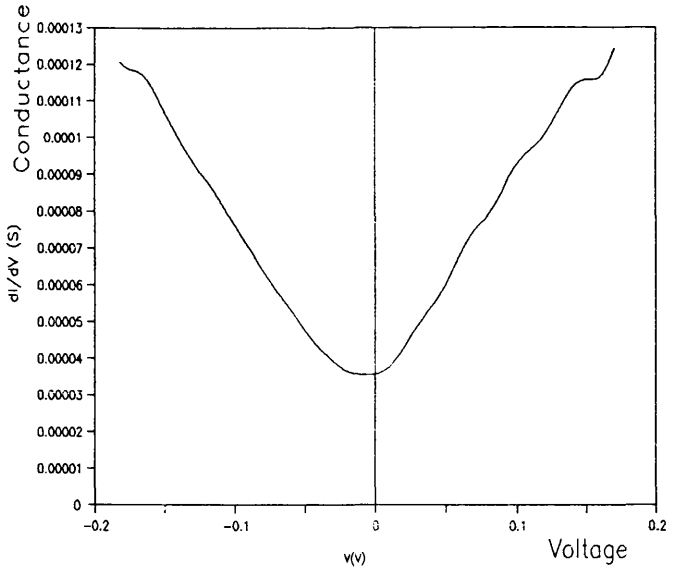

Fig. 5.88 Conductance vs voltage of J3&C, T=77 K

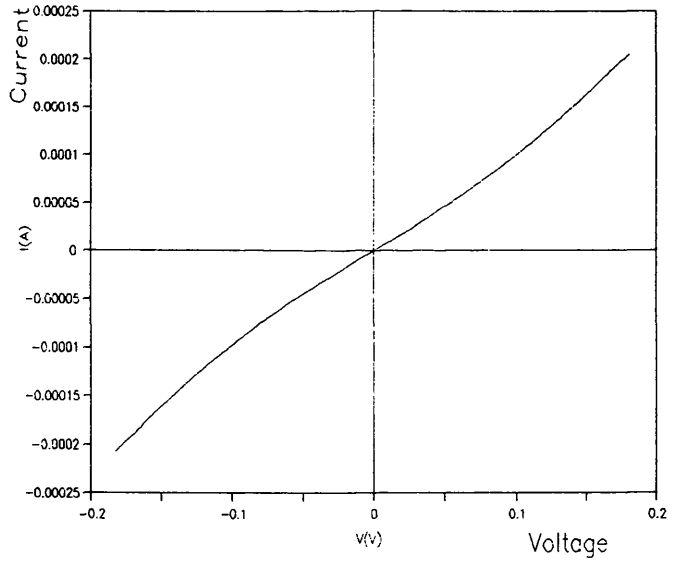

Fig. 5.89 IV curve of J14&C , T=77 K, V=+/-183 mV

Figure 5.89 shows the IV curve of J14&C which was measured over the voltage range +/-183 mV and is characterised by a smooth non-linear behaviour.

Figure 5.90 shows the IV curve of J14&C measured over the voltage range -193 mV to +193 mV. This curve repeats the smooth non-linear behaviour of figure 5.89 .

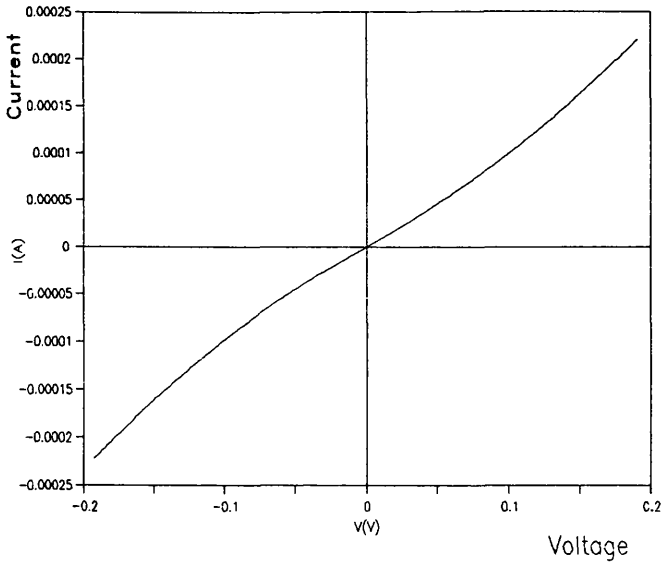

Fig. 5.90 IV curve of J14&C, T=77 K, V=+/-193 mV

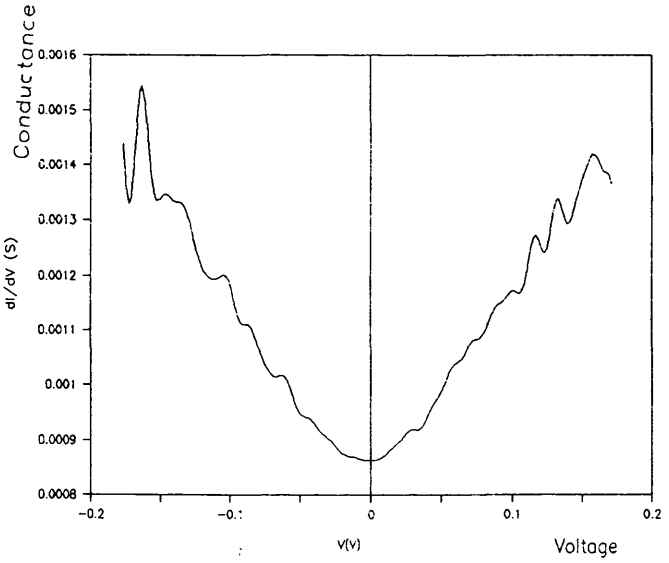

Fig. 5.91 Conductance vs voltage of J14&C, V=+/- 183 mV

Figure 5.91 shows the conductance against voltage of J14&C corresponding to the IV curve of figure 5.89 . This conductance variation a minimum at V=0 and shows small flat features at about -41 mV and + 28 mV . Beyond these two voltage values, the conductance increases with increasing voltage while exhibiting many peak-like features . These are more pronounced beyond | 100 | mV .

5.8.5 Measurement results of run 2

In this run, measurement of IV curves at different temperatures and voltage ranges were obtained from J11&C, J3&C, J14&C, and J8&C . The results will now be described .

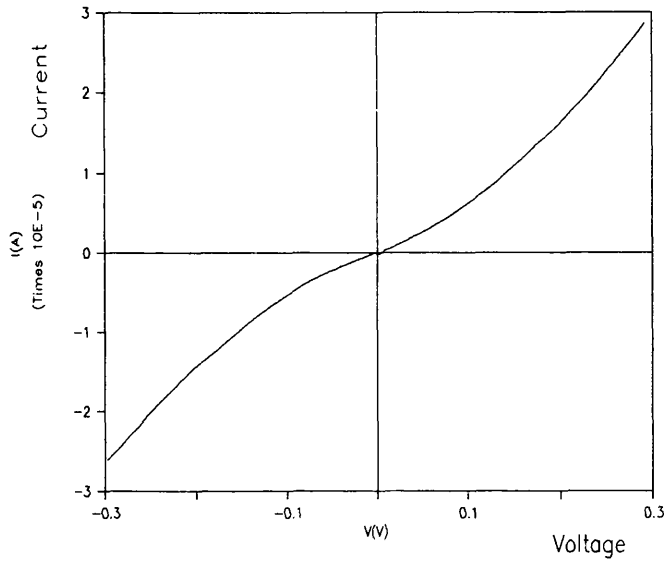

Fig.5.92 IV curve of J11&C, T=7 K

Figure 5.92 shows a well behaved IV curve of J11&C measured at T=7 K for voltages between -300 mV and +300 mV.

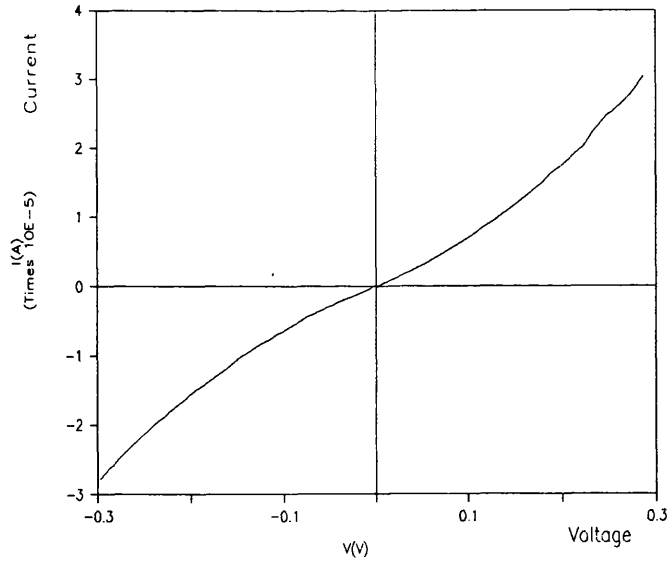

Fig.5.93 IV curve of J11&C, T=78 K

Figure 5.93 shows a well behaved IV curve of J11&C measured at T=78 K and voltage V between -300 mV and +300 mV.

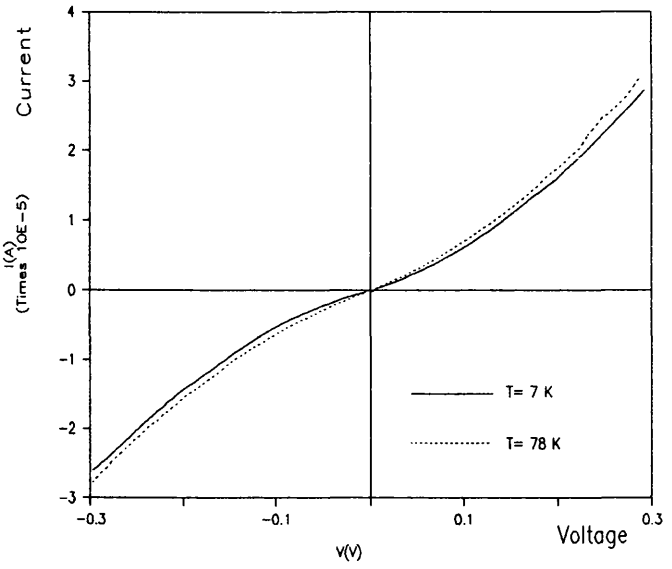

Fig.5.94 IV curve of J11&C at the indicated temperatures

The previous IV curves shown in figure 5.92 and 5.93 are presented together in figure 5.94. This figure (5.94) shows that the IV curve at higher temperature (77 K) is shifted upward relatively to the low temperature IV curve (7 K) indicating that the resistance of the junction decreases as the temperature increases. Although this shift is small, it is in agreement with the general properties of IV characteristics of superconductor tunnel junctions.

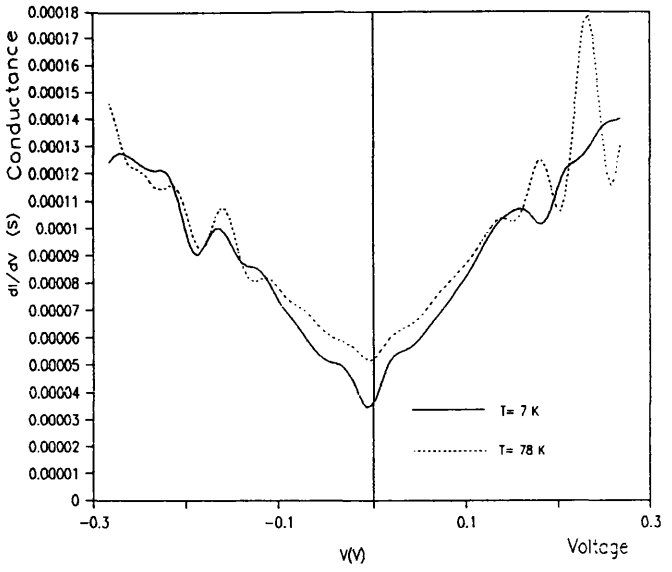

Fig.5.95 Conductance of J11&C at the indicated temperatures

Figure 5.95 shows a simultaneous presentation of the conductances verses voltage obtained from the data of the IV curves of figure 5.92 and 5.93 . Both conductance exhibit a gap like feature whose width decrease with temperature with increasing temperature . The width of the low temperature gap feature is 48 mV . Both curves have a subgap conductance which increases with increasing temperature . After the gap feature both conductances increase with increasing voltage and intercept each other at V=-116 mV and V=+131 mV .More features are observed on both curves beyond -116 mV and 131 mV but those on the right side of the curve taken at 78 K exhibit higher amplitudes.

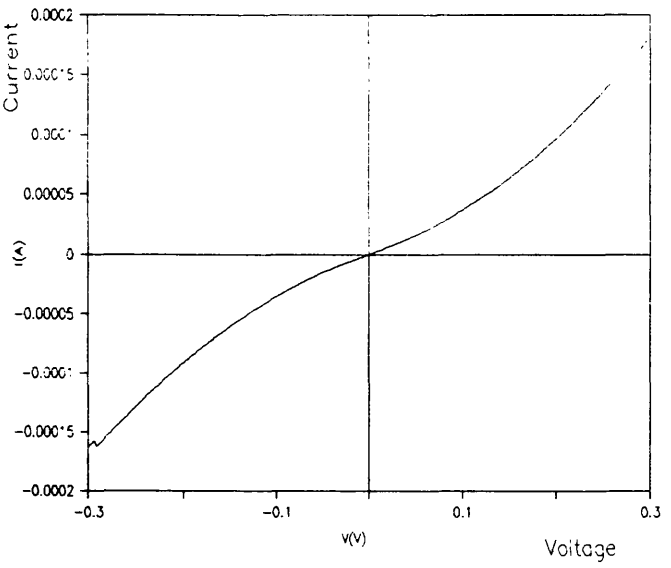

Fig.5.96 IV curve of J14&C, T=51 K

Figure 5.96 shows a well behaved IV curve of J14&C which was measured at T= 51 K.

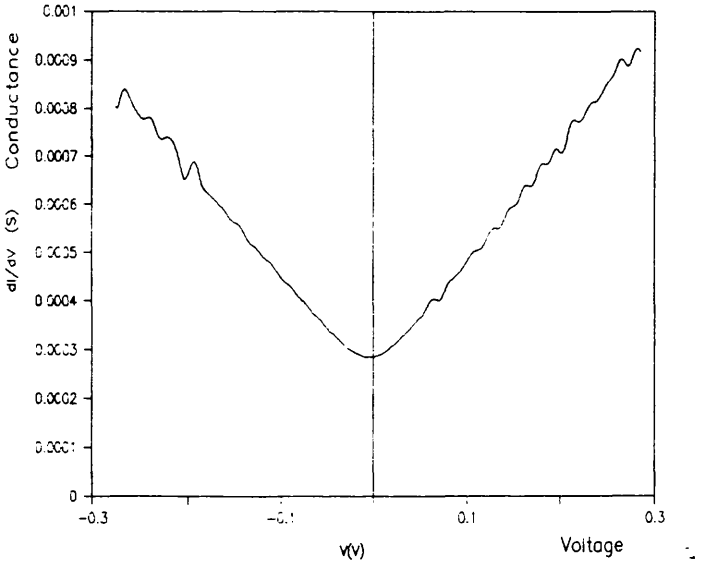

Fig.5.97 Conductance vs voltage of J14&C , T=51 K

The conductance against voltage presented in Figure 5.97 is obtained from the data of the IV curve of J14&C (figure 5.96). There are no pronounced peak features around the origin but the usual monotonous increase of the conductance verses voltage is observed with some features becoming more pronounced beyond 100 mV.

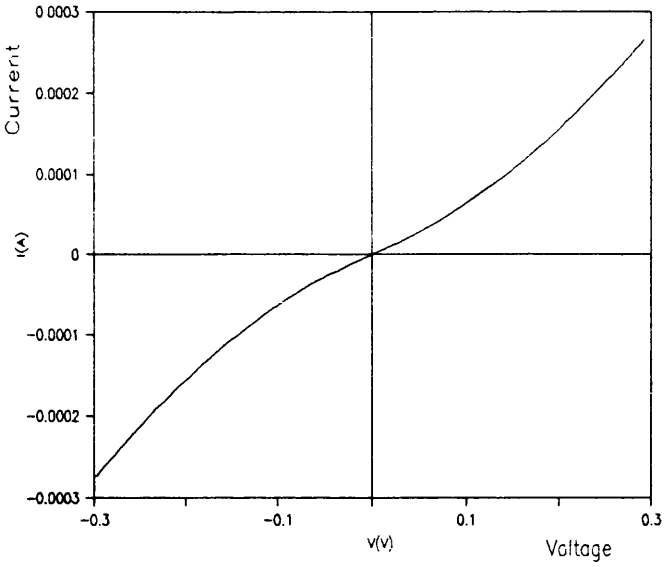

Fig.5.98 IV curve of J14&C, T=60 K

Figure 5.98 shows the IV curve of J14&C which was measured at T= 60 K .

Many IV curves measurements were carried out on junction J8&C at different temperatures and voltage ranges. The results are presented in the following figures .

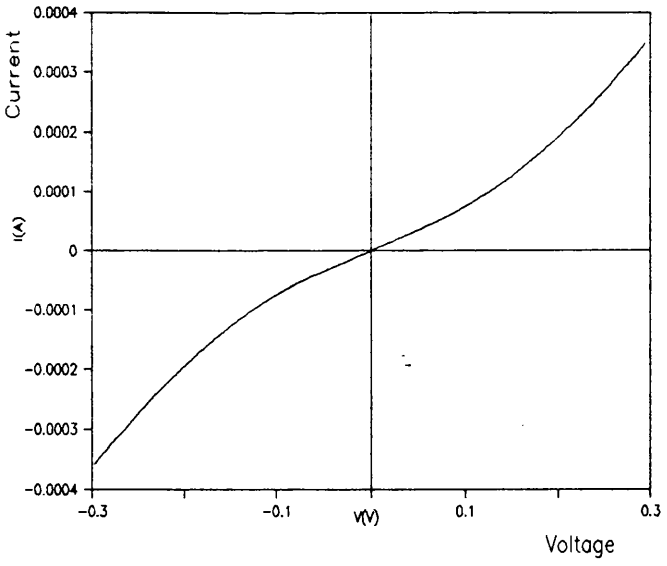

Fig.5.99 IV curve of J8&C, T=7 K

Figure 5.99 shows the IV curve of J8&C measured at T=7 K and over a voltage range between -300 mV and 300 mV.

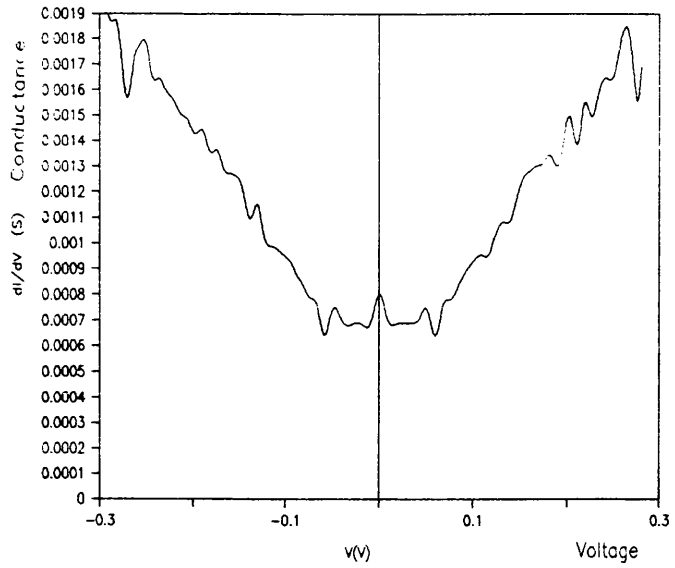

Fig.5.100 Conductance vs voltage of J8&C, T=7 K

Figure 5.100 shows the conductance against voltage corresponding to the IV curve of J8&C (figure 5.99) . This figure (5.100) shows many features that are indistinguishable in the IV curve. The current rises at zero voltage, followed by two flat regions . The first two symmetrical peaks are at +/- 49 mV. After these peaks the conductance decreases and thus two symmetrical valleys appeare at +/- 59 mV. The conductance then increases with increasing voltage with many step-like features followed by some oscilltions whose amplitudes increased at +-280 mV.

Figure 5.101 shows the IV curve of J8&C which was measured at T= 7 K for voltage range between -50 mV and 50 mV.

Figure 5.102 shows the IV curve of J8&C which was measured at T= 22 K for voltage range between -30 mV and 30 mV

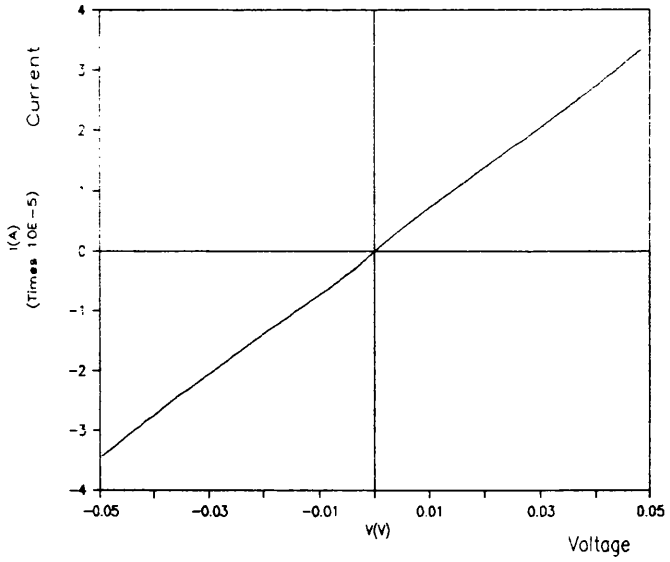

Fig.5.101 IV curve of J8&C, T= 7 K, -50 mV <V< +50 mV

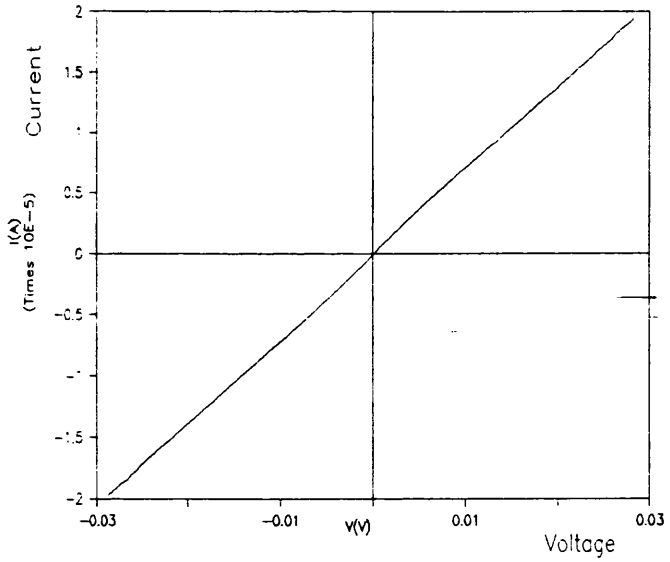

Fig.5.102 IV curve of J8&C, T= 22 K, -30 mV <V< +30 mV

Although the two last IV curves (figures 5.101 and 5.102) of J8&C were measured over a low voltage range, the increase of current at 0 V can only be noticed with careful observation.

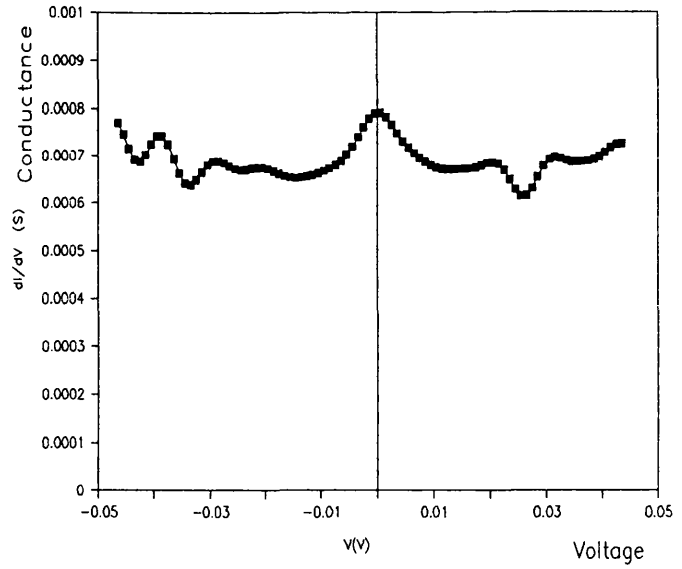

Fig.5.103 Conductance vs voltage of J8&C, T=7 K

The conductance variation against voltage corresponding to the IV curve of J8&C (figure 5.101) is presented in figure 5.103 . In this figure the increase in conductance around 0 V reflects very clearly the slight increase of current observed in the IV curves of figures 5.101 and 5.102 .

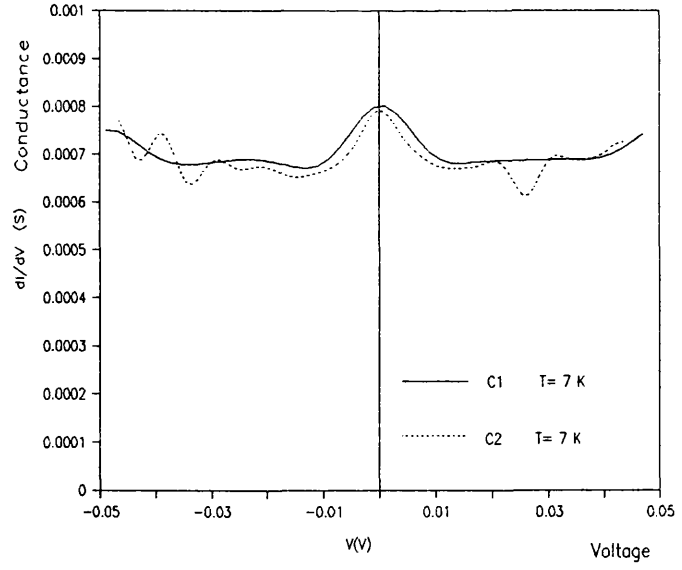

Fig.5.104 Conductance vs voltage of J8&C

The conductances against voltage curves shown separately in figures 5.100 and 5.103 are presented together in figure 5.104 . This graph shows close identity between the two curves . However the conductance C2 (obtained from the low voltage range of the IV curve of figure 5.101) has some additional valleys-like features at about -34 mV and +27 mV.

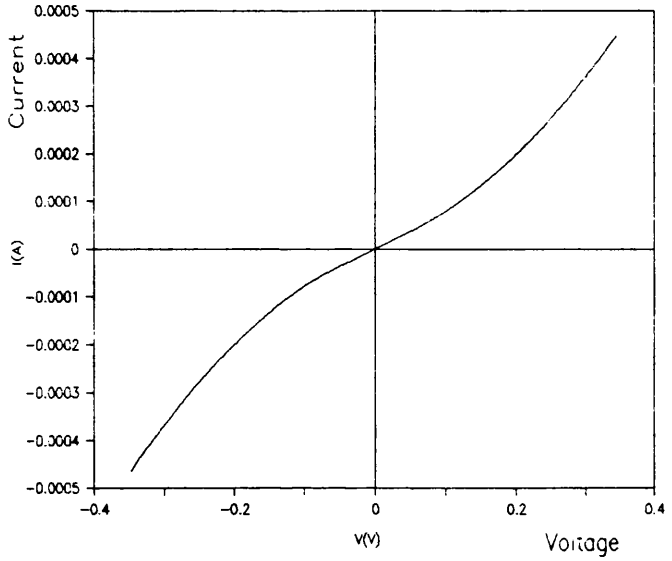

Fig.5.105 IV curve of J8&C, T= 35 K

Figure 5.105 shows the IV curve of J8&C measured at 35 K and over the wide voltage range from -300 mV to 300 mV.

Figure 5.106 shows the IV curve of J8&C measured at 45 K and wide voltage range between -300 mV and 300 mV.

Figure 5.107 is a simultaneous presentation of the IV curves of J8&C which were separately shown in figure 5.99 and 5.106 .

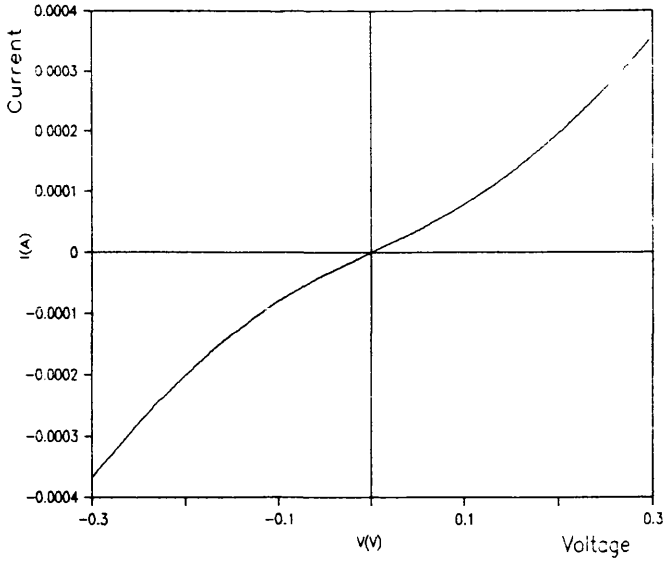

Fig.5.106 IV curve of J8&C ,T= 45 K

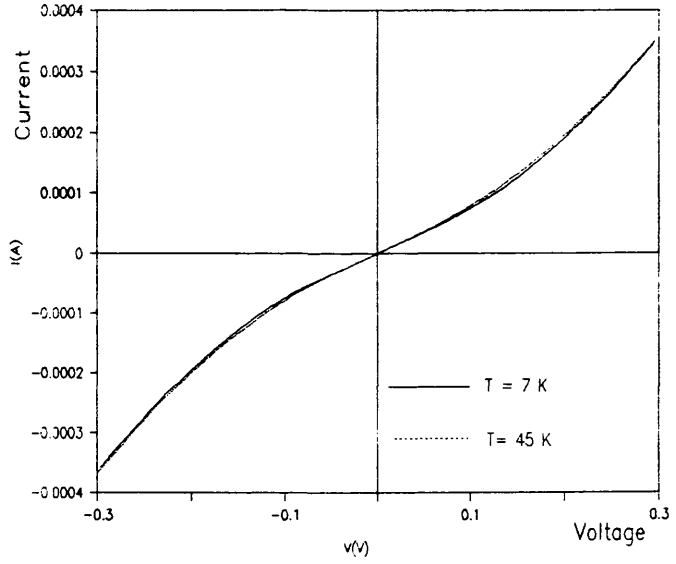

Fig.5.107 IV curves of J8&C, at tow different temperatures

Although the two curves were taken at different temperatures , this effect can hardly be seen . However the temperature difference can be more clearly revealed in the following figure.

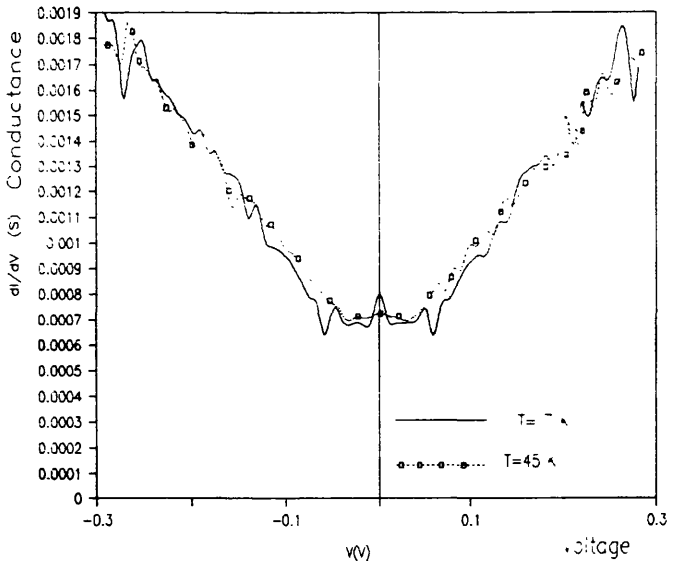

Fig.5.108 Conductance vs voltage of J8&C at the indicated temperatures

Figure 5.108 is a simultaneous presentation of the conductance against voltage corresponding to the IV curves in figures 5.99 and 5.106 . For voltages between -150 mV and 150 mV the conductance of T=45 K is higher than that of T=7 K. The maximum at V=0 which is present in the low temperature conductance has become almost flat for the conductance at T= 45 K. In addition the valleys that come just after the first peaks in the low temperature curve have vanished from the conductance at T=45 K. For voltages beyond |150| mV the conductance at the two temperatures have many similar features.

5.8.6 Measurement results of run 3

More measurements on junctions J11&C, J8&C, and J14&C were carried out during this run at different temperatures and voltages ranges . The results are presented in the following figures.

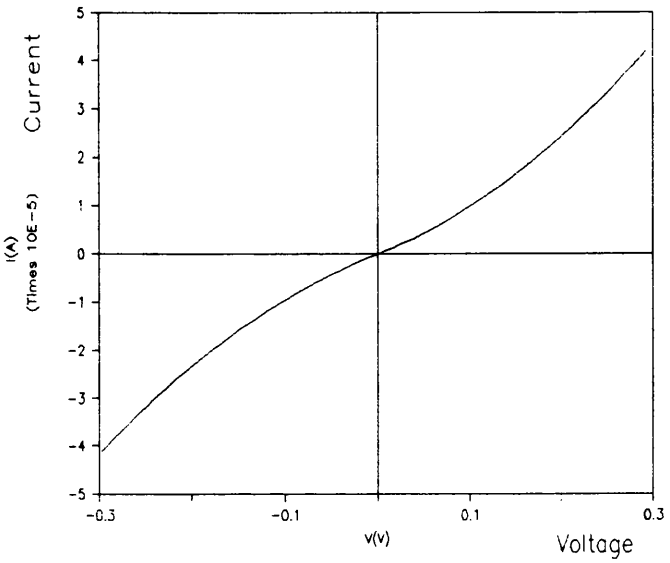

Fig.5.109 IV curve of J11&C, T= 24 K

Figure 5.109 shows the IV curve of J11&C measured at T = 24 K. This junction exhibits a well behaved non-linearity .

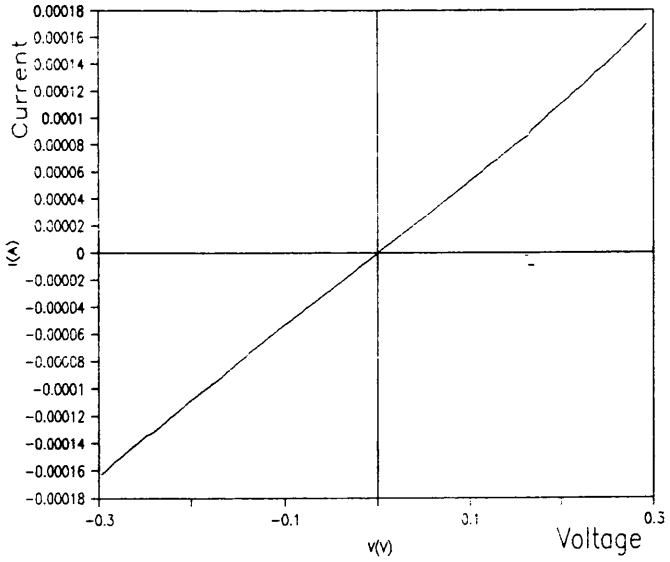

Fig.5.110 IV curve of J11&C At room temperature

Figure 5.110 shows the IV curve of J11&C taken at room temperature . This is a linear curve with a slope giving a junction resistance of 1.839 KΩ .

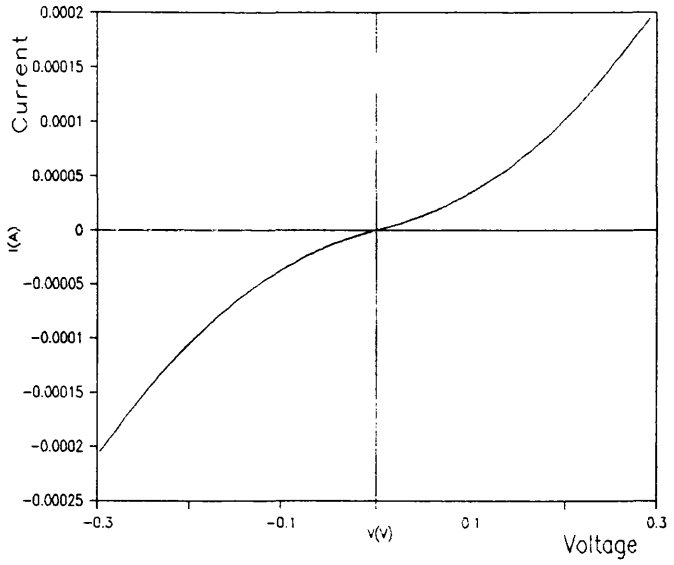

Fig.5.111 IV curve of J8&C, T= 38 K

Figure 5.111 shows a well behaved non-linear IV curve of J8&C measured at T = 38 between -300 mV and +300 mV.

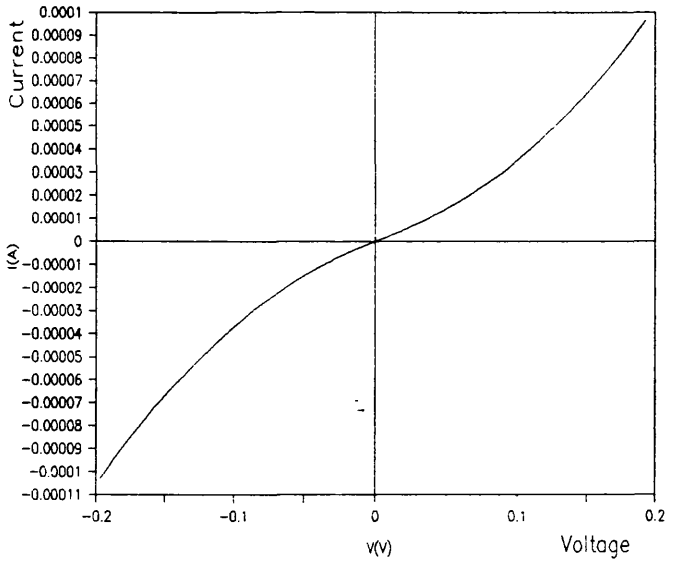

Fig.5.112 IV curve of J8&C, T= 41 K

Figure 5.112 shows the IV curve of J8&C measured at T = 41 K between -200 mV and + 200 mV.

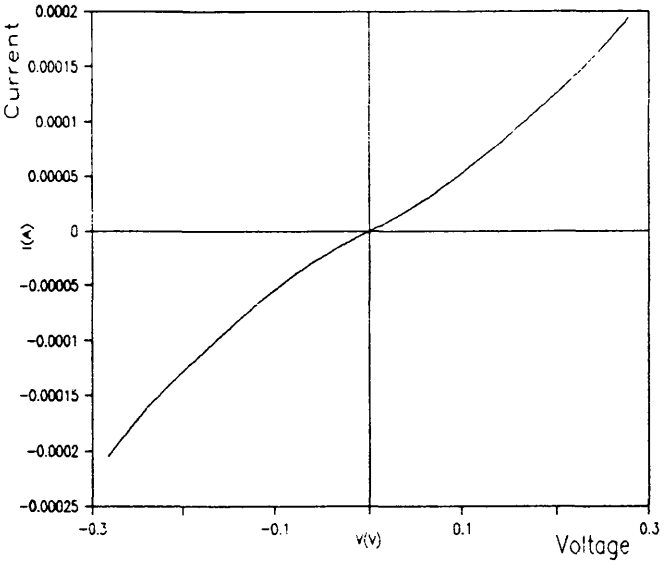

Fig.5.113 IV curve of J8&C, T= 77 K, -284 mV <V<284 mV

Figure 5.113 shows the IV curve of J8&C measured at T=77 K between -284 mV and + 284 mV . A series of four other IV curves similar to this one were measured from J8&C at T=77 and different voltage ranges . Only one of them wich was measured at T= 77 K is shown in figure 5.114 .

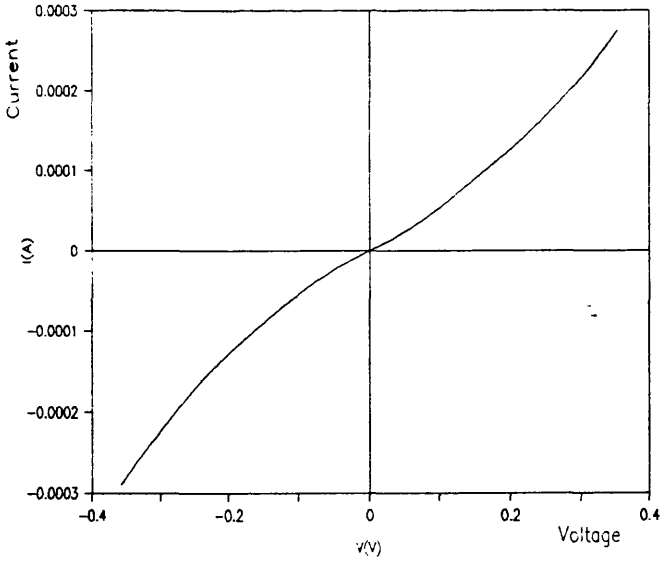

Fig.5.114 IV curve of J8&C, T= 77 K -358 mV <V<358 mV

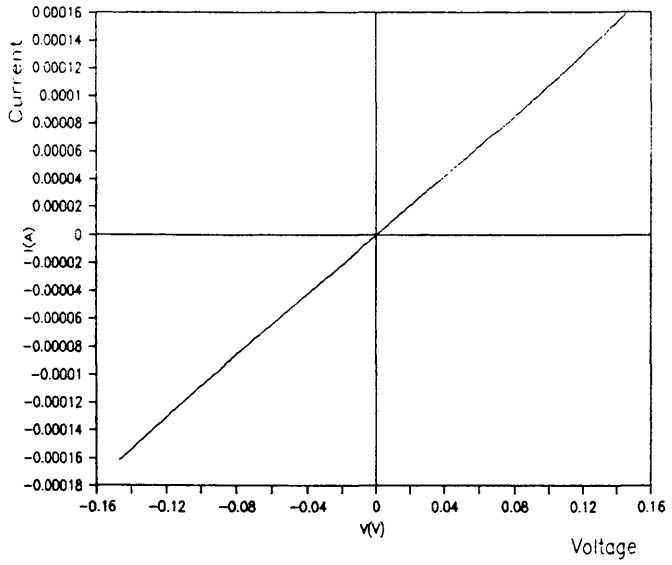

Fig.5.115 IV curve of J8&C at room temperature

Figure 5.115 shows the IV curve of J8&C measured at room temperature . This is a linear curve with a slope giving a junction resistance of 928 Ω .

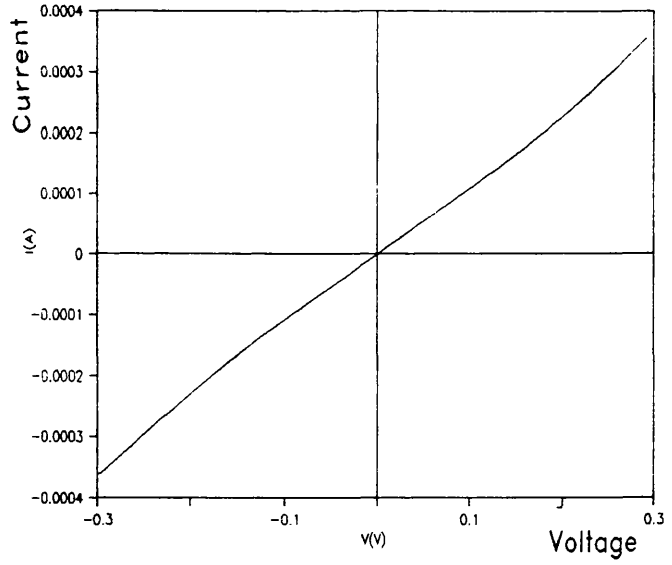

Fig.5.116 IV curve of J8&C at room temperature

Figure 5.116 shows the IV curve of J&&C measured at room temperature . This is linear and has a slightly higher resistance of 945 Ω . For voltages beyond |180| the curve exhibits a slight departure from the straight line.

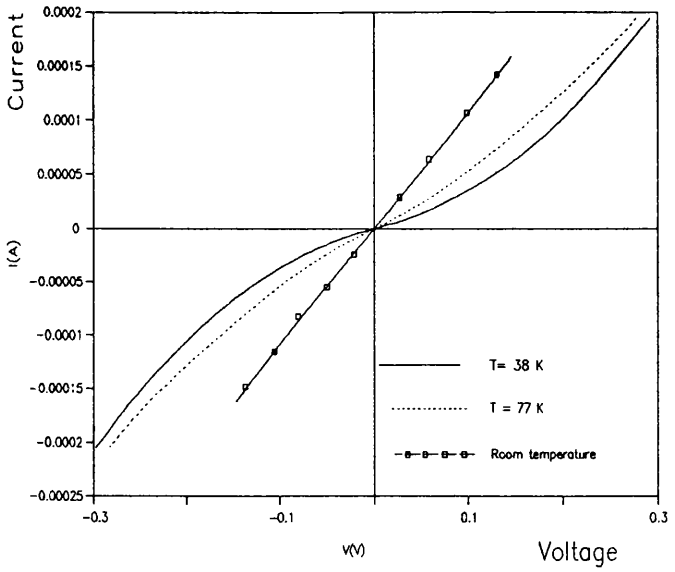

Fig.5.117 IV curve of J8&C at the indicated temperatures

The IV curve of J&&C taken at different temperatures (figures 5.111 , 5.113, and 5.115) are presented together in figure 5.117 . This shows that the non-linearity of the IV curve becomes less pronounced with increasing temperature until it becomes linear at room temperatrure. This behaviour is in agreement with the properties of superconductor tunnel junctions.

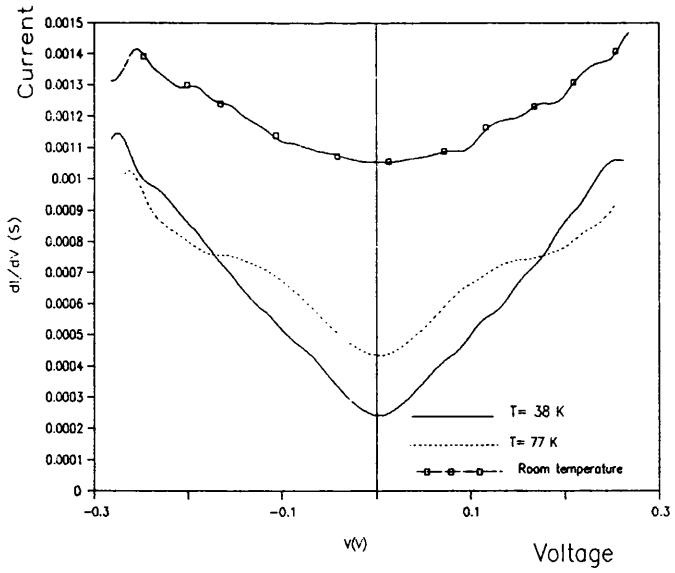

Fig.5.118 Conductances vs voltage of J8&C at the indicated temperatures

Figure 5.118 shows the conductances against voltage corresponding to the IV curves presented in figures 5.111 (38 K) , 5.113 (77 K) , and 5.116 (room temperature wide range) . At T=38 K the conductance has a minimum at 0 V and increases monotonously with voltage. For T =77 the position of the minimum is higher and than that of the curve measured at 34 K but less monotonous. Both curves intercept at +/- 170 mV. The room temperature conductance is higher than both of the previous and is almost featureless.

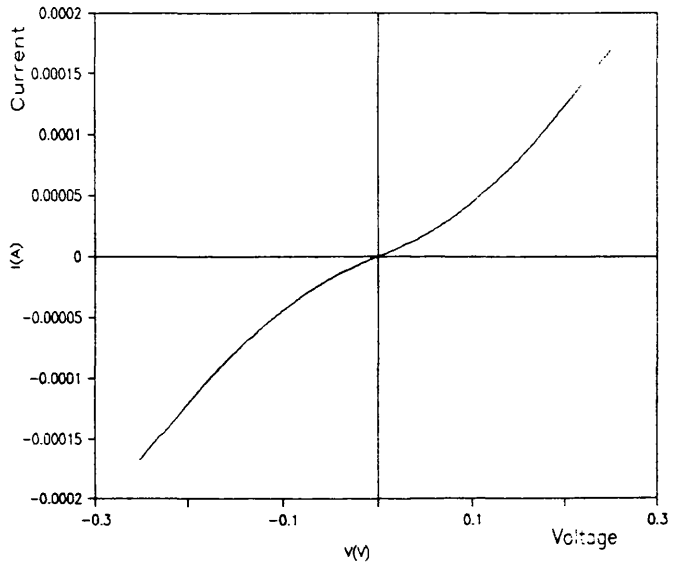

Fig.5.119 IV curve of J14&C , T= 58 K

Figure 5.119 shows the IV curve of J14&C measured at T=58 K between -250 mV and + 250 mV .

Figure 5.120 shows the conductance against voltage obtained from the data of the IV curve in figure 5.119 . The conductance is asymetric and monotonous with voltage until its first peak-like features appear at -66 mV and 75 mV. Beyond these two voltage values a variety of features can be seen.

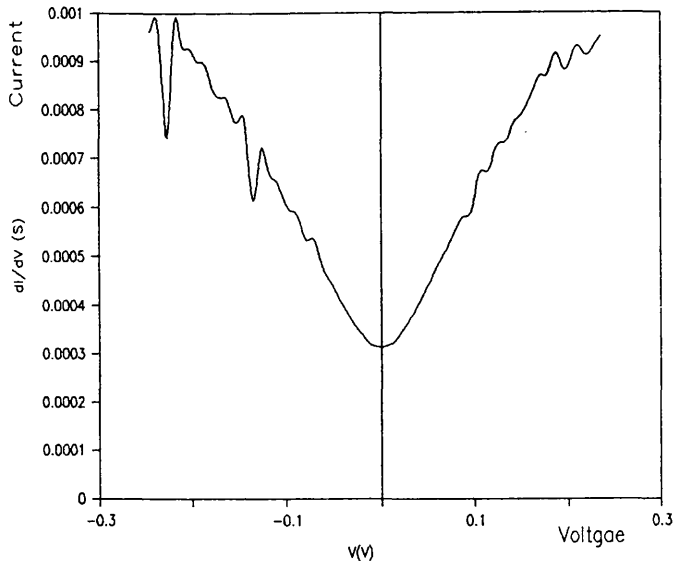

Fig.5.120 Conductance vs voltage of J14&C, T=58 K

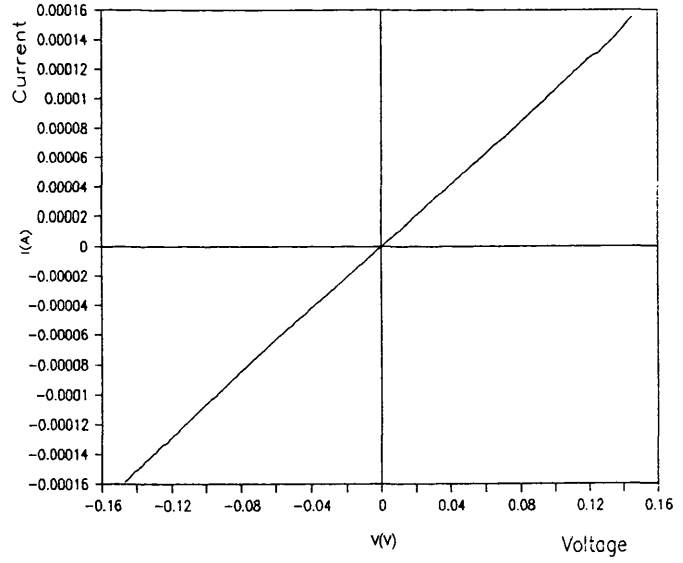

Fig.5.121 IV curve of J14&C at room temperature

Figure 5.121 shows a linear IV curve of J14&C taken at room temperature. The slope yields a junction resistance of 945 Ω at room temperature.

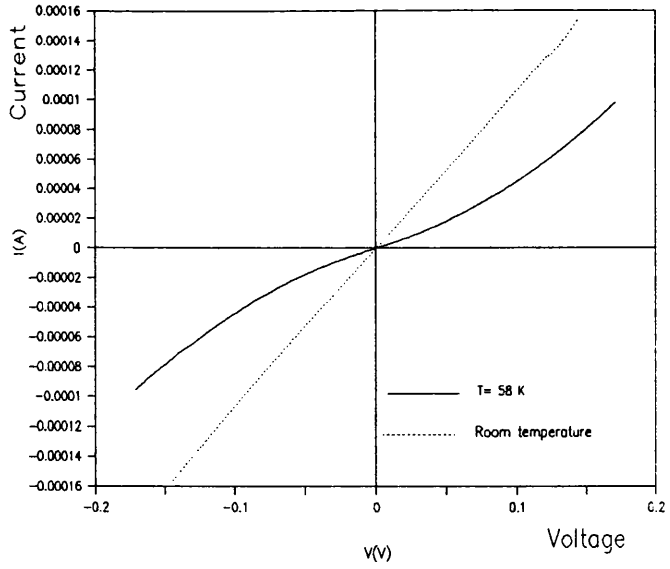

Fig.5.122 IV curves of J14&C at the indicated temperatures

The IV curves of figures 5.119 and 5.121 are shown together in figure 5.122 .

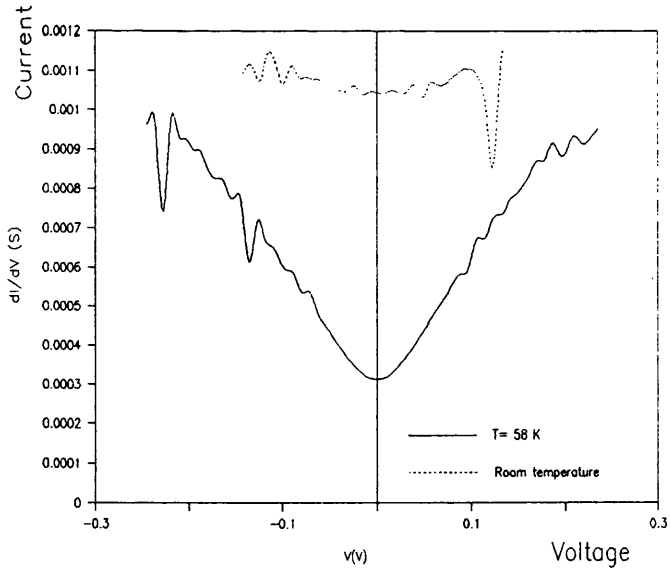

Fig.5.123 Conductances vs voltage of J14&C at the indicated temperatures

Figre 5.123 shows a simultaneous presentation of the conductance against voltage corresponding to figure 5.119 and 5.121 . As expected (from the IV curves of figure 5.122) the conductance at room temperature is higher than at low temperatures . However the former has anomalous oscillations-like features which increase with increasing voltage .

5.8.7 Layout of runs 4 and 5

In these two runs, some of the dots that were used in the previous runs were replaced by new ones . The selected dots were connected according to the configuration shown in figure 5.124.

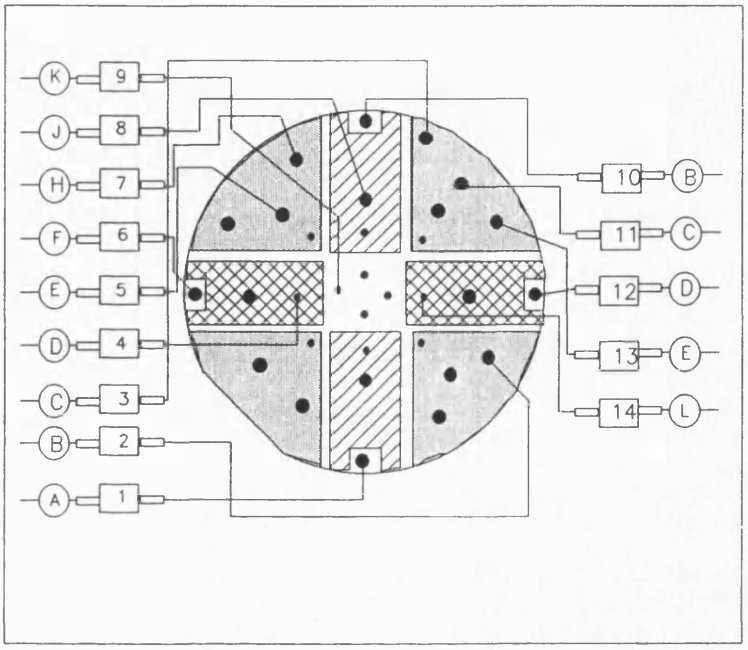

Fig.5.124 Contact layout used for run 4 and 5

In these two runs the common electrode of all the junctions is the dot connected to pin number 1. According to the previous method of junction numbering, the junctions should be referred to as JN&1, where N=2,3,4 etc . However, for simplifications purposes the two characters (&1) will be dropped and the junction will be referred to as JN (N= 2, 3, etc) .

5.8.8 Measurement results of run 4

All the measurement of IV curves of this run were carried out at about 6 K and voltages between -100 mV and 100 mV.

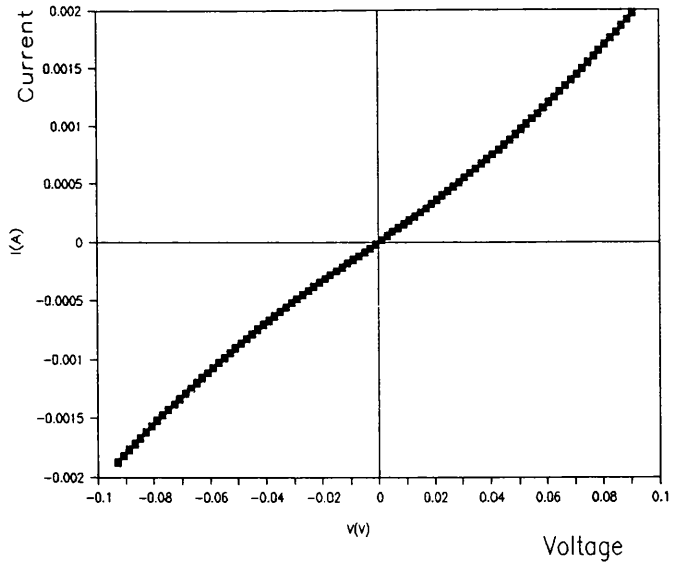

Fig.5.125 IV curve of J2, T= 6 K

Figure 5.125 shows the IV curve of J2 measured at 6 K . This curve is slightly non-linear but has no pronounced features .

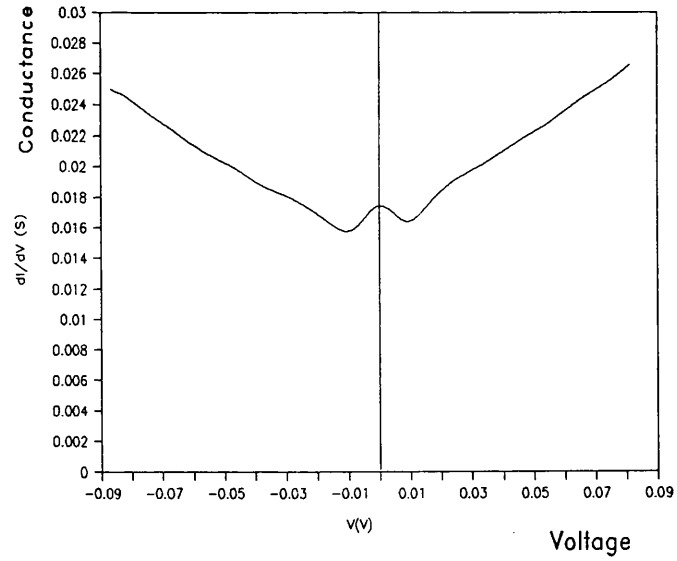

Fig.5.126 Conductance vs voltage of J2, T= 6 K

Figure 5.126 shows the conductance against voltage of J2 obtained from the data of the J2 IV curve . An increase of conductance around 0 V can be seen . For higher voltages the conductance increase monotonously with voltage .

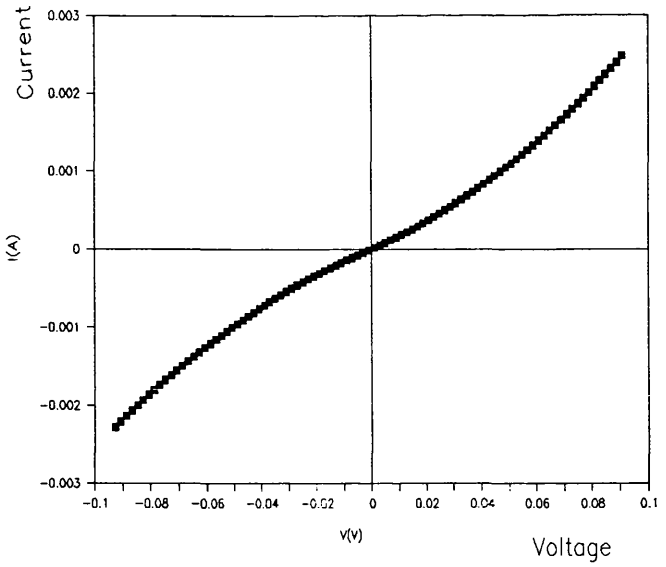

Fig.5.127 IV curve of J3, T= 6 K

Figure 5.127 shows the IV curve of J3 measured at 6 K. A slight non-linear behaviour can be seen on this curve.

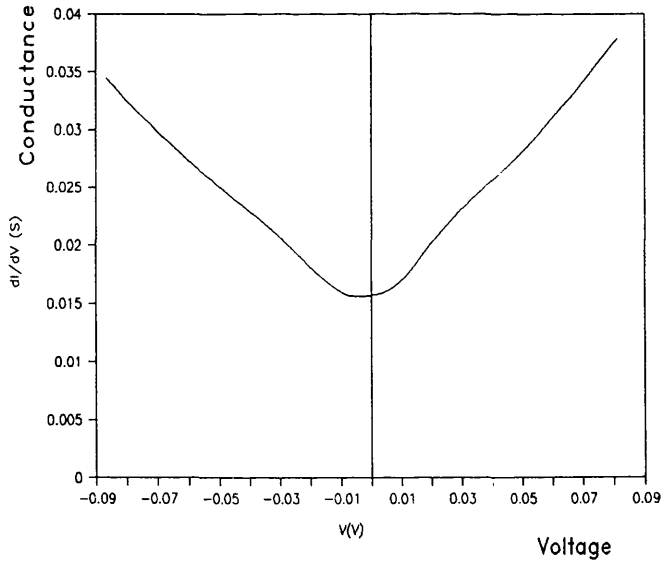

Fig.5.128 Conductance vs voltage of J3, T= 6 K

Figure 5.128 shows the conductance against voltage of J3 corresponding to the IV curve of J3. This is characterised by a dip around 0 V. For voltages greater than |30| mV, the conductance increases monotonously with voltage.

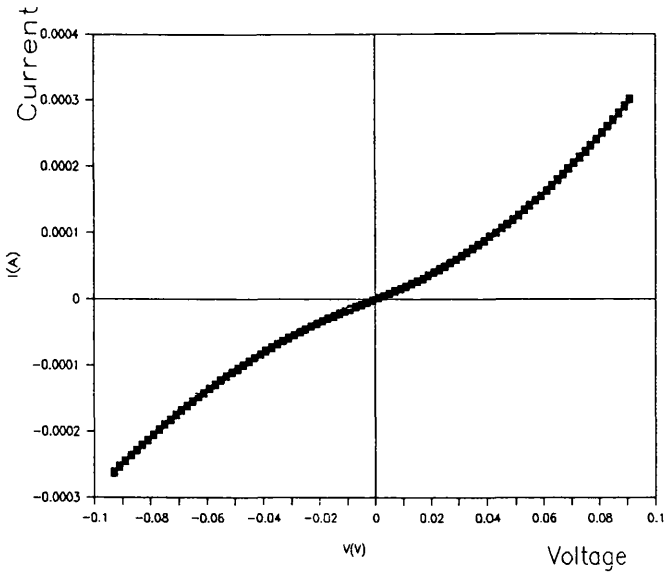

Fig.5.129 IV curve of J7, T= 6 K

Figure 5.129 shows the IV curve of J7 which exhibits a non-linear behaviour with a dip around 0 V and monotonous increase of the conductance with the voltages greater than |30| mV .

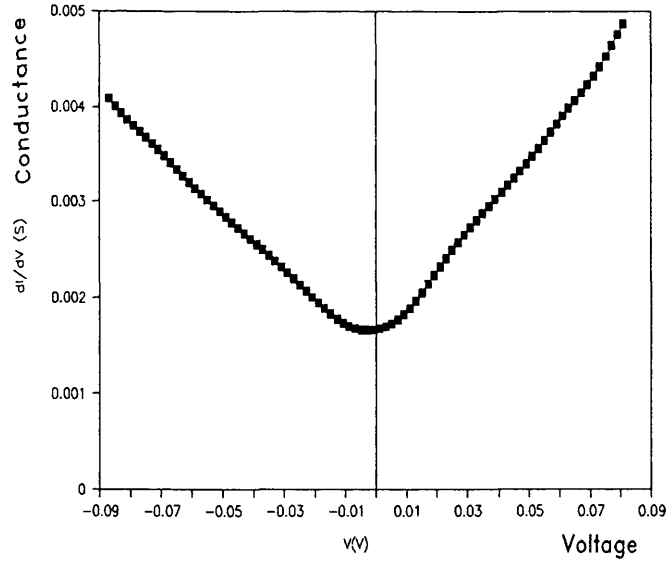

Fig.5.130 Conductance vs voltage of J7, T= 6 K

Figure 5.130 shows the conductance against voltage of J7 corresponding to the IV curve of J7.

Figure 5.131 shows the IV curve of J13 measured at 6 K. A close examination of this IV curve reveals a slight increase

of current around 0 V. This can be seen more clearly in the conductance vs voltage presentation shown in the following figure.

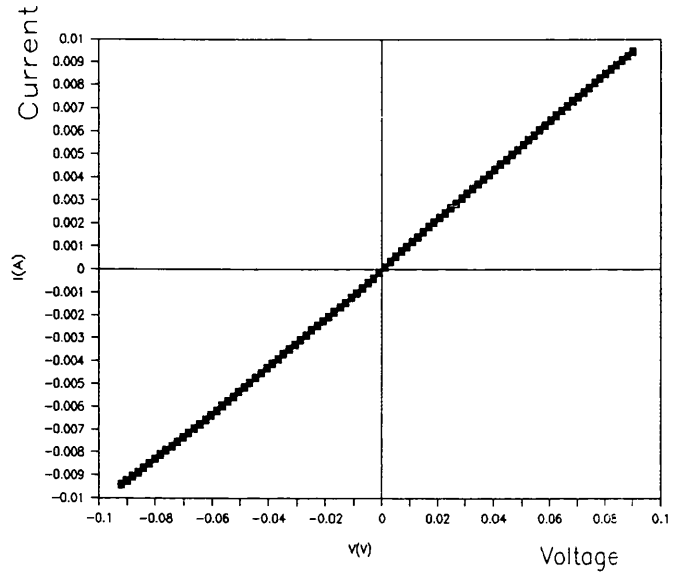

Fig.5.131 IV curve of J13, T= 6 K

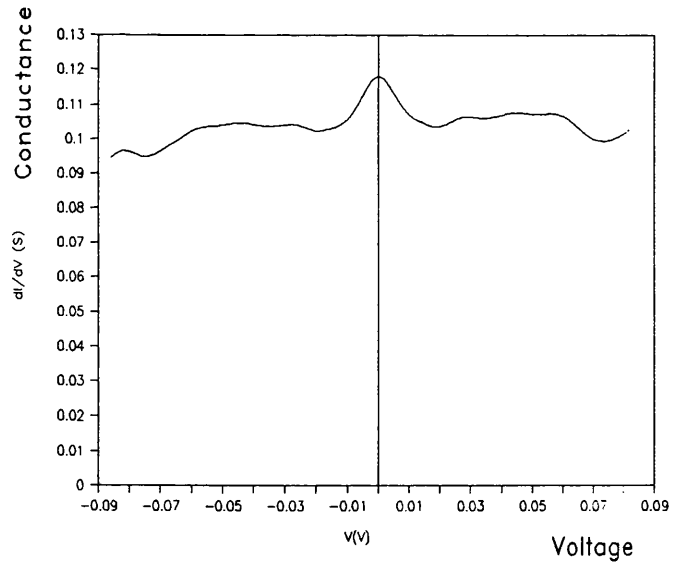

Fig.5.132 Conductance vs voltage of J13, T= 6 K

Figure 5.132 shows the conductance against voltage of J13 corresponding to the IV curve of J13. This conductance increases for voltage approaching zero and reaches a maximum

at 0 V .

Figure 5.133 shows the IV curve of J14 . This exhibits a well behaved non-linearity .

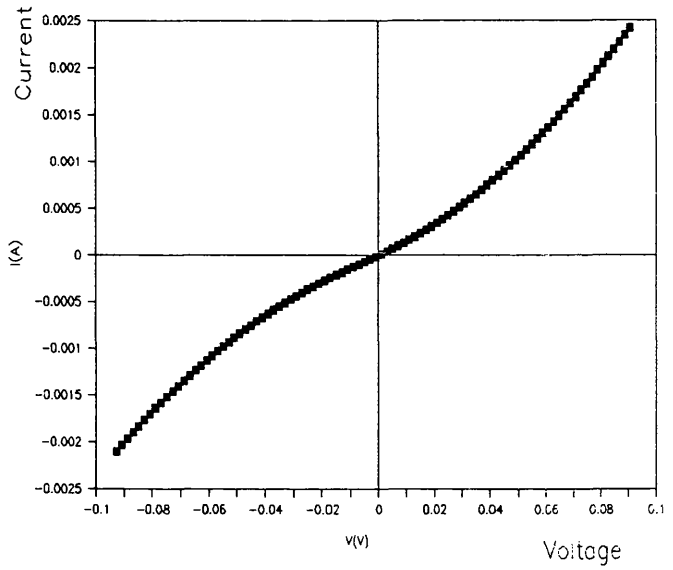

Fig.5.133 IV curve of J14, T= 6 K

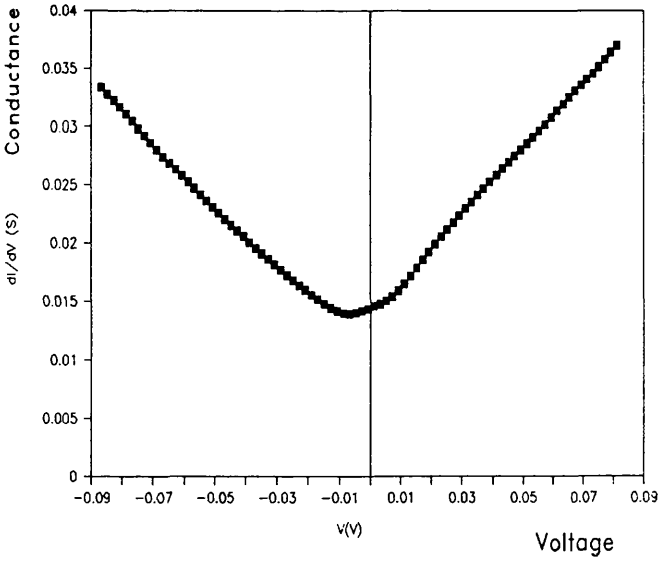

Fig.5.134 Conductance vs voltage of J14, T= 6 K

Figure 5.134 shows the conductance against voltage of J14 corresponding to the IV curve of J14. This is slightly asymmetric, exhibits a dip around 0 V and increases monotonously with increasing voltage

5.8.9 Measurement results of run 5

More IV curve were taken according to the layout of figure 5.124 at different temperature and voltage ranges . The results obtained are presented in the following figures .

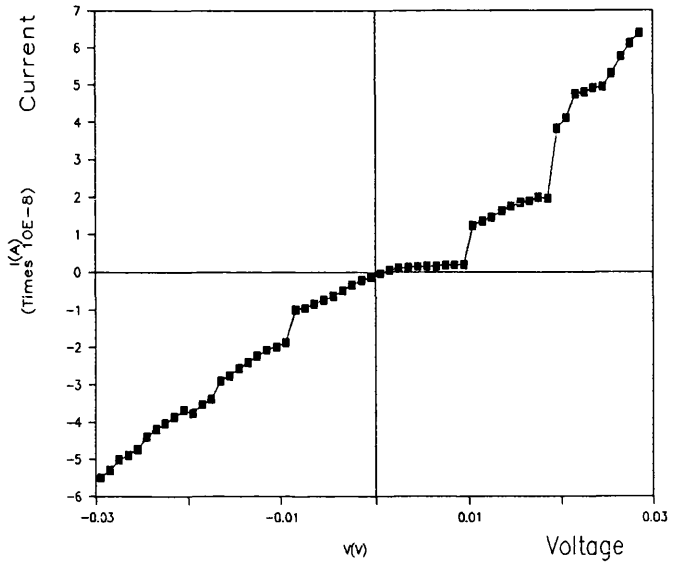

Fig.5.135 IV curve of J11, T= 28 K

Figure 5.135 shows the IV curve of J11 which exhibits a striking non-linear behaviour. The IV curve is slightly asymmetric and has very pronounced features such as the sharp change of current occurring at - 8 mV and 10 mV. The current is nearly zero for voltages between 0 and 10 mV . Another sharp increase of current can be seen at about 19 mV

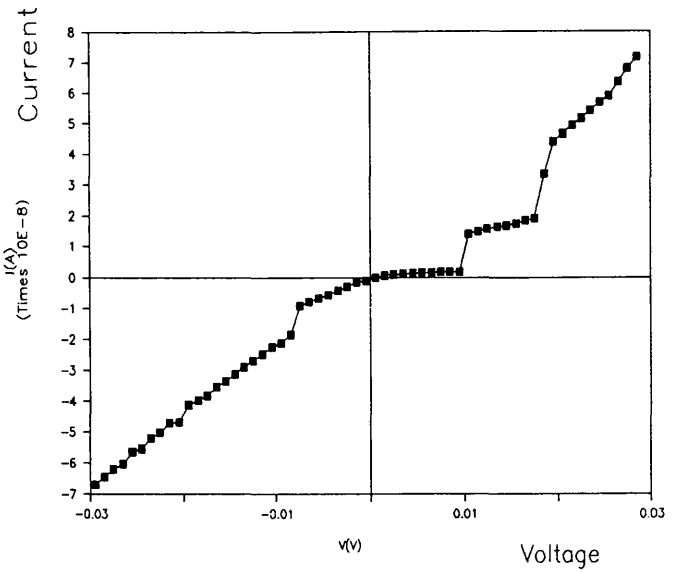

Fig.5.136 IV curve of J11, T= 28 K

Figure 5.136 shows the IV of curve of J11 obtained during a second scan. This shows that all the features observed in the first IV curve of J11 (figure 5.135) are present and thus indicates the reproducibility of the IV curve of J11 .

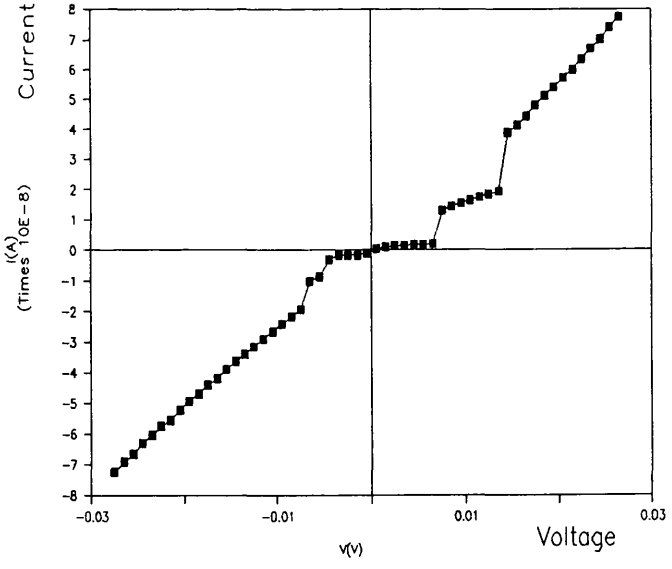

Fig.5.137 IV curve of J11, T= 40 K

Figure 5.137 shows the IV curve of J11 taken at T=40 K. This is slightly asymmetric but exhibits an almost ideal IV curve of a superconductor tunnel junction with zero current between -5 mV and 7 mV . At -5 mV a small current variation occurs, followed by a small knee and then a more important variation is observed . On the right side an abrupt current increase occurs at 7 mV, followed by a knee which extends up to 14 mV where a second sharp increase is observed. For voltages less than 7 mV and greater than 14 mV a linear behaviour is observed.

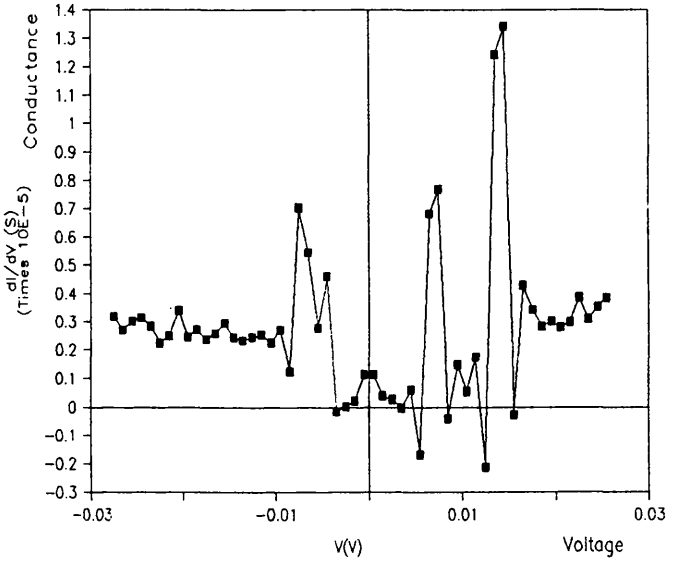

Fig.5.138 Conductance vs voltage of J11, T= 40 K

Figure 5.138 shows the conductance against voltage corresponding to the IV curve of figure 5.137 . The slight asymmetry of the IV curve can be seen reflected in this conductance curve . The conductance is zero around 0 V and the first two peaks are separated by 14 mV. Another high peak is situated at 15 mV.

Two IV curves of J11 shown earlier in figures 5.135 and 137 are presented together in figure 5.139. This indicates that when the temperature increased from 28 K to 40 K, the flat region became narrower and the junction resistance lower.

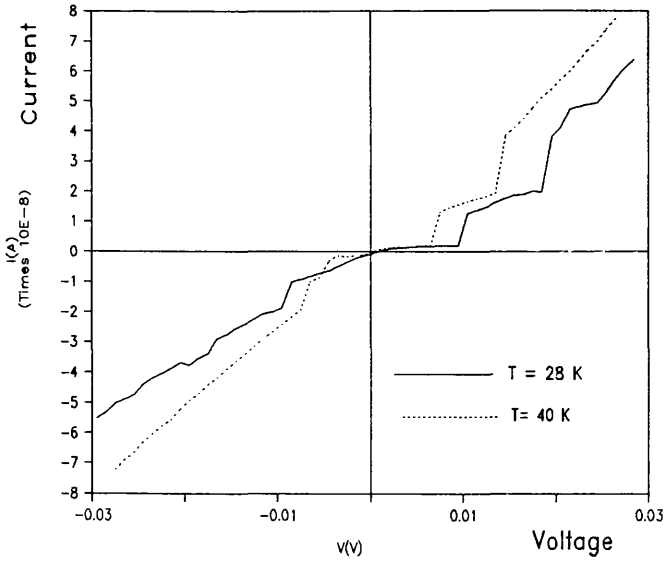

Fig.5.139 IV curves of J11 at the indicated temperatures

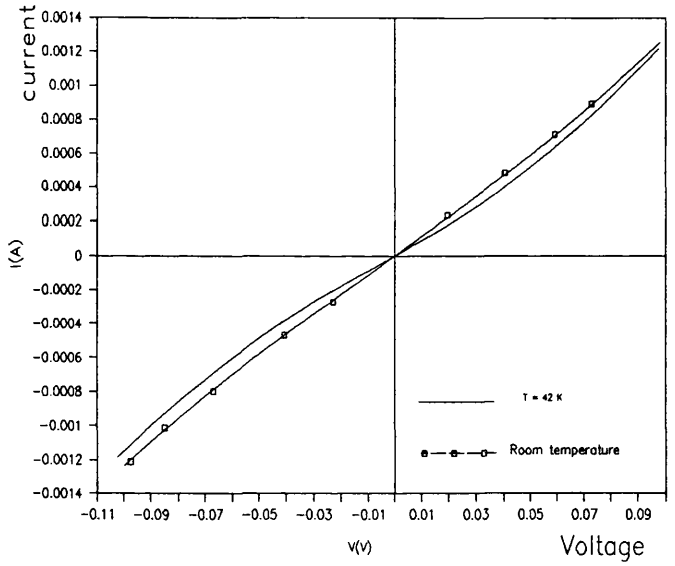

Fig.5.140 IV curves of J2 at the indicated temperatures

Figure 5.140 show two IV curves of junction J2 taken at T= 42 K and room temperature . The low temperature curve is slightly non-linear and approaches the room temperature curve at voltages greater than 85 mV .

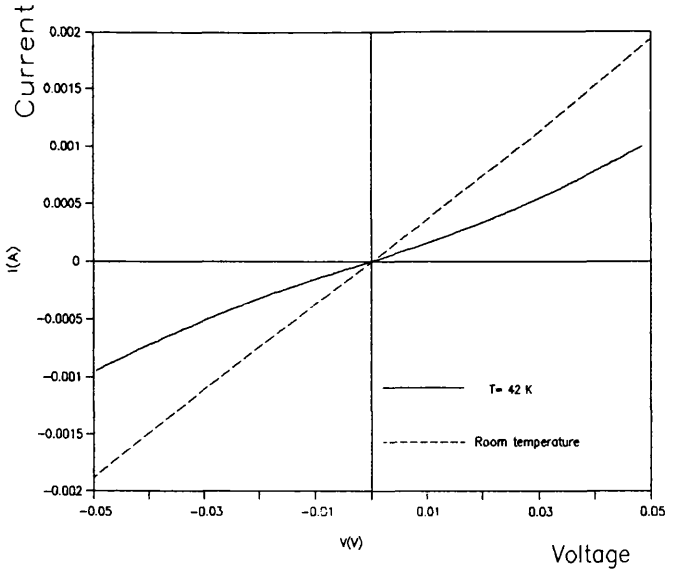

Fig.5.141 IV curves of J3 at the indicated temperatures

Figure 5.141 show two IV curves of junction J3 measured at T= 42 K (solid line) and room temperature (dashed line) . The low temperature curve exhibits a non-linear behaviour .

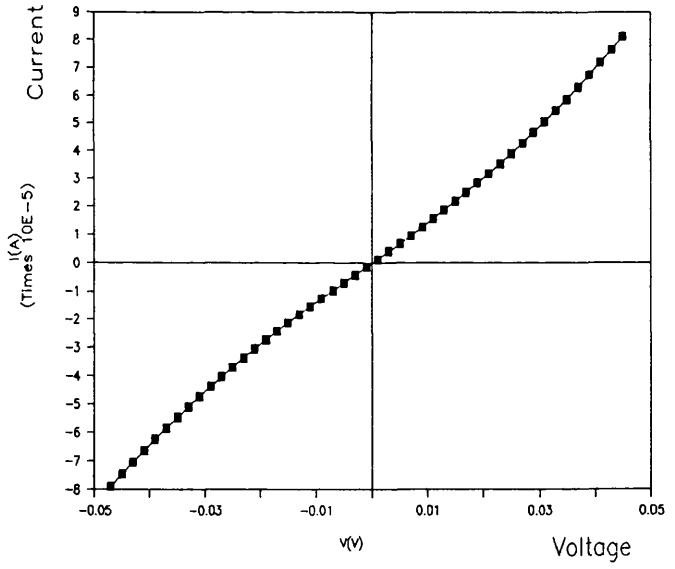

Fig.5.142IV curve of J7, T= 62 K

Figure 5.142 show the IV curve of junction J7 measured at T=62 K and showing a slight non-linearity.

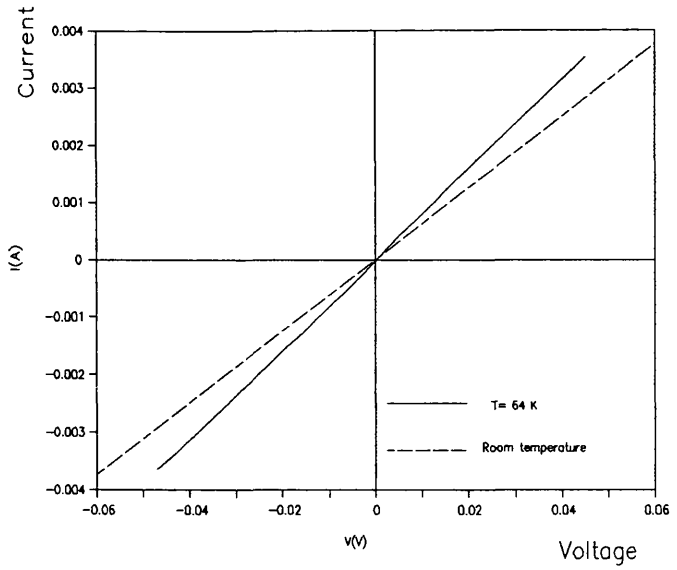

Fig.5.143 IV curve of J13 at the indicated temperatures

Figure 5.143 show two IV curves of junction J13 measured at T= 64 K (solid line) and room temperature (dashed line) . The slope of the room temperature curve yields a junction resistance of 15 Ω , with the junction at 64 K exhibiting a lower resistance and a slight non-linearity around 0 V which can be seen more clearly in the conductance vs voltage graph presented in the next figure .

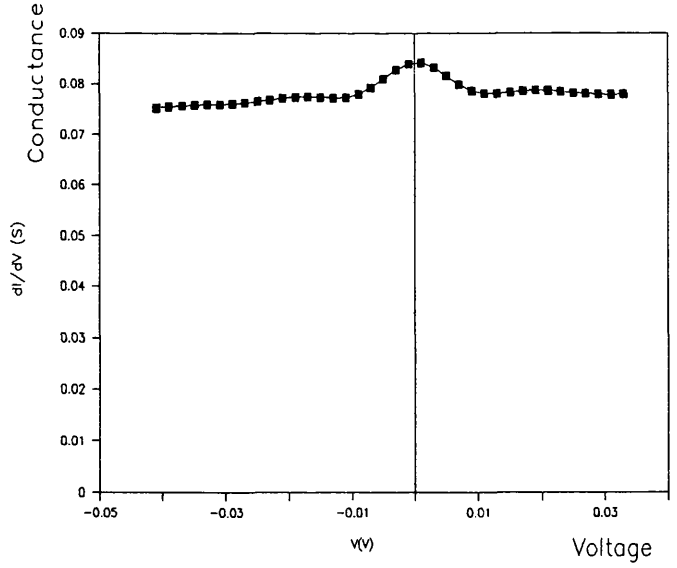

Fig.5.144 Conductance vs voltage of J13 at T= 64 K

Figure 5.144 show the conductance against voltage corresponding to the IV curves of J13 presented in figure 5.143 (solid line). This curve shows that the conductance increases when the voltage approaches zero and reaches its maximum at this value . This increase of the conductance reflects an increase of current around 0 V at T=64 K (solid line in figure 4.143).

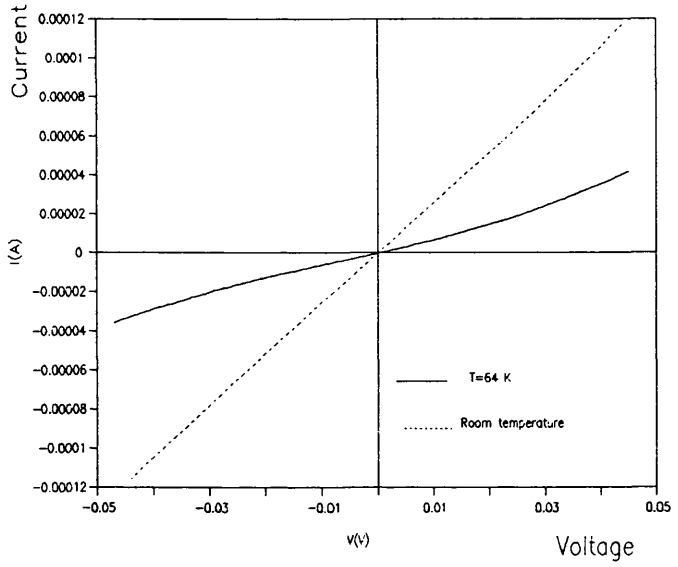

Fig.5.145 IV curve of J14 at the indicated temperature

Figure 5.145 shows a simultaneous presentation of two IV curves of J14 one taken at T= 64 K (solid line) and the other at room temperature (dashed line). The slope of the room temperature curve gives a junction resistance of 370 Ω .

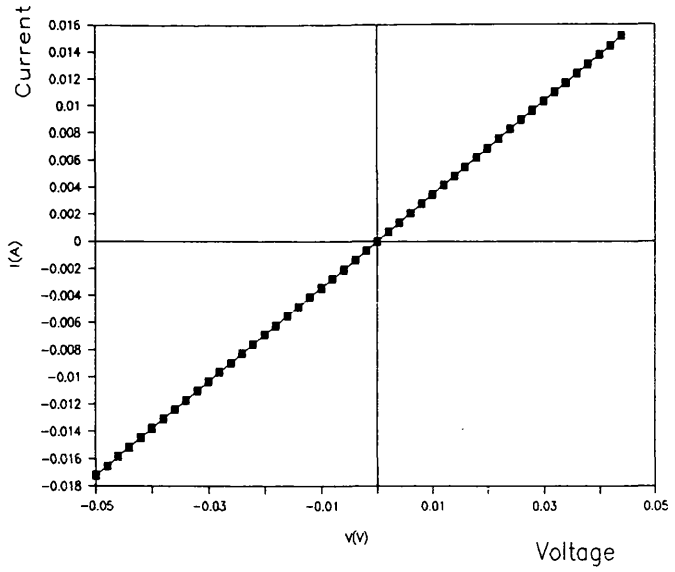

Fig.5.146 IV curve of J6 (direct contact) at room temperature.

Figure 5.146 shows the IV curve of J6 which is a direct contact (ie the measurement of the IV curve using the dots 6 and 1 which are without dielectric) on the superconductor. The slope of the curve yields a resistance of about 2.8 Ω which is fairly low if one consider that the resistance of the connecting wire alone is about 0.8 Ω for the cryostat used in this experiment .

Figure 5.147 shows the IV curve of J10 which is also a direct contact on the superconductor. The slope of the IV curve yields a resistance of 2 Ω .

Figure 5.148 shows the IV curve of J12 (dots 12 and 1 are used) . The slope of the IV curve of these direct contacts yields a resistance of about 1.8 Ω which is fairly low .

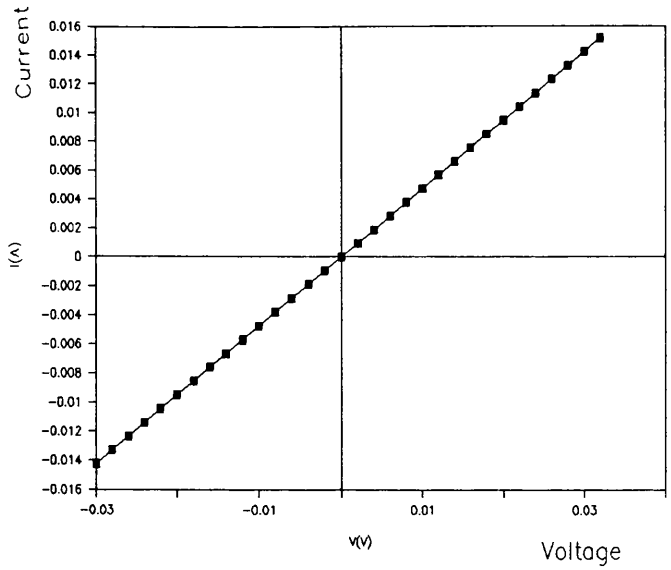

Fig.5.147 IV curve of J10 (direct contact) at room temperature

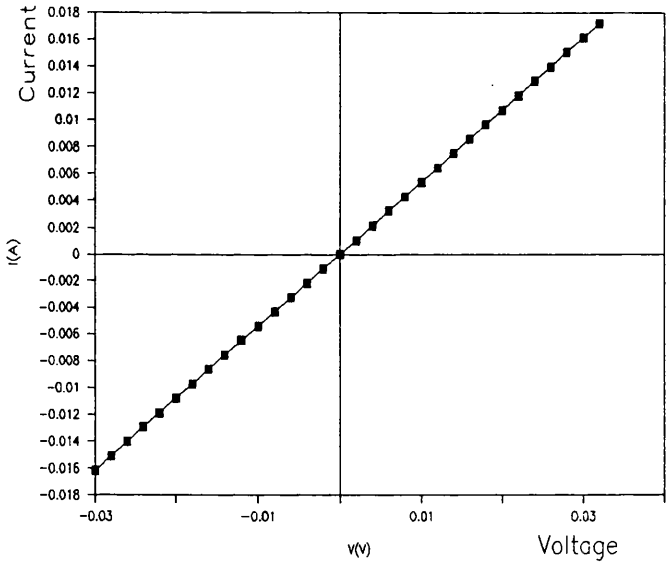

Fig.5.148 IV curve of J12 (direct contact) at room temperature

From the measurement on the direct contacts (figures 5.146, 5.147, 5.148) the linear IV curves show that these contacts are ohmic and of good quality . This an indication of the efficiency of the method of contact making onto high Tc superconductors which was developed during the project.

5.8.10 Layout of run 6

As seen in the previous runs, some junctions gave highly non-linear IV curves. These were selected for this run to test their reproducibility and observe the effect of magnetic field on them by using a superconducting magnet cryostat. The selected dots for this run are as indicated in figure 5.149 .

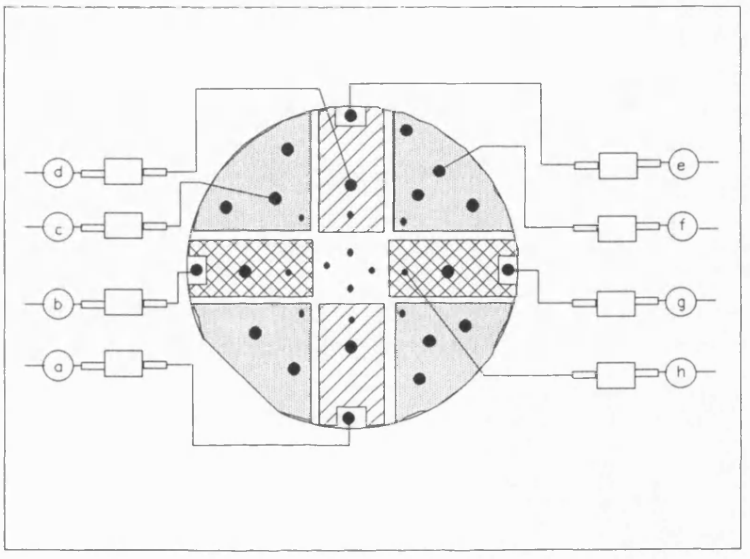

Fig.5.149 Electrical contact layout of run 6

For this run the junction are given the same number which they were referred to in the runs 4 and 5. Therefore the junctions connected for this run are as follows:

J8 between a and d
J5 between a and c
J11 between a and f
J14 between a and h

Resistance between different dots was measured using a digital multimeter and the following results have been found:

Rab= 6.5 Ω

Rae= 6.5 Ω

Raj= 6.2 Ω

Rad = 23.3 Ω

Rac = 1.2 KΩ

Raf= 24 Ω

Rah=10 KΩ

5.8.11 Experimental set up

The sample was fixed to a specially made sample holder that can be inserted into a magnetic field produced by the superconducting magnet as represented schematically in Figure 5.150 .

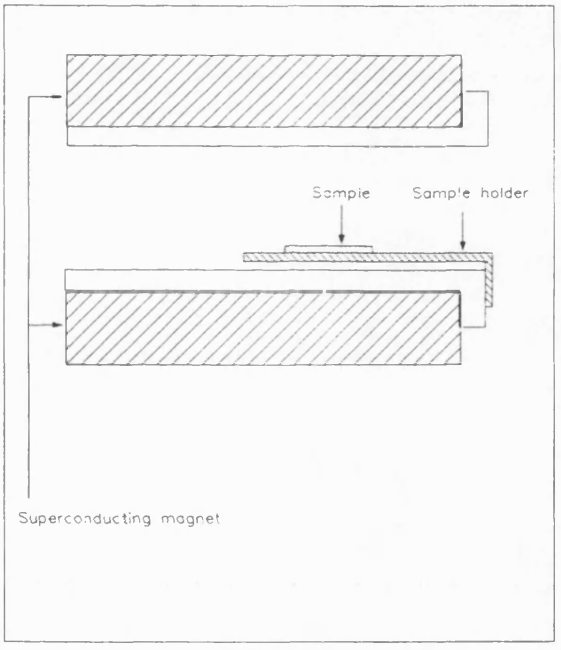

Fig.5.150 Schematic representation of the sample in the superconducting magnet

The measurements were carried out using the computer controlled system connected to the superconducting magnet cryostat as shown in figure 5.151 .

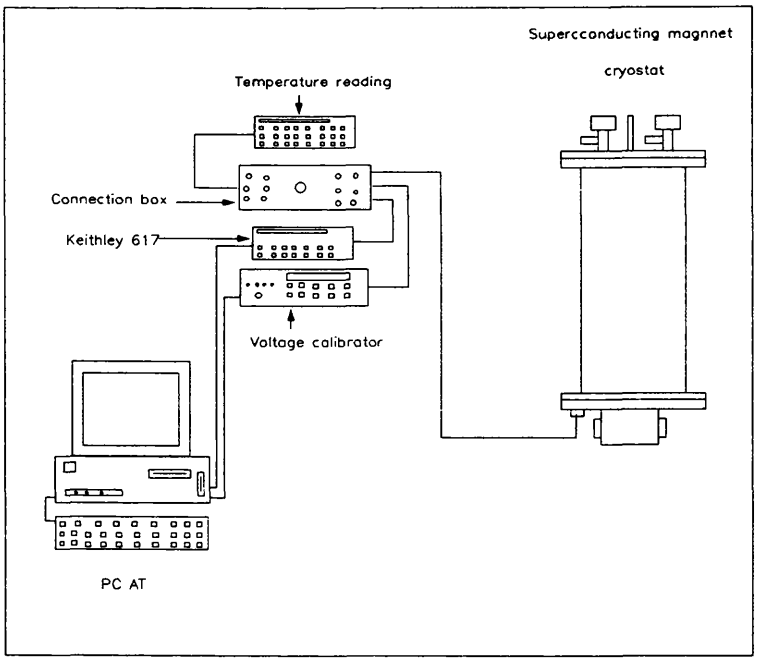

Fig.5.151 Computer controlled set up for run 6

5.8.12 Measurement results of run 6

The sample was cooled to 4.2 K in the cryostat and the superconducting magnet was used to observe effects of the magnetic field. During this run the measurements were concentrated on junctions J11 and J14 . These junctions gave non-linear IV characteristics which will be described in the next sections.

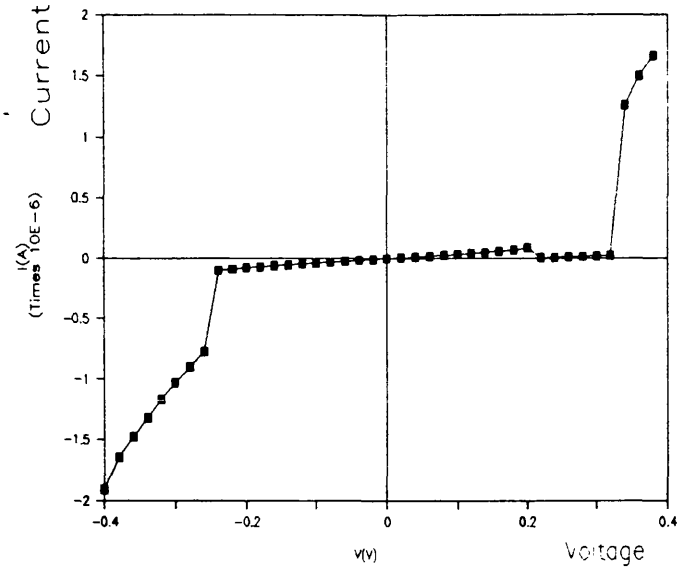

Fig.5.152 IV curve of J11, B=1 Tesla

Figure 5.152 shows the IV curve of J11 taken at liquid helium temperature with a magnetic field of 1 Tesla . This curve exhibits striking non-linear behaviour consisting of sharp variation of current at - 304 mV and , followed by a small linear current between -241 mV and 208 mV. At 203 mV the current reaches a peak and then decreases to zero . Although these features occur at quiete high voltages, they can be of interest, particularly the peak feature which may be anisotropic and thus gives a striking evidence of the anisotropy of energy gaps in high T_c superconductors as discussed in Chapter 4. Although the concept of energy gap anisotropy in HTS is well established , observation of this kind of peak in HTS has not been mentioned in any of the published data so far. However peaks resulting from gap anisotropy in Low Tc superconductors have been observed in the late sixties as will be discussed in Chapter 6 .

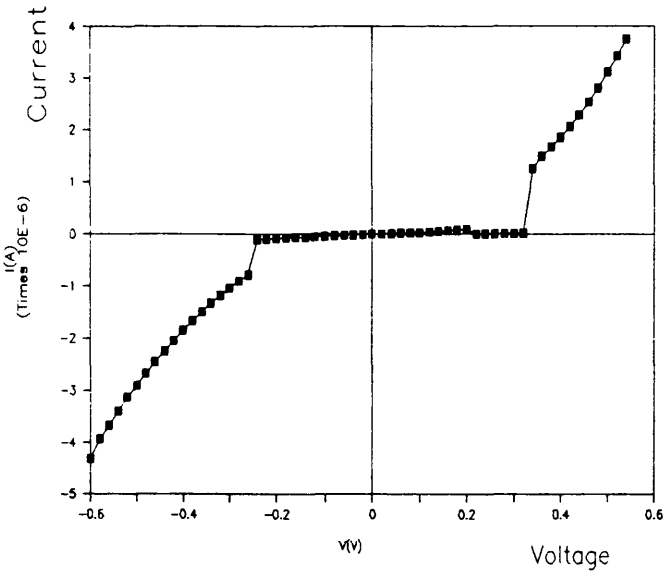

Fig.5.153 IV curve of J11, B=1 Tesla

Figure 5.153 shows the IV curve of J11 taken at liquid Helium temperature with a magnetic field of 1 T taken over a wide voltage range (-600 mV to 580 mV) . This exhibits similar features as figure 5.154 .

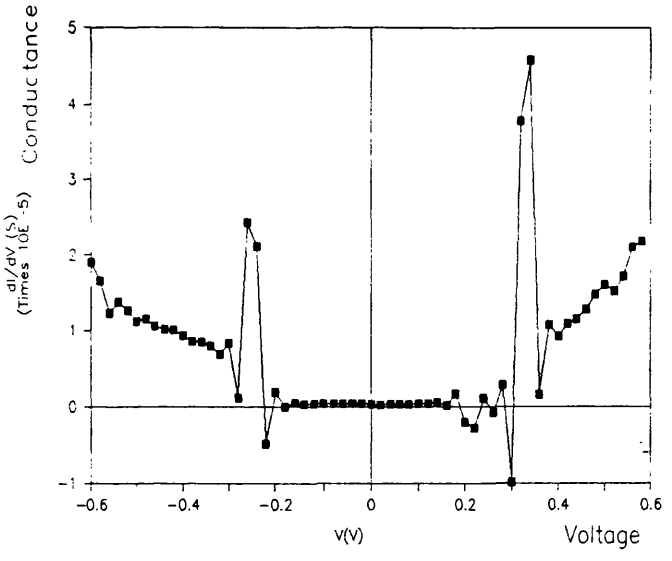

Fig.5.154 Conductance vs voltage of J11

Figure 5.154 shows the conductance against voltage corresponding to the IV curve of figure 5.153 . The non-linear features of the IV curve are reflected here with

two large peaks separated by 608 mV. Two smaller peaks can also be seen one at - 75 mV and the other at 105 mV ie 180 mV apart . These smaller peaks are followed by two negative conductances. These small features of peaks and valleys suggest the existence of a smaller peak on the left side of the IV curve similar to that on the right side, but smaller and thus not visible on the IV curve. If the two peaks were clearly visible the IV curve of this junction would exhibit an ideal IV curve of SIS' junctions showing striking anisotropy of gap structure of differently oriented YBCO grains (grain of chain and plane being side by side)

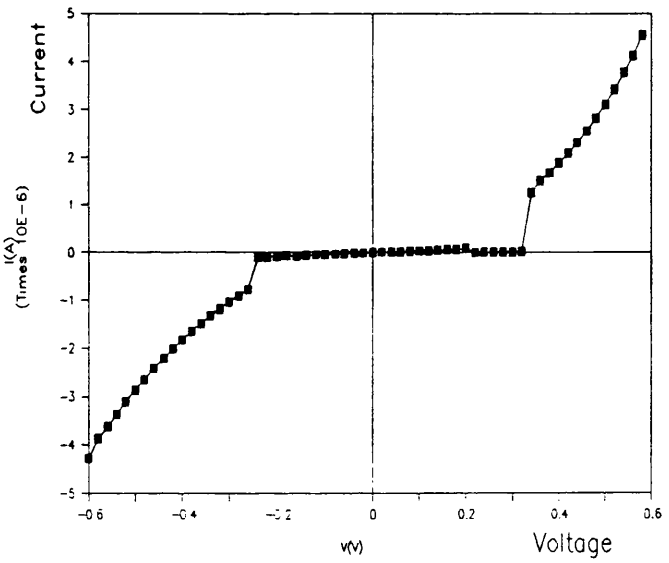

Fig.5.155 IV curve of J11, B=0.666 Tesla

Figure 5.155 shows the IV curve of J11 taken at liquid Helium temperature with a magnetic field of 0.66 T .

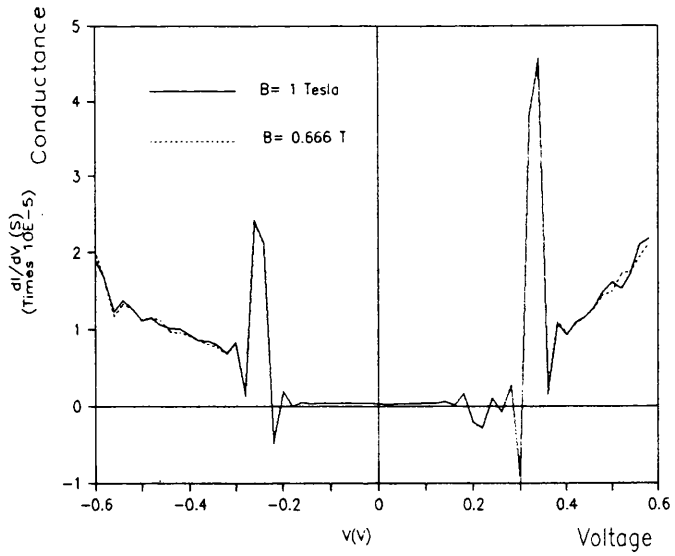

Fig.5.156 Conductance vs voltage J11 at the two indicated magnetic field values

Figure 5.156 shows the conductances vs volyage corresponding to the IV curves of figures 5.153 and 5.155 which were taken at the at 1 T and 0.666 T respectively . There is no effect of these two differnt values of the magnetic field on the conductance vs voltage of J11 for voltage between -400 mV and + 400 mV . Beyond |400| mV this figure (5.156) shows a slight increase of conductance with increasing magnetic field .

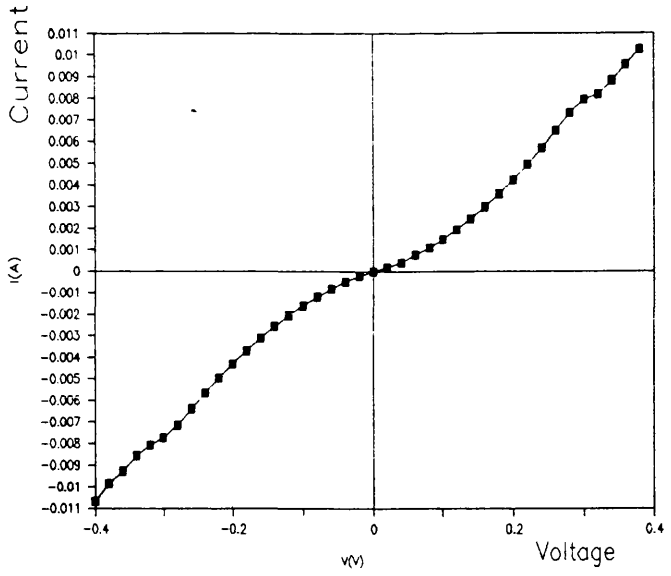

Fig.5.157 IV curve of J14, B=0 Tesla

Figure 5.157 shows the IV curve of J14 measured at liquid Helium temperature in the absence of a magnetic field. This is a well behaved nonlinear IV curve which exhibit shoulder structure at +/- 302 mV . Two similar IV curves were measured at 0.333 T and 0.6666 T and are presented with that of figure 157 in the following garphs .

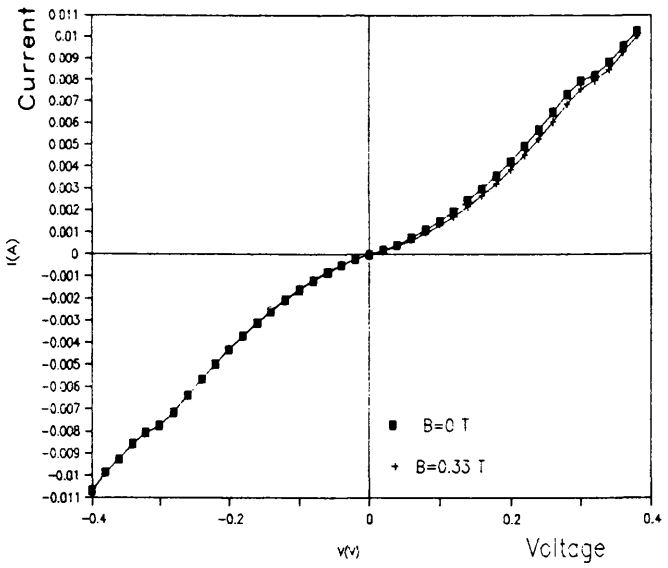

Fig.5.158 IV curve of J14 at the two indicated magnetic field

Figure 5.158 shows a simultaneous presentation of the IV curves of J14 taken at indicated magnetic field values . For B=0.333 T a slight shift to the right occurs for voltages between 100 mV and 250 mV. Beyond 250 mV the two curves almost coincide. For negative voltages the two curves are indistinguishable.

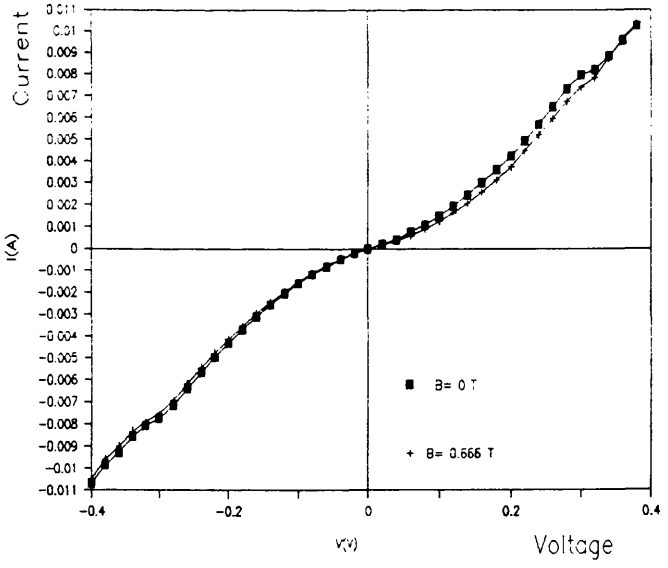

Fig.5.159 IV curve of J14 at the two indicated magnetic field values

Figure 5.159 shows a simultaneous presentation of the IV curves of J14 at the indicated magnetic field values . For a a higher magnetic field (0.666 T), a slight shift feature similar to that of figure 5.158 is observed. However when the voltage falls below -200 mV, a slight separation can be seen .

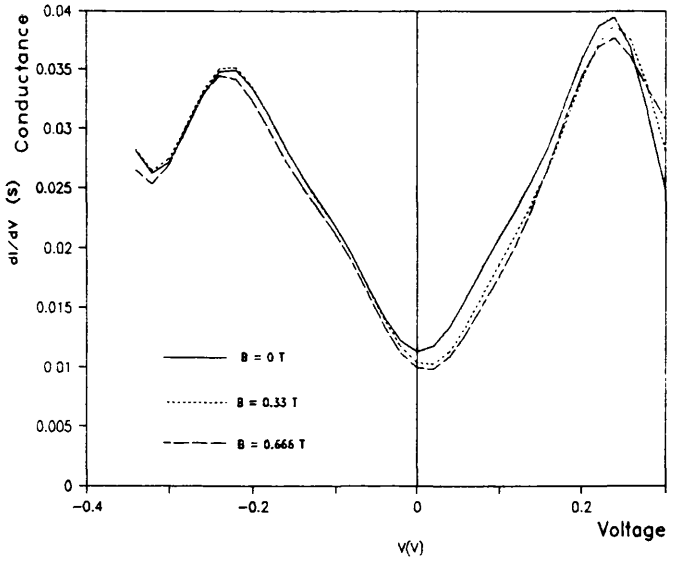

Fig.5.160 Conductance vs voltage of J14 at the indicated magnetic field values

Figure 5.160 shows a simultaneous presentation of the conductances against voltage corresponding to the three IV curves of J14 measured at three different magnetic fields. This figure shows that a higher magnetic fields causes the conductance to be slightly lowered between about -232 mV and + 252 mV. For voltages less than -240 mV the three curves almost coincide. The conductance curves with an applied magnetic field intersect at 158 mV, where the conductance of the junction in the higher magnetic field becomes slghtly higher than that of lower magnetic field . For voltages greater than 252 mV the conductance is shown to exhibit a small increase with the magnetic field. From the result of these curves it can be concluded that the effect of the magnetic field was negligeable.

5.9 Thin films attempt

Thin film making has been attempted several times using simple DC sputtering. In this attempt the target used was a 19 mm pellet situated at 20 mm from allumina and strontium titanate substrates. The sputtering was carried out at room temperature in a mixture of argon and oxygen. The ratio of argon to oxygen was 3:1 . The deposition continued for 48 hours, when the allumina substrate was covered with a black opaque film. The film on the SrTiO3 crystal was black, smooth and had a shiny surface as indicated by the photograph presented in figure 5.161 .

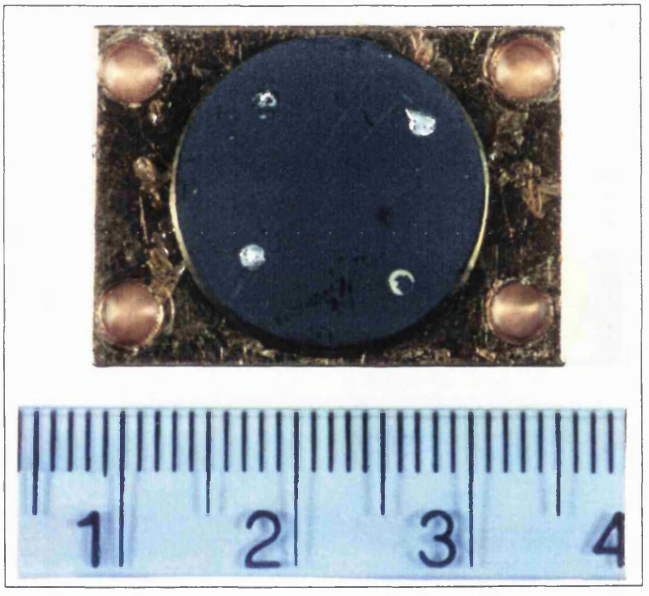

Fig.5.161 Photograph of YBCO film on SrTiO3

Both films which were deposited on allumina and Strontium titanate substrates were annealed in flowing oxygen according to the diagram shown in figure 5.162 .

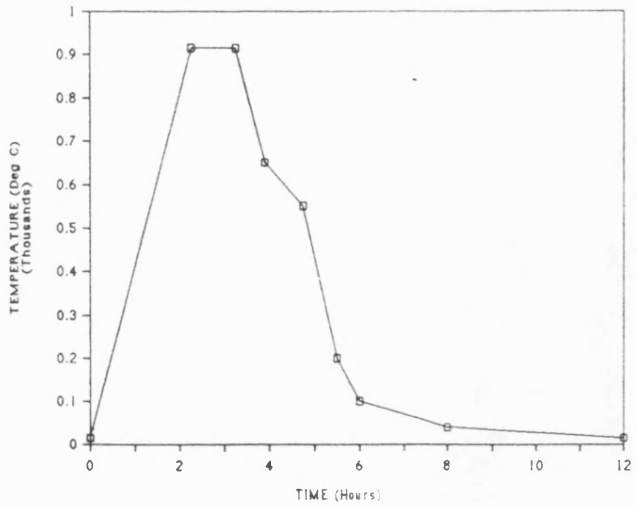

Fig.5.162 Annealing diagram of YBCO films

After this anneal an XRD pattern was recorded and is shown in figure 5.163 .

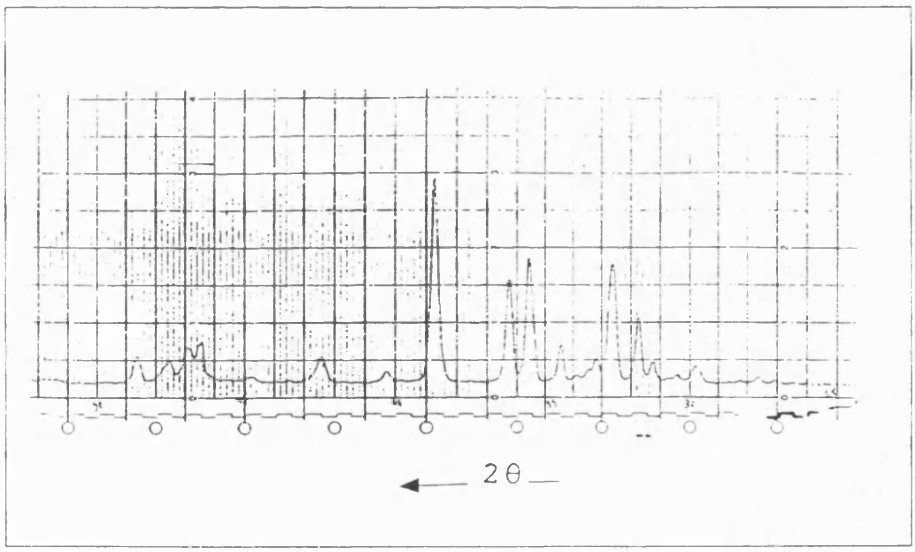

Fig.5.163 XRD pattern of YBCO film on SrTiO3

This is to be compared with a reported XRD pattern of YBCO thin film which is indicate in figure 5.164 .

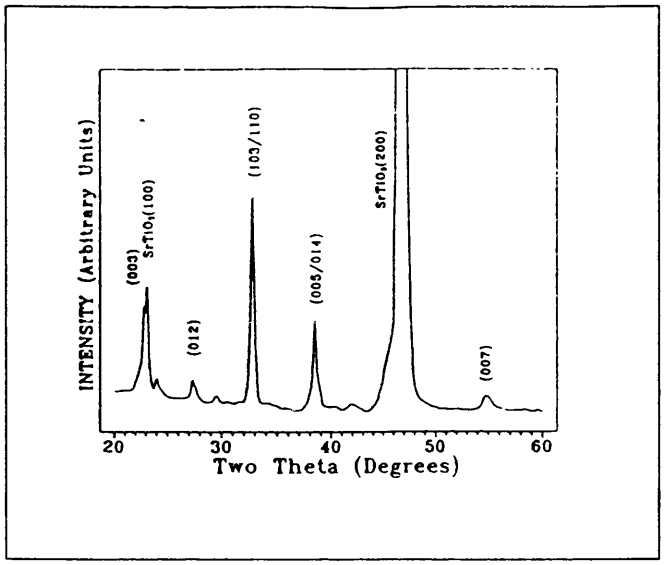

Fig.5.164 XRD pattern of YBCO film on SrTiO3 (from ref. [1])

5.9.1 R vs T measurement of thin film on SrTiO3

The sample on SrTiO3 was fixed in the low temperature cryostat and the R vs T measurement carried out using a DC four probes method. The result obtained is as shown in figure 5.165 .

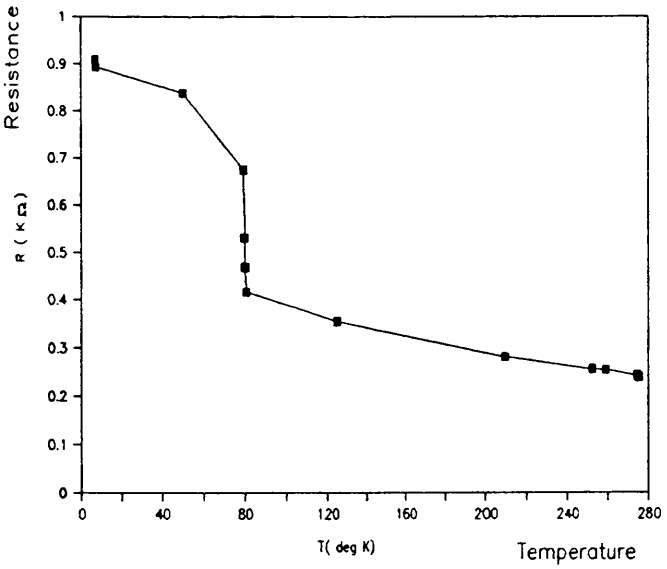

Fig.5.165 R vs T of YBCO thin film on SrTiO3

5.9.2. R vs T measurement of thin film on allumina

During the cooling down of the sample the resistance started to rise. At temperatures below 220 K, the resistance becomes too large to measure . The result of this measurement is shown in figure 5.166 .

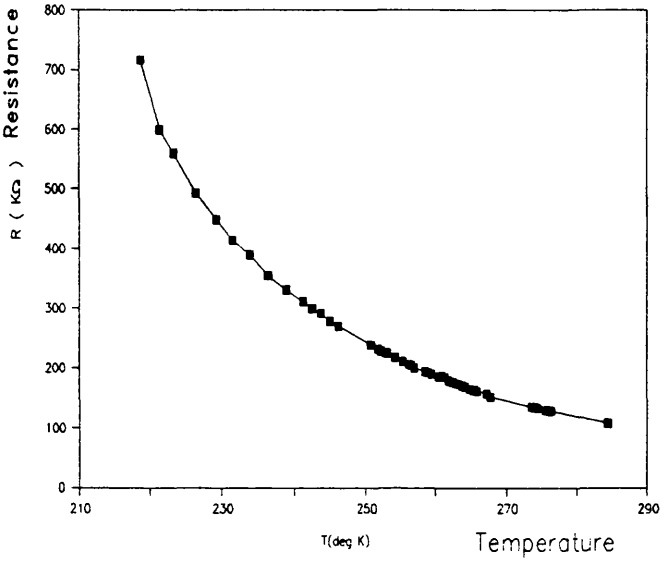

Fig.5.166 R vs T of YBCO thin film on allumina

This shows that the sample has a semiconducting-like behaviour.

5.9.3 Comparison of the previous R vs T

The simultaneous presentation of R vs T of strontium titanate and allumina films is shown in figure 5.167 . In this graph the symbol (x100) indicates that the values of R of the film on SrTiO3 have been multiplied by a factor of 100 so they can be presented in this simultaneous graph. This shows very clearly a striking poisoning effect of allumina on YBCO thin film .

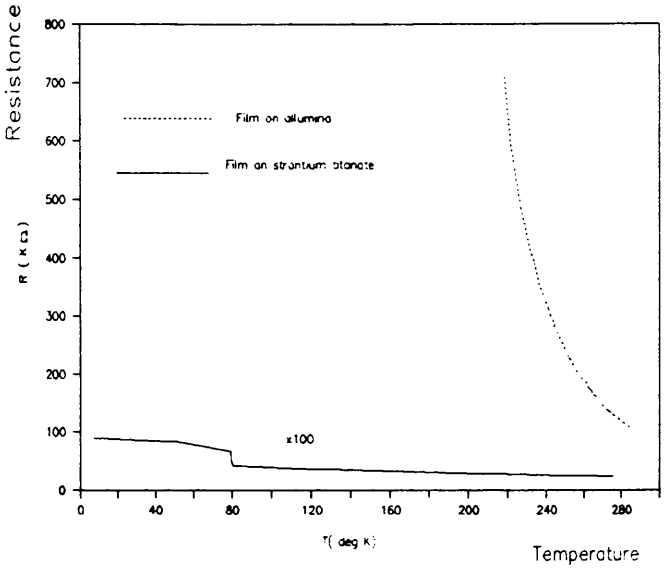

Fig.5.167 R vs T of films on allumina and strontium titanate

This semiconducting behaviour has been observed [2] [3] and found to result from a combination of many factors such as oxygen pressure [4], substrate nature, substrate temperature, and annealing procedure .

Most thin film depositions are carried out at relatively high temperature (>500 C) and involve complicated procedures such as plasma assisted laser deposition [5], electron beam evaporation [6], RF magnetron sputtering [7] and electron cyclotron resonance with oxygen plasm assisted evaporation [8].

The advantage of the procedure used in this attempt is that it was carried out at room temperature using simple dc sputtering . The film obtained on SrTiO3 had a mirror-like surface coinciding with the description of a recent report on thin film deposition on SrTiO3 using a more complicated approach namely the plasma-enhanced organometallic chemical vapour deposition [1]. This indicates that the approach followed during this attempt is not far from giving satisfactory results but more optimization is needed.

Chapter 5 references

1 J. Zhao, H. O. Marcy, L. M. Tonge, B. W. Wessels, T. J. Marks, and K. C.R. Kannewurf, "Deposition of high Tc Superconducting Y-Ca-Cu-O thin films at low temperature using a plasma-enhanced organnometallic chemical vapour deposition approach", Solid State Communications 74, pp.1091-1094, 1990.

2 B. Hauser and H. Rogalla, "Study of the preparation and properties of YBaCuO-films ", preprint 1987, to be published in: Proceeding of the Berkley workshop on novel mechanism in superconductivity.

3 J.R. Galver and A.I. Braginski, " near surface atomic segregation in YBCO thin film ", Physica C 153-155, pp : 1435-1436,1988.

4 J. Q. Zheng, M. C. Shih, S. Williams, S. J. Lee, H. Kjiwama, X. K. Wang, Z. Zhao, K. Viani, S. Jacobson, P. Dutta, R. P. H. Chang, J. B. Kettreson, T. Robert, R. T. Kampwirth, and K. A. Gray, " Effect of oxygen partial pressure on the in situ growth of Y-Ba-Cu-O thin film", Appl. Phys. Lett. 59, pp:231-233, 1991.

5 S. Witanachi, H. S. Kwoke, X. W. Wang, and D. T. Shaw, Appl. Phys. Lett. 53, p.234, 1988.

6 A. B. Berzin, C. W. Yuan, A. L. de Lausann, S. M. Garrisson, and R. W.Barton, " YBCO thin film on sapphire with epitaxial MGO buffer ", IEEE trans. Magn. MAG-27, p.970, 1991.

7 K. Mizuno, M. Miyachi, K. Setsune, and K. Wasa, Appl. Phys. Lett. 54, p. 383, 1989.

8 T. Aida, A. Tsukamoto, K. Imagawa, T. Fukazawa, S. Satito, K. Shindo, K. Tagagi, and K. Miyauch, Jpn. J. Appl. Phys. 28, L653, 1989.

CHAPTER 6: DISCUSSION OF RESULTS

6.1 Introduction

As most of the results consist of current vs voltage (IV) curves and conductance vs voltage (CV) curves it may be useful to refer to chapter 3 where the ideal IV curve of SIN or SIS junctions were presented at temperatures approaching zero . In these ideal cases the IV curves exhibit very strong non-linearities which can be used to infer the energy gap of the material considered from the voltage at which the non-linearities of the IV curves of these devices occur [1] . Other techniques such as the use of differential conductance, dI/dV, and even d^2I/d^2V plotted against voltage are used to uncover features which cannot be observed in IV simple characteristics [1] [2] [3]. Both types of curves have been used to characterise high temperature superconducting tunnelling devices . In high T_c superconductors the CV and IV characteristics are affected by many properties of the materials . Firstly the anisotropy of YBCO parameters (which is common to most HTS superconductors), and particularly the coherence length which is very small in the c-direction (less than 10 Å as discussed in chapter 4) . Secondly the sensitivity of this material to oxygen stoichiometry which can be altered by environmental or interfacing chemical compounds (as discussed in chapter 4) results in structural disorder and inhomogenieties in the sample . These and other effects, lead to different values for parameter such as the energy gap . This has led different authors to suggest different methods and models for interpreting IV and CV characteristics [4] [5] [6] [7] .

In this chapter the results described in chapter 5 will be summarised and the most important features will be discussed and compared, when possible, with reported results.

6.2 SAMPLE 1 S1P

The IV curves of S1P junctions exhibit two types of non-linearities:

A) IV curve with pronounced non-linearities as was shown in figure 5.7. These features were reflected in the conductance vs voltage (figure 5.8) by peak features one at 0 V and two others at +/- 35 mV. The 0 V peak has been reported in the conductance vs voltage in junctions having artificial barrier and was referred to as an anomaly [8] [9] [7]. This anomaly has also been observed in point contact junctions and was explained in term of a superconducting weak link or a Josephson like current flowing through a non-ideal barrier [5], [6] [10]. However a dip feature in the conductance against voltage was found to occur in results from junctions having either native barrier [11] [12] or artificial barrier [13] [14] . This difference in behaviour at 0 V is not properly understood yet . In the case of the peak features similar to that of figure 5.8 , a method of energy gap determination was suggested [6] and is presented in figure 6.1 .

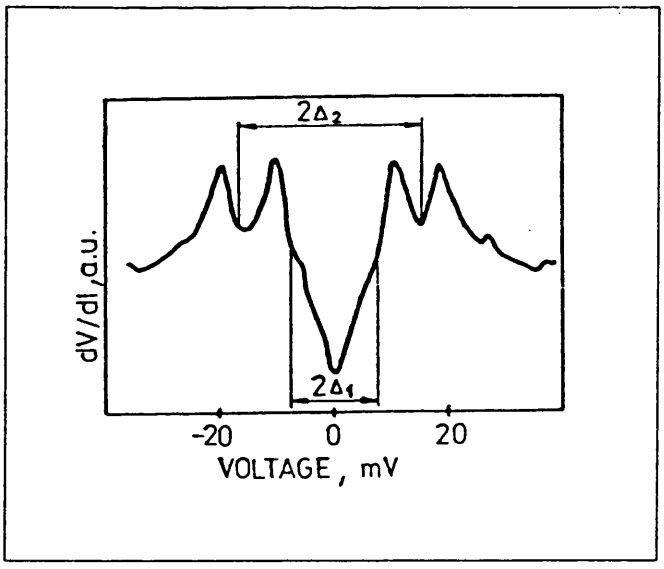

Fig.6.1 Conductance vs voltage showing the two energy gap structures (From [6])

This is similar to a recent method [7] in which the 0 V peak of the conductance was interpreted to be due to an energy gap along the c axis, Δ_c , and the two other peaks which enclose it , were identified with the energy gap in the (a,b) planes, Δ_{ab} , as indicated in the model shown in figure 6.2 .

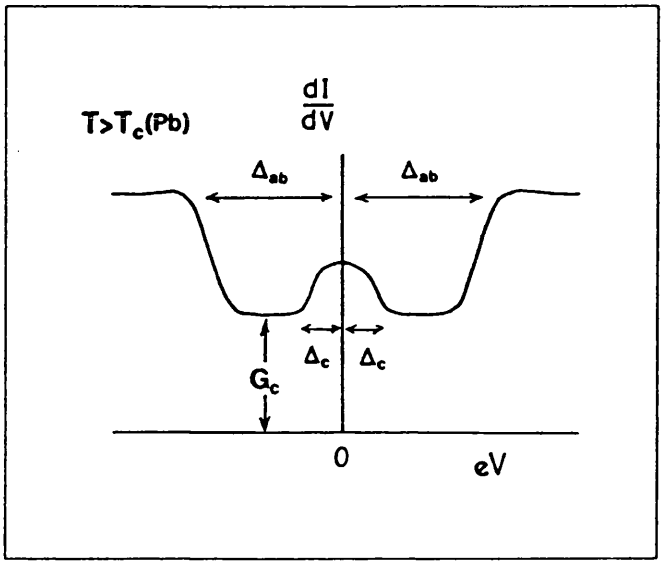

Fig.6.2 Model of conductance vs voltage showing the two energy gaps Δ_c and Δ_{ab} (From [7])

This model was suggested as a result of an investigation into the origin of the dip and peak features at 0 V of YBCO/I/Pb tunnel junction fabricated in situ and ex-situ. The values of Δ_c and Δ_{ab}suggested in this investigation [7] are:

$$\Delta_c = 5 \text{ meV}$$

$$\Delta_{ab} = 16 \text{ to } 20 \text{ meV}$$

If this second method is applied to the features of figure 5.8 one obtains the energy gap values of 11 meV in the c direction and 33 meV in the in the (a,b) planes. As the reported values ofΔ_c fall in the range 3 to 6 meV [6] [7], this suggests the existance of an array of N junction so that one can write:

$$N\Delta_c = 11 \text{ meV}$$

$$N\Delta_{ab} = 33 \text{ meV}$$

For N=2

$$\Delta_c = 5.5 \text{ meV}$$
$$\Delta_{ab} = 16.5 \text{ meV}$$

For N=3

$$\Delta_c = 3.6 \text{ meV}$$
$$\Delta_{ab} = 11 \text{ meV}$$

B) Secondly curves with an NDR features (figure 5.11 and 5.12). These features were reproducible over many scans. The conductance vs voltage curve (figure 5.13) gave a highly symmetrical structure of peaks including one at 0 V, and valleys with one having negative value at +/- 83 mV. A possible NDR behaviour has been noticed in one of the reports investigating single-electron tunnelling in YBCO point contact junctions [15] as can be seen in figure 6.3 .

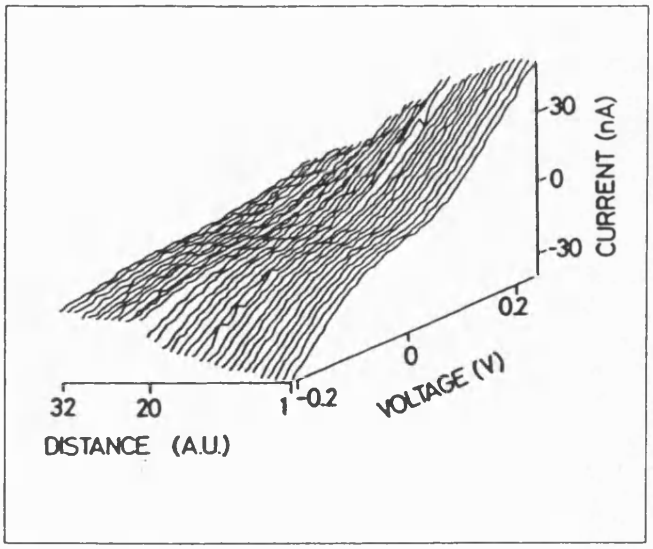

Fig.6.3 IV curves where NDR can be seen (From [15])

6.3 SAMPLE 2 K1B

The IV characteristic of this sample are characterised by a well behaved nonlinearity at low temperature and are similar to IV curves obtained in a recent report [9] .

The junction considered in this sample has no artificial barrier and its conductance against voltage curve (figure 5.22) had a dip at 0 V . This 0 V dip in the conductance of junctions with native barrier has been observed [11] [12]. The conductances of figure 5.22 increase slightly with increasing temperature around 0 V and then converge beyond |10| mV where they continue to increase monotonously with increasing voltage. This increase of the conductance with the voltage is one of the most common properties which characterise the conductance vs voltage curves of high T_c superconductors and has been observed in numerous reports [5] [6] [9] [7] [16] [17]. Figure 5.22 exhibits a finite conductance at zero biasing voltage. This behaviour has been observed by many teams [5] [18] [19] [20] [13] [7] and in one case, [11] it was described as perplexing and was suggested to be due to the presence of a continuum of states below the gap. However very low sub gap conductance was observed by other teams [21] [22] [23] and one of them [21] inferred the absence of quasiparticles states below the energy gap.

6.4 SAMPLE 4 S1DE (S1E and S1D)

The IV curves of junctions formed on the pellet and on the bar without dielectric exhibit an increase of current around 0 V. This increase is reflected by a maximum at 0 V in the conductance vs voltage of figure 5.36 (solid line).

The R vs T of the bar exhibits a knee around the transition temperature. This behaviour is referred to as double transition and has been observed in many reports and is believed to be due to the presence in the sample of different phases with different critical temperatures [24] .

6.5 SAMPLE 5 S2A

The IV curves of junctions with or without dielectric exhibit an increase around 0 V . This is reflected by a peak at 0 V in the conductance vs voltage like that of junction A for instance (figure 5.51) . At high voltages the conductance increases monotonously with voltage . A 0 V peak in conductance against voltage similar to that of figure 5.51, has been observed by many workers. A result taken from one of the reports [9] is shown in figure 6.4 .

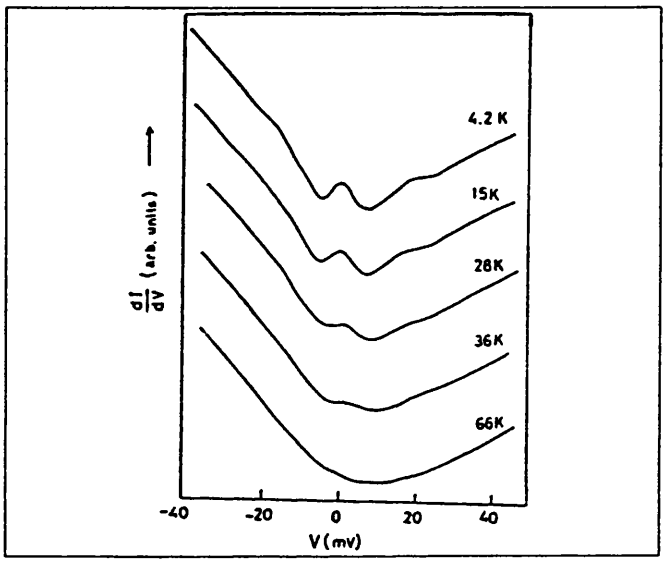

Fig.6.4 Conductance vs voltage similar to S2A (from [9])

The measurement results from this sample have revealed that two direct contacts on the sample surface have different IV curves (figure 5.56). This suggests that the sample surface is not homogeneous. This can result from different crystal orientations or local variation of the stoichiometric composition of the sample. This behaviour has been reported by many teams [21] .

6.6 SAMPLE 6 BD1

This sample gave well behaved non linear IV curves . Two junctions on the same sample and thus prepared under the same conditions gave distinct IV curves at the same temperature (figure 5.65). This kind of difference in behaviour is often due to inhomogenieties of the surface of the superconducting sample as has been pointed out in many reports [21].

6.7 SAMPLE 7 SDO

Many measurements were carried out on different junctions of the sample over many runs . Some of the results obtained from IV curves and conductances against voltage will be discussed in the following sections .

6.7.1 Run 1

During this run, junction J7&C gave striking non-linear IV but asymmetric IV curves at liquid nitrogen temperature (figures 5.76 to 5. 80). These had a fairly wide zero current region followed by sharp current variations and linear asymptotes at higher voltages. The conductance versus voltage (figure 5.81) revealed more features particularly the interesting negative valleys . These suggest the presence of small peaks in the low current region of the IV curves as in the case of an SIS junction with different superconductors having different gap parameter (if the asymmetry of figure 5.81) is neglected. As there is only one type of superconductor involved, this behaviour can only be explained if anisotropic gap parameters Δ_c and Δ_{ab} are considered . From figure 5.81 the following values of peaks separations are obtained :

Small peaks separation : 76.6 mV

Large peaks separation : 123 mV

If an array of N SIS junctions is assumed the following equations can be written:

$$N(\Delta_{ab}+\Delta_c)=123/2 \quad =61.7 \text{ meV}$$

$$N(\Delta_{ab}-\Delta_c)=76.6/2 \quad =38.3 \text{ meV}$$

These lead to:

$$N\Delta_c = 11.7 \text{ meV}$$

$$N\Delta_{ab} = 50 \text{ meV}$$

For different values N the possible values of Δ_c and Δ_{ab} are as indicated in table 6.1.

Table 6.1 Possible values of Δ_{ab} and Δ_c

N	Δ_{ab} (meV)	Δ_c (meV)
2	25	5.8
3	16.6	3.9
4	12.5	2.9

At room temperature the conductance vs voltage of J7&C gave oscillations-like feature with decreasing amplitude for voltages around zero . Similar behaviour has been reported [23] .

Junctions J3&C and J14&C gave well behaved non-linear IV curve . Their respective conductances against voltages had a dip around 0 V, increased with increasing voltage and had sub gap conductance .

6.7.2 Run 2

In this run junctions J11&C gave well behaved non-linear IV curves at 7 K and 77 K. Their conductances against voltage characteristics (figure 5. 95) had gap features. The low temperature conductance (solid line) gap is 62 mV

wide. This V shaped gap structure is thought to be a consequence of gap depression which is caused by a reaction between YBCO and its interfacing compound [7]. This results in a weakening of Δ_{ab} and a vanishing of Δ_c . Consequently the IV and CV characteristics obtained in this situation can be considered to be of the SIN type where only Δ_{ab} is involved. The gap feature of figure 5.95 yields Δ_{ab} =24 meV. Gap parameter values of this order have been obtained from junctions with artificial barriers exhibiting a dip at 0 V as shown in figure 6.5 where two the results of two investigations are shown , one using a junction on thin YBCO film (solid line) [13], and the other using a junction on YBCO single crystal (dashed line) [14].

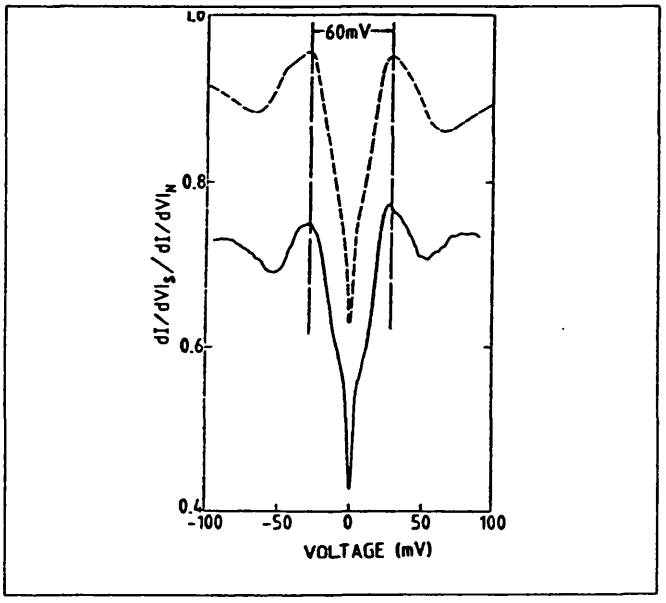

Fig.6.5 Conductances vs voltage of junctions on YBCO thin film (solid line) [13], and single crystal (dashed line) [14]

J8&C gave a well behaved IV curves at 7 K (figure 5.99). The conductance against voltage curve corresponding to it (figure 5.100) shows many features of peaks and valleys in addition to sub-gap conductance. The 0 V peak has a width V_{g1}=20 mV and the separation between the two other

peaks enclosing it is V_{g2}= 96 mV. These peak features can be interpreted using the model shown in figures 6.1 [6] or that of figure 6.2 [7] which are similar as discussed above. Applying the model of figure 6.2, one gets (from figure 5.100) the following values :

$$2\Delta_c = 20 \text{ meV}$$
$$2\Delta_{ab} = 96 \text{ meV}$$

As these values are much higher than those suggested in the above reports [6] [7], they can be interpreted as resulting from an array of N junctions so as one can write:

$$2N\Delta_c = 20 \text{ meV}$$
$$2N\Delta_{ab} = 96 \text{ meV}$$

The possible values of N, Δ_{ab}, and Δ_c are shown in table 6.2.

Table 6.2 Possible values of Δ_{ab} and Δ_c

N	Δ_{ab} (meV)	Δ_c (meV)
2	24	5
3	16	3.3

This idea of arrays or networks of junctions is widely used in high T_C superconductors [21], [25] and results from the micro structure of the pellet which consists of a network of tiny grains which are randomly oriented as shown in figure 6.6.

Fig.6.6 Granular structure of polycrystalline YBCO (the bars are 10 μm (from [27]) .

When polycrystlline samples are used for device applications short circuits are almost inavoidable as shown in figure 6.7. In this situation weak links below the tunnel barrier become important .

In the polycrystalline specimen coupling between the adjacent grains is weakened as a result of misalignments and contaminations by impurity phases at the grains boundaries [28] [29]. These grain boundaries act as weak links and reduce the critical current in sintered samples [30] [31]. These same week links have been used in many application such as detection, mixing, and radiation emission as was discussed in chapter 4 (section 4.12 to 4.14). Different types of grain boundaries can occur in polycrystalline systems and some of them are indicated in figure 6.8.

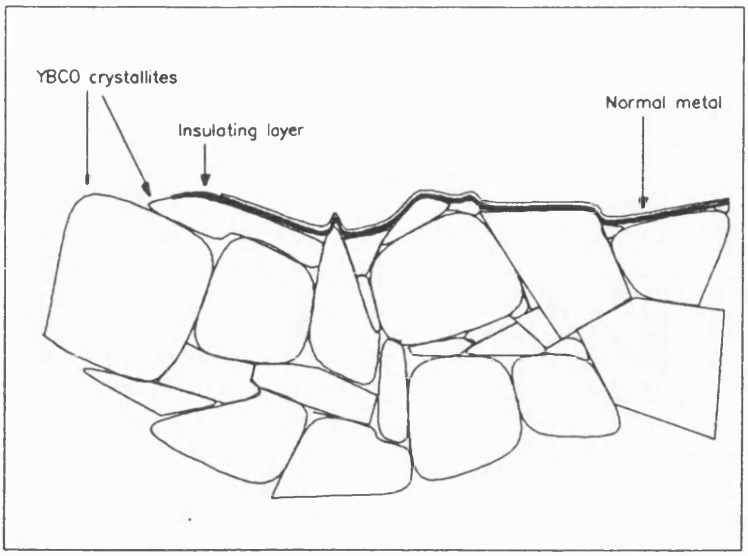

Fig.6.7 Schematic representation of a cross section of YBCO pellet with insulating and normal metal layers on its surface.

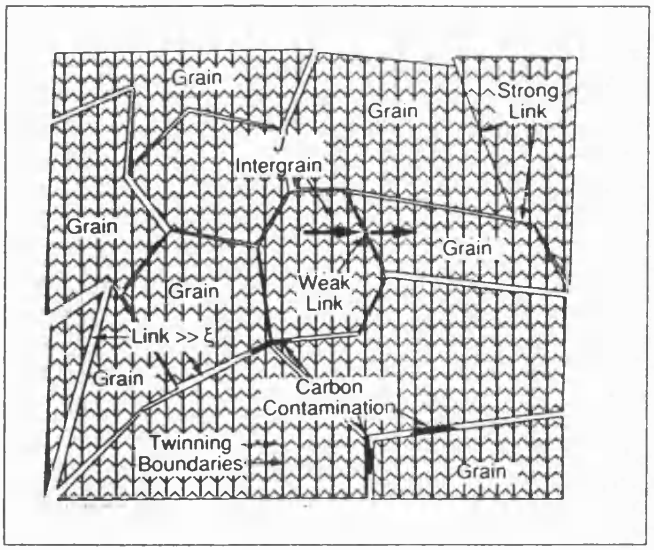

Fig.6.8 Schematic presentation of grain boundary effects in policrystalline samples (from [32]).

These differences in the nature of the grain boundary which lead to different type of barriers can cause the supercurrent

to flow through preferential paths and give rise to high tunnelling current density at the normal metal interface. It has been reported that angle grain boundary (AGB) which were present in investigated YBCO thin film can form different type of barriers and thus give different types of junction such as SIS, SNS, SSES (Superconductor SEmiconductor superconductor), SNIS and SNINS [32] . In another tunnelling experiment [33] using a point contact on a sintered polycrystalline BISCCO sample, all the contacts between grains (shown in figure 6.9 (a)) were assumed to be weak links of the Josephson junction type. By replacing each weak link by its equivalent Josephson junction circuit (shown in figure 6. 9 (b)), an equivalent circuit of this polycrystalline specimen was suggested and is shown in figure 6.9 (c) .

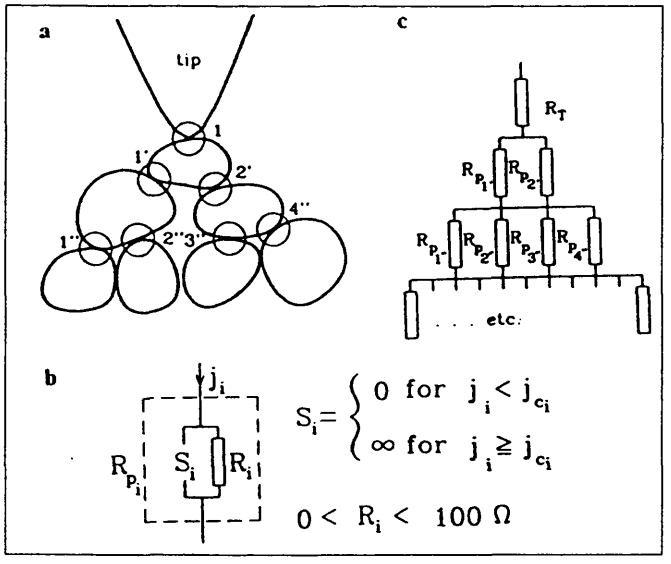

Fig.6.9 Schematic presentation of microstructure using weak links (numbered 1' 2' ...) . R_T is the tunnelling resistance between the point contact and the sample . R_i the normal resistance of the contact i when (Ji>Jc R_{pi} the parallel resistance of the contact (from [33])

From these examples one can conclude that the final shape of the tunnelling characteristics of HTS is determined by the type of junctions created by the grain boundaries that are present in the path(s) of the tunnelling current. Efforts have been made to reduce these weak links and considerable progress has been achieved using the melt textured growth (MTG) technique [34] which gives better aligned and connected grains and thus higher critical current.

It is interesting to note that most of the peaks and the valleys were greatly reduced when the temperature increased from 7 K to 45 K as was shown in figure 5.108.

6.7.3 RUN 3

Again J8&C gave well behaved non-linear features which became less pronounced with increasing temperature (figure 5.117). The conductances vs voltage curve presented in figure 5.118 shows a dip around 0 V whose minimum increases with increasing temperature. The room temperature conductance is slightly bent with a minimum at 0 V. This behaviour of the conductance versus voltage at room temperature has been reported elswhere [19], [11] [35] .

The conductances of J14&C shows a dip around 0 V at T=58 K (figure 5.120). However at room temperature, the dip at 0 V vanished but the CV characteristic then exhibited oscillation features (figure 5.123). A similar oscillating behaviour has been reported [23] and is shown in figure 6.10 .

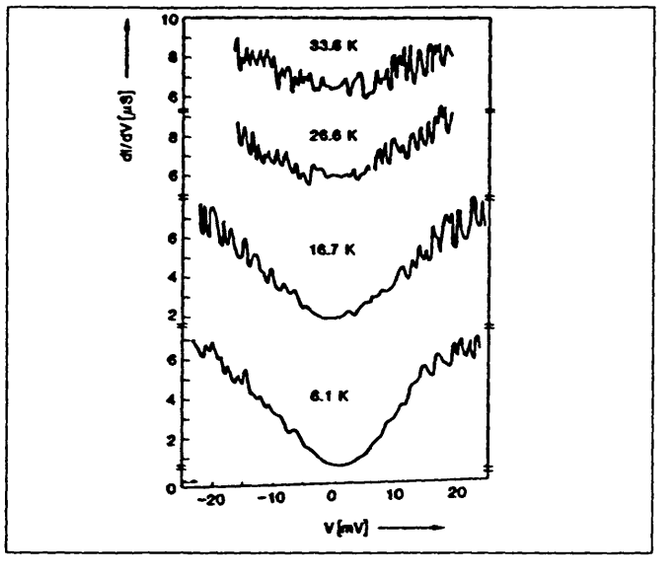

Fig.6.10 Conductance vs voltage (from ref [23])

6.7.4 Run 4

Junction J2 exhibits a slightly non-linear IV curve and its conductance vs voltage characteristic shows the 0 V peak and a fairly high sub-gap conductance. All the other junctions had well behaved non-linear IV curves and their CV curves had a dip at 0 V. J13 is the exception as it its conductance against voltage shown a peak at 0 V but did not exhibit the familiar monotonous increase with voltage. If the model discussed above [7] is used, the highest peak at 0 V is due to Δ_c and the two more smeared peaks enclosing it are due to Δ_{ab} . From the width of the peaks of figure 5.132 one can obtains Δ_c=5 meV, and Δ_{ab}=27 meV. The fact that the peak due to Δ_c is more pronounced than that due Δ_{ab} suggests that the structure is dominated by tunnelling in the c-direction [7] .

6.7.5 Run 5

During this run junction J11 gave striking non-linear IV curves which approach the ideal IV curve of a superconducting tunnel junction . The conductance vs voltage of figure 5.138

shows no sub- gap conduction and four peaks . The first two peaks enfolding the zero current region are separated by 12 mV and the second peaks are separated by 32 mV . This curve again can be interpreted in term of the anisotropic gap properties of YBCO . The two energy gaps resulting from this figure are as follow :

$$\Delta_c = 6 \text{ meV}$$
$$\Delta_{ab} = 16 \text{ meV}$$

In addition the simultaneous presentation of the IV curve of J11 at two different temperatures (figure 5.139) shows that when the temperature increased, the conductivity of the junction increases and the energy gap was reduced.

The IV curve of J2 converged with that of the device at room temperature at higher voltage (figure 5.140). A similar behaviour has been obtained using Scanning Tunnelling Microscope (STM) as a way to " get around the difficult technical problems involved in making conventional junctions on these materials " [18] ie High T_C superconductors . In this investigation La-Sr-Cu-O which has a T_C of 36 K was used and the result is shown in figure 6.11.

Junction J13 continued to exhibit the 0 V peak (figure 5.144) which was found to be due to Δ_c in the above discussion. At this fairly high temperature the peak was greatly reduced (in comparison with that of figure 5.132) and the peaks due to Δ_{ab} almost vanished .

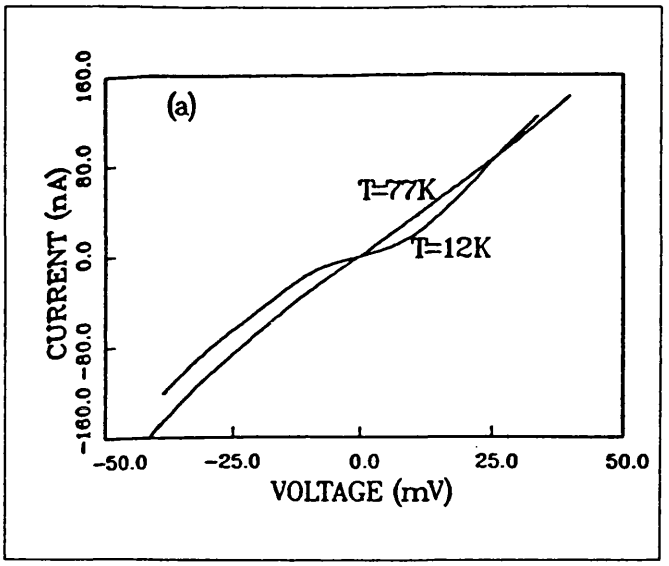

Fig.6.11 . IV curve of a junction built on La-Sr-Cu-O (T_C=36 K) at two different temperatures (from ref [18])

6.7.6 Run 6

During this run two junctions gave two types of non-linear IV curves .

A) Junction J11 gave IV curves with striking nonlinearities. In addition to the very sharp variation of current, there were smaller peak features in the low current regions (figures 5.152, 5.153 and 155) . This may be a striking direct observation of high T_C gap anisotropy using IV characteristics . The presence of peaks in both sides of the low current region was clearly shown in the conductance vs voltage of figure 5.154 . In low T_C superconductors similar small peaks resulting from gap anisotropy were observed in the IV curves of junctions and were found to be due to different orientation of crystallites if one of the superconducting film layer is thick [37] [38] . As discussed in chapter 4 and the present one, gap anisotropy is well established in high temperature superconductors. However the direct observation of gap anisotropy using IV

curves measurements has not been reported . Most of the published gap anisotropy data was obtained using conductance (or resistance) against voltage curves.

The features of figure 5.154 can be interpreted as an array of junctions where tunnelling in the (a, b) plane and c-direction are simultaneously present but with the major contribution coming from (a,b) tunnelling . Anisotropic properties due to both types of tunnelling were observed in junction built on a single type film as confirmed by XRD pattern [7].

As the separation between the large peaks was found to be 608 mV and that between the small peaks 190 mV, The gap voltage resulting from figure 5.154 can be obtained using:

$$2N(\Delta_{ab} + \Delta_c) = 608 \text{ meV}$$

$$2N(\Delta_{ab} - \Delta_c) = 190 \text{ meV}$$

These equations give :

$$N\Delta_{ab} = 199.5 \text{ meV}$$

$$N\Delta_c = 104.5 \text{ meV}$$

The possible values of N Δ_{ab} and Δ_c are indicated in table 6.3.

Table 6.3 Possible values of Δ_{ab} and Δ_c

N	Δ_{ab} (meV)	Δ_c (meV)
25	7.9	4.2
24	8.3	4.3
23	8.6	4.5
22	9.1	4.7
21	9.5	4.9
20	9.9	5.2
19	10.5	5.5
18	11.1	5.8
17	11.7	6.1
16	12.4	6.5

B) Junction J14 gave well behaved non linear IV curves characterised by the presence of a gap-like feature but at quiet high voltages. This gap structure is reflected by two peaks at +/- 232 mV in the conductance vs voltage curve of figure 5.160 . Once more, this is a fairly wide feature that can be explained only in term of array of junctions. As there is no anisotropic feature , the peak separation can be assumed to result from an array of N junctions where tunnelling in (a, b) dominates . If these junctions are assumed to be of the SIN type then one can write $N\Delta_{ab}$=232 meV. This yields different possible values of Δ_{ab} and Δ_c obtained for different values of N and these are indicated in table 6.4.

Table 6.4 Possible values of Δ_{ab} and Δ_c

N	8	9	10	12	13	14	15	16	17
Δ_{ab} (meV)	29.7	25.7	23.2	21.1	19.3	17.8	16.5	15.4	13.6
N	18	19	20	21	22	23	24	25	26
Δ_{ab} (meV)	12.8	12.2	11.6	11	10.5	10.1	9.6	9.3	8.9

The voltages involved in this run are quiet high which could be due to the formation of additional insulating layers between superconducting grains and thus resulting in the array of junctions. This may have occurred during the storage of the sample in laboratory environment for about two months before the measurements of the present run were carried out . In the previous runs the sample was kept continuously under vacuum .

6.8 Summary of gap parameters

In the above discussion gap parameters have been found to be in reasonable agreement with those reported in the literature . The different possible values of Δ_{ab} and Δ_c obtained in this chapter are summarised using statistical method and presented in figure 6.12 where N, the number of occurrences (or possible occurrences) of Δ_{ab} and Δ_c is presented as a function of different energy ranges.

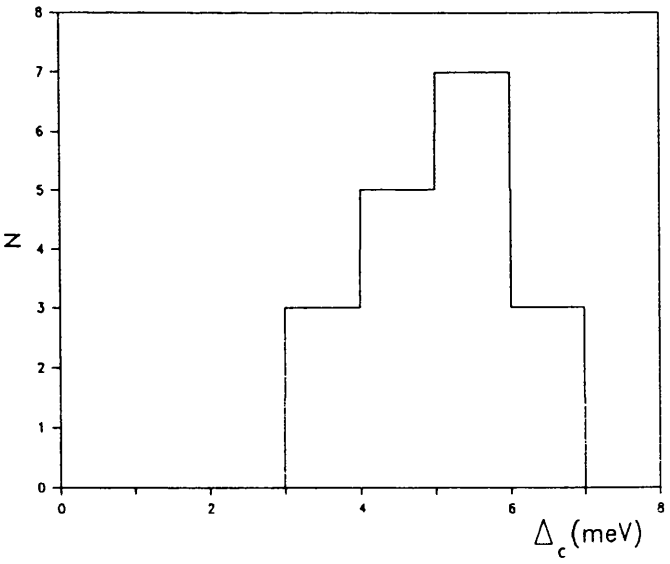

(a)

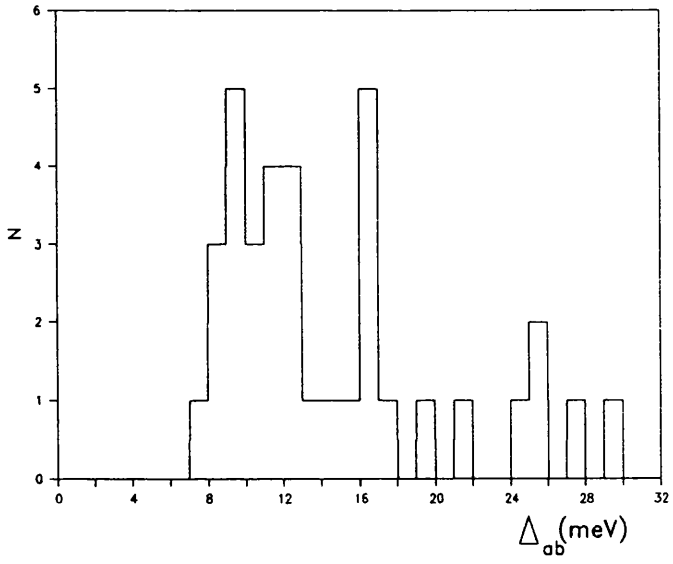

(b)

Fig 6.8 (a) Number of occurrences of Δ_c vs different energy ranges

(b) Number of occurrences of Δ_{ab} vs different energy ranges

6.9 General conclusion

The above discussion shows that the measurement results obtained in this project exhibited most of the feature reported in the literature including the most recent results. In many cases anisotropic properties of YBCO have been seen. These latter were only observed in unconventional tunnel junction (break junctions) or more recently in thin film planar junctions where sophisticated techniques were used.

Some of the results show striking non-linearities similar to ideal SIS and SIN junctions but at higher voltage gap values V_g (V_g =5 to 30 meV depending on the direction considered). This suggest that detection and mixing up to the terahertz range are possible using devices based on high temperatures superconductor materials . In fact it has been recently reported that ideal SIS behaviour was achieved using Nb/BKBO and Nb/NdCeCuO junctions and the author declared that there is no fundamental problem in forming tunnel junctions on high T_c superconducting materials [38].

However many features such as the 0 V dip or peak ,the increase of conductance with voltage and the sub-gap tunnelling are not yet properly understood. More work is also needed to definitely overcome problems that are inherent to high temperature superconductors such as the short coherence length (in c-direction of YBCO), the oxygen stoichiometry, and the effect of interfacing compound as well as that of the environment . Fortunately the enormous effort which is being spent in high temperature superconductors research is continuing and this will insure eliminating all the obstacles and bring high T_c applications at the industrial level .

6.10 Future work

Considering the intrinsic properties of high T_c materials many applications can be envisaged :

1) Detection and mixing using the following :
   - Granular properties of these materials
   - Single crystal (in the (a,b) direction
   - Thin film of uniform and shiny surface

2) Planar antennas, filters and transmission lines : these also require high quality thin films in the (a,b) orientation.

3) A combination between planar antennas and SIS junction using (a,b) thin film could lead to give interesting results

Chapter 6 references

1 I. Giaver and K. Megerel, " Study of superconductors by electrons tunnelling", Phys. Rev. 122, pp:1101-1111, 1961.

2 I. Giaver, " Energy gap in superconductors measured by electrons tunnelling", Phys. Rev. Lett. 5, pp:147-148,1960.

3 J. M. Rowell and L. Kopf, " Tunnelling measurements of phonon spectra and density of states in superconductors", Physical review 137, pp:A907-A915, 1965.

4 J. R. Kirtley, R. T. Collins, Z. Schlesinger, W. J. Gallagher, R. L. Sandstorm, T. R. Dinger, and D. A. Chance, " Tunnelling and infrared measurements of the energy gap in high-critical-temperature superconductors Y-Ba-Cu-O", Phys. Rev. B 35, pp:8846-8849, 1987.

5 T. Ekino and J. Akimitsu, " Superconducting tunnelling in YBCO", Jpn. J. Appl. Phys. 26, pp:L452-L453, 1987.

6 M. Reiffers, P. Samuely, M. Kupka, O. Hudak, P. Diko, K. csach, J. Miskuf, V. Kavecansky, N. M. Ponomarenko, "Point contact properties of YBaCuO and SmBaCuO", Physica C 153-155, p.1387-1388, 1988 .

7 I. Iguchi and Z. Wen, "tunnel gap structure and tunnelling model of the anisotropic YBaCuO/I/Pb junctions", Physica C 178, pp:1-10, 1991.

8 I. Iguchi, M. furyama, T. Kusumori, K. Shirai, S. Tomora, M. Nasu, and H. Ohtake, Jpn. J. Appl. Phys. 29, p.L614, 1990.

9 M. Furyama et Al " In situ fabrication of reproducible YBCO/Au tunnel junctions with artificial barrier", Jap. Jour. Appl. Phys., pp:L459-L462, 1990.

10 N. Hohn, R. Koltune, H. Schmidt, S. Blumenroder, H. Genearl, G. Guntherodt, D. Wohllebern, " Tunnelling and point-contact spectroscopy of high T_C superconductors M-$Ba_2Cu_3O_{7-x}$ (M= y, La, Eu)", Physica C 153-155, 1988.

11 M. Gurvitch M. Gurvitch, J. M. Valles, Jr. A. M. Cucolo, R. C. Dynes, J. P. Garno, L. F. Schneemeyer, and J. V. Wasczack, " Reproducible tunnelling data on chemically etched single crystal of YBa_2CuO_7", Phys. Rev. Lett. 63, p:1008-1011, 1989.

12 J. Kwo, T. A. Fulton, M. Hong, and P.L. Gammel, Appl. Phys. Lett. 56, p.788, 1990 .

13 J. Geerk, G. Linker, O. Meyer, Q. Li, R. L. Wang, and X. X. Xi, " The tunnelling gap of high T_c superconductors", Physica C-162-164, pp: 837-840, 1989.

14 A. Fournel, I. Oujia, I. Sorbier, Europhys. Lett. 6, p.653, 1988 .

15 P. J. Van Bantum, H. Van Kempen, L. E. C. Van Leemput, and P. A. A. Teunissen, " Single electron tunnelling observed with point-contact tunnelling junctions", Phys. Rev. Let. 60, pp:369-372, 1988.

16 J. H. James, B. Dwir, M. Affronte, A. Munzner, T. Naucler, B. J. Kellett, and D. Pavuna, " Window-type tunnel devices on $YBa_2Cu_3O_{7-x}$", Supercond. Sci. Technol. 4, pp:S136-S138, 1991.

17 J. Geerk, R. L. Wang, H. C. li, G. Linker, O. Meyer, F. Ratzel, R. Smithey, and H. Keschtkarb, " Electron tunnelling into 1-2-3 HTSC thin films", IEEE trans. Mag. 27, pp:3085-3089, 1991 .

18 S. Pan, K. W. Ng, and A. de Losanne, " Measurements of the superconducting gap of La-Sr-Cu-O with scanning -tunnelling microscope ", Phys. Rev. B 35, pp:7220-7223, 1987.

19 M. Sera , S. Shamoto, and M. Sato, " Electron tunnelling studies of high-T_c superconductors $YBa_2Cu_3O_{7-x}$", Solid State Comm. 65, pp:997-999, 1988 .

20 M. A. Ramos, and S. Vieira, "Tunneling specroscopy at 4.2 K and 56 K on $Bi_4Ca_3Sr_3Cu_4O_{16-\delta}$", Physica C 162-164, pp:1045-11046, 1989.

21 P. J. M. V. Bentum, H. F. C. Hoever, H. V. Kempen, L. E. C. V. De Leemput, M. J. M. F. De Nivell, L. W. M. Schreurs, R. T. M. Smokers, and P. A. A. Teunissen, " Determination of the energy gap in YBa2Cu3O7-x by tunnelling, far infrared reflexion and Andreev reflection", Physica C 153-155, pp:1718-1723, 1988 .

22 J. R. Kirtley, R. M. Feenstra, A. P. Frein, S. I. Raider, W. J. Gallgher, R. Sandstorm, T. Dinger, M. W. Shafer, R. Coch, R. Laibwitz, and B. Bumble, "Study of superonductors using a low-temperature high-field scanning tunnelling microscope", pp:259-262, 1988 .

23 M. A. M. Gijs, A. M. Gerrits, D. Scholten, and T. V. Rooy, "Proximity effect based $YBa_2Cu_3O_{7-x}$-Ag-Al-AlO_3-Pb Josephson junctions", Supercond. Sci. Technol. 4, p:S133-S135, 1991.

24 M. Ishikawa, Y. Nakasawa et Al, " Specific heat study on YBCO with double superconducting transition ", Physica C 153-155, pp:1089-1091, 1988.

25 M. G. Balmire, G. W. Morris, R. E. Somekh, and J. E. Evetts , "Fabrication and properties of superconducting device structure in YBa2Cu3O7-x thin films ", J. Phys. D: Appl. Phys. 20 pp: 1330-1335, 1987 .

26 J. D. Doss, " Engineer's guide to high temperature superconductor ", p.252, Published by J. Wiley & sons, 1989.

27 G. Bogner and H. E. Hoenig, " High Tc superconductors", Adv. Mater. 2, pp:473-477, 1990 .

28 J. D. Verhoeven, A. J. Bevolo, R. W. McCallum, E. D. Gibson, and M. A. Noack, " Auger study of grain boundary in large-grained $YBa_2Cu_3O_x$ ", Appl. Phys. Lett. 52, pp:745-747, 1988.

29 P. Chaudari, J. Manhart, D. Dimos, C. C. Tseui, J. Chi, M. Mopryssko, and M. Scheuermann, "Direct measurement of the superconductive properties of single grain boundary in $YBa_2Cu_3O_{7-\delta}$", Phys. Rev. Let. 60, pp:1653-1655, 1988.

30 D. Dimos, P. chaudari, J. Manhart, and F, K, LeGoues, "Orientation dependance of grain boundary critical current in $YBa_2Cu_3O_{7-\delta}$ bicrystal", Phys. Rev. Let. 61, p:219-222, 1988 .

31 J. D. Doss, " Engineer's guide to high temperature superconductor ", p.122, Published by J. Wiley & sons, 1989.

32 J. Chen, T. Yamashita, H. Sasahara, H. Suzuki, H. Corosawa, and Y. Hirotsu, " Possible three-Terminal device with angle grain boundary ", IEEE Trans. on Applied Superconductivty 2, pp:102-106, 1991.

33 R. Koltune, M. Hoffmann, P. C. Splittgerber-Hunnekes, C. Jarchow, G. Guntherodt, V. V. Moshkhalove, and L. I. Leonyuk, "Energy gaps and phonon structure in tunneling spectra of $Bi_2Sr_2Ca_1Cu_2O_{8+x}$, and $Bi_2Sr_2Ca_2Cu_3O_{10+y}$ superconductors", Z. Phys. B condensed matter 82, pp:53-59, 1991.

34 S. T. H. T. Jin, R. C. Sherwood, R. B. Van Dover, M. E. Davis, G. W. Kammlott, and R. A. Fastnacht, " Melt-textured growth of policrystalline $YBa_2Cu_3O_{(7-x)}$ with high transport Jc at 77 K", Phys. Rev. B 35, pp:7850-7853, 1988.

35 A. M. Cucolo and R. C. Dynes, J. M. Valles Jr, and L. F. Schneemeyer, "Planar tunnel junction on 90 K and 60 K YBCO single crystals superconducting and normal properties". et Al, Physica C 179, p.69, 1991 .

36 C. K. Campbell and D. G. Walmsley, Can. J. Phys. 45, p.159, 1967 .

37 M. L. A. Mac Vicar and R. M. Rose, J. Appl. Phys. 39, p. 1721, 1968 .

38 J. F. Zasdzinski and N. Tralshawala, "Tunnelling spectroscopy measurement on low leakage junctions of $Nd_{1.85}Ce_{0.15}CuO_{4-y}$ and $Ba_{1-x}K_xBiO_3$", IEEE Trans. Magn. MAG-27, pp:833-836, 1991.

Chapter 7: ACKNOWLEDGMENTS

I am deeply indebted to my supervisor Dr. Nigel J. Cronin who has been a continual source of guidance, support and encouragement throughout the duration of the project, the preparation of the thesis, and for securing much appreciated financial support from the School of Physics for the last few months .

Special Thanks must be given to Mr. Robert Draper for his invaluable help in the practical side of several parts of the project. I wish also to thank him for the photograph appearing in this thesis .

I would like to thank my colleagues Charles Summut for use of his derivative calculation programme, and Derradji Boumrah for helping in the final layout of the thesis.

I am grateful to the algerian ministry of higher education for the scholarship .

Appendix A1

Elements of Tunneling

The problem of one dimentinal abrupt potential barrier shown in figure 2.2 is solved using the Shrodinger equation :

$$-\frac{\hbar^2}{2m}\frac{d^2\psi}{d^2x}+V\psi=E\psi \qquad (1)$$

The general solution has the form :

$$\psi = A_1 e^{ikx} + B_1 e^{-ikx} \qquad (2)$$

where is given by the followimg expression :

$$k^2=\frac{2m}{\hbar^2}(E-V) \qquad (3)$$

1) In region 1 $E > V_1 = 0$, the wave functions are plane waves, and thus equation (2) becomes:

$$\psi = A_1 e^{ik_1x} + B_1 e^{-ik_1x} \qquad (4)$$

with $k_1^2=\frac{2m}{\hbar^2}(E-V_1)$

2) In region 2 $E < V_b$ and by writing $k=i\kappa_2$ one obtains:

$$\kappa_2^2=\frac{2m}{\hbar^2}(V_b-E) \qquad (5)$$

Then equation (2) becomes :

$$\psi = A_2 e^{-\kappa_2 x} + B_2 e^{\kappa_2 x} \qquad (6)$$

The wave function are now exponnentially growing and decaying.

By taking the wave functions and their derivatives at x_1 and x_2 a set of two equations linear in A_1, B_1, A_2 and B_2 are obtained . These can be arranged in the form :

$$\begin{vmatrix} A_1 \\ B_1 \end{vmatrix} = [R_1] \cdot \begin{vmatrix} A_2 \\ B_2 \end{vmatrix} \tag{7}$$

where $[R_1]$ is the following matrix :

$$[R_1] = \frac{1}{2k_1} \begin{vmatrix} (k_1 + i\kappa_2) & e^{-i(k_1 - i\kappa_2)x_1} & (k_1 - i\kappa_2) & e^{-i(k_1 + i\kappa_2)x_1} \\ (k_1 - i\kappa_2) & e^{i(k_1 + i\kappa_2)x_1} & (k_1 + i\kappa_2) & e^{i(k_1 - i\kappa_2)x_1} \end{vmatrix} \tag{8}$$

3) In region 3, $E > V_3 = 0$, and the solution is similar to equation (2) wave in this region :

$$\psi = A_3 e^{ik_3 x} + B_3 e^{-ik_3 x} \tag{9}$$

with $k_3^2 = \frac{2m}{\hbar^2}(E - V_3)$

As there is no reflected wave in region 3, $B3=0$.
A similar relation to (6) can be written at the boundary between region 2 and region 3.

$$\begin{vmatrix} A_2 \\ B_2 \end{vmatrix} = [R_2] \begin{vmatrix} A_3 \\ B_3 \end{vmatrix} \tag{10}$$

By substitution of (8) in (6) one obtains :

$$\begin{vmatrix} A_1 \\ B_1 \end{vmatrix} = [R_1][R_2] \begin{vmatrix} A_3 \\ B_3 \end{vmatrix} \tag{11}$$

Using this equation and $B3=0$, one can write :

$$A_1 = \{[R_1][R_2]\}_{11} A_3 \tag{12}$$

If a the following approximation is assumed $e^{-\kappa_2 w} \ll e^{\kappa_2 w}$ (with $w = x_2 - x_1$) equation (12) gives :

$$A_3 = \frac{4k_1\kappa_2\phi e^{-\kappa_2 d}}{(k_1^2+\kappa_2^2)(k_3^2+\kappa_2^2)} A_1 \qquad (13)$$

where d is the barrier thickness and ϕ is a phase factor given by :

$$\phi = ie^{i\beta}e^{i(k_1x_1-k_3x_2)} \qquad (14)$$

where $\beta = \tan^{-1}(\kappa_2/k_1)+\tan^{-1}(\kappa_2/k_3)$ (15)

The expressions of current density J_1 and J_3 are relatrd to A_1 and A_3 by the the following equations :

$$J_1 = -\frac{\hbar k_1 e}{m}|A_1|^2 \qquad (16)$$

$$J_3 = -\frac{\hbar k_1 e}{m}|A_3|^2 \qquad (16)$$

From equations (15) and (16) one obtains:

$$\frac{J_3}{J_1} = \frac{16k_1k_3\kappa_2^2}{(k_1+\kappa_2^2)(k_3+\kappa_2^2)} e^{-2\kappa_2 w} \qquad (17)$$

This equation shows that the barrier transmission is symetric in the indices 1 and 3 . This implies that the same relation holds for tunneling through the barrier in either direction. It shows also that the tunneling current is exponnentially dependant on the product of the barrier thickness d and $(V_b - E)^{1/2}$

APPENDIX A2

A2.1 Anomalous behaviour of bars SHS1B and S1C

Two bars SHS1B and S1B were cut from pellets described in section 5.4 . The resistance against temperature of these two samples shown anomalous dip at fairly high temperatures without transition to the superconducting state at liquid nitrogen . The experimental set up and the results of these two samples will be described in the following sections.

A2.2 Sample SHS1B

An YBCO bar, referred to SHS1B, of dimension 1x1.5x11 was cut from one of the pellets of S1B and fixed to rectangular piece of PCB board . Very thin gold wires were attached to the bar using silver paint and soldered to the cooper strips as indicated in figure A2.1.

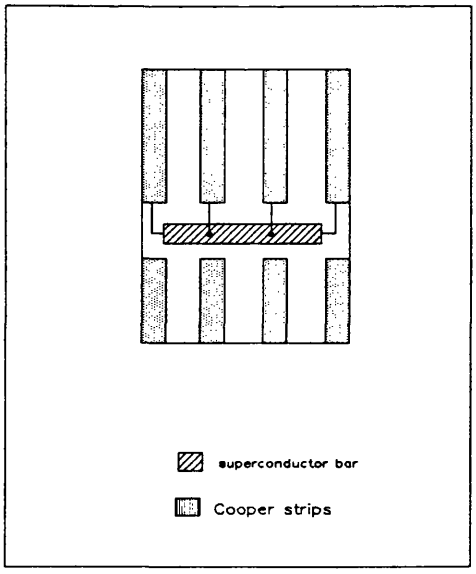

Fig.A2.1 Layout of sample SHS1B

A2.2.1 Experimental set up of SHS1B

The sample on its pcb substrate was fixed to a sample holder that can be incorporated in liquid N2 dewar. The sample holder was provided with a thermocouple for temperature reading and connected to a computer controlled set up as shown in figure A2.2.

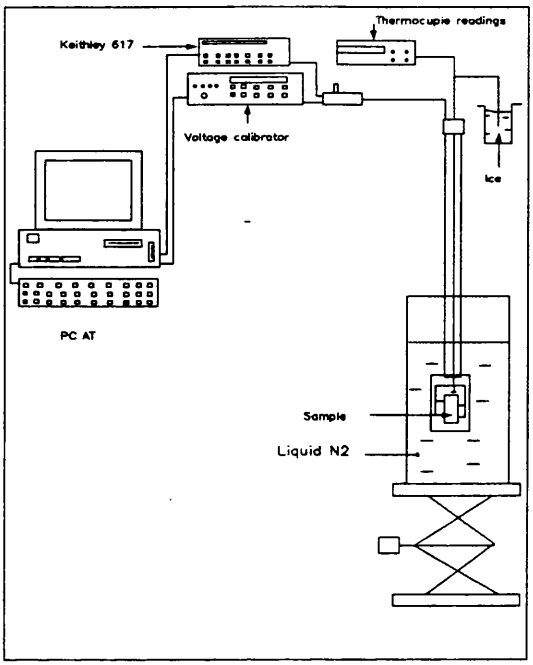

Fig.A2.2 Experimental set up of SHS1B

A2.2.2 Measurement results of SHS1B.

Figure A2.3 shows R vs T during cooling down of the sample. This shows a sharp onset of decrease of the resistance starting at 268 K followed by two plateaux at 260 and 230 K, and an anomalous dip between 190 and 210 K. After the dip the resistance started to rise and reached a maximum at 150 K and started to fluctuate without showing the superconducting transition.

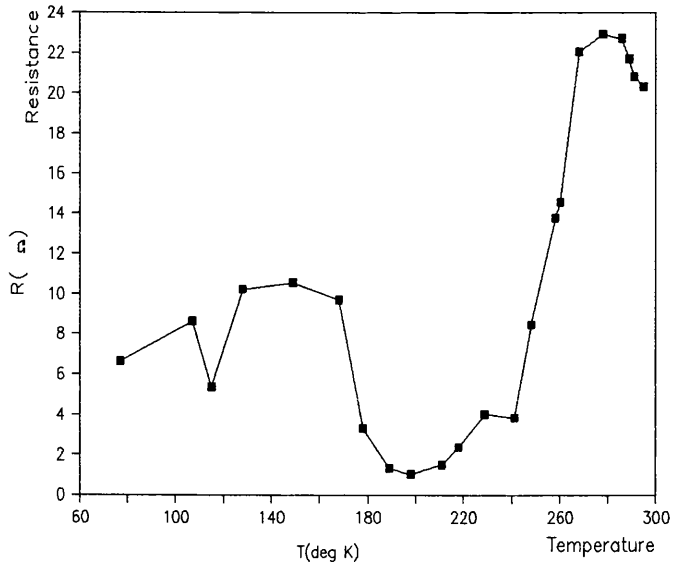

Fig.A2.3 Measurement of R vs T during cooling down, I=1mA

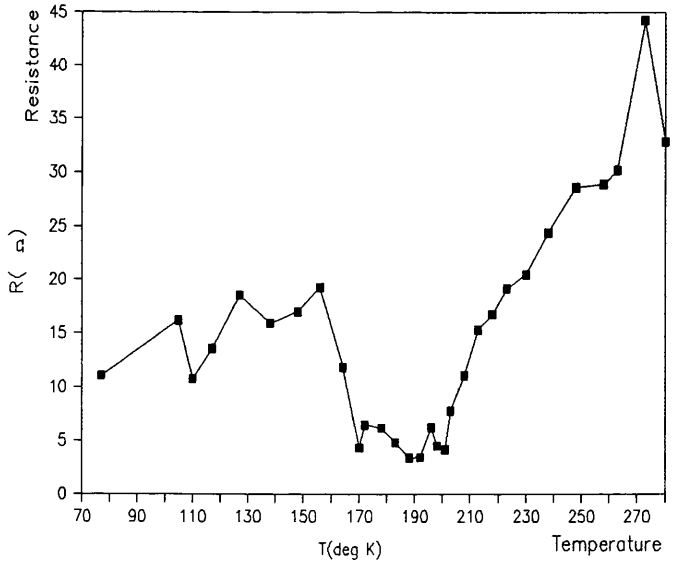

Fig.A2.4 Measurement of R vs T during warming up, I=1 mA

Figure A2.4 shows R vs T during the warming up of the sample . An anomalous low resistance behaviour can be seen between 164 K and 200 K.

A2.3 Sample 4 referred to as S1C

A bar (referred to as S1C) of dimension 1x2x5 mm^3 was cut from this pellet and fixed on a four pin holder. The electrical contacts between the pins and the sample were made using thin Au wire (37 microns) which was soldered to the four pins and fixed to the bar using silver paint . The layout of the bar on its sample holder is shown in figure A2.5.

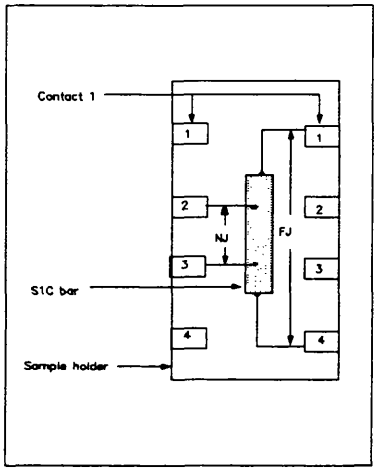

Fig.A2.5 Layout of S1C sample holder

These four dots were used for two purposes. Firstly the measurement of R vs T using the four points methods. Secondly the measurement of IV curves between the far dots referred to as FJ and the near dots referred to as NJ in as shown in the previous figure

A2.3.1 Experimental set-up .

The four pin holder was fixed to a long stick sample holder allowing for the sample to be incorporated into liquid N_2 dewar. This sample holder was also provided with a thermocouple for the reading of the temperatures. The measurement were carried out using a computer controlled set up similar to that of sample SHS1B which was represented in figure A2.2.

A2.3.2 Measurement results of S1C

Prior to cooling down the sample, IV curves measurements were carried at room temperature using the near dots (NJ), and the far dots (FJ) . The results obtained from both types of junctions are presented in figure A2.6 and figure A2.7 respectively .

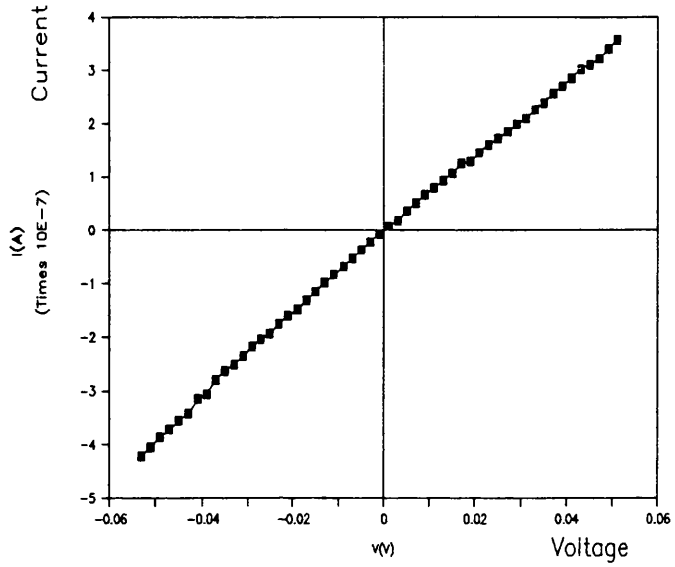

Fig.A2.6 IV curve of NJ at room temperature

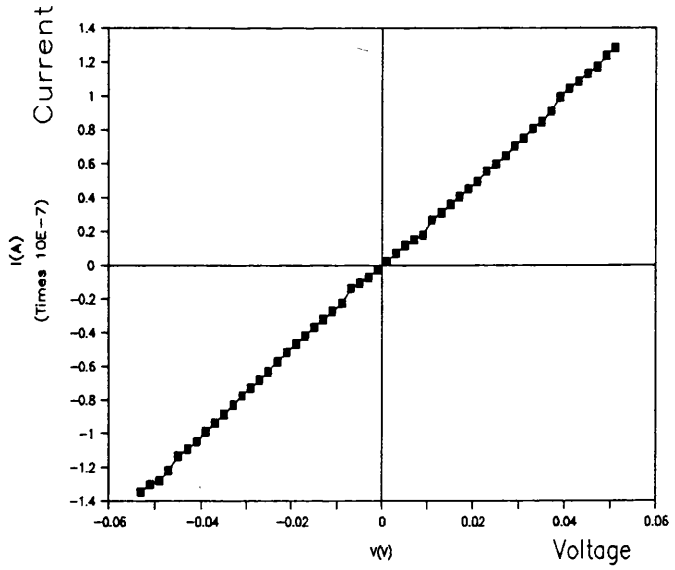

Fig.A2.7IV curve of FJ at room temperature

Although the resistance of the bar is about 2Ω , the IV curves show that the resistance of the junctions are very high : 142 KΩ for the near dots and 2.7 MΩ for the far dots. These high resistance values suggest the presence of insulating layer resulting from the interaction of the sample with both the environment and silver paint used to make the contacts .

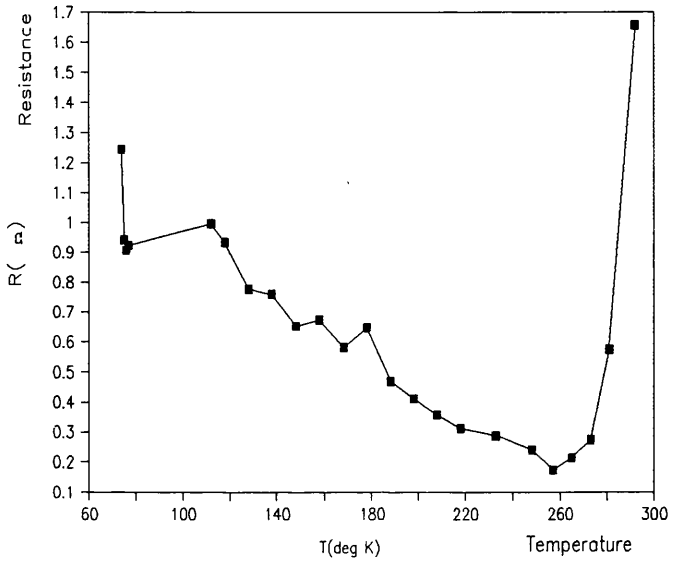

Fig.A2.8 Measurement of R vs T during the cooling down of the sample

Figure A2.8 shows R vs T during the cooling down of the sample . Once again the anomalous behaviour observed with the previous sample is repeated with this one. The minimum is located at 257 K and no transition to the superconducting state occurs when the temperature decreases to 77 K. This can be due to either an intrinsic phase of the sample or to a possible effect of liquid nitrogen on the sample .

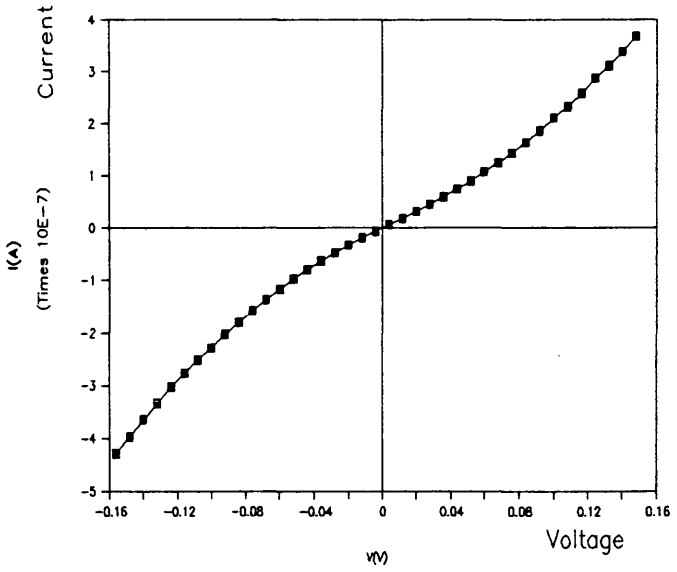

Fig.A2.9 IV curve of NJ at T=77 K

Figure A2.9 shows a slightly non linear IV curve of NJ at 77 K .

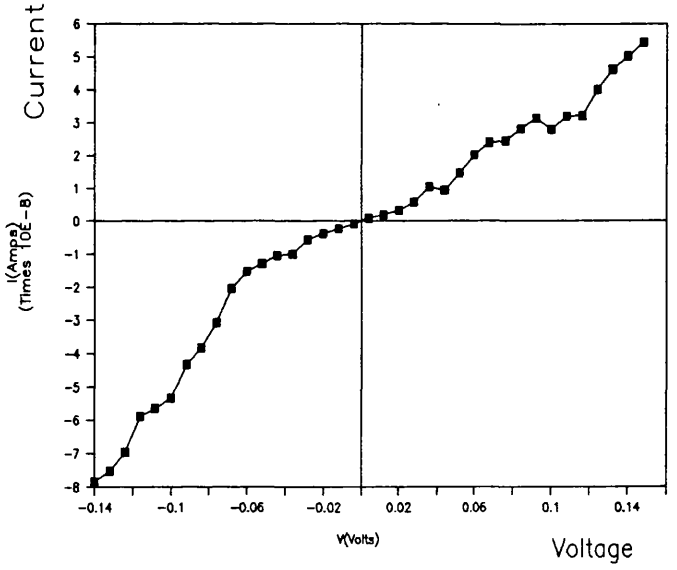

Fig.A2.10 IV curve of FJ at T=77 K

Figure A2.10 shows the IV curve of far FJ at 77 K which exhibits non-linear behaviour.

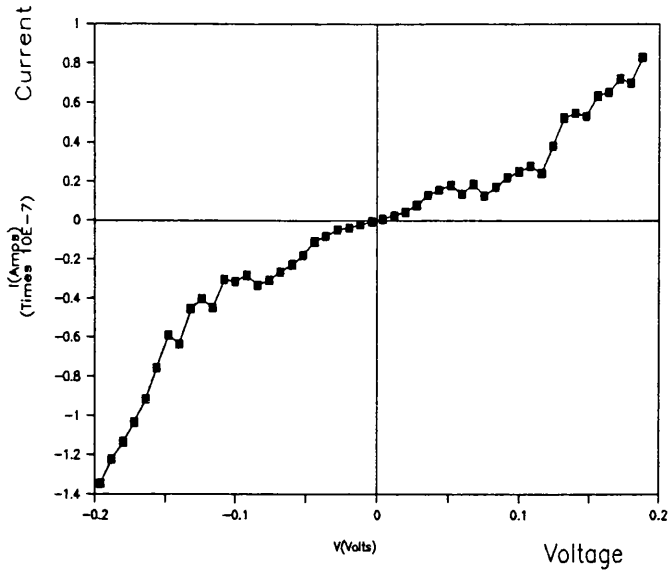

Fig.A2.11 IV curve of FJ ,T=77 K

Figure A2.11 shows the IV curve of far FJ at 77 K.

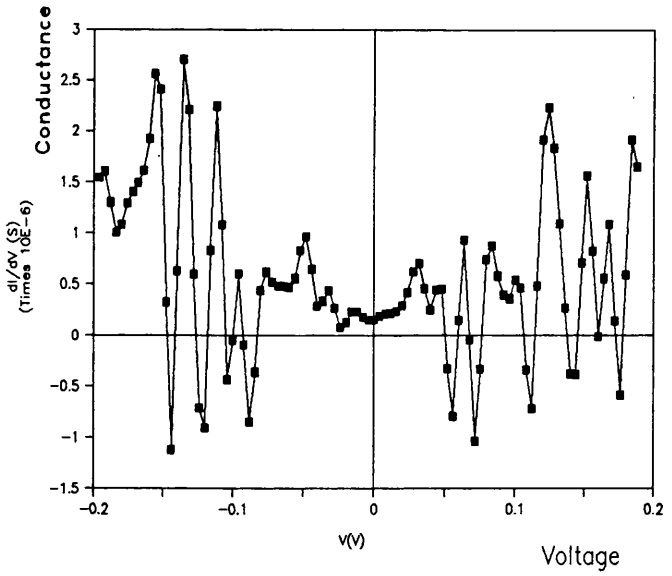

Fig.A2.12 Conductance vs Voltage of FJ, T=77 K

figure A2.12 is the conductance vs voltage corresponding to the IV curve of FJ. This is slightly asymmetric and exhibits a dip at 0 V enclosed by two peaks . The first two peaks are 79 mV apart.

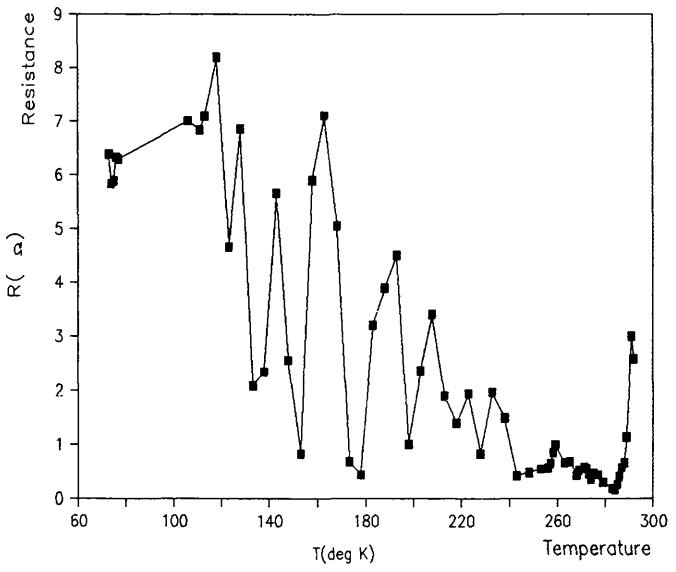

Fig.A2.13 R vs T during warming up of the sample

The sample holder was raised slowly to get the sample out of liquid N_2 in order to raise the sample temperature. The result obtained is shown in figure A2.13 . Despite the irregularities at low temperature the curve became more stable and repeated the low values of R but over a wider range of temperatures extending from 245 to about 285 K with the lowest value at 282 K .

After warming up to room temperature the sample was cooled down again to liquid N_2 and measurements IV curves of NJ were carried out in the region where the resistance exhibited a minimum (T= 257 K). The results gave striking non-linearities as indicated in the following graphs.

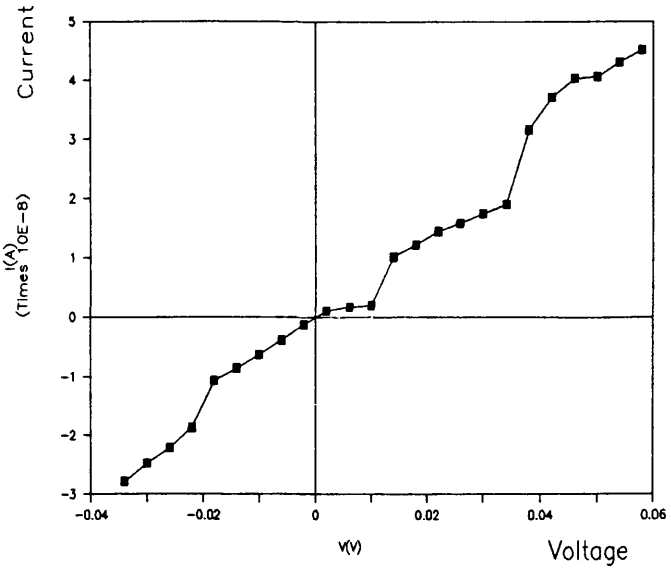

Fig.A2.14 IV curve of NJ at 257 K

Figure A.14 shows the IV curve of NJ exhibiting fairly strong non-linear features.

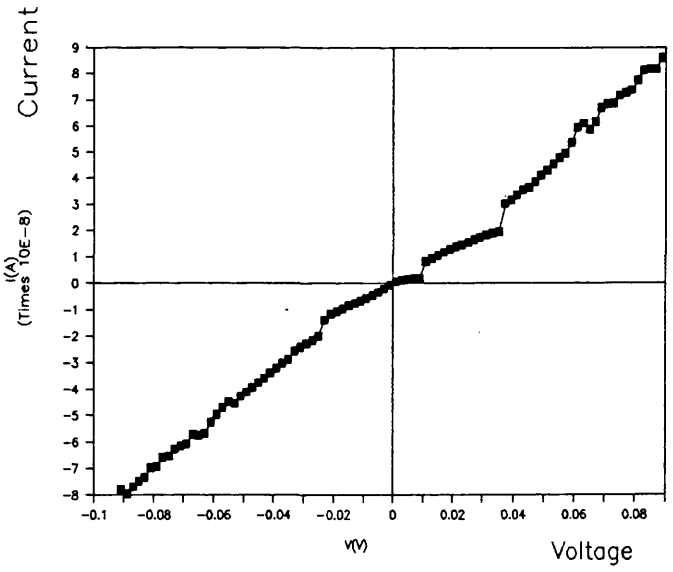

Fig.A2.15 IV curve of NJ at 257 K

Figure A.15 shows the IV curve of NJ over a wider voltage range . Many pronounced non-linear features can be seen. Two Sharp increases of the current can be seen

at +11 and +34 mV. On the left side a sharp decrease of the current occurs at -20 mV. More features including an NDR-like behaviour can also be seen at +-60 mV.

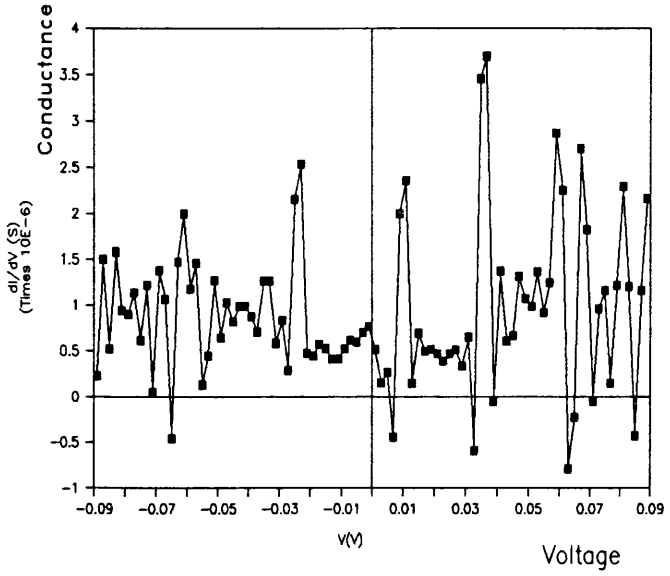

Fig.A2.16 Conductance of NJ at 257 K

Figure A2.16 is the conductance vs voltage obtained from the previous IV curve of NJ (figure A2.15). This is slightly asymmetric exhibiting a peak near 0 V whose width is 10 mV. Two stronger peaks enclose the 0 V peak and are distant by 38 mV. If the model of figure 6.2 is used the 0 V peak width coincide with $2\Delta_c$=10 meV and the two other peaks enclosing it are due to Δ_{ab} ie $2\Delta_{ab}$=36 mV. These values are similar to those reported in [7] in the previous discussion.

COMPUTER PROGRAM

```
10 REM PROGRAM TO OUTPUT ANY VOLTAGE IN VOLTS IN R3
20 REM FROM 9848 VOLTAGE CALIBRATOR AND GET CURRENT FROM
K617 ELECTROM.
30 'FILE(S)
40 REM ** K17VCW3.BAS DERIVED FROM K17VCW1.BAS, MODIFIED
CONV.SUB +R2,R3,R4
50 DIM VSAR(410)
60 DIM VG(401)
70 DIM VFAR(410)
80 DIM V(410)
90 DIM IC(410),IRES(410),ICAV(410),INC(410)
100 DIM R(410)
110 DIM VVP(410)
120 DIM IVP(410)
130 DIM RVP(410)
140 DIM VX(410)
150 DIM IY(410)
160 DIM RY(410)
170 DIM VS$(410)
180 DIM A$(410)
190 DIM ICR(20)
200 REM OPEN FILE$ FOR APPEND AS #1
210 REM *** INITIALISE IEEE BUS ***************************
220 GOSUB 4230
230 REM *** OUTPUT ROUTINE ********************************
240 REM
250 REM
260 LMAX=3
270 CU$=" AMPS "
280 VU$=" VOLTS "
290 DTAVG$="0.005 mV"
300 REM
310 RFACT1=1
320 RUNIT$="Ohm"
330 MAT1$="  Sample SDO:Silicon dioxide deposited "
340 MAT2$="  on High Tc at 3 different thicknesses "
350 MAT3$="  in E.Eng. School "
360 MAT4$="  Run 5. FILE KIND :JxPRTy.SD5  "
370 MAT5$="  Measurement Temp.:Room Temperatur"
380 RS=0:RS$="0 OHMS"
390 RSUM=0
400 REM
410 REM *** ADJUS.VARIABLES ******
420 LICF=5:REM THE NUMBER OF AVERAGING OF READING OF CUR.
430 JNC$="j13PRT"
440 FEXT$=".TRY"
450 REM
460 INPUT  "INPUT NUM";NUM
470 REM INPUT "input AMU";AMU$
480 AMU$="K":REM USING KEITHLEY.
490 NUM=NUM+1:REM ***  START. NUMB. ****
500 RCH=3
```

```
510 IF RCH=2 GOTO 540
520 IF RCH=3 GOTO 640
530 IF RCH=4 GOTO 760
540 RNGE$="R2":REM RNGE=R2=100 mV"
550 VMXR2=15:VSTA=VMXR2
560 VPR2=12
570 STPR2=2:STPR2$="0.004 VOLTS"
580 VPSTP2=5*STPR2
590 STP=STPR2
600 'VSTA=VMXR2+STP/2
610 VPF=VPR2-VPSTP2
620 HHF=INT(((VMXR2-VPF)/VPSTP2))
630 GOTO 860
640 REM ******* RNG=R3 *********
650 RNGE$="R3":REM RNGE=R3=1V"
660 VMXR3=.006
670 VPR3=4.000001E-03
680 STPR3=.002
690 'VSTA=VMXR3
700 VPSTP3=5*STPR3
710 STP=STPR3 :STP$=STR$(STP)
720 VSTA=VMXR3
730 VPF=VPR3-VPSTP3
740 HHF=INT(((VMXR3-VPF)/VPSTP3))
750 GOTO 860
760 REM ***** RNGE=4 **********
770 RNGE$="R4":REM RNGE=R4=10V"
780 VMXR4=3:VSTA=VMXR4:REM OUT IN VOLTS
790 VPR4=2
800 STPR4=.05:STPR4$="0.020 VOLTS"
810 VPSTP4=5*STPR4
820 STP=STPR4
830 'VSTA=VMXR4+STP/2
840 VPF=VPR4-VPSTP4
850 HHF=INT(((VMXR4-VPF)/VPSTP4))
860 REM HHF=
870 HMX=HHF+1
880 FRD=0
890 FDR$=JNC$+MID$(STR$(NDR),2,LEN(STR$(NDR))-1)+".DRW"
900 FF$="KDF.DRW"
910 GOSUB 2250
920 REM ************** START OF #1 ************
930 OPEN FDR$ FOR APPEND AS #1
940 PRINT #1,HHF
950 FOR HH=1 TO HHF
960 FRD=FRD+1
970 JNB$=STR$(NUM)
980 JN=LEN(JNB$):JB=JN-1
990 FL$=JNC$+MID$(JNB$,2,JB)+FEXT$
1000 REM ********   INIT.VARIABLES******************
1010 REM IF RCH=4  THEN GOTO 940
1020 IF RCH=2 GOTO 1070
1030 IF RCH=3 GOTO 1090
1040 REM RCH=4
```

```
1050 VPF=VPF+VPSTP4
1060 GOTO 1100
1070 VPF=VPF+VPSTP2
1080 GOTO 1100
1090 VPF=VPF+VPSTP3
1100 REM
1110 KH=INT(VPF/STP)+1
1120 VIN=-VSTA:VIN$=STR$(VIN)
1130 KMX=2*KH+1
1140 KMXD=KMX+1:REM THIS IS NUM.DATA AS K STARTS FROM 0
1150 PRINT #1,FL$,KMX
1160 IF HH<HHF GOTO 1200
1170 PRINT #1,"  F.DRAW NAME >"FDR$,"   F.NUMB "HHF," DATE
= "DAT$
1180 REM
1190 IVSZ=0
1200 GOSUB 2320:REM  ***** SCREEN OUTPUT  ******
1210 REM *** START OF #2 ***"
1220 OPEN FL$ FOR APPEND AS #2
1230 FOR K=0 TO KMX
1240 JCS=JCS+1
1250 IF JCS=17  THEN GOSUB 2320
1260 FOR LM=1 TO 10:NEXT LM
1270 NDT=0
1280 IZ=1
1290 GOSUB 2410:REM output zero voltage
1300 GOSUB 3120:REM **** CUR. READING FROM KEITHLY ******
1310 IRES(K)=ICAV(K)
1320 IF IVSZ=0 THEN GOTO 1430
1330 IF IVSZ=1 THEN GOTO 1370
1340 IF IVSZ=2 THEN GOTO 1400
1350 'VS=VIN+K*STP
1360 'GOTO 1290
1370 VS=STP/2
1380 IVSZ=IVSZ+1
1390 GOTO 1440
1400 VS=VIN+(K-1)*STP
1410 GOTO 1440
1420 REM
1430 VS=VIN+K*STP
1440 IZ=IZ+1
1450 REM
1460 IF VS=0 THEN GOTO 1480
1470 GOTO 1500
1480 VS=-STP/2:REM OVOID SENDING ZERO VOLTAGE THAT IS COMING
FROM INCREMENT.
1490 IVSZ=IVSZ+1
1500 VSAR(K)=VS:REM DESIRED VOLTAGE
1510 VG(K)=VSAR(K):REM VSAR(K)=VOLT,VG(K)=VLTS
1520 IF RNGE$="R4" THEN GOTO 1610
1530 IF RNGE$="R3" GOTO 1550
1540 IF RNGE$="R2" GOTO 1580
1550 VFACT=1
1560 IF ABS(VS)>1.3 THEN PRINT"MAXIMUM VOLTAGE VS=1 V FOR
```

```
R3":ND=ND+1:GOTO 2410
1570 GOTO 1630
1580 VFACT=.001
1590 IF ABS(VS)>110 THEN PRINT"MAX. VOLTAGE VS=110 mV FOR
R2":ND=ND+1:GOTO 2410
1600 GOTO 1630
1610 VFACT=1
1620 IF ABS(VS)>13 THEN PRINT "MAX. VOLTAGE VS=13 V FOR
R4":ND=ND+1:GOTO 2410
1630 REM
1640 'IF VS=0 THEN GOTO 1460
1650 'GOTO 1510
1660 'VS=-STP/2:REM OVOID SENDING ZERO VOLTAGE THAT IS COMING
FROM INCREMENT.
1670 'IVSZ=IVSZ+1
1680 'PRINT " VS ="VSAR(K)," VS=0.VFAR(K)= "VFAR(K)
1690 REM
1700 'GOTO 1630
1710 GOSUB 2550:REM CONVERT NUMERIC VS TO READABLE STRING
VARIABLE VS$
1720 VS$(K)=VS$:REM PRINT " VS NOT=0. VS$1   ="VS$(K)
1730 REM GOSUB 1620:REM CHECK STATUS
1740 REM
1750 GOSUB 4370:REM SET RANGE
1760 SEND$=VS$+T$
1770 CALL SEND(ADDR%,SEND$,STATUS%)
1780 REM
1790  VFAR(K)=VAL(VS$):REM  GENER.  VOLTAGE  AFTER  DOUBLE
CONVERSION
1800 REM input "input Am.used"
1810 IF AMU$="K" THEN GOTO 1830
1820 IF AMU$="T" THEN GOTO 1850
1830 GOSUB 3120:REM **** CUR. READING FROM KEITHLY ******
1840 GOTO 1860
1850 GOSUB 4570:REM **** CUR. READING FROM THIRLBY ******
1860 INC(K)=ICAV(K):REM INC > NON CORRECTED CURR.
1870 REM
1880 IC(K)=INC(K)-IRES(K):REM  IRES(K) SEEM TO NEGATIF FOR
ALL VOLTAGES.
1890 REM
1900 V(K)=VSAR(K)*VFACT-RS*IC(K):REM V(K) IN VOLTS
1910 REM
1920 REM PRINT "VSA="VSAR(K),"VFAR(K)= "VFAR(K),"VG= "VG(K)
1930 REM PRINT "V(K)=  "V(K),"IC(K) ="IC(K)
1940 'VS=0:REM ISF=0
1950 IF ABS(IC(K))<(1E-15) THEN GOTO 2000
1960 R(K)=RFACT1*ABS(V(K)/IC(K))
1970 PRINT #2,V(K),IC(K),INC(K),IRES(K),VFAR(K),R(K)
1980 REM  PRINT "   R(K)="R(K),RUNIT$
1990 GOTO 2010
2000 REM R(K)=R(K-1)
2010 PRINT K,V(K),IC(K),R(K),IRES(K)
2020 RSUM=RSUM+R(K)
2030 IF IZ=1 GOTO 1350
```

```
2040 VFIN=V(K):REM TO BE PRINTED IN FILE #2
2050 NEXT K:REM *******  END FILE  ****************
2060 RAV=RSUM/KMXD
2070 GOSUB 2410:REM SET GENER. OUTPUT=0 AT END FILE
2080 REM
2090 IF AMU$="T" THEN GOTO 2120
2100 GOSUB 3400:REM *****ZERO CHECK OF THE KEITHLY ******
2110 REM
2120 GOSUB 4420:REM CLOSE FILE
2130 CLS
2140 GOSUB 3590:REM FILE DISPLAY
2150 FOR IDIS=1 TO 100:NEXT IDIS
2160 IF HH=HHF THEN GOTO 2180
2170 CLS
2180 NEXT HH
2190 CLOSE #1:REM CLOSE #1
2200 IF HH=HMX THEN GOTO 2240
2210 'GOSUB 4210:REM CLOSE FILE
2220 CLOSE:REM CLOSE #1
2230 GOSUB 3400:REM *****ZERO CHECK ******
2240 GOTO 2300
2250 REM *** OPEN FFFF ******
2260 OPEN "O",#3, FF$
2270 PRINT #3,FDR$
2280 CLOSE #3
2290 RETURN
2300 REM SYSTEM
2310 END
2320 REM ****  SCREEN TITLE SUB **********
2330 CLS
2340 PRINT "**********************************************
**********************"
2350  PRINT  "FDR="FDR$,"TFN="HHF,"FNAM>"FL$,"F.OR>"FRD,"
NDAT="KMXD
2360 PRINT "**********************************************
**********************"
2370 PRINT "  K  ","    V(V)  ","    I(A)","      R  (O)"
,"INC(A)","IRES(A)"
2380 PRINT "***"," ***** "," ***** "," ***** ","  ****","
*****"
2390 JCS=0
2400 RETURN
2410 REM ****SET OUTPUT VOLTAGE TO ZERO*****
2420 'IF ABS(VSAR(K))>0 THEN GOTO 2190
2430 'GOSUB 4070:REM SET RANGE
2440 SEND$="D"+T$:REM PRINT "SEND$=D=0"SEND$
2450 CALL SEND(ADDR%,SEND$,STATUS%)
2460 'IF ND=0 GOTO 2280
2470 'GOTO 2010
2480 RETURN
2490 REM CHECK STATUS% FOR GOOD TRANSFER
2500 REM ******************************
2510 IF STATUS%=0 THEN RETURN
2520 PRINT "IEEE TIME-OUT, NO DATA TRANSFER"
```

```
2530 ND=ND+1
2540 GOTO 2410
2550 REM SUBROUTINE TO CONVERT NUMERIC TO STRING CHARACTER
2560 REM ************************************************
2570 A$=STR$(VS)
2580 A$(K)=A$
2590 IE=INSTR(A$,"E")
2600 LT=LEN(A$)
2610 IF IE=0 THEN VS$=A$:GOTO 2890
2620 ID=INSTR(A$,"."):REM LD=ID-2
2630 REM PRINT "LT ="LT," ID ="ID," IE ="IE
2640 IDR=ID+1:IDL=ID-1
2650 LDF=ID-2:REM LEFT DOT FIELD
2660 RDF1=IE-IDR:REM RIGHT DOT FIELD
2670 RDF=RDF1-3:REM RIGHT DOT FIELD USED
2680 REM PRINT "LDF="LDF," RDF1=" RDF1," RDF="RDF
2690 REF=LT-IE
2700 NIN$="9"
2710 NINA$=MID$(A$,IDR,1)
2720 IF NIN$=NINA$ THEN RDF=RDF1: REM GO TO 2107
2730 REM
2740 REM PRINT "A$="A$
2750 NGS$="-"
2760 NSP=INSTR(A$,NGS$)
2770 PS$="+"
2780 PSP=INSTR(A$,PS$)
2790 REM PRINT "NSP="NSP,"PS+P="PSP," REF="REF
2800 B$=MID$(A$,2,LDF)+MID$(A$,IDR,RDF):REM  GOTO 1780
2810 VREF=ABS(VAL(RIGHT$(A$,REF)))
2820 IF NSP=1 THEN VS$=NGS$+"." :GOTO 2840
2830 VS$=PS$+"."
2840 NZ=VREF-LDF:REM PRINT "VREF ="VREF," NUM ZER.="NZ
2850 FOR J=1 TO NZ
2860 VS$=VS$+"0"
2870 NEXT J
2880 VS$=VS$+B$
2890 VS$(K)=VS$
2900 REM IF IE=0 THEN GOTO 2440
2910 REM PRINT "  A$(K) ="A$(K),"  VS$(K) ="VS$(K)
2920 RETURN
2930 REM
2940 REM
2950 REM
2960 REM ** DRAW X Y AXES**
2970 SCREEN 2,,0,0
2980 PSET (0,100)
2990 DRAW "R640"
3000 PSET(320,0)
3010 DRAW "D200"
3020 'DRAW "R640"
3030 REM PSET (10,170)
3040 RETURN
3050 REM **DRAW GRADUTIONS**
3060 FOR I=1 TO 64 STEP 3
```

```
3070 COR=I*10
3080 PSET(COR,100):REM IF I=30 THEN DRAW"U170"
3090 DRAW"D5"
3100 NEXT I
3110 RETURN
3120 REM SUB FOR CUR. READING FROM K617
3130 REM ******************************
3140 TRANSMIT=3:RECEIVE=6:REM IF K>0 THEN GOTO 896
3150 REM
3160 CMD$="MTA UNL 12":CALL TRANSMIT(CMD$,STATUS%)
3170  CMD$="MTA    LISTEN    25  DATA  'F1R0B0C0G1X'":CALL
TRANSMIT(CMD$,STATUS%)
3180 FOR J=1 TO 2000:NEXT J
3190 TIC=0
3200 REM LICF=2  SEE BIGINNING OF THE PROG(LINE 430)
3210 CMD$="MLA TALK 25 "
3220 FOR L=1 TO LICF
3230 R$=SPACE$(40)
3240 CALL TRANSMIT(CMD$,STATUS%)
3250 FOR J=1 TO 2000:NEXT J
3260 CALL RECEIVE(R$,LENGTH%,STATUS%):B=LEN(R$)
3270 ICR(L)=VAL(RIGHT$(R$,B))
3280 TIC=TIC+ICR(L)
3290 ICD=TIC/L
3300 'PRINT "iz,L,ICR(L),TIC,ICD"
3310 'PRINT IZ,L,ICR(L),TIC,ICD
3320 NEXT L
3330 ICAV(K)=(TIC/LICF)
3340 'PRINT "icav(K)"
3350 'PRINT ICAV(K)
3360 'IF IZ=1 THEN IRES(K)=ICAV(K),ELSE INC(K)=ICAV(K)
3370 'IF IRES(K)<0 THEN IC(K)=ICAV(K)+ABS(IRES(K))
3380 'IC(K)=ICAV(K)-IRES(K)
3390 RETURN
3400 REM **** RNGE  CORRECT AND ZERO CHECK *******
3410 REM
3420 TRANSMIT=3
3430  CMD$="MTA  LISTEN  25  DATA  'F1R3C1X'":CALL  TRANS-
MIT(CMD$,STATUS%)
3440 FOR JK=1 TO 2000:NEXT JK
3450  CMD$="MTA  LISTEN  25  DATA  'F1R2C1X'":CALL  TRANS-
MIT(CMD$,STATUS%)
3460 FOR JK=1 TO 1000:NEXT JK
3470  CMD$="MTA  LISTEN  25  DATA  'F1R1C1X'":CALL  TRANS-
MIT(CMD$,STATUS%)
3480 FOR JK=1 TO 1000:NEXT JK
3490  CMD$="MTA  LISTEN  25  DATA  'F1R1C1X'":CALL  TRANS-
MIT(CMD$,STATUS%)
3500 FOR JK=1 TO 1000:NEXT JK
3510   CMD$="MTA   LISTEN   25   DATA'C1X'":CALL   TRANS-
MIT(CMD$,STATUS%)
3520 FOR JK=1 TO 1000:NEXT JK
3530 IF HH<HHF THEN GOTO 3570
3540 CMD$="IFC":CALL TANSMIT(CMD$,STATUS%)
```

```
3550 REM CMD$="DCL":REM CALL TANSMIT(CMD$,STATUS%)
3560 CMD$="GTL":CALL TANSMIT(CMD$,STATUS%)
3570 RETURN
3580 REM
3590 REM *****FILE DISPLAY*****
3600 KMAX=KMX
3610 PRINT "KMAX= "KMAX
3620 VMAX=.000001
3630 RMAX=1:IMAX=1E-15
3640 FOR J=0 TO KMAX
3650 IF ABS(V(J))<VMAX THEN GOTO 3670
3660 VMAX=ABS(V(J))
3670 IF ABS(IC(J))<IMAX GOTO 3690
3680 IMAX=ABS(IC(J))
3690 IF R(J)<RMAX GOTO 3710
3700 RMAX=R(J)
3710 NEXT J
3720 REM
3730 REM
3740 REM SCREEN VISUALISATION
3750 GOSUB 2960:GOSUB 3050
3760 YIFACT=100/IMAX
3770 XVFACT=320/VMAX
3780 YRFACT=100/RMAX
3790 REM
3800 REM
3810 LV=0
3820 REM
3830 NH=0
3840 FOR K=0 TO KMAX
3850 NH=NH+1
3860 IF LV=1 THEN GOTO 4140
3870 VVP(K)=ABS(V(K))*XVFACT:REM VALUE OF V(K) INNUMBER OF
POINTS
3880 IVP(K)=ABS(IC(K))*YIFACT
3890 RVP(K)=YRFACT*R(K)
3900 REM
3910 IF (V(K)<0 AND IC(K)<0) THEN GOTO 3970
3920 IF (V(K)<0 AND IC(K)>0) THEN GOTO 4000
3930 IF (V(K)>0 AND IC(K)<0) THEN GOTO 4030
3940 IF (V(K)>0 AND IC(K)>0) THEN GOTO 4060
3950 GOTO 4150
3960 REM
3970 IY(K)=100+IVP(K)
3980 VX(K)=320-VVP(K)
3990 GOTO 4080
4000 IY(K)=100-IVP(K)
4010 VX(K)=320-VVP(K)
4020 GOTO 4080
4030 IY(K)=100+IVP(K)
4040 VX(K)=320+VVP(K)
4050 GOTO 4080
4060 IY(K)=100-IVP(K)
4070 VX(K)=1*(320+VVP(K))
```

```
4080 RY(K)=100-RVP(K)
4090 IF NH>1 THEN GOTO 4120
4100 PSET(VX(0),IY(0))
4110 GOTO 4150
4120 LINE -(VX(K),IY(K))
4130 GOTO 4150
4140 PSET (VX(K),RY(K))
4150 NEXT K
4160 LV=LV+1
4170 IF LV=1 THEN GOTO 3830
4180 REM
4190 PRINT FL$
4200 PRINT "Rav  ="RAV
4210 PRINT "NDATA="KMXD:REM KMXD=KMX+1 AS K STARTS FROM K=0
4220 RETURN
4230 REM SUB DEFIN. START OF IEEE ROUTINES IN MEMORY
4240 DEF SEG=&HE000
4250 INIT=0
4260 ADDR%=21
4270 LEVEL%=0
4280 CALL INIT(ADDR%,LEVEL%)
4290 REM
4300 ADDR%=12:REM SEND ALL DATA TO DEVICE 12
4310 SEND=9:REM DEFINE ADDRESS OF SEND ROUTINE
4320  T$=CHR$(13):REM  DEFINE  CARRIAGE  RETURN  AS  STRING
DELIMINATOR
4330 REM INITIALISE PC AS SYSTEM CONTROLLER, WITH DEVICE
NUMBER 21
4340 TRANSMIT=3:RECEIVE=6
4350 CMD$="MTA REN ":CALL TRANSMIT(CMD$,STATUS%)
4360 RETURN
4370 REM ******* RANGE SUB *************
4380 SEND$="RNGE$"+T$:REM SET RANGE
4390 REM GOSUB 1620:REM CHECK STATUS
4400 CALL SEND(ADDR%,SEND$,STATUS%)
4410 RETURN
4420 REM
4430 PRINT #2,"  "VU$,"               "CU$," "VU$
4440  PRINT  #2," JUN.VOLT.","            JUN.CURRENT   ","
VOLT.OUTPUT"
4450 PRINT #2," VIN="VIN," VFIN."VFIN
4460 PRINT #2," STP="STP," VOLT.RANGE="RNGE$
4470 PRINT #2,"NB.OF DATA:"KMXD," FILENAME: "FL$
4480 PRINT #2,"RS= "RS$," Rav ="RAV,RUNIT$
4490 PRINT #2,"DATE :"DATE$,"TIME :"TIME$
4500 PRINT #2,MAT1$
4510 PRINT #2,MAT2$
4520 PRINT #2,MAT3$
4530 PRINT #2,MAT4$
4540 PRINT #2,MAT5$
4550 CLOSE #2
4560 RETURN
4570 REM SUB TO READ CURRENT FROM THIRLBY
4580 REM ************************************
```

```
4590 TRANSMIT=3: RECEIVE=6
4600 TIC=0
4610 REM LICF=5 :REM SEE BEGINNING OF THE PROGRAMM LINE 430
4620 FOR IJ=1 TO 2000:NEXT IJ
4630 FOR L=1 TO LICF
4640 CM$="UNT  UNL MLA TALK 11 DATA SEC 10"
4650 CALL TRANSMIT(CM$,STATUS%)
4660 REM
4670 REM
4680 CMD$="UNT UNL MLA TALK 11 "
4690 CALL TRANSMIT(CMD$,STATUS%)
4700 REM
4710 R$=SPACE$(40)
4720 REM
4730 FOR IJ=1 TO 2:NEXT IJ
4740 CALL RECEIVE(R$,LENGTH%,STATUS%)
4750 B=LEN(R$)
4760 IF LEFT$(R$,1)="R" THEN B=LEN(R$)-1
4770 CUR=VAL(RIGHT$(R$,B))
4780 'IF L=1 THEN GOTO 4460
4790 TIC=TIC+CUR
4800 ICD=TIC/L
4810 'IF L=LICF THEN GOTO 4450
4820 PRINT "L=";L,"CUR";CUR," ICD=";ICD
4830 FOR IB=1 TO 1000 :NEXT IB
4840 NEXT L
4850 'FOR LL=2 TO LICF
4860 REM CURRENT UNIT ICFACT
4870 ICFACT=.000001:REM CURRENT FROM THUR. IS IN micA
4880 IC(K)=ICFACT*TIC/(L-1)
4890 PRINT "L="L," IC(K)="IC(K)
4900 PRINT "**********************************"
4910 FOR IK=1 TO 8000:NEXT IK
4920 RETURN
```